Veröffentlichungen der Schweizerischen Meteorologischen Anstalt
Publications de l'Institut suisse de météorologie
Pubblicazioni dell'Istituto svizzero di meteorologia

1996

56

Data Assimilation and Mesoscale Weather Prediction: A Study with a Forecast Model for the Alpine Region

by Christoph H. Schraff

Data Assimilation and Mesoscale Weather Prediction:

A Study with a Forecast Model for the Alpine Region

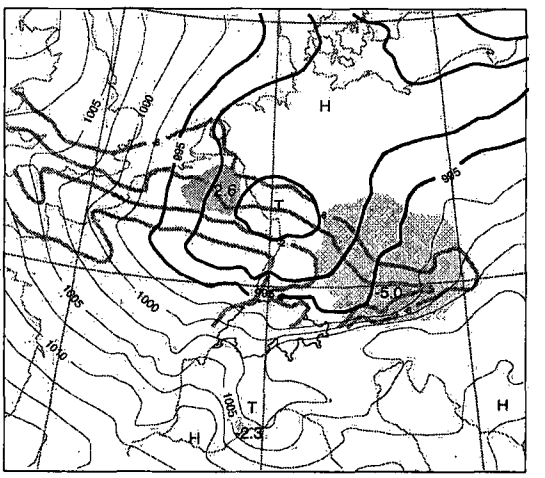

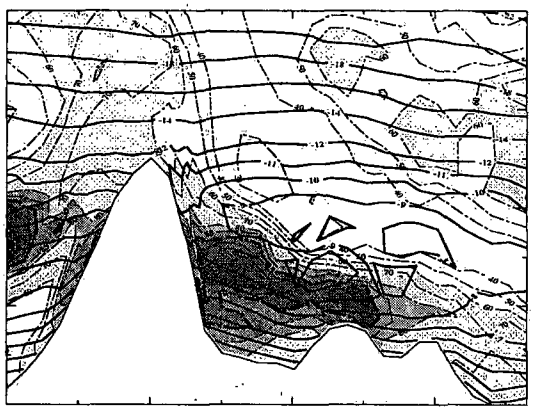

Christoph H. Schraff

SMA Publication No.56

Zürich, 1996

The present text is equivalent to Ph.D. dissertation No. 11627 of the Swiss Federal Institute of Technology Zürich.

Table of Contents

Abstract

A scheme based on the nudging method (Newtonian relaxation) is developed for direct assimilation of rawinsonde and screen-level data into a mesoscale model for the Alpine region. It is applied to routine observations in various meteorological situations to examine its potential capabilities and limitations for numerical weather prediction (NWP) purposes. Aspects of primary interest are the impact of different data, the influence of steep orography particularly with low stratus, and the benefit from the nudging for mixed-layer simulation in typical summertime smog conditions.

The impact of different types of data is first studied with idealized experiments designed to relate to basic theoretical considerations. A version of the operational model (mesh width: 14 km) of the Swiss Meteorological Institute is used to assess the scheme's performance. The benefit from different data is then examined with observing system simulation experiments (OSSE's) and real data experiments using the complete set of routinely available observations. The OSSE approach is also deployed for tuning and refinement of the scheme. The set of meteorological cases includes events with mesoscale convective systems, mesoscale cyclones, fronts, wintertime low stratus, or strong advection.

Linear geostrophic adjustment theory is shown to provide some guideline for estimating the degree of assimilation of the observational information, but its applicability is limited due to advective and orographic effects. The benefit from nudging of surface pressure is small, and does not improve with the use of a geostrophic wind correction. However, most of the pressure error is eliminated by nudging of the rawinsonde wind and temperature profiles which constitute the backbone of the assimilation scheme. Additional nudging of humidity profiles is also beneficial, and generally, errors in precipitation patterns are often reduced efficiently. Remarkably, the temperature information is found to be generally as important as the wind information, particularly in the boundary layer. This applies to 12-hourly rawinsonde data, and, in an exploratory case study, to additional hourly profiler data from a dense, simulated profiler network. It suggests that the promotion of future routine temperature profilers should not be neglected due to concentration of efforts on wind profilers.

In relation to air-quality studies, time series of mixed-layer depth are computed for summertime cases with weak winds and little cloudiness. Continuous nudging towards routine data, and in particular nudging of linearly interpolated 12-hourly temperature profiles within the mixed layer, adjusts effectively the evolution of the mixed layer and its depth. Hence in such cases, the nudging approach has a good potential to significantly improve diagnostic data sets generated with the model. However in a forecast, the positive impact of the nudging on the mixed-layer depth disappears comparatively rapidly.

The influence of orography upon data assimilation is studied in detail with wintertime low stratus episodes. In these conditions, the operational analyses - interpolations of large-scale analyses - and forecasts have been notably poor in the immediate environs of the Alps. Nudging is shown to introduce finer vertical structures and to benefit from increased vertical model resolution. However, the humidity advection scheme and, near steep terrain, particularly the horizontal model diffusion of the thermodynamic varia-

bles are shown to generate spurious vertical smoothing. In effect, forecasts benefit from the nudging only if the diffusion is significantly reduced.

Specific problems arise near steep orography, when rawinsonde observation increments over low terrain are spread laterally along the terrain-following σ-surfaces to high terrain, i.e. areas for which the observation is not often representative. A new concept for σ-layer models is introduced by spreading the observational information along isentropic surfaces. This leads to modest improvement of low stratus prediction over steep and moderate terrain. An attempt to take advantage of the steep Alpine terrain is made by applying this concept to screen-level humidity information from a high-resolution Swiss network of surface stations located at various altitudes. The quasi-horizontal spreading of the Alpine data increments over the Swiss Plateau improves the analyses, however significant benefit from screen-level humidity data on the humdity and temperature structure does not often pertain to 12-hour forecasts.

If compared to optimum interpolation, nudging often yields more consistent analyses and forecasts of inversions, associated vertical humidity gradients, cloud top heights, and cloud cover, notably near steep orography. However on occasions, the forecasts have a greater tendency to erroneously dissipate low cloud as a result of the stronger vertical gradients in the nudged analyses and of the spurious vertical smoothing present in the model.

In general, nudging towards direct observations is shown to be an appropriate method for assimilation of rawinsonde and screen-level data into a mesoscale model for the Alpine region, and appears to be promising for operational NWP.

Zusammenfassung

Zur kontinuierlichen Assimilation von Daten von Radiosonden und Bodenstationen in ein mesoskaliges Wettervorhersagemodell für die Umgebung der Alpen wird ein auf der 'Nudging'-Methode (Newton'sche Relaxation) basierendes Schema entwickelt. Dieses wird in einer Reihe verschiedener meteorologischer Situationen auf routinemässig gemessene Daten angewandt, um die Stärken und Schwächen der Methode zur Bestimmung des Modellanfangszustandes im Hinblick auf die Anwendung auf die numerische Wettervorhersage (NWV) zu untersuchen. Von besonderem Interesse sind die Auswirkungen von verschiedenen Daten, der Einfluss von steiler Orographie insbesondere bei Hochnebelfällen, sowie der Nutzen von 'Nudging' für die Simulation der Mischungsschicht in Situationen, die typisch für sommerlichen Smog sind.

Das in dieser Studie verwendete Modell ist eine Version des operationellen 'Schweizer Modells' (Maschenweite: 14 km) der Schweizerischen Meteorologischen Anstalt. Der Einfluss von verschiedenen Datentypen wird in idealisierten, auf theoretischen Überlegungen basierenden Experimenten untersucht, sowie in Experimenten mit simulierten (OSSE) und realen Daten, wobei hier alle routinemässig verfügbaren Beobachtungen berücksichtigt werden. Die OSSE Methode wird auch für das Tuning und die Verfeinerung des Schemas verwendet. Die Reihe der betrachteten Fälle besteht aus Episoden mit mesoskaligen konvektiven Systemen, mesoskaligen Tiefdruckgebieten, Fronten, winterlichem Hochnebel oder starker Advektion.

Es wird gezeigt, dass mit der linearen 'geostrophen Adjustment Theorie' der Grad der Assimilation von Beobachtungsinformation qualitativ abgeschätzt werden kann. Einer weitergehenden Anwendung der Theorie werden jedoch durch advektive und orographische Effekte Grenzen gesetzt. 'Nudging' des Bodendrucks ist nur von geringem Nuzzen, der auch durch geostrophe Windkorrekturen nicht erhöht wird. Hingegen werden Fehler in den Druckfeldern weitgehend eliminiert durch das 'Nudging' von Wind- und Temperatur-Radiosondenprofilen, welche die wichtigste Informationsquelle bilden. Zusätzliches 'Nudging' von Feuchteprofilen ist nützlich, und Fehler in Niederschlagsfeldern werden meist effizient reduziert. Interessanterweise erweist sich die Temperaturinformation als ebenso wichtig wie die Windinformation, insbesondere in der Grundschicht. Dies trifft sowohl auf 12-stündliche Radiosondendaten zu als auch auf in einem Fall zusätzlich erzeugte stündliche Profile von einem dichten simulierten Profilernetzwerk. Das deutet darauf hin, dass die Förderung von zukünftigen operationellen Temperaturprofilern nicht vernachlässigt werden sollte aufgrund einer (möglichen) Konzentration der Mittel auf Windprofiler.

In Bezug auf Studien über Luftverschmutzung werden Zeitreihen von simulierten Mischungsschichthöhen für sommerliche Fälle mit schwachen Winden und geringer Bewölkung berechnet. Kontinuierliches 'Nudging', insbesondere von linear interpolierten 12-stündlichen Temperaturprofilen innerhalb der Mischungsschicht, korrigiert in effektiver Weise die Evolution der Mischungsschicht und deren Höhe. Dies deutet darauf hin, dass 'Nudging' die Qualität von mit dem 'Schweizer Modell' produzierten diagnostischen Datensätzen in solchen Situationen signifikant verbessern kann. In der Prognose hingegen verliert sich die positive Auswirkung des 'Nudging' auf die Mischungsschichthöhe relativ rasch.

Der Einfluss von Orographie auf die Datenassimilation wird eingehend in Hochnebelfällen untersucht. In solchen Fällen sind die operationellen Analysen - Interpolationen von grobmaschigeren Analysen - und Vorhersagen für die unmittelbare Umgebung der Alpen oft ausgesprochen mangelhaft. Es wird gezeigt, dass das 'Nudging' feinere Vertikalstrukturen ins Modell einführt, insbesondere bei geringerer vertikaler Maschenweite. Allerdings verursachen das Feuchteadvektionsschema und, in der Nähe von steilem Gelände, vor allem die horizontale Modelldiffusion der thermodynamischen Variablen künstliche Glättungseffekte in der Vertikalen. Als Folge davon profitieren die Hochnebel-Vorhersagen von der Anwendung des 'Nudging'-Schemas nur wenn die Diffusion signifikant reduziert wird.

Spezifische Probleme ergeben sich, wenn Radiosondeninformation aus den untersten Schichten seitlich entlang den terrain-folgenden σ-Flächen von tief- zu hochgelegenem Gelände ausgebreitet wird, für welches die Information nicht repräsentativ ist. Als alternatives, neues Konzept für Modelle in σ-Koordinaten wird daher diese Information entlang von Isentropenflächen ausgebreitet. Daraus ergibt sich tendenziell eine weitere Verbesserung der Hochnebelprognosen über steiler und mässiger Orographie. In einem Versuch, das steile alpine Gelände auszunützen, wird dieses Konzept auch auf Feuchtedaten von einem dichten schweizerischen Netzwerk von Bodenstationen angewandt, welches Höhenlagen bis 2500 Metern gut repräsentiert. Die quasi-horizontale Ausbreitung dieser alpinen Information über das Schweizer Mittelland erhöht die Analysenqualität, hingegen bleibt die signifikante Verbesserung der Feuchte- und Temperaturstruktur nicht oft bis zur 12-Stunden Prognose erhalten.

Im Vergleich zur optimalen Interpolation, welche heutzutage die meistverwendete Methode zur Bestimmung des Anfangszustandes eines NWV-Modells ist, führt 'Nudging' oft zu konsistenteren Analysen und Vorhersagen von Inversionen, damit verbundenen vertikalen Feuchtegradienten, Hochnebelobergrenzen, und der horizontalen Ausdehnung des Hochnebels, insbesondere in der Nähe von steilem Terrain. Allerdings kann als Folge der schärferen vertikalen Gradienten in den 'genudgten' Analysen und der im Modell vorhandenen, bereits erwähnten unrealistischen vertikalen Glättungseffekte gelegentlich eine erhöhte Tendenz zu fälschlicher Hochnebelauflösung auftreten.

Insgesamt zeigt die vorliegende Studie, dass 'Nudging' eine geeignete Methode zur Assimilation von Radiosonden- und Bodenschichtdaten in ein hochauflösendes Modell für die Alpenregion ist und für die operationelle NWV vielversprechend zu sein scheint.

Résumé

Un schéma se basant sur la méthode du "nudging" (ou relaxation de Newton) a été développé pour assimiler de façon continue dans un modèle numérique de prévision du temps à méso-échelle les données des radio-sondages et des stations au sol pour un domaine centré sur les Alpes. Ce schéma est employé pour une série de situations météorologiques avec des données d'observation opérationnelles afin de faire apparaître les forces et les faiblesses de cette méthode dans sa capacité à déterminer les conditions initiales d'un modèle numérique de prévision du temps en vue de son utilisation opérationnelle. Particulièrement étudié a été l'impact des différentes données d'observation et l'influence des fortes pentes de l'orographie par situation de brouillard élevé, ainsi que l'utilité de la méthode pour la simulation de la couche limite dans les situations météorologiques qui sont typiques du smog estival.

Le modèle utilisé pour cette étude est une version du "Swiss Model" (résolution horizontale: 14 km) de l'Institut suisse de météorologie. L'influence de différents types de données d'observation est étudié dans des expériences idéalisées se basant sur des considérations théoriques ainsi que par des expériences utilisant des données simulées (OSSE) ou réelles. Dans ce dernier cas, toutes les données opérationnelles disponibles ont été utilisées. La méthode OSSE est aussi utilisée pour la mise au point et l'ajustement de la méthode du "nudging". La série des cas traités se compose d'épisodes caractérisés par des systèmes convectifs à méso-échelle, par des dépressions de petite échelle, par des fronts, par des situations de stratus hivernaux ou par une forte advection.

On montre qu'avec la théorie linéaire de l'ajustement géostrophique le degré de l'assimilation de l'information contenue dans les observations peut être qualitativement estimé. Néanmoins, les effets orographiques imposent des limites à l'utilisation de cette théorie. Le "nudging" de la pression au sol est d'une utilité très limitée qui n'est pas accrue par l'utilisation d'une correction géostrophique du vent. Par contre les erreurs dans les champs de pression sont en grande partie éliminées par le "nudging" des profils de vent et de température des radio-sondages. Ces derniers sont la source d'information la plus importante. Si en plus on "nudge" les profils d'humidité, on améliore la qualité des champs des précipitations. Il est important de noter que l'information de température est aussi importante que celle du vent, particulièrement dans la couche limite. Ceci est vrai aussi bien lorsque l'information des radio-sondages n'est disponible que toutes les 12 heures que dans le cas où à partir d'un réseau simulé de profileurs l'on dispose de profils horaires. Cela implique que la demande pour de futurs profils opérationnels de température ne devrait pas être négligée au profit des profileurs classiques mesurant le vent.

En relation avec les études de la qualité de l'air, des séries temporelles de la hauteur de la couche de mélange sont calculées pour des situations estivales avec des vents faibles et peu de nuages. Le "nudging" continu des profils de température de la couche de mélange interpolés linéairement dans l'intervalle d'observation de 12 heures ajuste d'une façon efficace l'évolution et la hauteur de la couche de mélange. Dans ces situations le "nudging" peut ainsi sensiblement améliorer la qualité des données diagnostiques produites par le modèle. Toutefois cet effet positif du "nudging" sur la hauteur de la couche de mélange se perd relativement rapidement dans la prévision.

L'influence de l'orographie sur l'assimilation des données est étudiée en détail pour des situations de stratus hivernaux. Dans ces cas les analyses opérationnelles - interpolations d'analyses à plus large-échelle - et les prévisions à proximité immédiate des Alpes sont nettement déficientes. La méthode du "nudging" introduit des structures verticales plus fines et bénéficie d'une résolution verticale accrue. Néanmoins des effets de lissage fictifs dans la verticale sont introduits par le schéma d'advection d'humidité et, dans les régions à forte pente, particulièrement par la diffusion horizontale des variables thermodynamiques du modèle. De ce fait les prévisions de cas de stratus hivernaux ne profitent du "nudging" que si l'on réduit de manière significative la diffusion.

Des problèmes spécifiques résultent lorsque les incréments d'observations des radiosondages dans les basses couches se répandent latéralement le long des surfaces σ du modèle d'un terrain bas à un terrain élevé, c.à.d. dans des zones où l'information des observations n'est pas représentative. Un nouveau concept qui répand cette information le long de surfaces isentropes est introduit pour les modèles utilisant la coordonnée verticale σ. Il en résulte une ultérieure légère amélioration des prévisions de stratus hivernaux dans les régions à pente forte ou modérée. Pour tirer profit du terrain alpin pentu, ce concept est aussi appliqué sur les données d'humidité du réseau suisse de stations au sol à différentes altitudes. La répartition quasi-horizontale de cette information alpine sur le Plateau suisse augmente la qualité de l'analyse, par contre l'amélioration significative de la structure des champs d'humidité et de température ne persiste souvent pas jusqu'à 12 heures de prévision.

En comparaison avec l'interpolation optimale, qui est aujourd'hui la méthode la plus répandue pour la détermination des conditions initiales pour les modèles de prévision numérique du temps, le "nudging" produit souvent des analyses et des prévisions d'inversions plus consistantes. Il en est de même des gradients verticaux d'humidité, des hauteurs supérieures et des extensions horizontales du stratus associés à l'inversion. Ceci est surtout vrai à proximité des forts gradients d'orographies. Cependant quelques fois les prévisions ont une plus grande tendance à dissiper d'une façon incorrecte les nuages bas à cause des plus forts gradients verticaux de l'analyse "nudgée" et du trop grand lissage vertical du modèle.

D'une façon générale, le travail présenté montre que le "nudging" est une méthode appropriée pour assimiler les données des radio-sondages et des stations au sol dans un modèle à méso-échelle pour la région des Alpes et que cette méthode semble être très prometteuse pour les prévisions numériques opérationnelles du temps.

Riassunto

Per permettere l'assimilazione continua di dati provenienti dalle radiosonde e dalle stazioni al suolo in un modello a mesoscala di previsioni meteorologiche per la regione alpina, viene sviluppato uno schema basato sul metodo di rilassamento newtoniano (*nudging*). Il metodo viene applicato a misurazioni sistematiche in situazioni meteorologiche diverse per esaminarne le capacità potenziali e le limitazioni nel determinare le condizioni iniziali del modello nell'ottica di un'applicazione nelle previsioni numeriche. Di particolare interesse sono le conseguenze di diversi dati, l'influsso di un'orografia ripida, soprattutto nei casi di nebbia alta, come pure l'utilità del sistema di rilassamento per la simulazione dello strato di mescolamento, tipico per le situazioni di smog estivo.

L'impatto dei differenti tipi di dati viene dapprima studiato con esperimenti ideali concepiti per essere messi in relazione con le considerazioni teoriche di base. Una versione operazionale del modello (con una larghezza di maglia di 14 km) dell'Istituto svizzero di meteorologia è utilizzato per giudicare l'esecuzione dello schema. L'apporto dei differenti dati è poi esaminato usando esperimenti di simulazione di sistemi osservanti (Observing System Simulation Experiments, OSSE) ed esperimenti con dati reali di tutte le serie di osservazioni disponibili normalmente. L'approccio con OSSE è pure impiegato per l'aggiustamento e l'affinamento dello schema. Il ventaglio di casi meteorologici comprende eventi di sistemi convettivi a mesoscala, cicloni a mesoscala, fronti e situazioni invernali di strati bassi o di forte avvezione.

Viene mostrato che la teoria di aggiustamento geostrofico lineare dà un'indicazione per stimare il grado di assimilazione dei rilevamenti, ma la sua applicazione è limitata dagli effetti orografici e avvettivi. Il beneficio del rilassamento sulle superfici di pressione è limitato e non aumenta usando una correzione del vento geostrofico. Comunque la gran parte dell'errore della pressione è eliminato rilassando la radiosonda, che costituisce la parte portante dello schema di assimilazione. Un ulteriore rilassamento del profilo dell'umidità ha pure un effetto positivo e, in generale, gli errori della distribuzione delle precipitazioni vengono spesso ridotti efficacemente. Da notare che i rilevamenti della temperatura risultano generalmente altrettanto importanti quanto le informazioni sul vento, in particolare nello strato limite. Ciò concerne i dati dei radiosondaggi principali (ogni 12 ore) e in analisi di studio di prospezione anche i dati orari supplementari dei *profilers* di una densa rete di *profilers* simulati. Ne consegue che il promuovimento dei futuri *profilers* operazionali della temperatura non dovrebbe venir trascurata a causa della concentrazione degli sforzi sui *profilers* del vento.

Nell'ambito di studi sulla qualità dell'aria, sono state analizzate serie temporali sullo spessore dello strato di rimescolamento per eventi estivi con venti deboli e poca nuvolosità. Il rilassamento continuo sui dati correnti, e in particolare il rilassamento sui profili della temperatura nello strato di rimescolamento rilevati ogni 12 ore e interpolati linearmente, corregge efficacemente l'evoluzione e lo spessore dello strato di rimescolamento. Perciò, in questi casi, la tecnica del rilassamento ha un buon potenziale per migliorare significativamente la serie di dati diagnostici generati con il modello. Comunque, in una previsione, l'impatto positivo del rilassamento sullo spessore dello strato di rimescolamento scompaiono in maniera relativamente rapida.

L'influsso dell'orografia sull'assimilazione dei dati viene studiato in dettaglio con eventi invernali di strati bassi. In queste condizioni, le analisi operazionali (le interpolazioni delle analisi a grande scala) e le previsioni sono notoriamente di modesta qualità nelle immediate vicinanze delle Alpi. Il rilassamento induce una struttura verticale più fine e beneficia dell'aumentata risoluzione verticale dei modelli. Comunque, lo schema di avvezione dell'umidità e, in prossimità dell'orografia ripida, soprattutto il modello di diffusione orizzontale delle variabili termodinamiche mostrano la formazione di falsi lisciamenti verticali. In effetti le previsioni beneficiano del rilassamento solo se la diffusione viene significativamente ridotta.

Problemi specifici insorgono vicino a un'orografia ripida quando i rilevamenti della radiosonda vengono estesi lateralmente lungo le superfici σ sopra terreno montuoso, cioè su aree per le quali i rilevamenti spesso non sono rappresentativi. Un nuovo concetto per modelli a livelli σ viene introdotto, distribuendo le informazioni rilevate lungo le superfici isoentropiche. Ciò porta a un modesto miglioramento della previsione di strati bassi sopra un'orografia ripida o moderatamente ripida. Un tentativo di trarre vantaggio dalla ripida orografia alpina viene fatto applicando questo concetto ai rilevamenti dell'umidità a 2 m dal suolo forniti dalla densa rete di misurazione svizzera con stazioni ubicate a varie altezze. L'estensione quasi orizzontale degli incrementi dei dati alpini sull'Altopiano svizzero migliora le analisi, comunque un beneficio significativo sulla struttura dell'umidità e della temperatura dovuto ai rilevamenti dell'umidità a 2 m dal suolo spesso non si estende fino alle previsioni a 12 ore.

Se paragonato a un'interpolazione ottimale, il rilassamento spesso genera analisi e previsioni di inversioni più consistenti, con i parametri associati quali gradiente verticale dell' umidità, altezza del limite superiore delle nubi e copertura nuvolosa, in particolare vicino a un'orografia ripida. Comunque, ogni tanto, le previsioni hanno un'accresciuta tendenza a dissipare erroneamente la nuvolosità bassa, come conseguenza di un gradiente verticale più forte nelle analisi rilassate e dei falsi lisciamenti presenti nel modello.

In generale il rilassamento dei rilevamenti diretti si dimostra un metodo appropriato per l'assimilazione dei dati delle radiosonde e dei rilevamenti effettuati a 2 m dal suolo in un modello a mesoscala per la regione alpina, così come sembra promettente per modelli operazionali di previsioni numeriche.

1 Introduction

Numerical weather prediction (NWP) is the key tool for modern operational weather forecasting in the short (12 - 48 hours) and medium forecast range (3 - 7 days). Mathematically, the modelling and numerical prediction of the atmospheric evolution is an initial (and boundary) value problem. Hence, there are two distinct tasks to produce a numerical forecast: the determination of the initial condition by assimilating observational data into the model, and the model integration forward in time by solving the time-dependent system of (non-linear, partial differential) model equations. Recent predictability studies (Simmons et al., 1995; Rabier et al., 1996) suggest that better estimation of the initial state currently offers the principal path to more accurate forecasts (Simmons, 1995; ECMWF, 1995). However, there is still considerable scope for benefit from model improvement. To take full advantage of evermore increased model resolution made feasible by the rapid growth of available computer power, more accurate and detailed initial conditions are required (Weygandt and Seaman, 1994; Stauffer and Seaman, 1994). The present study is designed to contribute to the improvement of the initial conditions for a high-resolution limited-area NWP model in the presence of steep orography.

1.1 Methods and current trends in data assimilation

Data assimilation consists of the process which estimates the initial conditions of a forecast using as far as feasible all the available information. Since the number of degrees of freedom of the current NWP models is by orders of magnitude larger than the number of current observations available, the estimation problem is strongly underdetermined. It is therefore essential to carry forward in time information from past observations using the forecast model since it is the best information propagator available. This concept was first used by Bergthorsson and Döös (1955) and Cressman (1959). Both sources of information, i.e. the prior information contained in the gridded short-range model forecast, and the current, irregularly distributed observations, have errors. Filtering and interpolation are thus the main tasks of a data assimilation scheme. A comprehensive introduction on data assimilation is provided by Daley (1991), and excellent reviews on past and present days' methods, problems and trends include Bengtsson et al., (1981), Lorenc (1986), Hollingsworth (1986), Harms et al. (1992), Courtier (1994), and, with a focus on high-resolution applications, Gustafsson et al. (1995).

Most of the current operational data assimilation schemes are based on the optimum (statistical) interpolation (OI) method (Gandin, 1963; Thiébaux and Pedder, 1987). The whole processing consists here of four distinct steps: (i) data quality control to exclude bad data (cf. Gandin, 1988; Ingleby and Lorenc, 1993), (ii) 3-dimensional (3-D) objective analysis by OI, (iii) initialization to balance the initial wind and mass fields by suppressing undesirable high-frequency gravity waves (cf. Temperton, 1988; Lynch and Huang, 1992; Huang et al., 1994), and (iv) a short-range forecast to provide prior information for the subsequent analysis. OI provides a systematic framework for blending observations of differing error characteristics with the short-range forecast and is designed to minimize the analysis error in a statistical sense. However in practice, this is compromised by various simplifications and assumptions (cf. Daley, 1991; Courtier, 1995). A main problem is the modelling of the forecast error correlations which strongly

influence the final analysis since they largely determine the spreading of the information contained in the observations. These correlation models most often rely on isotropy and geostrophy (Courtier, 1994). Therefore they do not account for orographic effects, and the suitability of current implementations for mesoscale applications is limited (Kim et al., 1994).

Technological advances during recent years did and still do strongly influence data assimilation research and development in the following ways:

1) The increasing amount and quality of asynoptic satellite and aircraft data, and the prospect and advent of high-frequency data from ground-based remote sensing observing systems (cf. Clifford et al., 1994; Browning and Szejwach, 1994; Lafaysee, 1994; Ruffieux, 1995) has promoted interest in 4DDA (4-D data assimilation) methods which allow for continuous assimilation of data into a model (Charney et al., 1969; Seaman, 1990). This interest refers to (i) variational techniques using adjoint methods (4DVAR: Lewis and Derber, 1985; Le Dimet and Talagrand, 1986; Thépaut and Courtier, 1991), (ii) the Kalman-Bucy filter (KF: Kalman and Bucy, 1961; Ghil et al., 1981), and (iii) nudging (Anthes, 1974; Hoke and Anthes, 1976; Davies and Turner, 1977). These methods combine objective analysis, initialization, and short-range forecast in one step, and this reduces the spin-up problems (cf. Krishnamurti et al., 1988) of the hydrological cycle during the early forecast (Gustafsson et al., 1995). Further advantages include the at least implicit flow dependency of the forecast error correlations (cf. Thépaut et al., 1993; Thépaut et al., 1996), and the use of the non-linear model dynamics (instead of diagnostic relations) to couple and balance the mass and wind fields. However, 4DVAR and especially KF are computationally extremely demanding.

2) The rapid growth of available computer power has enabled the development of higher horizontal model resolution: Before 1992, there were very few operational (cf. Bougeault, 1992) and even research-orientated complex NWP models for the meso-β-scale (i.e. for flow features in the range of scales of 20 - 200 km (Orlanski, 1975), which are resolved by models with grid spacings of 5 - 50 km respectively). Nowadays, there is a considerable number of operational limited-area models with mesh widths of 10 - 20 km (cf. EWGLAM, 1995; Nielsen et al., 1996), or, run in experimental mode, even of ca. 4 km (Sidselrud, 1995; Nielsen et al., 1996). Non-hydrostatic models are studied using resolutions of 4 km or even less (Stauffer et al., 1994; Seaman et al., 1995; Lyons et al., 1995; Fast, 1995).

   A main objective of meso-β-scale NWP models is the short-range prediction of local weather parameters such as near-surface wind and temperature, clouds and precipitation (cf. Majewski, 1995). This requires realistic meso-β-scale flow features already in the initial conditions, including realistic fields of humidity and latent heating rates (to avoid spin-up of clouds and precipitation, cf. Stauffer et al., 1994; Lee and Krishnamurti, 1995). Particular research efforts on data assimilation are therefore devoted to (i) very high-resolution applications, (ii) initialization of cloud water (Huang and Sundquist, 1993; Carr and Zhao, 1994; Snook et al., 1995; Huang, 1996), (iii) adjustment of humidity by use of cloud analyses (Wright et al., 1994; Cram et al., 1995; Young and Zack, 1994) or total precipitable water (Kuo et al., 1993; Filiberti et al., 1994), and (iv) adjustment of moisture, latent heating rates and/or surface fluxes by use of observed precipitation rates (Krishnamurti et al., 1984; Wang and Warner, 1988; Manobianco et al., 1994; Mathur, 1995), and/or outgoing longwave radiation (Puri and Miller, 1990; Krishnamurti et al., 1995; Yap,

1995). Note that most of these quanities are observed with high frequency by remote sensing instruments, and are therefore likely to be best used with 4DDA methods (cf. Krishnamurti et al., 1994).

3) The (prospect of) increasing computer power has also promoted strong research efforts in 4DVAR (see e.g. Tellus special issue on adjoint applications, 1993, Vol, 45A, No. 5; list of literature: Courtier et al., 1993). Here, the initial state is adjusted in such a way that the model trajectory fits past and present observations in an optimal way over a certain period of time. Derber (1989) and Wergen (1992) demonstrated how to address a model bias in 4DVAR, and in the cycling 4DVAR approach (Courtier, 1994), explicitly flow dependent forecast error correlations and variances reflect the actual forecast error (as an approximation to KF). By deployment of several simplifications (incremental formulation: Courtier et al., 1994; nested loops with simplified model versions: Courtier, 1995) and a quasi-continuous approach (Järvinen et al., 1996) to cut down the requirements on computer resources, operational 4DVAR for medium-range forecasts is about to become feasible, and is planned at the ECMWF (European Center for Medium Range Forecasts) for 1997 (Simmons, 1995).

The main advantages of 4DVAR are: (i) Observed quantities (e.g. radiances from satellites, cf. Andersson et al., 1994; precipitation, cf. Zupanski and Mesinger, 1995; total precipitable water, cf. Kuo et al., 1996), which are non-linearly related to the prognostic model variables, can be used directly. (ii) The combination of optimal control and use of (at least implicit) flow dependent forecast error correlations makes 4DVAR (besides KF) the method most capable of correcting structures associated with the fastest growth of forecast error (Rabier et al., 1996). These baroclinic structures are usually related to cyclogenesis over the ocean, and their correct representation in the initial condition is crucial for medium-range NWP but less important for short-range NWP over continental areas with limited area models.

This may be one reason, why the tendency to move towards 4DVAR has been much slower for high-resolution models. Although 4DVAR has produced good results in recent applications for a limited-area model (Zupanski, 1993; Zupanski, 1994; Zou et al., 1995), it has not yet been attempted with meso-β-scale NWP models. A main reason is that operational short-range forecasting is too time critical to allow for operational 4DVAR in the near future. Technical problems, particularly asssociated with grid point models (cf. Gustafsson et al., 1995), add to these problems.

Hence, many new data assimilation schemes for high-resolution limited area models are based on observation nudging (Newtonian relaxation). Here, the model fields are relaxed towards the observations during the forward integration of the model. The advantages of this method include those mentioned above for continuous 4DDA methods, and it is conceptually and computationally simple. The direct influence of observations is more local than in OI or 4DVAR, e.g. no vertical correlation functions are used for complete vertical profiles, and as a result there is less tendency to smoothe vertical gradients which is especially important in short-range NWP (Gilchrist, 1984). A number of studies have demonstrated that observation nudging is able to reduce the error in the larger scales which are resolved by the observing network, while not suppressing realistic fine-scale structures produced by the model itself. Therefore, observation nudging appears to be attractive for meso-β-scale applications. Practical difficulty with nudging schemes include data quality control, and tuning since several aspects of the nudging

method are difficult to quantify. A 4DDA scheme based on nudging is operational at the UKMO (United Kingdom Meteorological Office: Lorenc et al., 1991).

1.2 Object of the present contribution

The Swiss Meteorological Institute (SMA) operates a limited area NWP model (Swiss Model: SM) with a mesh width of 14 km to produce short-range forecasts for Switzerland and the Alpine region. The initial conditions are derived from coarser-grid OI analyses. Figure 1-1 shows the (low) cloud cover for a case with widespread persistent deep fog and low stratus in the environs of the Alps, which is missed almost completely in the initial fields of the SM. Most of the error pertains in the subsequent forecast (see section 3.2.1), and similar shortcomings have often been found with low stratus cases, particularly in the Swiss Plateau. This clearly illustrates a need to improve the initial conditions.

The first main object of the present work is thus to develop a data assimilation scheme for conventional routine observations and to examine its potential for improving the initial states and forecasts of the SM. This requires the scheme's application to various meteorological situations and its evaluation with a focus on phenomena and quantities which are of particular interest for short-range forecasting in Switzerland and for meso-β-scale modelling in general. These phenomena and quantities include:

- low stratus: temperature inversions and low cloudiness
- mesoscale cyclones and fronts: surface pressure, temperature gradients, and precipitation
- mesoscale convective systems: precipitation

The selected assimilation method is nudging towards individual observations because of the scientific (compared with OI) and practical (compared with 4DVAR) advantages mentioned in the previous section. The nudging method can also be used to assimilate 3-D analyses, but this approach is less suitable for asynoptic data (Stauffer and Bao, 1993; Seaman et al., 1995) and high-resolution modelling since it is found to adversely affect realistic fine-scale structures produced by the forecast model (Wang and Warner, 1988; Stauffer and Seaman, 1994). Note, however, that the observation nudging approach as deployed here may have a tendency to introduce false divergences (Stauffer and Seaman, 1990) and to assimilate unrepresentative components of observations (Harms et al., 1992; Stauffer and Seaman, 1994).

The second central aim is to study the effects of steep orography (e.g. the Alps) on nudging. In the context of NWP, the discussion of this issue in the literature is limited. Some aspects related to wind field forecasting have been addressed by Leidner et al. (1994). Otherwise, however, either nudging was applied throughout the period of interest for diagnostic purposes (Warner et al., 1992; Stauffer and Seaman, 1994; Seaman et al., 1995), or it was applied only to wind data to study its impact on the flow field (Henmi, 1990; Fast, 1995), or the focus was not on orographic effects, or a method other than nudging was used to initialize the model (cf. Ballard et al., 1991; Golding, 1993).

For two reasons, orographic effects will be addressed here primarily with cases of low stratus (or deep fog). Firstly, there is a general lack of experience in data assimilation with cases of continental low stratus (see section 3.1.1), although the prediction of fog

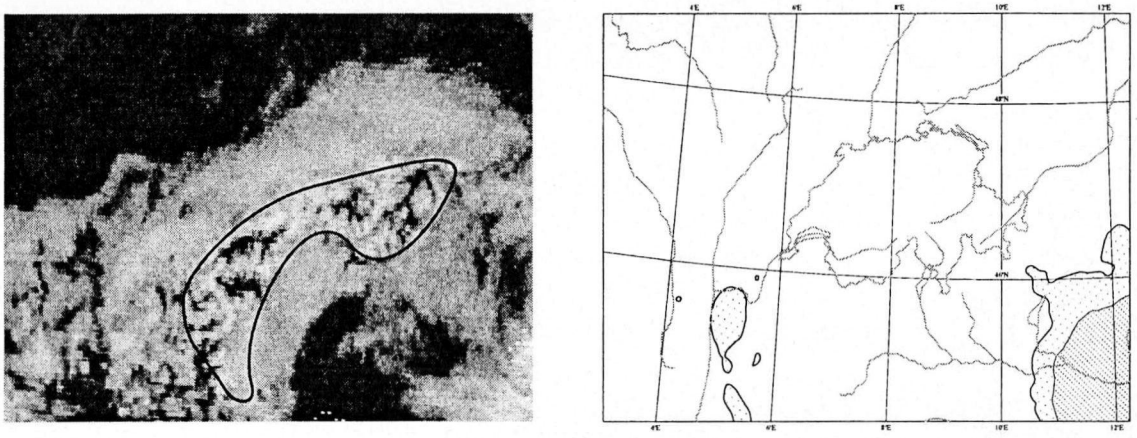

FIGURE 1-1. Low cloud cover in the environs of Switzerland for 1200 UTC, 20 November 1993. a): Section of VIS 1+2 channel image from METEOSAT 4. White areas are covered with low stratus except for cloudless, snow covered Alpine areas approximately encircled by the black contour b): Low cloud cover of operational initial state of the Swiss Model. Cloudiness in white areas is < 20 %, in light stippled areas 20 % to 80 %, in dark stippled areas > 80 %).

and low stratus is a primary task of short-range forecasting in many countries (e.g. Switzerland). Secondly, since the operational SM analyses and forecasts of low stratus are especially poor in the immediate environs of the Alps, orographic effects are likely to be important in these cases, and the scope for improvement by adjustment and refinement of the scheme appears to be relatively large.

A further objective is to address the potential of the nudging scheme for enhancement of the suitability of the SM for diagnostic purposes, namely in relation to air quality studies on summertime smog (e.g. POLLUMET, 1996). In this context, the diurnal cycle of the mixed-layer depth is of particular interest, and the impact of nudging on its simulation with mesoscale NWP models has been mixed in the past and depended on the temporal (and horizontal) resolution of the upper-air data (Stauffer et al., 1991; Seaman et al., 1995).

The data used in this study are conventional routine observations from rawinsondes and surface stations. Rawinsonde data still constitute the backbone of any data assimilation scheme today, and the rawinsonde's capability for resolving details of the thermodynamic structure in the vertical has yet to be duplicated by any of the new remote-sensing systems (Schwartz and Doswell, 1991). In the future, wind and temperature (RASS) profiler may provide routine data of sufficient quality and vertical resolution (except near inversions, cf. Martner et al., 1993) to be of value particularly for high-resolution models (Browning and Szejwach, 1994). However, networks of profilers have yet to be designed in Europe. Hence, a supplementary objective of this work is to contribute to information needed for such a design by examination of the impact of different observed parameters (wind, temperature, humidity) from hourly simulated profiler data in an exploratory case study.

1.3 Outline

It is important to develop an understanding of the effect which different types of data have on the model fields when using the nudging scheme. In particular, it would be useful to know whether there are theoretical considerations that help to estimate these

effects. After a short description of the model and a presentation of the nudging scheme, this issue is addressed in chapter 2 by means of idealized experiments with single data.

In order to examine the potential of the nudging scheme for meso-β-scale NWP in the Alpine region, there are two major tasks to be undertaken: Firstly the refinement and tuning of the scheme, and secondly its evaluation in a realistic setting, including a comparison with one (or several) current operational data assimilation schemes. Both tasks are addressed in each of chapters 3 and 4, and in practice, the progress has been characterized by a continuous mutual influence of the experimentation done in the two chapters.

Chapter 3 deals with the real-data application to low stratus, and evaluates the scheme's performance with a focus on orographic effects. The influence of some model components are addressed, and a comparison to two alternative methods (based on OI) to define the model's initial conditions is included. However, considerable effort is also given to the refinement of the scheme, for instance in relation to lateral spreading of the influence of data, or the use of screen-level humidity data.

In chapter 4, the 'OSSE' approach provides a suitable tool for further refinement, tuning, and control of the scheme. Some real data experiments are also undertaken, and the scheme's performance is examined for various meteorological situations with respect to e.g. the elimination of surface pressure errors or position errors of fronts and precipitation. The impact from different data is studied, and the diurnal cycle of the mixed-layer depth and the impact of simulated profiler data are also addressed.

Finally, the main conclusions are drawn in chapter 5.

2 Model structure and formulation of the nudging

2.1 The Swiss Model

The performance and detailed features of any data assimilation scheme, and particularly of a nudging scheme, is strongly related to the formulation of the model. Thus, it is appropriate to provide a short description of the model.

2.1.1 Short description of the Swiss model

The forecast model employed is a version of the Swiss Model (SM). The SM is the mesoscale NWP model that became operational at the Swiss Meteorological Institute (SMI) in September 1994. It has been developed in collaboration with the Deutscher Wetterdienst (DWD). They operate 2 NWP models with the same code as the Swiss Model - the Europa Modell (EM) with a horizontal resolution of 55 km and the Deutschand Modell (DM) with a resolution of 14 km. The nudging scheme has been implemented into the code of the version 2.9 (operational at the DWD in February 1994). A description of the EM can be found in Majewski (1991) and Schrodin (1995a). Here, a summary is provided with an emphasis on those model components, which are relevant for the discussion of the effect of the nudging, particularly with respect to the application to low stratus.

A. Coordinates and dynamics

The Swiss Model is a hydrostatic limited-area grid-point model written in a terrain-following hybrid σ - p coordinate system (henceforth, the model layers below the lowest constant pressure model level at 240 hPa will be simply denoted as σ-layers). The prognostic variables are surface pressure p_s, the horizontal wind components (u,v), total heat h and the total specific water content q_{vc}. The total energy h is defined as the sum of the enthalpy (or sensible heat) c_pT and of the latent heat Lq_v. Likewise, the total specific water content q_w is defined as the sum of the specific contents of water vapour q_v and of cloud water q_c. The (h, q_{vc})-system treats phase changes between water vapour and liquid water implicitly so that no condensation or evaporation rates become apparent. The model is formulated in advective form on an Arakawa-C grid using rotated geographical horizontal coordinates. The Eulerian version employs second order central differences in space and leap-frog time stepping with a semi-implicit correction, and it is run with a time step of 90 s. Alternatively, a version with a 2-D Semi-Lagrangian scheme permits larger time steps. It is used operationally in the SM and the DM with a time step of 240 s. Vertical advection and vertical turbulent fluxes are treated implicitly to avoid numerical instability. A rigid lid is used for the upper boundary.

B. Physical parameterization

The traditional thermodynamic variables temperature T, water vapour q_v and cloud water q_c are used in the physics package and determined diagnostically from (h, q_{vc}) by assuming water saturation in clouds. However, in the radiation scheme (Ritter and Geleyn, 1992), cloudiness can also occur in subsaturated layers. The convective cloud cover can reach 20 %, and a fractional grid scale cloud cover is diagnosed from the relative humidity using a relationship which depends purely on the vertical model coordi-

nate. To form 20 % grid scale cloud cover, 97 % relative humidity is needed in the lowest model layer, but only 90 % at 1000 m above the ground. Saturated layers always contain 100 % cloudiness. Since this relationship does not depend on the thickness of a model layer, the parameterization can account for sub-grid scale variability of cloudiness only in the horizontal, but not in the vertical. The resulting total cloud cover in a model layer (together with aerosols, water vapour and other trace gases) is considered as an optically active atmospheric constituent which influences the longwave thermal and the shortwave solar radiative transfer through scattering, absorption and emission.

A linear fourth-order horizontal diffusion for the 3-D prognostic variables is applied on the σ-levels. However, in the heat equation, the moist static energy h_p is diffused instead of the total energy h, where h_p is given by

$$h_p = h + \phi = c_p T + L q_v + \phi \qquad (2\text{-}1)$$

(ϕ denotes geopotential). This accounts for the slope of the model layers, but only if the equivalent potential temperature is approximately constant with height. In any other situation, this formulation results in a pseudo-vertical diffusion near sloping terrain. The diffusion of total specific water content has similar side effects. A discussion of these effects for the situation of low stratus is provided in section 3.2. The operationally used diffusion coefficient renders an e-folding decay time of two time steps for two-grid waves.

Vertical turbulent fluxes are parameterized with a second order closure scheme of hierarchy level 2 (Mellor and Yamada, 1974) for the Ekman layer and the free atmosphere (cf. Müller, 1981). The Dyer-Businger relations as modified by Louis (1979) are used in the surface layer.

Grid scale precipitation is parameterized with a Kessler-type scheme including an ice phase, whereas sub-grid scale moist convective processes are parameterized by a mass flux scheme (Tiedtke, 1989). A two-layer soil model (Jocobsen and Heise, 1982) predicts the soil temperature and soil moisture which are used for the computation of the vertical turbulent fluxes in the surface layer. Soil type, seasonal vegetation cover, root depth and roughness length over land are climatological input parameters for the soil model. In the model version used here, the roughness length is up to 12 m in rugged terrain.

C. Initial and lateral boundary conditions

Both the EM and the DM have their own 6-hourly intermittent data assimilation cycle based on optimal interpolation (OI). A brief description of the OI scheme is provided in section 3.6. An adiabatic implicit normal mode initialization (Temperton, 1988) is applied to the analyses to render balanced mass and wind fields for the initial condition. Separate analyses are performed for the sea surface temperature and the water content of the snow cover.

For the Swiss Model (SM), EM analyses are interpolated on the fine grid using the method of Majewski (1985) which is designed to preserve as far as possible the degree of balance in the coarse grid fields despite large differences between the coarse-grid and the fine-grid orography. This is achieved by a two-step adjustment of the horizontally interpolated surface pressure yielding smooth geopotential fields also over rough terrain. First, a vertical interpolation of temperature with conservation of the layer

mean temperature is accompanied by an adjustment of the wind field within the boundary layer using the stationary Ekman equation. In a second step, a divergence correction above the boundary layer ensures that the interpolated surface pressure tendency equals that of the coarse grid model. The scheme has been extended by Schubiger and de Morsier (1992) to inclued the interpolation of cloud water fields. Thereafter, the normal mode initialization is applied.

The lateral boundary fields of the SM (and the DM) are temporally linearly interpolated EM forecast fields which are updated hourly and interpolated to the fine-mesh grid in the same manner as the analyses. The boundary values are then assimilated by the boundary relaxation technique after Davies (1976) in a marginal zone of 8 grid points.

2.1.2 Model noise

It is often helpful to view atmospheric flow as consisting of low-frequency geostrophic Rossby modes and of higher-frequency divergent inertia-gravity modes with a time scale shorter than the inertial time scale f^{-1} (f being the Coriolis parameter, typically 10^{-4} s^{-1} in the mid-latitudes). The bulk of the energy of synoptic-scale flows over flat terrain projects onto the geostrophic modes, and such flows are said to be balanced. Irrespective of the scale, primitive equation models tend to partition too much energy into inertia-gravity wave components. The latter component is often regarded as noise and includes imbalances in the initial conditions, inconsistencies in the boundary conditions, or shortcomings in the model formulation itself, notably of the numerical scheme and the diffusion. Since such noise can adversely affect the assimilation process of data by nudging, it is appropriate to examine briefly the model with respect to (an unphysical level of) inertia-gravity wave activity and systematic unphysical flow features.

Generally, internal inertia-gravity waves show up particularly in the vertical velocity, whereas the surface pressure tendency is more influenced by external gravity waves. Time series of these quantities (cf. Figure 2-1a) at single grid points often show oscillations with periods of about 1 hour or less caused by small-scale modes within the first

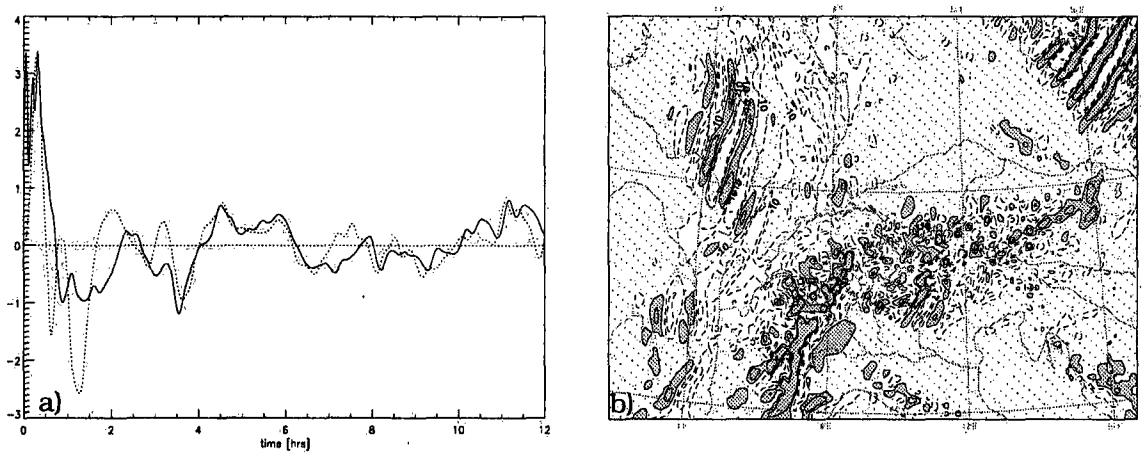

FIGURE 2-1. a): Time series of surface pressure tendency (in hPa/h) for the forenoon of 5 February 1993. Solid line: Payerne; dotted line: Zurich (about 140 km from Payerne).
b): Vertical velocity (in 10^{-1} Pa/s) at 700 hPa of the 30-hour Semi-Lagrangian forecast valid for 1800 UTC, 28 March 1995. Dark stippled areas: downward motion > 1 Pa/s; white areas: upward motion > 1 Pa/s.

2 hours of the integration. They are significantly affected by the normal mode initialization, and therefore caused by imbalances in the initial state. Thereafter, they largely disappear, and the general impact of the initialization becomes marginal which indicates that these modes interact little with the meteorological modes, and should have little impact on nudging. Little noise is usually apparent after this initial period. Weak external gravity waves originate from the lateral boundaries (cf. Miyakoda and Rosati, 1977), but they are also considered negligible.

In the presence of pronounced low-level stability and weak low-level winds, the initial low-level flow has a spurious tendency to be directed from higher to lower orography, and significant unphysical horizontal temperature gradients reach up to 2000 m above the ground. These gradients occur where orography differences between EM and SM vary strongly in the horizontal. The adjustment to a balanced flow where such spurious features are absent takes up to about 6 hours, and therefore, these features are likely to affect the nudging, particularly of surface data. Hence, the nudging period should preferably start from SM forecasts rather than interpolated EM analyses.

Small-scale horizontal patterns of vertical velocity are almost always found over topography throughout the integration. In the case shown in Figure 2-1b, they are attributable to orographic-induced inertia-gravity waves (cf. Smith, 1979) in the strong northwesterly air flow. The band of upward motion along the Rhine Valley in Figure 2-1b is associated with a warm front, and is realistic. In the southwestern part of the Alps, where the incident flow is perpendicular to the mountain chain, an elongated stationary mountain wave has formed. In the Eulerian version of the SM, such waves are probably often overestimated due to wave reflection at the upper boundary. In contrast, the Semi-Lagrangian version smoothes these mountain waves as part of a general tendency to smoothe strong gradients and strongly curved flow, and this smoothing, and hence the forecast, depends significantly on the time step (cf. McDonald and Haugen, 1992). Moreover, strong numerical propagating 'inertia-gravity waves' (cf. Figure 2-1b: northeastern corner, and northwest of Switzerland) often occur where the Courant number is greater than 1 (cf. Coiffier et al., 1987; Tanguay et al., 1992), particularly over steep orography (Rivest et al., 1994; Côté et al., 1995). In consideration of these defects in the Semi-Lagrangian scheme, the Eulerian version of the SM has been adopted for the work presented here.

To summarize, the Eulerian version of the SM appears to be reasonably well balanced with little spurious noise: inertia-gravity waves in the first 2 hours of the forecast; low-level adjustments near steep orography within the first 4 to 6 hours associated with a stable stratification; mountain wave reflection at the upper boundary associated with high wind speed; and small-scale vertical circulations over rough terrain (cf. section 3.2).

2.2 Implementation of the nudging scheme

A. The basic idea

Nudging or Newtonian relaxation consists of relaxing the model's prognostic variables towards prescribed values. For data assimilation purposes, these values can be 3-D analyses and/or direct observations. In the scheme developed here, nudging towards direct observations is performed. For this, a relaxation term is introduced into the

prognostic equations so that, assuming a single observation, the tendency of the prognostic variable $\psi(\boldsymbol{x},t)$ is given by:

$$\frac{\partial}{\partial t}\psi[x,t] = F[\psi[x,t],x,t] + G\left(\psi^{obs} - \psi\left[x^{obs},t\right]\right) \tag{2-2}$$

$F(\psi,\boldsymbol{x},t)$ denotes the dynamical and physical model, and ψ^{obs} is the value of the observation at $\boldsymbol{x}^{obs}$. The difference between the observation and model value at the observation point is called observation increment. Without dynamics and physics, the model fields would relax exponentially towards the observation with an e-folding decay time of the inverse of the weight G which contains the following constituents:

$$G = G_{\psi} \cdot \varepsilon \cdot w_{xy} \cdot w_p \cdot w_t \tag{2-3}$$

G_{ψ} is the nudging coefficient, which defines the time scale of the relaxation. The other factors vary between 0 and 1; ε depends on the quality of the observations, whereas the remaining weights depend on the horizontal, vertical, respectively temporal distance between the observation and the time-space model (grid) point.

It becomes evident from (2-2) and (2-3), that nudging towards direct observations consists of two major steps. The first step is to compute the observation increment in the vicinity of the observation point. This usually involves some kind of interpolation. The use of threshold values allows a rudimentary data quality control. The second step is to determine the weights and to spread the increments to the model grid points in some neighbourhood of the observation.

With finite time differences, the nudging is carried out as the last operation within a timestep except for the relaxation towards the lateral boundary fields. The implicit form of 2-2 then becomes for the leap-frog time stepping (cf. Yap, 1995)

$$\psi^{n+1} = \psi_F^{n+1} + \frac{2\Delta t \cdot G}{1 + 2\Delta t \cdot G} \cdot \left(\psi^{obs} - \psi_F^{n+1}\right) \tag{2-4}$$

where ψ_F^{n+1} is the model value after the updating with the dynamical and physical tendencies. Equation (2-4) forms the basis of the nudging. Evidently, a part of the observation increment is added to the model fields at each time step.

B. Multiple observations and varying data density

If an increasing number of observations influence a grid point the total nudging weight should be limited. Both the decreasing influence of an individual observation with increasing 4-D distance and the relative confidence of an observation with respect to the other influencing observations should also be taken into account. This is achieved by a weighted mean of weighted observation increments (Benjamin and Seaman, 1985). Equation (2-2) then takes the form

$$\frac{\partial \psi}{\partial t} = F + G_{\psi} \sum_k \frac{w_k}{\sum_k w_k} w_k \left(\psi^{obs_k} - \psi\right) \tag{2-5}$$

where $w_k = \varepsilon \cdot w_{xy} \cdot w_p \cdot w_t$ consists of the spatial and temporal weighting and the quality factor, and k runs over all the observation. The derivation of the according discrete equation is straightforward. This simple approach which is designed to improve particularly the gradients of the analyzed fields has been adopted by most authors (e.g. Stauffer and Seaman, 1990). A more correct, yet more expensive approach to account

for varying data density is to calculate the data density at the observation points rather than at the grid points and to include it in the quality factor ε (Bell, 1989; Lorenc et al., 1991). However, (2-5) is considered sufficient for the domain of the SM since the rawinsonde coverage over western and central Europe is fairly uniform.

C. Horizontal assignment of an observation to a grid point

To compute an observation increment, a spatial interpolation or an assignment of the observation to a model grid point has to be done first. Horizontally, the observation is assigned to the grid point (henceforth called 'observation grid point') within a search radius of $\sqrt{2} \cdot \Delta x$ (Δx being the mesh width) with the smallest orographical height difference to the observing station (except if a grid point exists within $\Delta x/4$ and a height difference < 40 m). For surface pressure data, the assignment is slightly modified (see below). The rather large search radius renders relatively small height differences, and is justified by the facts that (i) the error correlations of the SM are much broader than $\sqrt{2} \cdot \Delta x$, (ii) wavelengths smaller than $4\Delta x$ are not resolved properly, (iii) rawinsonde data provide good vertical resolution, and are best used (especially in the boundary layer) if orographic height differences to the model are small, and (iv) large height assignment errors of screen-level data can be disruptive.

Note, that the horizontal rawinsonde balloon drift is not taken into account. A recent examination (Macpherson, 1996) with a mesoscale model (Δx = 15 km) showed little impact of this approximation, albeit for relatively flat terrain.

D. Processing and nudging of surface pressure

The first part of the nudging scheme consists of updating the surface pressure p_s. For the vertical interpolation, consider first that the observation station height z_s^{obs} is greater than the model surface height z_s^{mod} of the observation grid point. The model pressure is then interpolated from the nearest model levels to the station height. This renders a pressure observation increment at that height, or equivalently, a geopotential increment at the interpolated model pressure. Since a pressure increment is needed at the model's orography z_s^{mod}, the pressure increment at the station height, $\Delta p[z_s^{obs}]$, is reduced adiabatically:

$$\Delta p_s\left[z_s^{mod}\right] = \Delta p\left[z_s^{obs}\right] \cdot \left(\frac{p_s^{mod}}{p^{mod}\left[z_s^{obs}\right]} \right)^{1 - R/c_p} \qquad (2\text{-}6)$$

$\Delta p_s[z_s^{mod}]$ then induces the same geopotential increment at the observation station height as $\Delta p[z_s^{obs}]$. The reduction can be regarded as an extrapolation of the observation increment, and the resulting error should be much smaller than if the surface pressure observation itself was extrapolated. If the height (above sea level) of the boundary layer top is assumed nearly constant within a 14 km grid box (as e.g. in low stratus situations), the method used here takes into consideration the observed fact that a surface pressure observation on a hill at z_s^{obs} is less influenced by the boundary layer than an observation at an average height z_s^{mod}.

If the observing station is lower than the model orography the observed pressure from vertical soundings can be simply interpolated to the model orography which should also result in small interpolation errors. For surface stations however, the observed surface pressure has to be extrapolated to the model surface height. For this, a

constant lapse rate (0.6 K / 100 m) temperature profile is assumed which starts from the model temperature at the lowest layer. Since the temperature error may be very large, the extrapolation error can become large as well (e.g. for a height difference of 100 m, a temperature error of 12 K results in an extrapolation error of 0.5 hPa, which is in the order of the expected observation error). Therefore, pressure data from surface stations are assimilated only if orography differences are in the interval $-100 \text{ m} < z_s^{obs} - z_s^{mod} < 400 \text{ m}$. The grid point assignment (cf. section C) is adapted accordingly, and the quality factor ε is a function of orography difference (with a Gaussian e-folding decay of -100 m respectively 400 m).

The resulting increment is then spread horizontally with the following autoregressive weight or correlation function (cf. Thiébaux et al., 1986; Lorenc et al., 1991) in the distance r between the observation point and target grid point:

$$w_{xy} = w_r = c + (1-c) \cdot (1 + r/s)\, e^{-r/s} \tag{2-7}$$

(Parameter values are chosen such that the weight function fits the geopotential error correlation used in the DM and EM OI scheme as until February 1994, cf. Buchhold and Paul, 1995. Alternatively, a more narrow function is also used, cf. Table 2-1.) Finally, the increments are multiplied with an adiabatic reduction factor analogous to (2-6) to account for the density difference between the observation grid point and the target grid point. Without this factor, the geopotential change at constant pressure surfaces is slightly greater over high orography than low orography for a given surface pressure increment (Figure 2-2).

Direct nudging of surface pressure will change the geopotential at every level. A pressure change at the surface is caused by a net mass divergence or convergence (with accompanying density or temperature changes) usually within the troposphere and lower stratosphere. The correlation of the geopotential with the surface pressure often decreases with increasing distance from the ground. Therefore, a temperature correction for surface pressure nudging (cf. Lorenc et al., 1991) is applied optionally, and this should aid the assimilation of surface pressure data (Lorenc, 1984). The correction is constant in the troposphere (below 240 hPa) to affect the lapse rate as little as possible, and decreases gradually to zero within the lower stratosphere in such a way that updating the surface pressure has no direct effect above the lower stratosphere.

A further extension, the geostrophic wind correction, will be discussed in section 2.3.3.

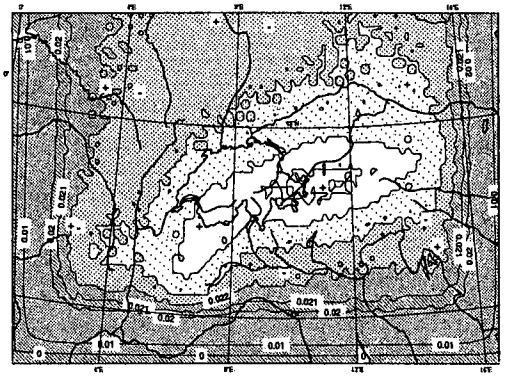

FIGURE 2-2. A section of the net impact on the 240 hPa geopotential of surface pressure nudging with a constant horizontal weight function a few time steps after the beginning of the nudging period, if no adiabatic reduction factor is applied to account for orography. The increased geopotential change over the Alps and the influence of the lateral boundaries in the west, south and east are evident. The orographic effect disappears after several hours of nudging.

E. Formulation of the nudging of the thermodynamic variables

The observed variables temperature T and specific water vapour content q_v are related to the model's thermodynamic prognostic variables, i.e. the total energy $h = c_pT + Lq_v$ and the total water content $q_{vc} = q_v + q_c$. If a zero nudging weight is assumed for q_c the linkage is simple for the formulation of the nudging since (i) the prognostic variables are a linear combination of the observed variables, and (ii) equation (2-4) is linear, which means that it will hold for h and q_{vc} if it holds for T and q_v. In this case, the nudging equations are set up for the observed variables. For temperature, it takes the form

$$T^{n+1} = T_F^{n+1} + \frac{2\Delta t\mu_T}{1+2\Delta t\mu_T}\left(\frac{\sum_k w_k^2\left(T_k^{obs} - T_{F,k}^{n+1}\right)}{\sum_k w_k^2}\right) + \frac{f_p \cdot 2\Delta t\mu_{p_s}}{1+2\Delta t\mu_T}\left(\frac{\sum_l w_l^2\left(p_{sl}^{obs} - p_{sF,l}^{n+1}\right)}{\sum_l w_l^2} + p_{sF}^{n+1} - p_s^{n+1}\right) \quad (2\text{-}8)$$

where $\mu_\psi = G_\psi \Sigma_m w_m^2 / \Sigma_m w_m$, and $w_{m(\psi)}$ consists of the spatial and temporal weighting and the quality factor. The summation is over all observations (k or l) influencing a grid point, and $T_{F,k}^{n+1}$ and $p_{s\,F,l}^{n+1}$ denote model values at observation points. The surface pressure term (where $f_p = RT_v/(c_pp) \cdot (dp/dp_s)$) accounts for the temperature change due to adiabatic compression induced by a pressure change which occurs at each σ-model layer if there is a surface pressure change. This term is modified if the temperature correction for surface pressure nudging (see above) is applied. The equation for the water vapour content is analogous, but without surface pressure term.

From the new values of T and q_v, new values of h and q_{vc} are computed, and these values are transformed back to the final values of T and q_v by the standard procedure (cf. section 2.1.1). This renders correct the transformation of latent heat into sensible heat (and vice versa) in saturated conditions when the nudging implies cooling (heating).

F. Nudging of wind

A number of authors obtained better results with nudging of only the non-divergent wind component instead of the total wind, or with nudging the divergence with a smaller weight. However, they used low-resolution large-scale models (Hoke and Anthes, 1976) or dealt with data assimilation in tropical of monsoon regions where diabatic heating rather than quasigeostrophy defines the vertical motion field (Ramamurthy and Carr, 1987; Davidson and Puri, 1992; Yap, 1995). For a limited area model in the mid-latitudes, Stauffer and Seaman (1990) have found that nudging only vorticity degraded the precipitation fields. Moreover, the divergent fraction is larger with smaller-scale flow. Thus, for a meso-β-scale model for the extra-tropics, nudging the total wind as done in many studies and operationally at the UKMO (Lorenc et al., 1991) is considered to be preferable. This renders nudging equations for the wind components that are analogous to (2-8) but excluding the surface pressure term.

G. Corrections to humidity data

Rawinsonde humidity data (e.g. data from the Vaisala sondes) are known to have a dry bias near saturation (cf. Schwartz and Doswell, 1991; Garand et al., 1992; Wade and Schwartz, 1993; Wang and Rossow, 1995). To compensate, a model-consistent bias correction can in principle be introduced (Lorenc et al., 1994). No such correction has been applied here, but saturation is assumed for observed relative humidity greater than 96%.

In the dynamic equations, the model distinguishes only between water vapour and liquid water, but not between liquid water and ice (cf. section 2.1.1). As a result, saturation pressure is always computed over water as opposed to the observed saturation pressure which is measured over ice below freezing. Nudging towards a saturated observation would then lead to subsaturation in the model if vapour pressure was used for the computation of the observation increment. Instead, relative humidities are compared. Equivalently, the observed vapour pressure e_{obs} can be multiplied with a correction to render model compatibility:

$$e_{obs}^{corr} = e_{obs} \cdot \frac{e_{Sat}^{water}[T]}{e_{Sat}^{ice}[T]} \tag{2-9}$$

A similar approach has been adopted by the DWD for the EM and DM analysis. In cases where supercooled water clouds are about to form or have just dissipated this may result in a wet bias which counteracts the overall dry bias to some extent.

H. Use, processing and quality control of rawinsonde data

All mandatory- and significant-level rawinsonde wind and temperature data from the ground up to 50 hPa are used in the scheme. Above 50 hPa, only mandatory-level data are used. Humidity data from all levels are used up to 300 hPa only, as rawinsonde humidity data at great heights are known to contain large errors (Richner and Phillips, 1982; Antikainen and Hyvönen, 1983; Ivanov et al., 1991).

First, the model wind components (u, v), temperature T and dewpoint T_d given at the model layer mid-points are interpolated (linearly in log(pressure)) to the height of the observations where observation increments are computed. Note that these increments are spot values and not generally representative of a whole model layer. If an increment exceeds a prescribed value given in Table 2-1 the observation is considered erroneous and is neglected. This rudimentary quality control is performed once per hour for all data.

The second step is to interpolate the observations vertically. To reduce representativeness (and measurement) errors (Ingleby, 1995), the procedure (cf. Woodage, 1985) is to adjust the vertical scale of the observations to the vertical scale resolved by the model layers. To achieve this, a continuous observed vertical profile is defined by interpolating the observed point values. The interpolation is linear in log(pressure) according to the WMO definition of significant levels (World Meteorological Organization, 1974). The continuous profile is then averaged between the bottom and the top of each model layer to produce scale-adjusted observations which are then used to determine the observation increments. This procedure is approximately hydrostatically consistent (the effect of moisture on the hydrostatic equation is not correctly accounted for) so that the model thickness between two pressure surfaces is adjusted towards the observed thickness by nudging the temperature. If surface pressure nudging is included it will allow an indirect (approximate) control of the geopotential. An alternative procedure is simple linear (in log(pressure)) interpolation to the model layer mid-points (see section 3.3).

Even with perfect humidity observations there is a dry bias (cf. Bell, 1994) because no cloud water is introduced directly by saturated observations, but the model fields can be deprived of cloud water in the presence of subsaturated observations. Whenever there are both saturated and unsaturated relative humidity data used for the interpola-

observations	TEMP: pressure, wind speed and direction, temperature and (only up to 300 hPa:) dewpoint depression. all mandary levels, significant levels up to 50 hPa SYNOP, ANETZ (Swiss automated surface station network): surface pressure; screen-level winds and relative humidity
observation increments with thresholds for quality control	surface pressure: 5 hPa ; rotated wind components: 12 m/s (potential) temperature: 8 K ; relative humidity: 40 %
temporal weighting	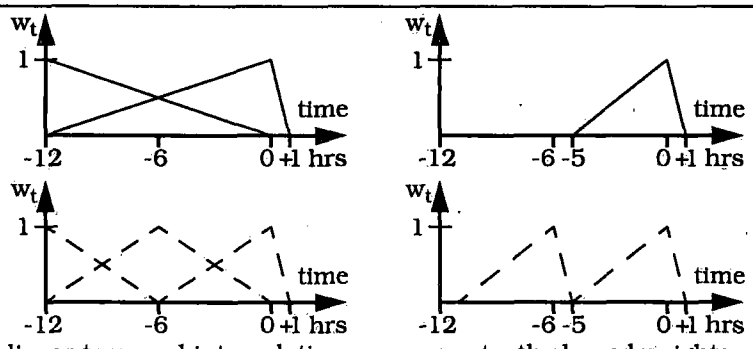 linear temporal interpolation or sawtooth shaped weights solid (dashed) lines: data available every 12 (6) hours (rawinsondes); time 0 denotes the beginning of the forecast period screen-level data: 1 or 3 hourly linear interpolation
surfaces along which increments are laterally spread	(hybrid) σ-model levels optionally: isentropic or isobaric surfaces
horizontal weight functions (they model horizontal forecast error correlations)	$w_{xy} = c + (1-c) \cdot (1 + r/s)\, e^{-r/s}$ s : 'correlation scale' surface pressure : s = 200km , c = 0.08 or s = 130km , c = 0 3-D rawinsonde data: s = 130km , c = 0 (or s = 100km, c = 0) screen-level data : s = 70km , c = 0
influence radius	infinite for surface pressure data 3.5 correlation scales for 3-D rawinsonde and screen-level data
nudging coefficient G_ψ	$6 \cdot 10^{-4}$ s^{-1}

TABLE 2-1. Standard parameter values used for the assimilation of rawinsonde and screen-level data.

tion and averaging, the value 1 from the saturated observations is replaced by a generalized relative humidity value derived from the model's total specific water content at the observation point provided that the model value is also saturated. This is designed to diminish additional spurious drying brought about by the vertical interpolation.

If a vertical sounding is incomplete at the top or at the bottom, is it vertically extended with the outermost available observation increment and weighted with a vertical structure function in the log(pressure) difference between the model layer containing the increment and the target model layer (Barwell and Lorenc, 1985; Lorenc et al., 1991):

$$w_p = e^{-3(\Delta \ln p)^2} \qquad (2\text{-}10)$$

Finally, the observation increments are spread laterally along the model's σ-layers with

the weighting given by the horizontal structure function as defined in equation (2-7). Since specific water content varies as a function of altitude mainly due to temperature and pressure, observation increments of relative humidity as opposed to mixing ratio are spread (cf. Ruggiero et al., 1994). Alternative ways of lateral spreading are discussed in sections 2.3.4 and 3.4. The standard choice of the parameters in (2-7) is given in Table 2-1. The resulting correlations are more narrow than the correlations used by the UKMO for their regional model (Lorenc et al., 1991), but are somewhat broader than the mean of the DM's longitudinal and transverse wind velocity correlations (cf. Buchhold and Paul, 1995), which equals the mean of the wind component auto-correlations (Daley, 1991). The influence of the correlation scale will be addressed in section 4.2.3.

I. Use and processing of screen-level data

Nudging of screen-level temperature (T_{2m}) data is not included in the present scheme. Stauffer et al. (1991) found that nudging near-surface temperature could be disruptive since a small change in the thermal structure easily lead to a major change in the diagnosed stability class and the PBL (planetary boundary layer) depth. Seaman et al. (1995) improved surface layer temperatures by nudging high-resolution temperature soundings in the upper and middle mixed layer, but they did not attempt to assimilate screen-level temperature data. They stressed that the problems related to these data are likely to depend on the PBL parameterization. However, problems have also been encountered with other models, e.g. by Cardinali et al. (1994) who argued that assimilation of screen-level temperature would require a consistent adaptation of the soil fields. McNider et al. (1994) suggested adjusting the surface specific humidity to balance the surface energy budget.

No such difficulty has apparently been found for nudging screen-level humidity data although their representiveness is also questionable. As these data have shown a positive impact namely on low stratus and fog prediction (Lorenc et al., 1994; Clark, 1994) they are incorporated into the assimilation process. As the relative humidity at screen-level and at the lowest model level are identical in the SM, the observation increment equals simply the relative humidity difference between the screen-level observation and the model value at the lowest model level. Differences between station height and model orography are only accounted for by neglecting observations from stations with $|z_s^{obs} - z_s^{mod}| > 160$ m, and by defining the quality factor ε as Gaussian in height difference with an e-folding decay of 160 m.

Surface wind data are nudged in the same way except for two modifications. Firstly, since the representiveness of these data is notoriously poor in rough terrain they are usually considered only from stations which lie below 700 m and satisfy $|z_s^{obs} - z_s^{mod}| < 100$ m. Secondly, for the vertical interpolation of the observed winds from the screen-level to the lowest model level, the model equation for diagnosing the screen-level model winds is reversed by making the following approximation. The turbulent transfer coefficients as defined in Müller (1981) are to a first order linear in the wind speed at the lowest model level. By approximating the unknown observed wind speed at the lowest model level with the model wind speed in the higher order terms, the diagnostic model equation can be reversed, and the interpolation becomes straightforward.

For the horizontal spreading of observation increments from screen-level data, the autoregressive function (2-7) is used. The correlation scale (see Table 2-1) is almost iden-

tical to that used in the UKMO mesoscale model for screen-level relative humidity (Maycock and Macpherson, 1994). The vertical aspect of the spreading is addressed in section 3.5.

J. Lateral boundary conditions, temporal weights, and nudging coefficients

No observations within the boundary zone are used for nudging. This prevents the boundary fields from directly affecting observation increments and hence (by lateral spreading of these increments) from directly influencing the inner domain. Hourly boundary values for the first 9 hours of a 12-hour nudging period are provided by the EM forecast starting at the beginning of the nudging period. Within the last 3 hours of the nudging period, the transition is made to the boundary fields provided by the new EM forecast starting at the same time as the forecast period of the SM nudging experiment. This transition period is long enough to keep the noise at a low level.

Two concepts for the temporal weighting are applied in this work (Table 2-1), i.e. linear interpolation or use of a saw tooth shaped weight function as deployed by the UKMO (but without varying the horizontal correlation scale here). They are compared in chapter 4. The nudging coefficients (Table 2-1) are similar to those used in most studies, and operationally by the UKMO. Their specification is discussed in section 4.2.5.

2.3 Nudging single simulated data

A fundamental issue is how well various kinds of data are assimilated into the SM by use of the present nudging scheme. There are some theoretical considerations to estimate the effect.

Data insertion and even multivariate data analysis procedures do not generally produce balanced initial model states (see Daley, 1991). If an unbalanced perturbation, i.e. a perturbation with a mass and wind field imbalance, is introduced into a primitive equation model, there is a period of adjustment until balance is restored. Linear geostrophic adjustment theory describes this adjustment process and the final balanced flow field.

Mesoscale flow, however, has more energy in the inertia-gravity modes, particularly near steep orography where it is often strongly ageostrophic. The dynamics of mesoscale flow phenomena, e.g. of mesoscale convective systems, can differ strongly from approximately geostrophic synoptic-scale flow. Furthermore, nudging perturbs the model continuously in time. Hence, the question arises to what extent the geostrophic adjustment theory can still provide a guideline for the estimation of the residual flow in a mesoscale model following a period of nudging.

In section 2.3.1, a description is provided of the theory, a discussion of its applicability to nudging in general, and a formulation of specific questions. These are addressed in the subsequent sections by means of idealized experiments which focus particularly on the influence of orography.

2.3.1 Geostrophic adjustment theory

Linear geostrophic adjustment theory was first formulated by Rossby (1938) and described in detail by Blumen (1972) and Økland (1970). The latter in particular put it in the context of primitive equation NWP models. The theory assumes that the inertia-

gravity modes are dispersed or dissipated leaving only the non-divergent modes as solutions. The final solution of the streamfunction ψ_f can then be written as the sum of the non-divergent part of the initial wind field ψ_0, and the geostrophic wind ψ_g derived from the initial mass field, i.e.

$$\psi_f = a\psi_0 + (1-a)\psi_g \tag{2-11}$$

The final geopotential is determined from ψ_f with the geostrophic relation. A simple idealized model with the wind and mass fields being expanded in orthogonal modes (e.g. as a Fourier series assuming cyclic lateral boundary conditions) allows the determination of a by

$$a = 1 - f^2/\sigma_{n,k}^2 \tag{2-12}$$

where $\sigma_{n,k}$ is the angular frequency of the mode with horizontal wave number k and vertical scale number n (Økland, 1970). It follows that for the high-frequency part of the fields, i.e. for which $\sigma_{n,k} \gg f$, the initial geopotential plays a little role in determining the final state, and the final wind field corresponds closely to the initial non-divergent component of the wind field. For the lower-frequency part with $\sigma_{n,k} \cong f$, the opposite is true and the wind field adjusts to the initial mass field.

By use of the hydrostatic dispersion relationship

$$\sigma_{n,k}^2 = \left(k^2/n^2\right)N^2 + f^2 \tag{2-13}$$

the coefficient a can be expressed as

$$a = \frac{1}{1 + (L/L_R)^2} \tag{2-14}$$

where L_R is the baroclinic Rossby radius of deformation defined as

$$L_R = \frac{N}{f} \cdot L_z \tag{2-15}$$

which can be regarded as a measure of the effective vertical scale. Here, $L = 1/k$ is the horizontal and $L_z = 1/n$ the vertical length scale, and N denotes the Brunt-Vaisala frequency which is a measure of static stability (ca. $1.2 \cdot 10^{-2}$ s^{-1} in the troposphere). For an equivalent depth, $h_e = N^2 L_z^2/g$, (2-15) takes the form $L_R = \sqrt{gh_e}/f$ in analogy to the shallow water equations. From (2-11), (2-14) and (2-15), it follows that the smaller the horizontal scale, the larger the vertical scale, the lower the latitude, and the stronger the static stability, the more the mass field tends to adjust to the non-divergent component of the wind field. And vice versa.

To estimate the rate of adjustment caused for instance by imperfect data assimilation procedures it is necessary to know the spectrum of the excited inertia-gravity waves. However, some idea of the residual information content, i.e. the balanced model fields after the adjustment, can be obtained in the linear case if the excited spectrum can be characterized by a typical horizontal wavelength and a Rossby radius of deformation since the final state is independent of the dispersion and dissipation process. For an initial wind perturbation, the first step is to analyze the perturbation into its rotational and divergent component. The latter projects almost entirely onto gravity modes. The second step is to infer horizontal and vertical scales and an amplitude of the rotational part. Then the residual flow is determined using (2-11), (2-14) and (2-15). Inferences

are that a wind perturbation has more effect if it is locally non-divergent and in approximate geostrophic balance, and that insertion of single-level wind data is more effective if spread in the vertical.

These predictions of the linear geostrophic adjustment theory were basically confirmed in numerical studies by Barwell and Lorenc (1985) and Barwell and Bromley (1988) who introduced idealized initial wind perturbations in nonlinear models. Note that the theory is linear and expressed in terms of non-interacting, independent modes only.

However, neither the geostrophic adjustment theory nor experiments with initial perturbations model the nudging technique as it perturbs the model continuously. Nudging is designed to prevent the generation of high-frequency modes (i.e. modes with periods less than double the insertion period) by relaxing gradually towards observed values over a certain period (of the order of about 6 hours). In an approximately steady atmosphere with little advection, the main effect of this is that the excited spectrum is not only restricted spatially by the spatial weight functions, but also temporally by the nudging period. Equation (2-13) relates these restrictions. Since nudging prevents a separation into independent modes, Barwell and Lorenc (1985) used a simple linearized model to compare the effect of nudging wind with that of an initial wind perturbation in the synoptic scale, and to study the partition of inertia-gravity and geostrophic modes. They found that for deep wind structures extending to half the tropospheric depth or more, nudging rendered the correct geostrophic flow, and the scheme did not need to contain explicit balancing of height and wind fields. In contrast, for small equivalent depth, inertia-gravity waves still tend to be excited because the period of the shallow modes is larger than the 6-hour nudging period. Carr et al. (1993) and Stauffer and Seaman (1990) found the geostrophic adjustment theory to be also consistent with the dynamical model response if real data of realistic density were nudged. In the presence of strong mean advection however, nudging generated spurious wind speed maxima downstream of the observations (Barwell and Lorenc, 1985). Note that in all these studies, the horizontal model resolution was 1° or less, and orographic effects were not considered.

This leaves open the issue about the effect of the nudging in the Swiss Model, and the applicability of the geostrophic adjustment theory in the mesoscale. More specifically, it prompts the following questions. To what extent does the SM retain the influence of nudging? Is there a need to control the noise? Does the geostrophic adjustment theory provide a guideline for the estimation of the residual flow for a mesoscale model? Is there a possibility of enhancing the assimilation in conditions, where the information content of an observation is not normally used well by simple nudging? Are there specific problems or features in the presence of steep orography, for instance in relation to terrain-following model coordinates?

2.3.2 Experimental design

To address these questions in the two subsequent sections, idealized nudging experiments will be presented using an adiabatic 30-layer version of the Swiss Model (but with horizontal diffusion and vertical turbulent fluxes included). In each experiment, a single datum or vertical profile of data of either wind, surface pressure, or temperature will be assumed. Humidity is not examined here as it is dynamically passive in the absence of phase transitions. The difference between the value of the assumed datum and the model value of the control integration (without nudging) at the beginning of an ap-

pointed forecast period will be called 'target increment'. In the nudging experiments, the assumed datum is then nudged with the use of horizontal weight functions (cf. Table 2-1) which provide the characteristic spatial scales of the spectrum that is excited by the perturbation.

Note that since neither the truth nor the 'observation error' of the assumed data is known with this experimental set-up, the 'correct' model response to the perturbations is not defined. The assumed data are to some extent arbitrary, and their assimilation tends to imply larger changes to the model fields than the assimilation of real, high-quality observations which represent a state of the atmosphere that should not hopefully differ enormously from the unperturbed first guess model fields. This may make it somewhat more difficult for the model to assimilate assumed data. However apart from this restriction, poor (good) retainment of the real data can be expected in the forecast period if the retainment of the effect of the assumed data is poor (good) in the present experiments.

In this study, the case of 5 February 1993 has been selected because of its weak synoptic forcing and absence of precipitation. Winds in the Alpine area were weak at low levels and moderate from the southeast in the middle and upper troposphere. All observations are assumed valid for Payerne (in the western Swiss Plateau). The temporal nudging weight function rises linearly from zero to one in the first hour of a prespecified nudging period and is held constant thereafter until the 'analysis time' (t=0) at the end of the nudging period. During the successive hour, the weight decreases to zero. The model's horizontal domain is 97*81 grid points.

2.3.3 Nudging surface pressure

Consider a single surface pressure observation of 976.3 hPa (with a target increment of +4 hPa), and a nudging period of 24 hours. Parameters for the horizontal structure function (2-7) are chosen to be c=0, s=130 km, and this implies a characteristic horizontal length scale of about L=220 km (where $\omega_r[r=L] = 0.5$) for the perturbation. Equa-

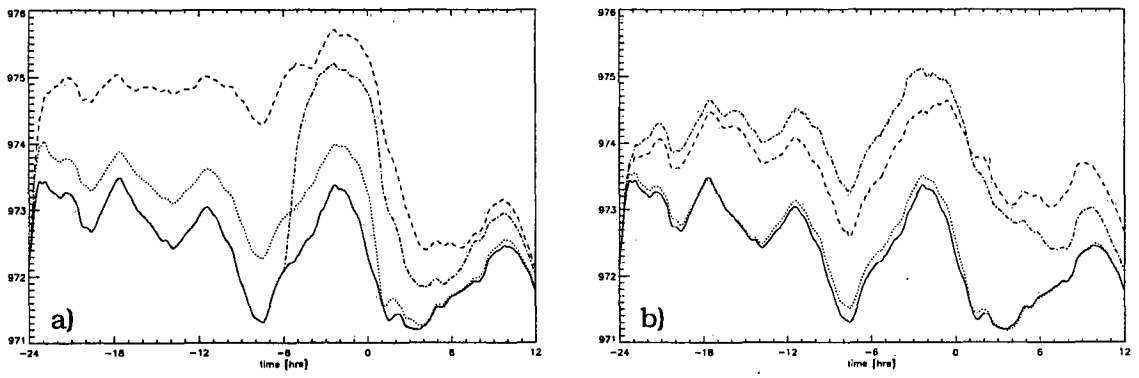

FIGURE 2-3. Time series of surface pressure at Payerne for the 24-hour nudging period, beginning at 0000 UTC, 5 February 1993, and the subsequent 12-hour forecast period. A single surface pressure observation of 976.3 hPa is assumed at Payerne. a): $G_\psi = 6 \cdot 10^{-4}\ s^{-1}$; solid: unperturbed; dotted: nudging surface pressure only; dashed: nudging surface pressure including the temperature correction; dash-dotted: same, but for a 6-hour nudging period. b): $G_\psi = 1 \cdot 10^{-4}\ s^{-1}$; solid: unperturbed; dotted: nudging surface pressure only; dashed: nudging surface pressure including the geostrophic wind correction; dash-dotted: nudging surface pressure including the temperature correction and the geostrophic wind correction.

tions (2-11) to (2-15) then suggest for a vertical wavenumber n=1 (as primarily excited by insertion of surface pressure), and an atmospheric scale height of about 8000 m, that the wind field will not adjust geostrophically (a=0.95 in (2-11)). As expected from linear theory, the assimilation of the surface pressure datum is poor in the experiment (Figure 2-3).

In the perturbation fields (i.e. the difference between perturbed (by nudging) and unperturbed (control) model fields), a divergent component corresponding to the external gravity mode quickly develops, persists, and prevents a more complete assimilation of the positive surface pressure target increment, although a geostrophic component also develops gradually due to the Coriolis effect (Figure 2-4a). When the nudging is turned off, the perturbation disappears almost immediately. This moment is the only time that significant high-frequency noise is produced in any of the experiments (otherwise it is suppressed by the nudging), but this noise vanishes quickly. Note that during the nudging period, the strongest horizontal gradient of the pressure perturbation is located at the lateral boundary zone so that the perturbation has a considerable constant component in the inner domain (Figure 2-4a). The rapid reduction of this component in the forecast period indicates that without external forcing it is largely determined by the lateral boundary condition which thus appears to have an integral influence on the pressure field (cf. Vukicevic and Paegle, 1989; Vukicevic and Errico, 1990).

The inclusion of the temperature correction as described in section 2.2 does not change the model response fundamentally. Since the geopotential is not changed directly above the lower stratosphere, it is the first internal gravity mode (n=2, for its typical vertical structure, see e.g. Temperton and Williamson, 1981) that is likely to be primarily excited. Equations (2-11) to (2-15) then suggest a geostrophic wind field adjustment of 17 %, i.e. about 17 % of the pressure target increment is expected to be preserved after the nudging period (i.e. about 0.7 hPa), and this agrees reasonably with the experiments for the first 10 hours of the forecast period (Figure 2-3a).

Although nudging is designed to promote balance, surface pressure is not assimilated significantly if the scheme does not contain explicit balancing of height and wind fields. To enhance the assimilation of pressure data, geostrophic wind increments can be added. They are computed locally from the mass field increments inserted at the each timestep with the following equation in σ-coordinates:

$$f(\boldsymbol{k} \wedge \Delta v) = -R(\nabla \ln p)\,\Delta T_v - RT_v\,\Delta(\nabla \ln p) - \Delta(\nabla \phi) \qquad (2\text{-}16)$$

Geostrophic wind increments have been used for many years to support mass perturbations (e.g. Hayden, 1973; Kistler and McPherson, 1975). They are found to have a significant impact with nudging (Barwell and Lorenc, 1985), and are applied in the UKMO analysis correction scheme operationally (Lorenc et al., 1991) also in the mesoscale. For the assimilation of a single pressure observation, the nudging coefficient has been reduced here ($G_\psi = 10^{-4}s^{-1}$), and the wind correction is applied without limitations to test its potential and reveal possible drawbacks. Whereas the pressure perturbation is 0.2 hPa or less throughout the nudging period without explicit balancing (not shown), it exceeds 2 hPa and is generally preserved after the end of the nudging period when the geostrophic wind correction is included in the scheme (Figure 2-3b, Figure 2-4b). However, the strong mesoscale anticyclonic vortex in the perturbation wind field is unrealistic and essentially unbalanced. This indicates the inadequacy of the geostrophic assumption, and is partly due to the presence of the Alps, where barrier effects modify the pressure perturbation strongly. Furthermore, there appears to be a compli-

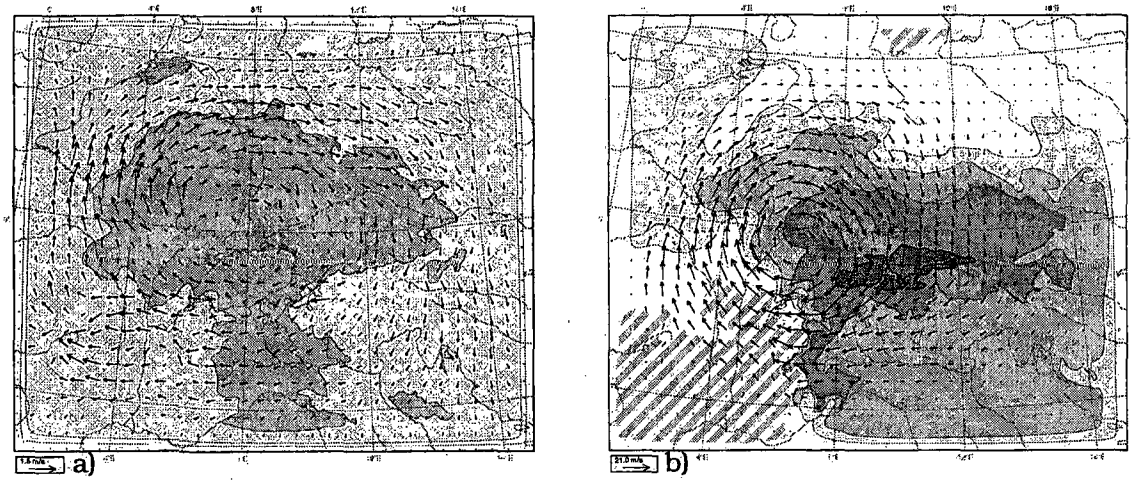

FIGURE 2-4. Differences between the perturbed (nudged) and the unperturbed surface pressure (contours and shading) and 700 hPa wind vector field after 12 hours of nudging (valid for 1200 UTC, 5 February 1993) towards a single surface pressure observation.
a): without any further corrections, and with a nudging coefficient of $6 \cdot 10^{-4}$ s^{-1};
b): with the geostrophic wind correction, and a nudging coefficient of $1 \cdot 10^{-4}$ s^{-1}.
Pressure difference contour values encircling increasingly dark shading are: +0.25, 0.5, 1, 2 hPa; differences < -0.25 hPa are hatched; in a), the +0.1 hPa contour is also plotted (without shading). Note that the wind vector arrows are displayed shortened by a factor of 14 in b) relative to a).

cated interaction with the lateral boundaries leading to negative pressure perturbations. The inclusion of the temperature correction in addition to the geostrophic wind correction has a negative effect on the efficiency of the wind correction in the forecast period (Figure 2-3b).

In this simple case, the potential of the geostrophic wind correction to help the assimilation of pressure data is evident. For this reason, it will be addressed further in a more realistic setting in chapter 4.

2.3.4 Nudging temperature or wind

Here, in relation to the assimilation of rawinsonde data, single prespecified (i.e. assumed) vertical profiles or single-level data of temperature or wind are nudged. To provide some indication of the flow response to be expected for a range of rawinsonde profiles, a set of three profiles is selected for each variable. Each set consists of a very shallow structure, a deep, relatively uniform structure, and a structure with a strong vertical gradient (cf. Table 2-2).

vertical structure of pseudo-data ↓ \ nudging variable →	temperature	wind
very shallow structure (single-level data)	NTS	NVS
deep, relatively uniform structure	NTD	NUD, NVD
structure with strong vertical gradient	NTI	NUVI

TABLE 2-2. Names of experiments on nudging of temperature or wind. See text for a detailed description of the experimental set-up.

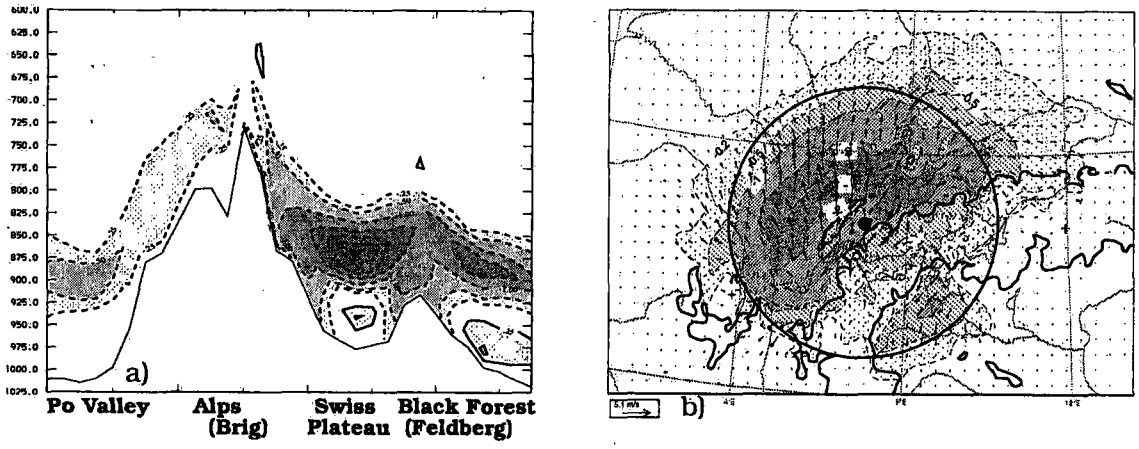

FIGURE 2-5. Experiment NTS with a temperature target increment of -2 K in model layer 25 (about 110 hPa above the ground). Perturbation fields at the end of the 6-hour nudging period. a): Cross section of the temperature perturbation. Contour interval is 0.5 K (without the 0 K contour, but with ±0.25 K contours), contours are solid for positive values and dashed for negative values. The grey scale increases with increasing absolute value of the perturbation.
b): Temperature perturbation at model layer 25 (contour values are -0.2 K, -0.5 K, -1 K, -2 K, -4 K) and wind field perturbation (arrows) at layer 26 (about 85 hPa above the ground). The black dot indicates the location of the observation at Payerne, the circle contours the specified a-priori area of influence for the temperature observation at Payerne, and the thick solid lines denote the 1000 m contours of the model orography.

The basic setting and configuration is the same as before, except that (i) the nudging period is chosen to be only 6 hours because the model fields should ideally be stationary during the nudging period, and (ii) the Cressman weight function ($w_r = (1 - r^2/s^2)/(1 + r^2/s^2)$ for $r < s$, $w_r = 0$ for $r \geq s$) is deployed for the lateral spreading with an influence radius of s=260 km (For small r, this is a second order equivalent to the weighting usually used for rawinsonde data, cf. Table 2-1). A zero weight for $r \geq s$ allows an easy evaluation of the differences between the explicit (a-priori) area of influence and effective (a-posteriori) area of influence of the nudging and enables the identification of outward propagating inertia-gravity noise. To examine the response to shallow structures resolved by rawinsonde data, a very narrow vertical correlation is used for single-level data (by replacing the parameter value 3 in equation (2-10) by a value of 1000 which yields a weight w_p of 0.45 in the adjacent model layers and less than 0.05 in more distant layers).

A. Temperature

In a first experiment NTS, a single temperature datum with a target increment of -2K is assumed to be representative at Payerne for model layer 25 (about 110 hPa above the ground). For a vertical length scale of the order of 500 m (cf. Figure 2-5a) and a horizontal length scale L=150 km (where $w_r[r=L] = 0.5$), the linear geostrophic adjustment theory predicts a geostrophic adjustment of the wind field (a=0.25 in (2-11)). (Note that for a vertical potential temperature gradient of about 7K / 1000 m, a vertical scale of 500 m yields an equivalent depth of about 7m, and this compares reasonably with the value used by Barwell and Lorenc (1985) to simulate single-level data assimilation.) Therefore, the temperature datum is expected to be assimilated well, and this is confirmed in the experiment (Figure 2-5). In the forecast period, the perturbation fades only gradually (not shown). This somewhat contradicts Ramamurthy and Xu (1993)

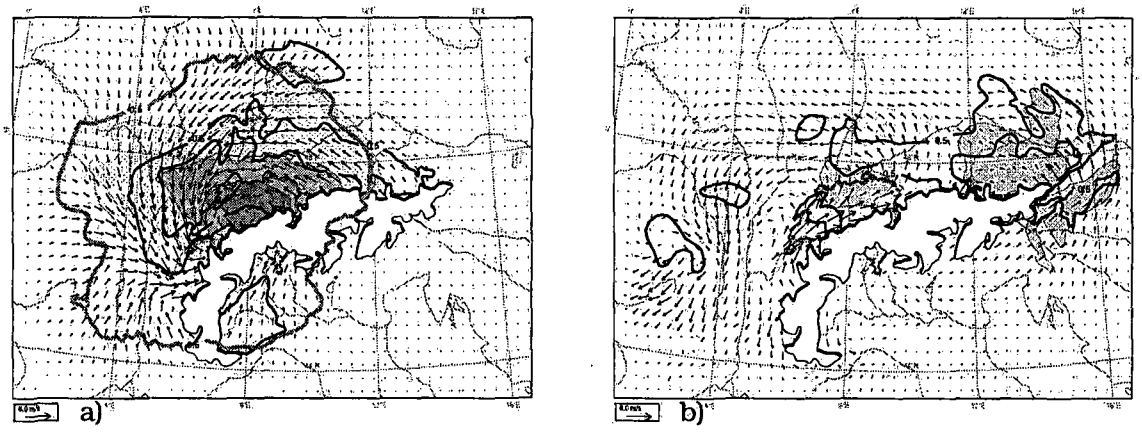

FIGURE 2-6. 850 hPa perturbation fields of experiment NTD, a): at the end of the 6-hour nudging period, b): of the 6-hour forecast. Arrows: wind field perturbation; black lines: temperature perturbation (contour values ±0.5 K, ±1 K, ±2 K); shading: geopotential perturbation (white: > -2.5 m; shaded areas between -2.5 m and -10 m with increasingly dark shading in 2.5 m intervals). In a), the 0.5 K contour of the 700 hPa temperature perturbation (thick grey line) is also shown. Areas with model orography above 1500 m are white.

who found that nudging real single-level data of temperature was ineffective without increased vertical coupling.

In NTS, cooling exclusively three model layers implies a small decrease of the geopotential and convergence further above. This in turn causes a geopotential rise, divergence and, as a result of the adjustment process, a weak anticyclonic flow component further below (between layers 26 and 30, e.g. in southern Germany, Piemont, Bourgogne, cf. Figure 2-5b). Two orographic effects modify the wind and temperature fields. Firstly, the increased density within the cooled layers (24 to 26) results in a tendency of the flow to be directed from higher towards lower orography (thermo-gravitational effect), and in a negative correlation of the cooling with orographic height. This effect is reversed for positive temperature target increments. Secondly, the temperature signal is negatively correlated to the ruggedness of the terrain, i.e. the cooling is attenuated over the Alps (cf. Figure 2-5). Since no indication has been found that this is due to inertia-gravity waves radiating energy away over rugged terrain, the cause is likely to be horizontal advection across the sloping σ-layers which distributes the perturbation to large areas. Note that due to advection and orography, the effective area of influence of the temperature datum is flow-dependent and to some extent adapted to the flow, and it can clearly exceed the prespecified radius of influence (cf. Figure 2-5b).

In experiment NTD, a deep temperature perturbation is assumed with positive target increments of up to 2K between layers 27 and 16, negative increments from layers 14 to 5, and parabolic profiles within both intervals. This renders small the direct geopotential change in the upper stratosphere, and external gravity waves are not greatly excited. For a horizontal scale of 150 km and a vertical wavelength of about 12 km (i.e. an equivalent depth of about 70 m, which corresponds roughly to the vertical mode n=5 (cf. Temperton and Williamsson, 1981)), the wind field is not expected to adjust geostrophically to a large extent (a=0.75 in (2-11)). However, the theory assumes a single insertion, but during the nudging period, adjustment processes extend the horizontal scale to about 300 km above about 700 hPa (Figure 2-6a). This causes a greater geostrophic adjustment of the wind field (the degree of balance of the perturbation is about

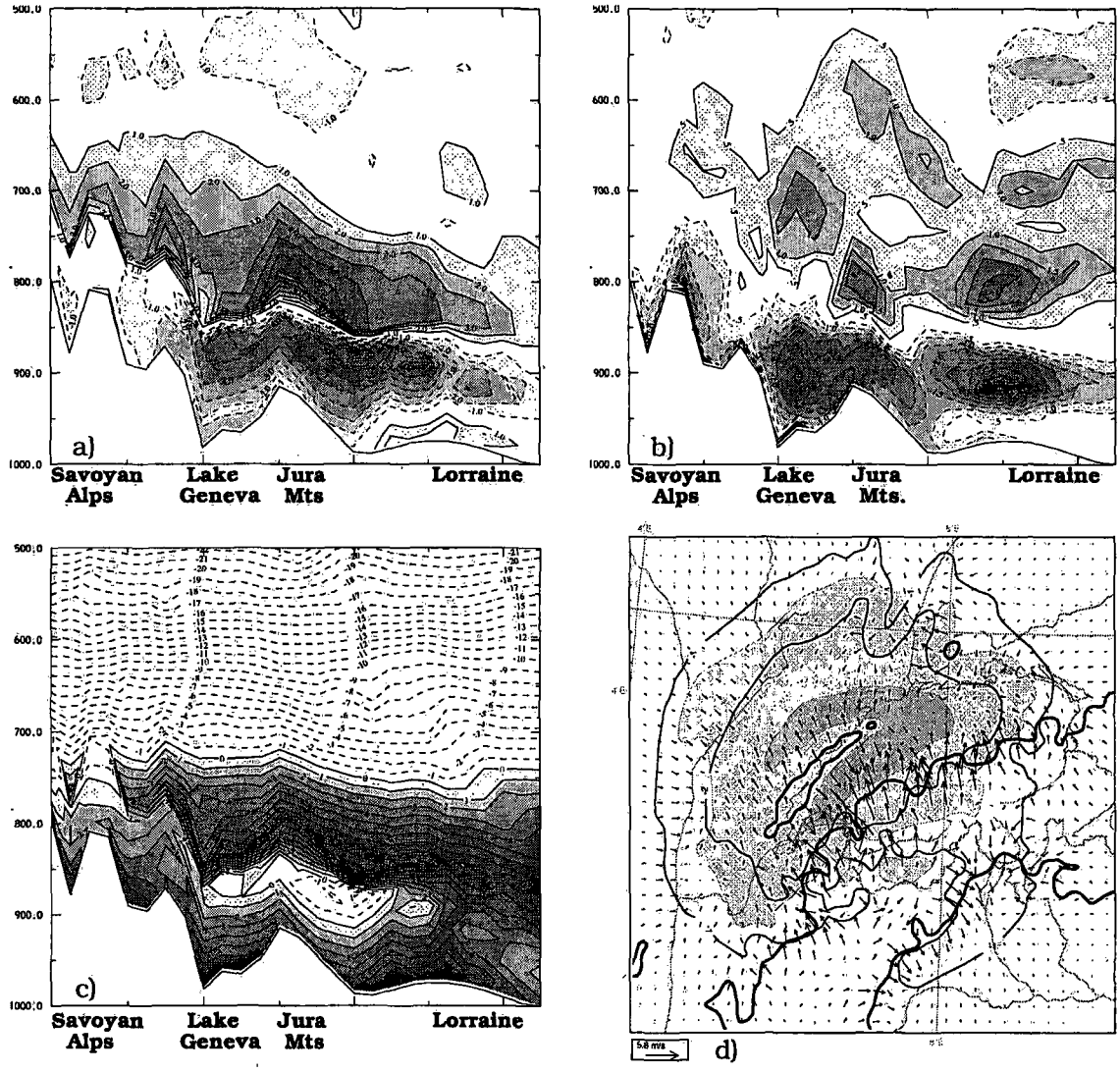

FIGURE 2-7. Experiment NTI for nudging of a temperature inversion with effective target increments of up to ±6 K. Here, the horizontal model diffusion is reduced by a factor of 10, and this inhibits some unphysical smoothing effects as discussed in section 3.2.
a): Cross section of the temperature perturbation at the end of the nudging period (i.e. at +0 h) as in Figure 2-5, but with a 1 K contour interval.
b): Cross section of the 6-hour forecast temperature perturbation with a 0.5 K contour interval.
c): Temperature cross section at +0 h; contour interval is 1 K, shading for positive values.
d) Perturbation fields after 1 hour of nudging; arrows: wind field perturbation at layer 26; solid lines: temperature perturbation (contour interval 1 K) at layer 26; shading: 850 hPa geopotential perturbation (white: > -5 m; light shaded: between -5 m and -10 m; dark shaded: < -10 m; geopotential is to be evaluated at constant pressure levels since the pressure of a model level depends on the perturbation); thick solid lines: 1000 m model orography contour.

50 % at the end of the nudging period, and slowly increasing thereafter), and inhibits a sharp attenuation of the perturbation in the forecast period.

The heating centered around 750 hPa leads to an increase of the potential vorticity below, and a Foehn-like effect induced by the cyclonic circulation moves the centre of the temperature and geopotential perturbation at 850 hPa to southeastern Bavaria in the 6-hour forecast (Figure 2-6b). Because the vertical gradient in the specified tempera-

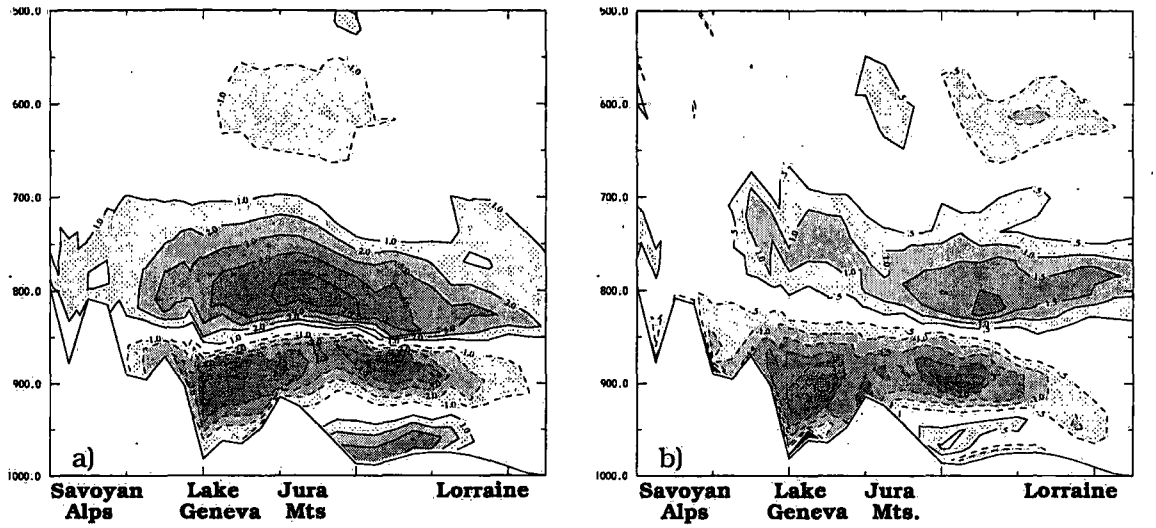

FIGURE 2-8. Temperature cross section as in Figure 2-7a, b, but with lateral spreading of observation increments along isobaric surfaces instead of σ-surfaces.

ture perturbation is weak, other orographic influences, e.g. related to the sloping of the σ-layers, remain small.

Finally, nudging of a temperature inversion is tested in experiment NTI. The effective temperature target increments decrease from 0 K at layer 30 to -6 K at layer 25 and from +6 K at layer 24 to 0 K at layer 19. As in NTS, the perturbation is shallow (the equivalent depth small), and the degree of assimilation, the orographical effects, and the adjustment of the wind field are generally similar. The inversion is assimilated almost completely except over the Alps, and the orographic thermo-gravitational effect is indicated by a strong tendency of the flow perturbation to be directed from higher towards lower orography in the cooled layers (Figure 2-7d). In the forecast period, the attenuation of the inversion in the perturbation fields (Figure 2-7b) is pronounced. The vertical turbulent fluxes are found to have little influence on the inversion, and the inversion perturbation is best preserved in some distance to steep orography. Thus, factors contributing to the attenuation may be spurious smoothing due to the sloping model σ-layers or adjustments due to imbalances.

The cross sections (Figure 2-7a-c) further reveal that the height of the inversion is highly correlated to the unphysical σ-surfaces, especially in the analyses. This heavily contrasts with the horizontally homogeneous structure and height typically observed with low-level inversions, e.g. if associated with low stratus (cf. section 3.1.2). It suggests that lateral spreading of observation increments along σ-surfaces can lead to unrealistic structures in the model fields, and that spreading along quasi-horizontal surfaces may therefore be beneficial. This alternative approach, the technique and the application to real-data cases will be discussed in section 3.4. The potential of this approach is shown here in Figure 2-8 for lateral spreading along isobaric surfaces which renders slightly weaker the inversion, but causes it to be largely horizontally homogeneous and uncorrelated to the σ-surfaces.

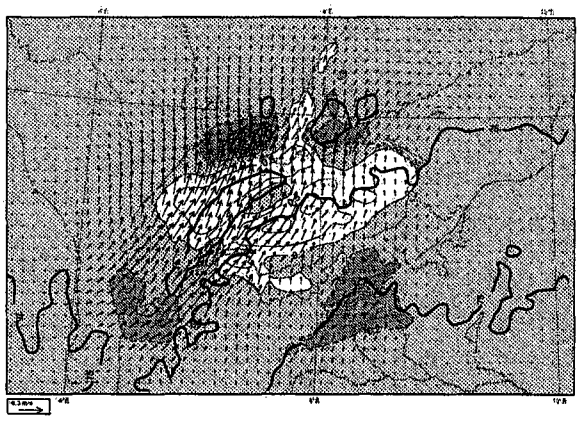

FIGURE 2-9. Perturbation fields of experiment NVS on model layer 25 at the end of the 6-hour nudging period. Arrows: wind field perturbation; thin lines and shading: temperature perturbation (contour values are ±0.2 K, ±0.5 K, ±1 K, values > 0.2 K are white, values < -0.2 K are dark shaded). The thick solid lines denote the 750 m model orography contour.

B. Wind

In experiment NVS, a single-level wind observation for layer 25 with an (approximately) meridional target increment of 4 m/s is assumed. The analogous theoretical estimation as for NTS predicts little geostrophic adjustment of the mass field, and this is confirmed in the experiment. The response of the mass field is mostly ageostrophic and orographically induced as indicated in the temperature perturbation by the blocking and Foehn effects in Figure 2-9. As a result, geostrophic adjustment of the wind field attenuates the perturbation quite quickly in the forecast period.

In experiments NVD and NUD, a deep, parabolic wind perturbation between levels 29 and 2 with an (approximately) meridional respectively zonal target increment of up to 5 m/s is nudged. The geostrophic adjustment theory predicts an almost complete gestrophic adjustment of the mass field to the non-divergent part of the wind perturbation, and the target increment is indeed largely assimilated in NVD and NUD (not shown). However, the degree of geostrophy is only about 50 % in the low troposphere. In the 850 hPa 6-hour forecast perturbation fields (Figure 2-10), the eastern (anticyclonic) vortex in NVD is pushed north(west)wards, and the southern (anticyclonic) vortex in NUD (north-)westwards by the influence of the Alps. Although the specified wind perturbation differs only by 90 degrees between NVD and NUD, the perturbation fields

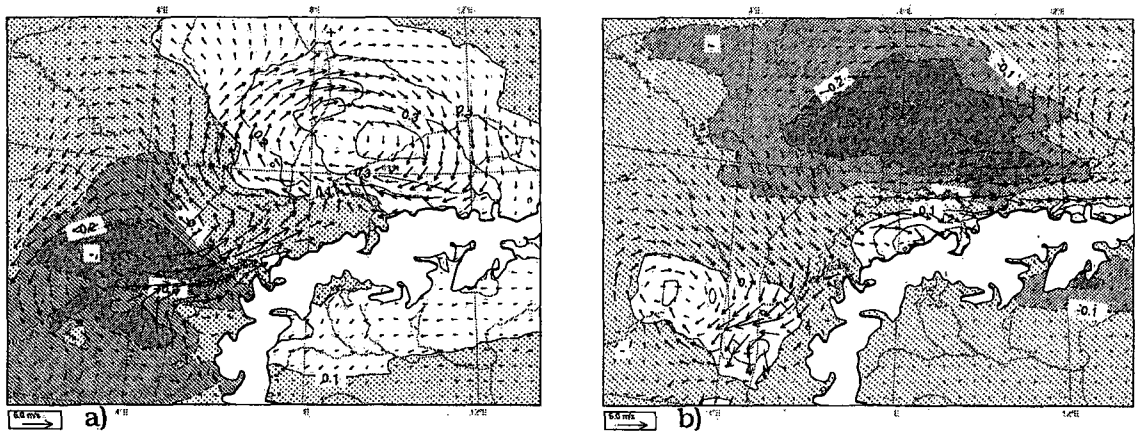

FIGURE 2-10. 6-hour forecast perturbation fields at 850 hPa. a): Experiment NVD; b): Experiment NUD. Arrows: wind field perturbation; thin lines and stippling: geopotential perturbation (contour interval: 1 m (without 0 m/s contour), values > 1 m are not stippled, values < -1 m are dark stippled). Areas with model orography above 1500 m are white.

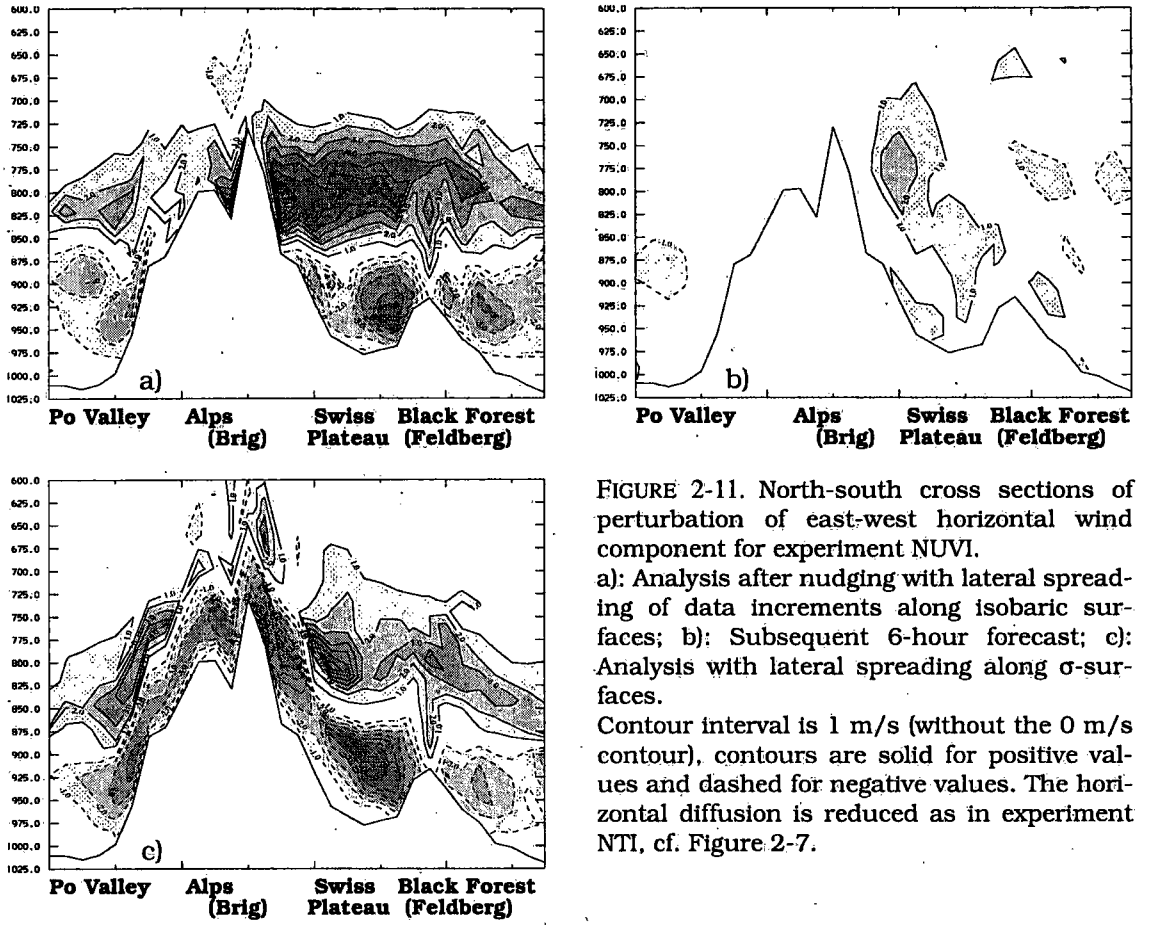

FIGURE 2-11. North-south cross sections of perturbation of east-west horizontal wind component for experiment NUVI.
a): Analysis after nudging with lateral spreading of data increments along isobaric surfaces; b): Subsequent 6-hour forecast; c): Analysis with lateral spreading along σ-surfaces.
Contour interval is 1 m/s (without the 0 m/s contour), contours are solid for positive values and dashed for negative values. The horizontal diffusion is reduced as in experiment NTI, cf. Figure 2-7.

are almost reversed. Thus, the residual flow namely in the low troposphere is significantly modified by steep orography, and the perturbation is rendered substantially ageostrophic with little decrease of its amplitude.

In experiment NUVI, the same shape of the vertical profile of target increments as in NTI is applied to produce a strong vertical wind shear. From the surface to layer 25, the effective target increments of wind data consist of a northeasterly component, that grows with height to 8 m/s, and from layers 24 to 19, they consist of an analogous, decreasing southwesterly component. This models a flow situation in the Swiss Plateau called Bise (cf. section 3.1.2) which is often associated with low stratus and is fairly uniform in the horizontal. This demand is satisfied far better in the analyzed wind perturbation if the lateral spreading of observation increments is performed along isobaric surfaces (Figure 2-11a) instead of sloping σ-surfaces (Figure 2-11c), but it is stressed that the truth, and hence the adequacy of the demand, is not known. With both ways of lateral spreading, and in agreement with geostrophic adjustment theory, the wind perturbation in NUVI is almost entirely unbalanced in the analysis, and disappears rapidly thereafter (Figure 2-11b). The dissipation of vertical shear is not due to increased turbulent instability and vertical model diffusion, and indicates that the concept for lateral spreading may be less important for wind data than for temperature data.

2.3.5 Summary and further remarks

The Swiss Model is robust and readily handles the perturbations induced by nudging. In general, despite large imbalances in several experiments, no significant deleterious increase of inertia-gravity wave activity results from the nudging. Except are the following cases. First, external gravity wave activity occurs within one hour of surface pressure nudging. Second, the mean absolute vertical velocity is increased whenever winds are enhanced over steep orography, but this is mostly due to physical stationary mountain waves rather than noise. Third, the mean absolute surface pressure tendency is significantly increased when the geostrophic wind correction is applied. Unless this correction is used the potential for noise control procedures appears to be limited. This is in line with Stauffer and Seaman (1990), but contrasts with Ramamurthy and Xu (1993) who found a large increase of the mean absolute surface pressure tendency without divergence damping in their eta model. Divergence damping is also used operationally at the UKMO (Lorenc et al., 1991). Note, however, that most studies on nudging do not mention the use of noise control procedures. Based on the present results, no such procedures have been included in the present nudging scheme for the SM.

The geostrophic adjustment theory is found to provide a guideline for estimating the degree to which (i) a target increment is assimilated and preserved in the early forecast period with a meso-β-scale model, and (ii) the mass field adjusts to a wind field perturbation induced by nudging, and vice versa. However, the residual flow is often substantially modified by the orography, notably by the Alps. Particularly near rough terrain and at low levels, the adjustment is only partly geostrophic.

In line with theory, surface pressure data is poorly assimilated, and strong vertical wind shears imposed by nudging a wind profile with strong shear or single-level wind data with little vertical spreading decrease rapidly in the forecast period. Whereas a geostrophic wind correction is shown to have a potential to enhance the assimilation of surface pressure despite strong unrealistic side effects in the case of a single pressure datum, it appears to be difficult to enhance vertical wind shear assimilation, at least without suitable temperature data.

The nudging of wind profiles without strong shears or temperature profiles (with or without strong vertical gradients) is basically effective, but orographical effects can hamper the model, e.g. winds can be deflected locally. Again, if a σ-layer is cooled, flow from higher towards lower orography induced by the increased density can carry the maximum of a temperature perturbation away from the observation location.

Specific problems arise near steep orography, when observation increments are spread laterally along the sloping terrain-following σ-surfaces. Shallow temperature perturbations are significantly attenuated over rough terrain as horizontal advection across several model layers distributes the perturbation in relatively large areas. For example close to the ground, areas over high orography may be influenced by observations over low orography which are not representative of the elevated areas, for instance in the case of low-level inversions. Lateral spreading along quasi-horizontal isobaric surfaces diminishes at least the latter problem.

3 Application to low stratus

3.1 Introduction

3.1.1 Motivation and strategy

The major, densely populated basins in the environs of the Swiss Alps (namely the Swiss Plateau, the Po Valley, the Saône and upper French Rhone Valley, the Upper Rhine Valley, and the area from the Danube Valley to the Alps in Southern Bavaria) are prone to persistent deep fog and low stratus during anticyclonic situations and situations with weak pressure gradients during autumn and winter. The forecasting of these events is of importance particularly because of the adverse effects of fog on air and road transportation. However, the ability to forecast its formation, evolution and dissipation has not improved much during recent years, and there is a great uncertainty in forecasting boundary layer stratiform clouds such as low stratus (Duynkerke, 1991; Smith, 1994).

Therefore, one of the aims for the development of the Swiss Model (SM) was to provide the local forecasters with additional guidance in fog and low stratus forecasting. However, in the (pre-) operational daily use of the SM (and the DM), it became evident that the low cloud cover was not well predicted. Over relatively flat areas, e.g. in Germany, overcast conditions for low stratus clouds were produced too often, possibly associated with an underestimation of the turbulent fluxes across the boundary layer top (Schrodin, 1995b). In contrast, fog and low stratus events over the Swiss Plateau were usually missed both in the analyses fields (cf. Figure 1-1) and in the forecasts if the cloud top was significantly below 1500 m.

Deficiencies in the simulation and prediction of fog and low cloud by means of operational NWP models are very common (Golding, 1990; Clark, 1994; Smith, 1994; Kvamstø, 1994; Bretherthon et al., 1994; Working Group Report, 1994). Shortcomings include the models' limited vertical resolution, inadequate parameterizations (e.g. of soil-atmosphere interactions, turbulence in stratified layers, cloud top entrainment, microphysical processes, radiation) and interactions between these parameterizations, and insufficient observations to adequately specify the initial conditions. A method to partly overcome the model shortcomings and to improve fog prediction for a given location is to use refined one-dimensional (1-D) high-resolution boundary layer models which may be forced with wind and advection from a mesoscale model (Musson-Genon, 1987; Bergot and Guedalia, 1994; Guedalia and Bergot, 1994), or which may consider advection by moving a column of air along a mean trajectory (Karlsson and Falk, 1984). Further studies with 1-D models include Turton and Brown (1987), Xinmei et al. (1990), and Duynkerke (1991). However, this method can only be applied successfully to flat regions with weak surface heterogeneity. Model prediction of fog and low stratus in other areas, for instance near steep orography, will therefore tend to rely on 3-D mesoscale models.

The literature on 3-D mesoscale modelling of continental radiation fog is limited. Nocturnal drainage flows that result in convergence lines and assist shallow radiation fog formation have been modelled by Golding (1993) for the coastal plain near Perth in Western Australia and by Branscome et al. (1994) for a 100 m deep valley in Tennessee. Gayno et al. (1994) simulated the diurnal cycle of summertime coastal advection fog in

California. However, these studies have put emphasis on the dynamical and physical processes and parameterization rather than initialization.

Studies with a focus on initialization have been made by Ballard et al. (1991) and Ballard et al. (1994) for sea fog and marine low stratocumulus. The key issue was found to be initialization rather than model formulation. The retention of cloud after the initial time was greatly improved when a nudging technique (Lorenc et al., 1991) was deployed instead of a static moisture analysis and initialization scheme (Wright and Golding, 1990). Note, however, that land and sea fog are physically fundamentally different (cf. Roach, 1994). Bell and Hammon (1989) added low cloud interactively to the model analysis over the North Sea and over Britain. The low cloud added overland erroneously disappeared within the first few hours of the forecast, whereas the low cloud over the sea remained and was then advected overland.

In relation to continental deep fog and low stratus near steep orography, there is a lack of experience on the behaviour of mesoscale NWP models and particularly on the aspect of data assimilation.

In light of the above there are several open issues related to data assimilation with low stratus, and these are now listed.

- What is the potential of a meso-β-scale model, namely the Swiss Model, to simulate persistent continental meso-α to meso-β-scale deep fog and low stratus?
- What is the potential of nudging towards conventional observations to improve the analyses in such situations, and how is this improvement preserved in subsequent forecasts?
- What specific problems arise near steep orography?
- What is the benefit from modifications to the model and to the standard formulation of the nudging scheme which are designed to tackle these problems?
- How does nudging compare to static initialization?

A series of experiments is undertaken to answer these questions on three events of winterly low stratus. The present chapter is organized as follows. Following a description of some physical aspects of low stratus, information is provided on the meteorological cases, the model configuration and orography, the dataset, and the evaluation strategy. In sections 3.2 and 3.3, nudging experiments are discussed with a focus on model aspects, namely the horizontal diffusion and the vertical resolution. In sections 3.4 and 3.5, refinements on the nudging scheme are addressed which are designed to tackle problems related to steep orography. This includes modifications to the lateral spreading of data increments, and the potential benefit from screen-level humidity data from a dense network of surface stations at different altitudes. Finally, a comparison of nudging and optimum interpolation is provided in section 3.6.

3.1.2 Physical aspects of low stratus

In mountainous areas, low stratiform cloud can be regarded as 'deep fog' or 'low stratus'. Well mixed deep fog behaves like a stratocumulus or stratus cloud sheet (Stull, 1988). Hence, no rigorous distinction is made between these terms here. The focus of this work lies on meso-α to meso-β-scale deep fog or low stratus rather than local shallow fog.

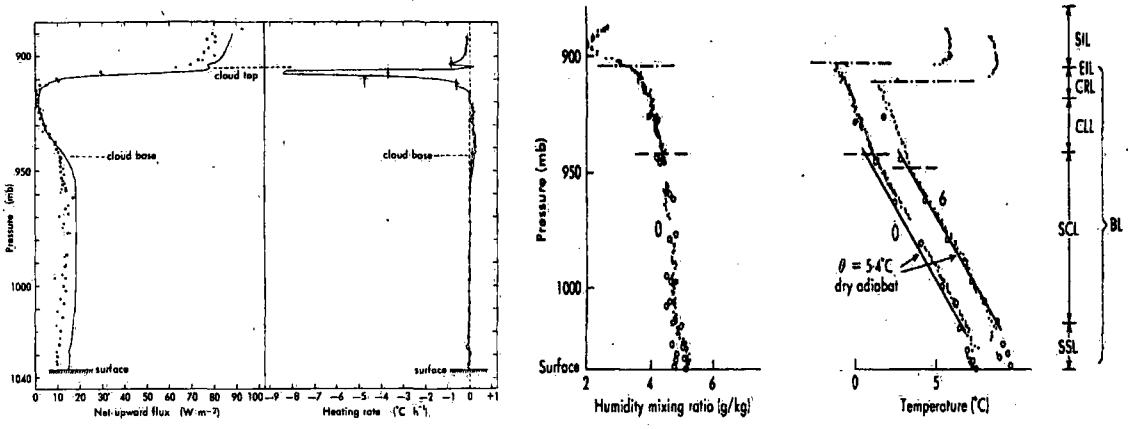

FIGURE 3-1. Vertical profiles at Cardington UK on 20 November 1976. Left: Observed (dotted) and theoretical (solid line) net infrared fluxes and heating rates at 0100 UTC (from Slingo et al., 1982). Right: Observed (dotted) and theoretical (solid line) humidity mixing ratio at 0000 UTC and of temperature at 0000 UTC and 0600 UTC (from Roach et al.,1982).
The abbreviations on the right denote: SIL: subsidence inversion layer; EIL: entrainment interface layer containing the major temperature step; CRL: cloud layer with a radiative flux divergence; CLL: remaining (lower) part of the cloud layer; SCL: sub-cloud dry adiabatic layer; SSL: stable surface layer.

When humid, warm air is advected over low-level cold air pools in the major Alpine basins, advection and mixing are primary processes in formation of deep fog or low stratus. By far the most common type of fog in the lowlands near the Alps is radiation fog. The present study deals with pre-existing mature deep fog or low stratus. Here, the expected structure of low stratus in the simulations and the potential factors contributing to (erroneous) dispersal of low stratus are discussed in the context of the typical structure of mature low stratus, the mechanisms for its dissipation, and the influence of orography. (For details on the formation of fog or low stratus, see e.g. Roach (1995), Bergot and Guedalia (1994), Fitzjarrald and Lala (1989) and Meteorological Office (1994).)

The typical vertical structure of (thin) low stratus is depicted in Figure 3-1. The base of a very sharp inversion coincides with the cloud top. Turbulence keeps the mixing ratio roughly constant below the inversion and maintains an adiabatic sub-cloud layer topped by a moist-adiabatic lapse rate within the cloud. Radiative cooling is confined to a thin layer just below the cloud top due to a net radiative flux divergence. Horizontally, the cloud top height is often regarded as largely homogeneous on the meso-β-scale. Variations inherent to low stratus which are due to downward convection and dry air entrainment (Roach et al., 1982; Lenschow, 1990) typically occur on smaller scales.

In isolation, fog or low stratus can persist for long periods. However, several mechanisms enhance its dissipation (Roach, 1995). Incursion of a cloud sheet not too far above the fog greatly reduces radiative cooling at the fog top, and droplet settling thins the fog. A pronounced increase in wind speed leads to enhanced warm and dry air entrainment across the fog top. In contrast, heating by absorption of solar irradiation is inefficient at mid-latitudes in the winter season (Brown and Roach, 1976). Anticylonic subsidence reduces the top height of fog or low stratus and may eventually assist in fog dissipation (Roach et al., 1982).

Orography has various influences on fog and low stratus. Hill fog occurs as a result of the lowering of the cloud base over hills. Classical upslope fog usually forms on the slope of higher mountains, often under cyclonic conditions. Extensive fog formation due to orographic lifting can also occur in fair-weather winterly conditions, for instance, when sufficiently humid low-level air moves slowly upwards from the northeast towards the higher-elevated pre-Alpine areas in Southwest Germany and the Swiss Plateau, causing deep fog in these areas rather than in the lower-elevated Danube basin (Eigenwillig and Ungewitter, 1993).

The confluence of the Jura Mountains and the Alps towards the west has special implications on fog and low stratus in the Swiss Plateau. With northeasterly winds, called 'Bise' (Wanner and Furger, 1990), the foggy cold-air body is partly dammed by the confluence, and the cloud top rises. The reverse effect is observed with westerly to southwesterly flow. Given weak large-scale winds, the confluence and thermal effects also cause a diurnal fog cycle in the Swiss Plateau which is opposite to the typical evolution in smaller-scale deep mountain valleys (Whiteman, 1982). Since the ratio of mountain areas above the cloud, which are heated during the daytime, relative to areas below the cloud top is larger in western Switzerland compared to northeastern Switzerland, there is more updraft in the west. The resulting pressure anomaly leads to a northeasterly wind and thus to a rising of the fog top in the Swiss Plateau during the day. During the night, southwesterly wind and lowering of the fog top is observed (Wanner, 1979).

Over the Swiss Plateau, cloud top heights of low stratus of up to about 1100 m corresponding to about 600 m above the valley floor are most common (Bachmann and Bendix, 1993), but they can also reach 2000 m. Persistent low stratus occurs most often from October to January (Wanner, 1979).

3.1.3 Meteorological cases

A series of experiments have been conducted for three persistent low stratus type meteorological cases. Cloud top heights were rather large, but typical for the Swiss Plateau. The synoptic situations, and the development and evolution of the low stratus in the environs of the Alps are described. In each case, the analysis time(s) denote the end of the data assimilation period or, equivalently, the beginning of the forecast period(s) for the experiments.

Case A: Analysis times: 19 November 1993, 1200 UTC (case A1),
20 November 1993, 1200 UTC (case A2).

After the eastward passage of a strong cyclone over the Alpine region, cold and moist air from the north was blocked by the Alps causing snowfall. Advection of drier air and subsidence associated with an anticyclone over northern Central Europe subsequently decreased the cloud top height to 1500 m. On 19 November, very cold air aloft associated with an upper-level trough decreased the temperature gradient of the inversion. A strengthening of the wind over Germany and Eastern Europe reduced the stability further, and caused the stratus dissipation (cf. section 3.1.2) over large areas (Figure 3-2a, b). However, the Swiss Plateau, the area of Bavaria adjacent to the Alps, the Lyon region including the southern part of the Saône basin, and the Massif Central remained mostly under a thick layer of low stratus with a cloud top height at around 1500 m associated with a moderate inversion until the forenoon of 21 November (Figure 3-2c). The Jura Mountains, its northern slopes, and the remaining part of the Saône basin were mostly cloud-free. Damming of moist air resulted in regionally (e.g. Ticino) per-

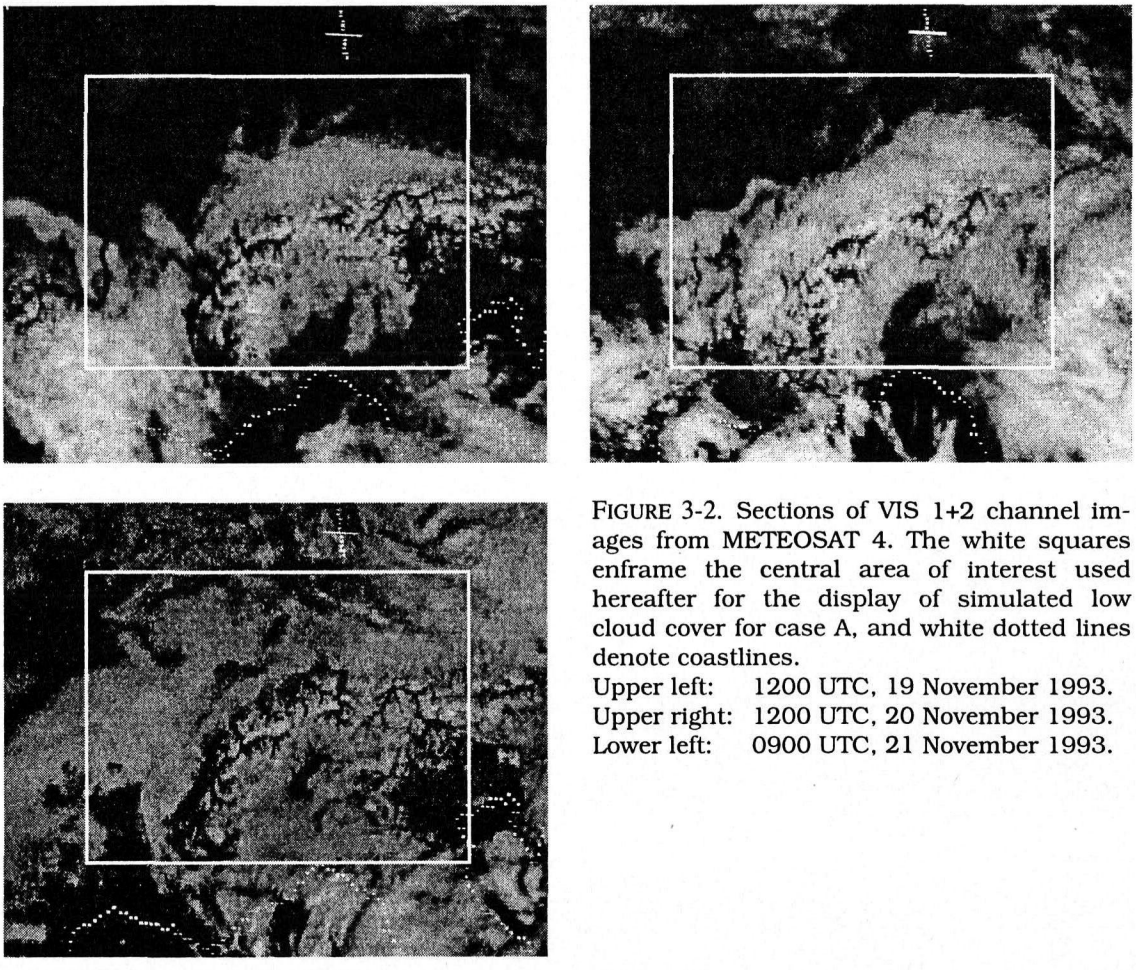

FIGURE 3-2. Sections of VIS 1+2 channel images from METEOSAT 4. The white squares enframe the central area of interest used hereafter for the display of simulated low cloud cover for case A, and white dotted lines denote coastlines.
Upper left: 1200 UTC, 19 November 1993.
Upper right: 1200 UTC, 20 November 1993.
Lower left: 0900 UTC, 21 November 1993.

sistent stratus along the northeastern Po Valley, reaching up to 2200 m at the Alpine slopes. Winds in the environs of Switzerland were weak easterlies below the cloud without significant vertical shear across the inversion. The Bise in the Swiss Plateau was slightly stronger in the daytime, indicative of a weak diurnal cycle (cf. section 3.1.2).

Case B: Analysis time: 28 November 1993, 0000 UTC.

A moderate Bise associated with a strong, large anticyclone centered over Russia caused patchy radiation fog to grow to a contiguous layer of fog with a depth of 500 m over the Swiss Plateau on 26 November. Deep fog also formed over parts of France. During 27 and 28 November, the situation was quasi-steady (Figure 3-3). A persistent thick blanket of low stratus with a cloud top height of 1000 to 1200 m (above sea level) was topped by an inversion of up to 15 K over the Swiss Plateau, Southern Germany, and most of France. In Switzerland, fog was reported down to 500 m. The satellite images indicate that the Jura Mountains, the Black Forest, and the Vosges penetrated the cloud cover. Low-level winds were generally weak in Switzerland and without a diurnal signal. South of the Alps, cloudiness associated with a cyclone over the Mediterranean prevented fog from being persistent.

Associated with an upper-level trough crossing the eastern Alps, advection of cold air above the inversion reduced the stability during the night to 29 November. Some mid-level cloudiness and an increase of the wind speed further contributed to a break-up of

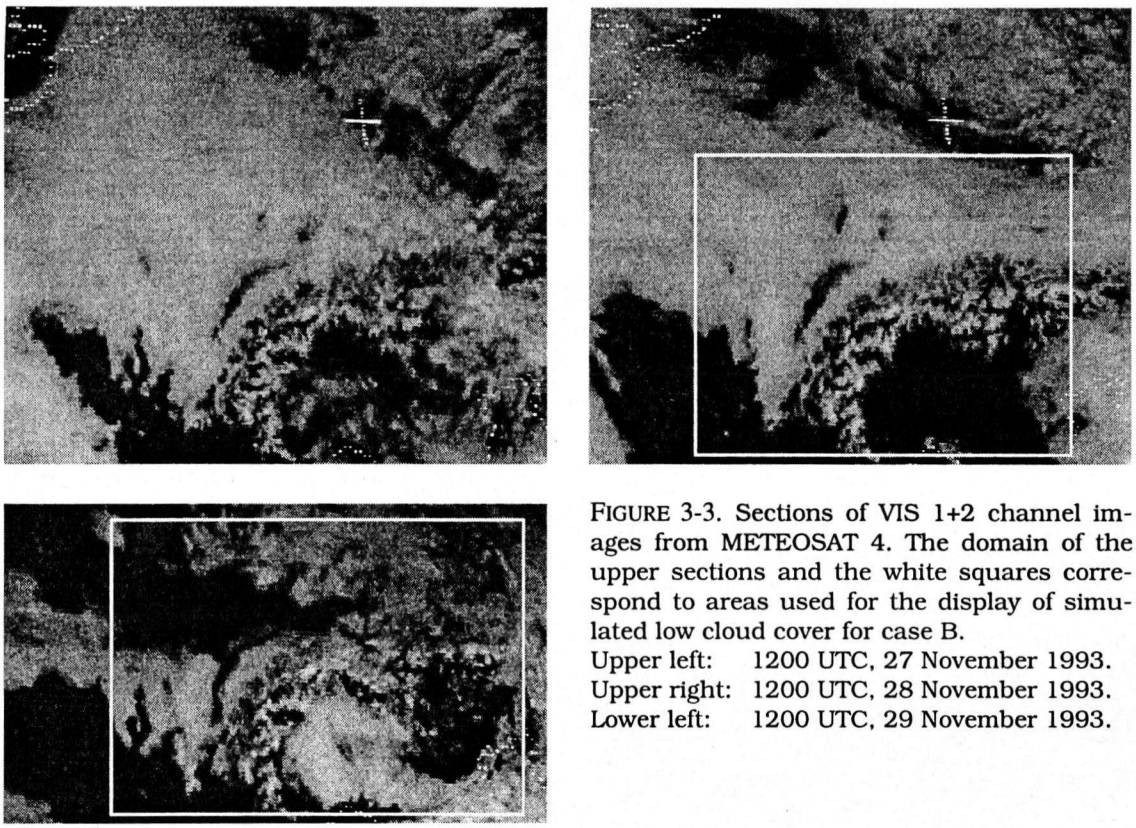

FIGURE 3-3. Sections of VIS 1+2 channel images from METEOSAT 4. The domain of the upper sections and the white squares correspond to areas used for the display of simulated low cloud cover for case B.
Upper left: 1200 UTC, 27 November 1993.
Upper right: 1200 UTC, 28 November 1993.
Lower left: 1200 UTC, 29 November 1993.

the cloud cover. However along the Alps, the damming effect and the Bise caused the stratus to persist, and to extend up to 1700 m in the Swiss Plateau.

Case C: Analysis time: 30 November 1994, 1200 UTC.

A large anticyclone moved from England to Poland, and the cloud cover that was left after a frontal passage dispersed in large parts of western to central Europe. Over the Swiss Plateau, the low stratus mostly broke up during 29 November. The following night, it formed again at about 900 m following slight moistening of the whole boundary layer, and by noon of 30 November, the typical moist adiabatic lapse rate within the thick cloud layer was reestablished. The low stratus with its top at 1000 m persisted that day and on 1 December (Figure 3-4). Low stratus was also observed over parts of southern Germany and northeastern France on both days. South of the Alps, fog was present on 30 November over the eastern Po Valley, and thickened and expanded quickly thereafter due to moist-air advection.

3.1.4 Model configuration, dataset and its use, and evaluation strategy

a. Model configuration and orography

All experiments in this chapter are performed on a 97*91 grid point domain (Figure 3-5a) centered over Switzerland, i.e. a domain considerably smaller than the operational SM domain with 145*145 grid points. The main area of interest comprises the lower troposphere around the western and central part of the Alps and their environs especially to the north and west. Since winds are relatively weak in the Alpine environs in all three cases, one expects the influence of the initial conditions to dominate over

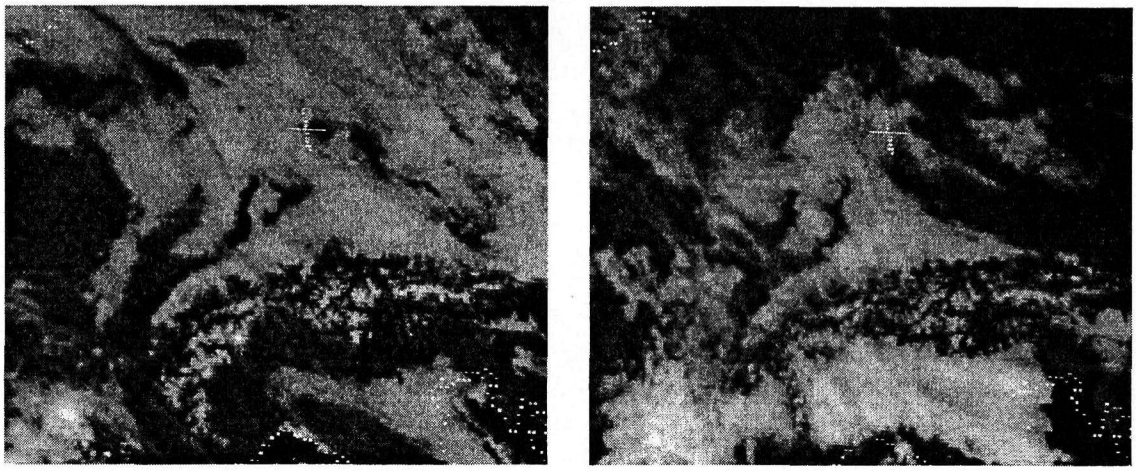

FIGURE 3-4. Sections of VIS 1+2 channel images from METEOSAT 4.
Left: 1200 UTC, 30 November 1994. Right: 1200 UTC, 1 December 1994. This relates to case C.

the influence of the lateral boundary conditions for the first 24 to 36 hours of the forecast.

The model topography is also displayed in Figure 3-5. Note that the Swiss Plateau is resolved, but its valley floor is only one or two gridpoints wide in its western part. Its eastern parts, the Upper Rhine Valley, the French Rhone Valley (including the Lyon region), and particularly the Po Valley are better resolved.

In all experiments, the model parameterizations are identical to the operational version 2.9 except where noted otherwise. However, the horizontal diffusion is reduced in sections 3.3 to 3.6.

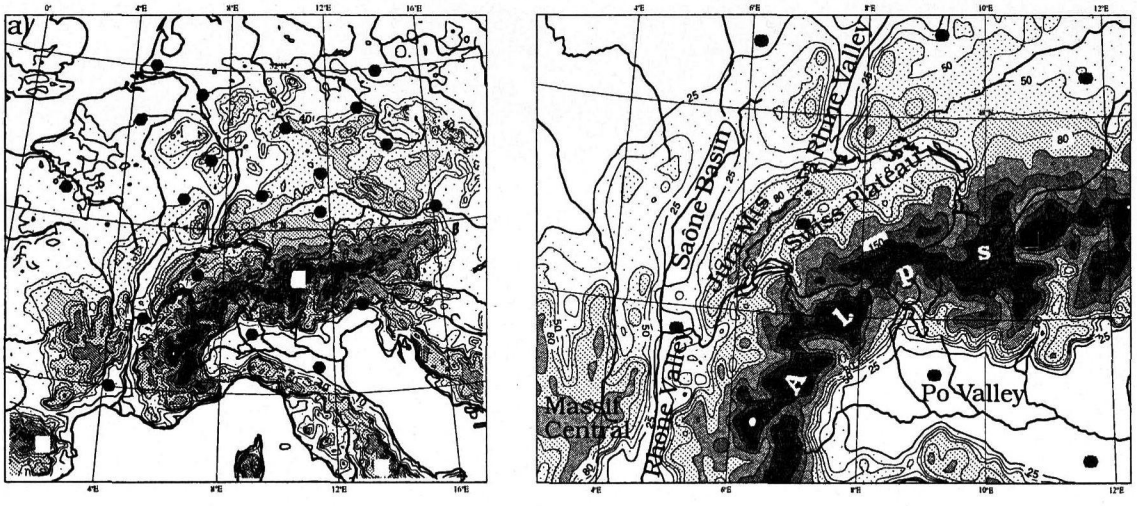

FIGURE 3-5. a): Model domain with orography as used for all experiments in this chapter. Isolines are at 100, 250, 400, 500, 600, 800, 1000, 1500, 2000, 3000 metres above sea level. The black dots denote the locations of rawinsonde stations, of which TEMP reports assigned to the analysis time could be utilized for nudging in at least one case.
b): Same as left, but for the central area of primary interest. The isoline at 100 m is replaced by an isoline at 2500 m. The seven rawinsonde stations indicated here are (from north to south): Stuttgart, Nancy, Munich, Payerne, Lyon, Milano, San Pietro (Bologna).

b. dataset and its use

All rawinsonde data used in this study are retrieved from the MARS (Meteorological Archive System) of the ECMWF. The locations of the rawinsonde stations are indicated in Figure 3-5. All relevant stations issued TEMP (temperature, dewpoint and wind profiles) reports every 12 hours. In case A, Payerne also reported every 6 hours, but Milano was not used due to insufficient resolution. In case B, Munich, Milano and San Pietro (Bologna) were missing.

Rawinsonde temperature and humidity data have high vertical resolution, and are capable of defining the base and thickness of cloud layers (Lorenc et al., 1994; Wang and Rossow, 1995) and of inversions. In contrast, their horizontal and temporal resolution is rather poor. Since persistent low stratus varies strongly in the vertical, but only slowly in time, it is better represented by the rawinsonde network than other mesoscale meteorological phenomena. Yet, the data resolution particularly in the horizontal is still insufficient due to mesoscale variations of the environment of the low stratus (cf. section 3.1.2).

The data base of surface observations consists of the SYNOP reports available in the MARS archive of the ECMWF, and in cases A and B of all 72 hourly reporting stations of the high-resolution automated surface station network ANETZ of Switzerland (all Swiss SYNOP stations belong to the ANETZ). Elimination of stations which do not match the maximum elevation difference condition (e.g. 160 m for screen-level humidity, cf. section 2.2) excludes highly localized signals from exposed mountain peaks and deep valleys, and leaves 40 ANETZ stations elevated between 316 m and 2472 m and about 120 SYNOP stations outside Switzerland. Middle and high orography is quite well represented in Switzerland and its close environs to the southeast. Anywhere else, the data coverage above 750 m is extremely poor (with only three more stations, elevated below 1050 m).

In subsequent nudging experiments, all available TEMP reports are used to derive observation increments of surface pressure and of vertical profiles of wind components, temperature and humidity as described in section 2.2. Surface data are used in sections 3.4 to 3.6. Nudging parameter values are defined in section 2.2 (e.g. Table 2-1), and linear temporal interpolation is deployed during nudging periods of (at least) 12 hours.

c. Evaluation strategy

The model results are subjectively compared with observations, i.e. satellite images (Figure 3-2 to 3-4), SYNOP reports, and rawinsonde soundings. Furthermore, vertical cross sections of different experiments are evaluated with respect to their consistency with observations and to their compatibility with the knowledge about the typical structure of low stratus (cf. section 3.1.2). The focus is on orographic effects. For sounding sites with different distances to steep orography, errors in the vertical profile can have different physical or numerical causes. This calls for an evaluation of specific quantities like amplitude and height of an inversion for each individual station and limits the value of statistical verification.

3.2 Influence of horizontal diffusion

3.2.1 Combined impact of nudging and of reduced horizontal diffusion in the case of November 20, 1993.

As a first step to address the questions raised in section 3.1.1, the nudging scheme is applied to case A2. The operational, interpolated EM analysis (cf. Figure 1-1) misses the widespread low stratus observed in the low basins around the Alps. In the subsequent 12-hour forecast (Figure 3-6) with a 30-layer version (experiment C30), the model produces low cloud in Southern Bavaria, but not in the Swiss Plateau and the Lyon region. Thus, the model's ability to compensate for the serious shortcomings in the initial state appears to be limited.

A comparison is made between operational initialized analyses (experiment C30) and the initial states after a nudging period, henceforth called 'nudged analyses' (experiment N30). Comparison is also made of subsequent 12-hour forecasts. 30 vertical layers are used in both experiments to provide a vertical resolution more adequate for low stratus. Daily comparison of 30-layer 12-hour to 36-hour forecasts (starting from operational analyses) with the operational 20-layer forecasts from November 1993 to January 1994 indicates that this increase in vertical resolution has a negligible impact. Note however that the effective vertical resolution of the operational initial state is never more than 20 layers - the vertical resolution of Europa Modell.

The nudging introduces significantly more low cloudiness (e.g. in Southern Bavaria and southwest of the Jura Mountains) and more realistic vertical structures matching the observations far better than the operational analysis. The vertical profiles of temperature, dewpoint and horizontal wind for Payerne (Figure 3-7a) indicate that in the nudged analysis, temperature errors are strongly reduced compared to the operational analysis, and the inversion, although too weak, is located at the correct height. Also, the relative humidity decreases more sharply above the inversion even though the vertical gradient is still too weak and saturation is not attained. Nudging also corrects the

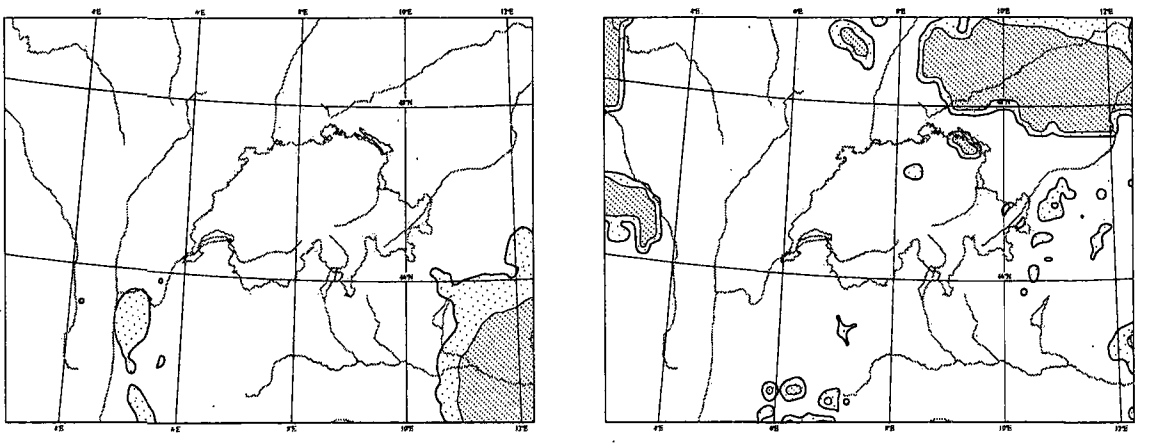

FIGURE 3-6. Areal extent of low cloud cover, as defined as model cloudiness beneath approximately 1500 metres above the ground. White areas < 20 %, light stippled areas 20 % to 80 %, dark stippled areas > 80 % cloud cover.
a): Operational SM analysis for case A2 (valid for 1200 UTC, 21 November 1993); b): subsequent 30-layer 12-hour forecast (control experiment C30), valid for 0000 UTC, 21 November 1993.

low-level winds. Similar, but often less pronounced differences between C30 and N30 are observed at other locations.

However, in the subsequent 12-hour forecast (Figure 3-7b), the fine vertical structures introduced by the nudging disappear completely at Payerne. The same applies to Lyon, and the low cloud erroneously dissipates in the central and western Swiss Plateau and the Lyon region. Nevertheless at other stations, the significant benefit from nudging pertains in the forecast. In summary, the model rejects fine vertical structures in the thermodynamic variables near steep orography, but is able to keep the structures introduced by the nudging elsewhere.

A potential contribution to this process is the linear, fourth-order horizontal diffusion of moist static energy and of total water content along the terrain following sigma (σ) surfaces (see section 2.1.1). The effects of the diffusion near steep orography are sketched in Figure 3-8. Moist static energy h_p is approximately proportional to equivalent potential temperature Θ_e,

$$h_p \cong c_p \Theta_e \tag{3-1}$$

where c_p denotes specific heat of dry air. Thus, even if the temperature and the specific water vapour content are horizontally uniform, the diffusion of moist static energy affects the total heat field in the presence of orography as soon as the lapse rate deviates from the moist adiabatic lapse rate. In the case of a stable stratification (in terms of Θ_e), 'warm' air aloft is diffused downwards along the mountain slopes and vice versa. This results in 'heating' (in terms of Θ_e) over concave orography (where the Laplacian of the

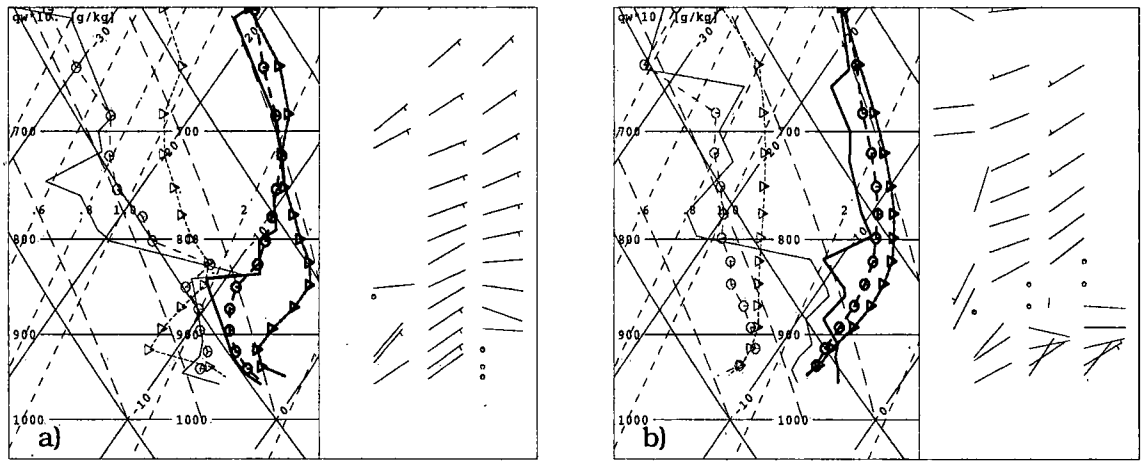

FIGURE 3-7. Vertical profiles of Payerne. Emagramme on the left side of each plot, with temperature profiles (bold lines and symbols) and dewpoint profiles (thin lines and symbols). Vertical profiles of horizontal wind vector on the right side of each plot (WMO wind symbols).
Case A2. a): Analyses; b): 12-hour forecasts (valid for 0000 UTC, 21 November 1993). The following three profiles are shown (winds from left to right): solid lines: observation; circles: experiment N30, starting from nudged analysis; triangles: experiment C30, starting from interpolated Europa Modell analysis (operational analysis).
Note, that dew point is computed over water per definition. Therefore, the observed dew point would always be less than the observed temperature below the freezing point even if saturation (over ice) was measured with a perfect instrument. In contrast, the specific water vapor content is always calculated over water in the model, and the model dew point can equal the temperature without restriction. Note also that there is often a dry bias in the observed rawinsonde dew point near saturation (namely above freezing).

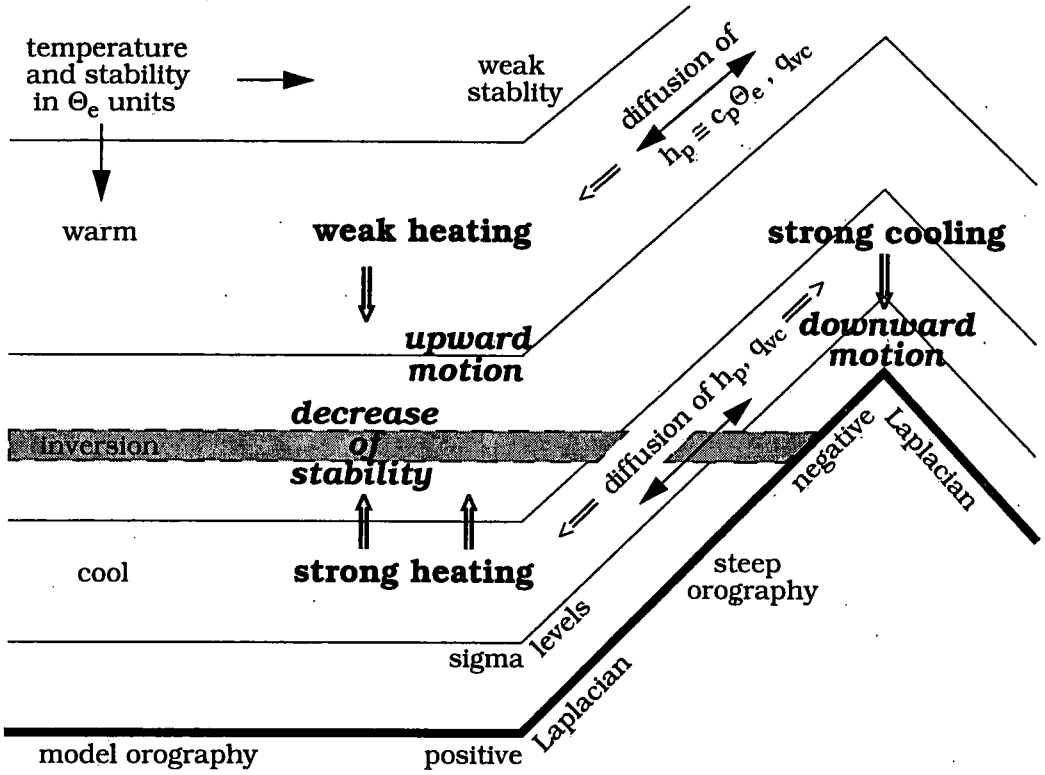

FIGURE 3-8. Illustration of the thermal effects of diffusion of moist static energy h_p and total water content q_{vc} along sigma (σ) levels. Θ_e denotes equivalent potential temperature. Underlying assumptions and initial conditions are in regular letters, primary effects in bold letters, implications and secondary effects in italic bold letters. For further explanation, see text.

orography is positive), namely at the foot of the mountains, and in 'cooling' over the mountain peaks. For typical low stratus conditions (cf. Figure 3-1), diffusion of total specific water content along the σ-surfaces induces drying at the foot of the mountains (cf. Mills and Logan, 1994). Combination of increasing Θ_e and of drying implies an increase of sensible heat. As the heating is strongest below stable layers, the stability and inversions are reduced at the edge of the low basins adjacent to the Alps (cf. Figure 3-8), and the vertical coupling between model layers is spuriously enhanced.

In addition, the heating relative to its lateral environs results in upward vertical motion, and downward motion occurs over convex orography due to the cooling there. In stable, non-convective situations like case A, these spurious secondary vertical circulations (Figure 3-9) are significant and extend up to the height (about 240 hPa) where the model's σ-levels pass into the model's pressure levels further up, which coincides approximately with the height of the tropopause.

A sequence of experiments were conducted in which the coefficient for the horizontal diffusion was reduced for all variables by factors of 4, 10, 16 or 100 relative to the operational value. Only experiment N3A with a 10-fold reduction will be discussed (the other experiments show qualitatively similar results). In N3A, no spurious vertical motions are apparent (Figure 3-9). The comparison of N30 and N3A reveals that the low-level heating due to the horizontal diffusion can reach several degrees at the foot of the Alps. At Payerne (Figure 3-10d), this difference is up to 1.5 K. However, there is still no fine vertical structure in the temperature profile unless the diffusion is reduced further,

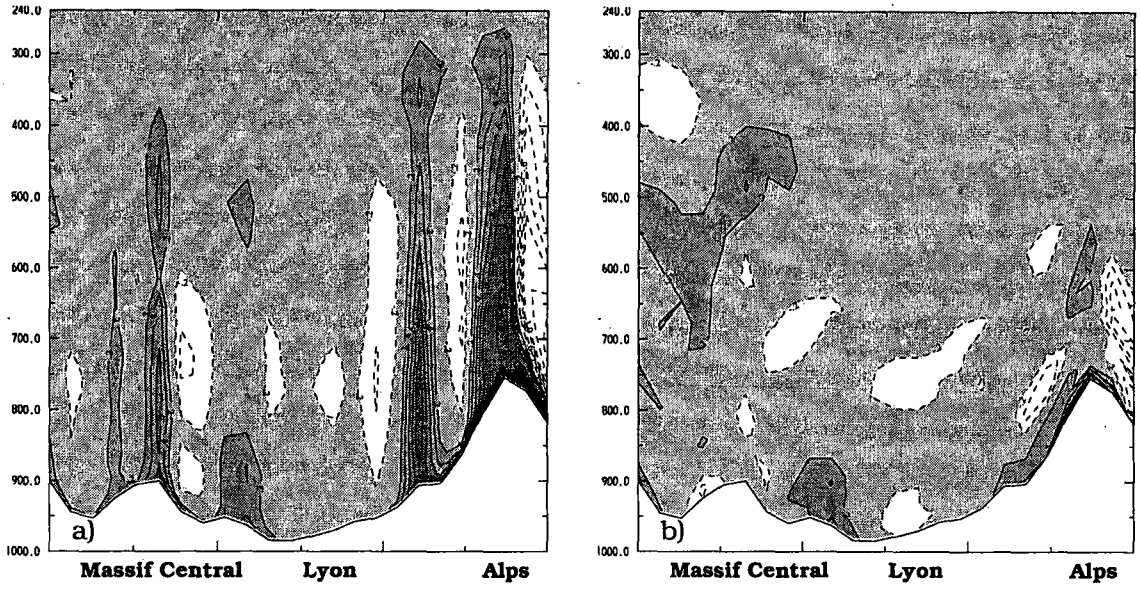

FIGURE 3-9. Vertical cross sections of vertical velocity through the upper French Rhone Valley. 12-hour forecasts for case A2. a): Experiment N30 with full horizontal diffusion; b): Experiment N3A with horizontal diffusion reduced by a factor of 10. Units are in Pa/s, positive values (solid contours, dark shading) denote downward motion.

which indicates that the 10-fold reduced diffusion still contributes to smoothing effects near sharp orographic changes.

The largest impact of the reduced diffusion is at Lyon (Figure 3-10e). The 12-hour forecast with full diffusion does not retain an inversion or saturation. The simulation with reduced diffusion also misses some of the observed fine-scale details, but captures the main inversion quite well and predicts a reasonable humidity structure except close to the ground. The low cloud predicted over the Swiss Plateau and the Lyon region (including the southern part of the Saône basin, cf. Figure 3-10b) also compares favourably with the observations (cf. Figure 3-2b, c). A control experiment C3A starting from the operational analysis, but integrated also with 10-fold reduced diffusion, fails to predict the inversion at Lyon (Figure 3-10e) and most of the forementioned low stratus (Figure 3-10c).

In conclusion, the improved forecast performance of N3A derives from a combination of nudging and reduced horizontal diffusion. Analogous experiments for case B comfirm this result.

3.2.2 Further remarks

The experiments indicate that nudging is able to improve the vertical structure of the initial state during episodes of low stratus. Near steep orography, there is also improvement in the forecast period if the horizontal diffusion along the model's σ-layers is considerably reduced.

Horizontal diffusion is also a matter of concern in the context of fog prediction (Clark, 1994). Ballard et al. (1991) report, that if this diffusion was removed for the thermodynamic variables more deep sea fog would correctly be retained close to the orography of the northeast Scottish coast. However, the horizontal diffusion is required with most

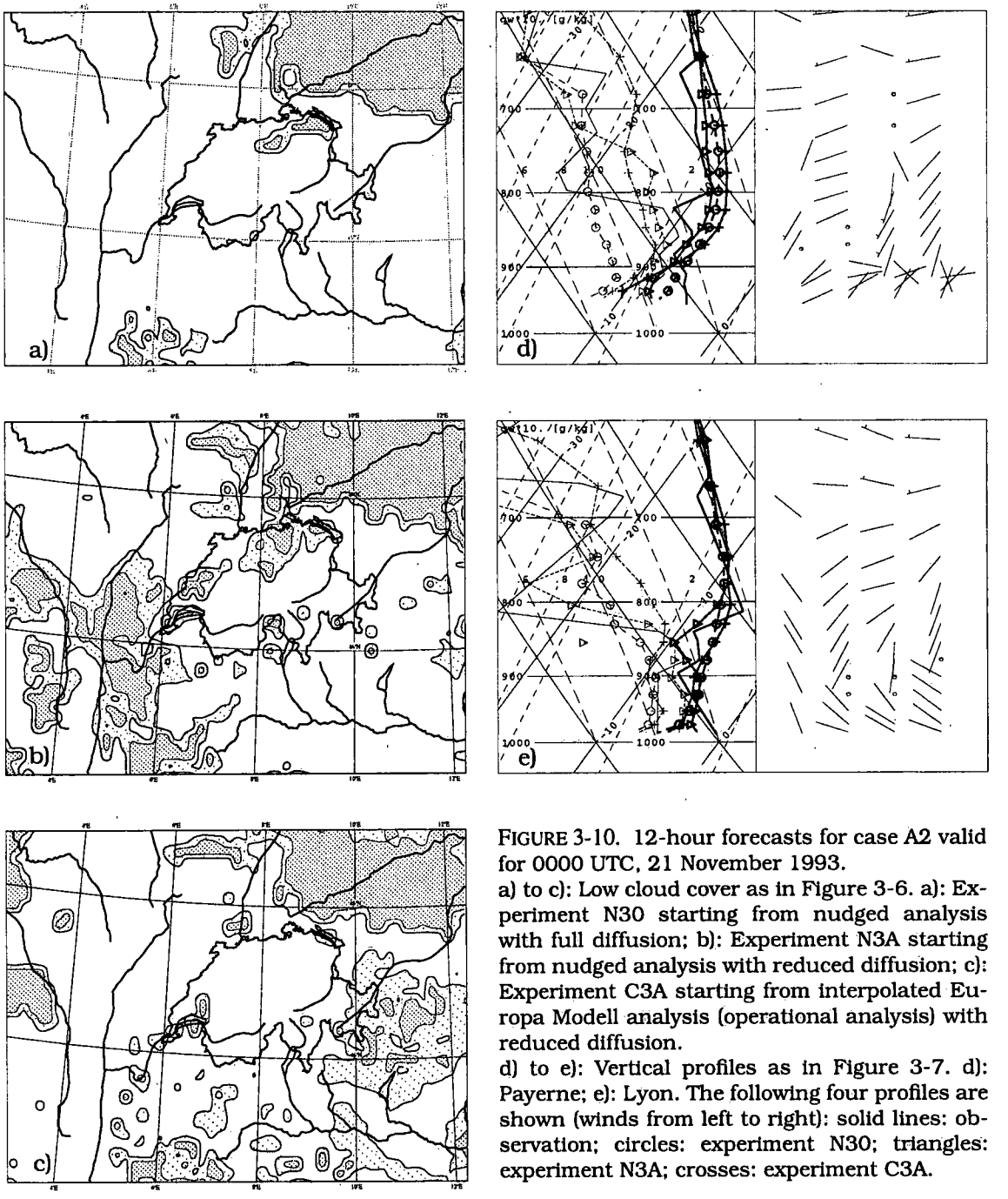

FIGURE 3-10. 12-hour forecasts for case A2 valid for 0000 UTC, 21 November 1993.
a) to c): Low cloud cover as in Figure 3-6. a): Experiment N30 starting from nudged analysis with full diffusion; b): Experiment N3A starting from nudged analysis with reduced diffusion; c): Experiment C3A starting from interpolated Europa Modell analysis (operational analysis) with reduced diffusion.
d) to e): Vertical profiles as in Figure 3-7. d): Payerne; e): Lyon. The following four profiles are shown (winds from left to right): solid lines: observation; circles: experiment N30; triangles: experiment N3A; crosses: experiment C3A.

advection schemes to remove the energy that is transfered by nonlinear downscaling to the small scales (cf. Haltiner and Williams, 1980).

Forecasts with an overall reduction of the horizontal diffusion by a factor 10 were compared to the (full diffusion) operational SM forecast daily from December 1994 to February 1995, and showed consistent improvement in low stratus prediction near steep orography. However, there was evidence of grid-scale noise (particularly in the precipitation fields during severe events). Moreover, on occasions, single grid points in valleys underwent radiative cooling by tens of degrees within few hours at low levels. The cold air was trapped and did not mix if the diffusion was too low. The full diffusion of the operational model is able to counteract this deficiency. Thus, an operational reduction

of the diffusion is problematic. A different formulation for the horizontal diffusion, which acts purely along truly horizontal surfaces is attractive, but can still cause problems (cf. Ballard et al., 1991).

The results in section 3.2.1 clearly show that the benefit from the nudging is model dependent, and hence, care must be taken in generalizing the results. Irrespective of the method to determine the initial state, a modification to the diffusion is required to predict low stratus near steep orography. It is appropriate both from a practical and a scientific point of view to carry out all subsequent experiments in this chapter with the horizontal diffusion reduced by a factor of 10.

3.3 Influence of vertical resolution

This section addresses two aspects related to vertical resolution. The first is the problem of representing sub-grid scale variability given the vertical model grid spacing, and the second aspect is the influence of the vertical grid spacing on vertical temperature and humidity gradients and on the cloud cover if the observed layer of low stratus extends over at least one model layer.

If a cloud layer is thinner than the model layer at the same height it should be parameterized. Alternatively it could be included by nesting a 1-D PBL representation with high vertical resolution, or an adaptive grid in the vertical could be deployed (Working Group Report, 1994). Most present-day cloud-parameterization schemes account for horizontal rather than vertical sub-grid variability (Dastoor, 1994). In the Swiss Model, non-convective cloudiness is dignosed within the radiation scheme (Ritter and Geleyn, 1992) as a function of relative humidity and model layer only. Grid-scale sub-saturation never results in 100 % cloudiness. The vertical averaging within a model layer can result only in sub-saturation with thin layer cloud sheets, and the model cloud scheme interprets the profile as containing much less cloudiness than is seen by a surface observer (Maycock and Macpherson, 1994; this problem occurs even in new prognostic cloud schemes, cf. Tiedtke, 1993).

The same happens also to observed profiles if the layer-averaging vertical interpolation (see section 2.2) is used for the nudging. This technique tends to make it more difficult to introduce cloudiness even for cloud layers comparable to the vertical grid spacing. Given the current cloud parameterization, the radiational properties of such cloud sheets may be better represented if the model relative humidity is nudged towards the maximum observed relative humidity value within the model layer. However, Lorenc et al. (1994) obtained inferior vertical structures as dryer layers become poorly represented. They achieved better results with mid-point interpolation of observed relative humidity. This approach has been tested here with the 30-layer version for case A1. It tends to produce slightly more low cloudiness, and is therefore used henceforth. Mid-

Number of model layers	20	30	40	49
Resolution (in hPa) within the lowest 200 hPa (the resolution of the lowest model layer is fixed at 8 hPa)	25 - 50	25	15	10

TABLE 3-1. Vertical grid spacing within the lowest ca. 200 hPa of the model atmosphere for various model configurations differing in their total number of model layers.

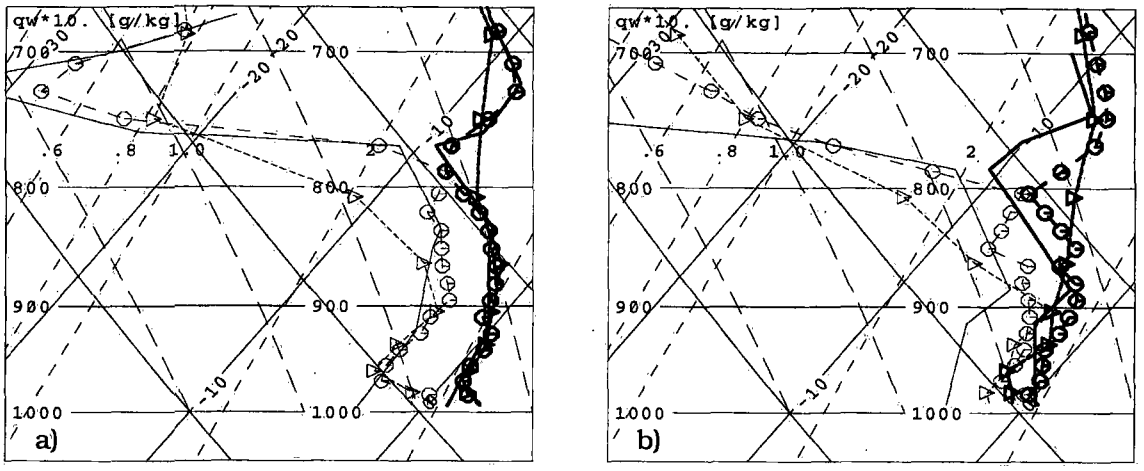

FIGURE 3-11. Vertical profiles as in Figure 3-7, for Lyon. Case A1. a): Analyses; b): 12-hour forecasts (valid for 0000 UTC, 20 November 1993). The following three profiles are shown: solid lines: observation; circles: nudging experiment with 40 model layers; triangles: nudging experiment with 20 model layers. Although the displayed observed dewpoint depression is not zero, saturation over ice is likely to have occured, because the Lyon SYNOP reported 90 % respectively 100 % cloud cover for these times. The discrepancy is explained by the fact that the dewpoint is defined (and displayed) over water, and by observation errors of the radiosonde.

point interpolation has also been attempted for temperature and wind, but the impact is marginal.

Now consider the second aspect related to vertical resolution. In the operational setting, an increase from 20 to 30 model layers has a negligible effect (cf. section 3.2). Here, we examined whether this also holds when the initial state is determined by nudging towards direct observations, and with different values for the horizontal diffusion coefficient. Experiments are carried out with 20, 30, 40, and 49 model layers, and the extra resolution is mainly in the low troposphere (cf. Table 3-1).

The 49-layer experiment with full diffusion analyzes significantly more low cloud near steep orography than the 30-layer experiment (N30), but the differences are not retained in the 12-hour forecast. With reduced diffusion, comparison is made of 20- and 40-layer integrations for case A1. In contrast to Payerne, where smoothing effects of the horizontal diffusion are still significant, the benefit from increased vertical resolution is retained around Lyon in the forecast period. With 40 layers, the humidity and temperature structure at Lyon (Figure 3-11) is well analyzed and predicted. Cloud tops are strongly correlated to the base of inversions (see cross section, Figure 3-12a), and the sharp vertical humidity gradients appear to be realistic. In contrast, the 20-layer version completely misses the inversion throughout the period, and lacks fine vertical structures (Figure 3-12b). Saturation is attained only in the forecast, but at far too low a level. As a result, the forecast of the low cloud cover does not benefit strongly from extra resolution in this case, although the 40-layer analysis contains significantly more low cloud which is more confined to low terrain and in better agreement with the observations.

In cases B and C, the inversions are less elevated and stronger at the initial time, and their representation in the 20-layer model version is more reasonable. Therefore, the influence of vertical resolution is less pronounced, although significant in some areas. The following remarks summarize the inferences from the experiments.

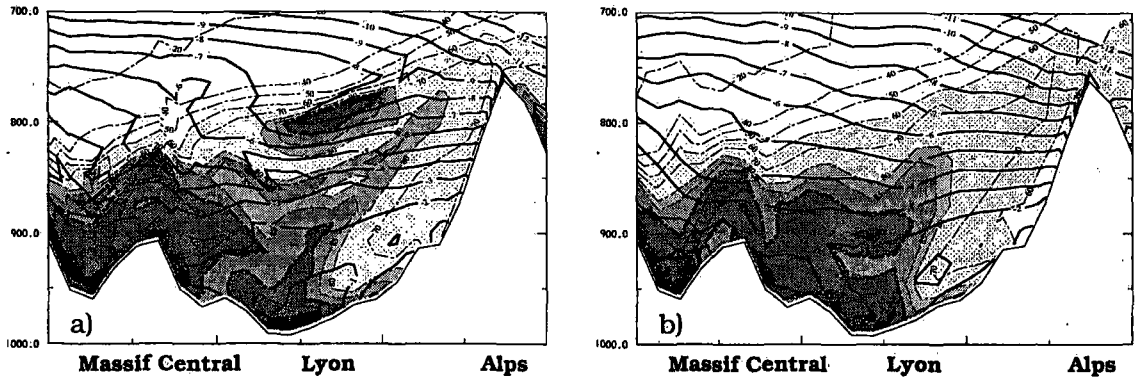

FIGURE 3-12. Vertical cross sections of relative humidity (shading and dashed contours for 20, 40, 50, 60, 70, 80, 85, 90, 95, 100 %) and of temperature (solid lines, in °C) through the upper French Rhone Valley. Above about 90 % humidity (thick dashed lines), the model produces cloudiness except close to the ground. - 12-hour forecasts for case A1.
a): Nudging experiment with 40 model layers; b): Nudging experiment with 20 model layers.

- The higher the vertical resolution and the thinner the model layers, the better the model values should match the observed point values. Nudging towards direct rawinsonde observations is found to often draw the vertical temperature and humidity gradients close to the observed gradients, and in effect, it enhances the effective vertical resolution of the initial state. Moreover, the initial states appear to be sufficiently balanced so that the forecasts of the inversions, low cloud cover, and cloud top height benefit from the extra vertical resolution. Similar results have been obtained by Ballard et al. (1994) for sea fog. However, the degree of benefit is shown here to depend strongly on the model formulation (i.e. diffusion), and upon the geographic location.
- To improve forecasts of low stratus by increasing the model's vertical resolution, it is often necessary that the initial state also has an increased effective vertical resolution. An exception occurs in case B over Central France (e.g. Paris, Figure 3-13) where the vertical structure, and hence the effective vertical resolution is similar in the 20- and 40-layer simulations at the initial time. However, in contrast to the 40-layer simulation, the 20-layer 12-hour forecast is far from saturation and has too little cloudiness. The layer of maximum relative humidity is too low and does not coincide with the inversion base. This case will be discussed in more detail in section 3.6.
- Onset and dissolution of low cloudiness at the inversion base is a decision point with strongly non-linear radiative feedback. Vertical ageraging and smoothing due to insufficient vertical resolution may inhibit cloud formation or cause cloud dissipation. As a result, the impact of increased vertical resolution is not necessarily gradual, i.e. extra vertical resolution can lead to fundamentally different properties in the forecast.
- In the context of boundary layer clouds, it has been noted (Working Group Report, 1994), that increasing vertical resolution, although desirable from a physical point of view, can create numerical problems associated with the representation of vertical advection in the presence of sharp gradients. Such problems have not been observed in the present experiments but it is conceivable that such effects could appear if the resolution was further increased.

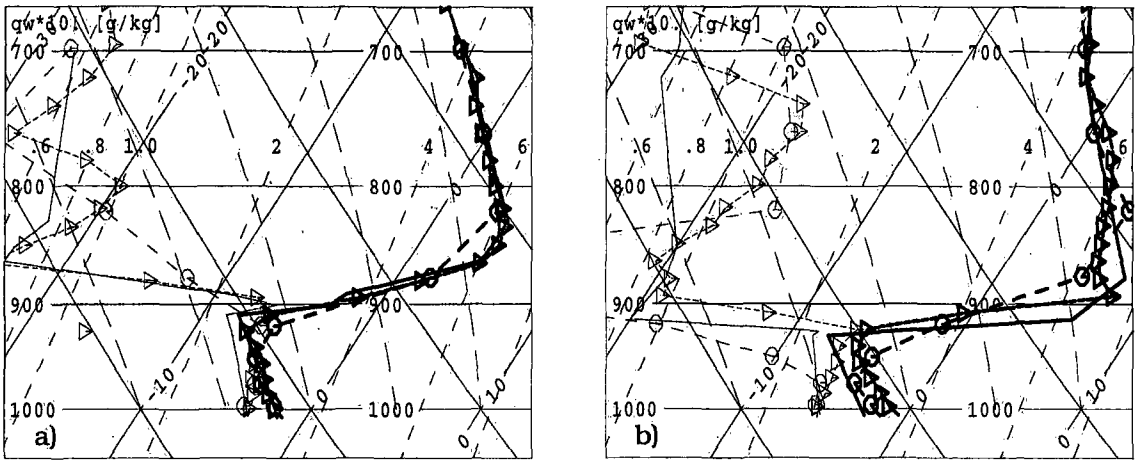

FIGURE 3-13. Vertical profiles as in Figure 3-7, for Trappes (Paris). Case B. a): Analyses; b): 12-hour forecasts. The following three profiles are shown: solid lines: observation; circles: nudging experiment with 20 model layers; triangles: nudging experiment with 40 model layers.

3.4 Lateral spreading of observation increments in steep orography

Near steep terrain, a specific problem arises with the present formulation of the nudging scheme. Rawinsonde observation increments are spread laterally along the model's terrain-following σ-surfaces so that low-level observational information in a valley floor can be spread upslope to areas, for which it is not often representative (cf. Fast, 1995). In the Alpine region, the problem is accentuated by the lack of rawinsonde stations at middle and high altitude, and in principle, this occurs with any data assimilation scheme which models the horizontal correlations in σ-coordinates, like e.g. variational assimilation schemes (Courtier, 1994). It is less prominent with other analysis techniques performed on pressure levels or on isentropes (e.g. Benjamin et al., 1991). Low-level inversions will be sensitive to this process (cf. section 2.3.4), since the air mass below the inversion is often significantly decoupled from the air above it.

Approaches to tackle this problem are either to use non-isotropic structure functions, or to perform the lateral spreading along surfaces which are physically more appropriate. Both approaches are tested here, and Table 3-2 lists the experiments for cases A1 and B.

3.4.1 Use of non-isotropic horizontal weight function

Various flow-dependent (non-statistical) non-isotropic structure functions for the spreading of upper air observations have been used in the past to retain sharper gradients in the atmospheric fields (Atkins, 1974; Benjamin and Seaman, 1985; Spero et al., 1994). Reduced representiveness due to orographic blocking effects have been accounted for by use of non-isotropic correlation functions in spatial analysis methods by Lanzinger and Steinacker (1990) and by Vrhovec (1990). For nudging, non-isotropic weight functions accounting for reduced representiveness due to orography have been used only for screen-level data by inclusion of differences in surface pressure (Stauffer

and Seaman, 1994) or in surface elevation and potential temperature (Miller and Benjamin, 1992).

A similar approach (experiment T3A-NONISO) is adopted here for rawinsonde data by multiplying the horizontal weight function (2-7) with the following term which accounts for potential temperature differences $\Delta\Theta$ between observation point and target grid point:

$$e^{-(\Delta\Theta/\Theta_c)^2}$$

Θ_c is set to 5 K. By using potential temperature differences instead of height or pressure differences, the restriction of the impact of observations as a function of terrain depends on the stability of the atmosphere, i.e. the spreading of information across an inversion is diminished selectively. (Reduced representiveness of observations across air mass discontinuities like surface fronts is also accounted for.) With this choice of Θ_c, the nudging weights are usually small over elevated Alpine terrain (above about 1500 metres).

Comparison of experiments T3A and T3A-NONISO (cf. Table 3-2) reveals (Figure 3-15) that with the use of the non-isotropic weight function, the analyzed low cloud cover is more confined to low orography and tends to agree better with the observations in case

Experiment name	case	number of model layers	horizontal weight function isotropic	surfaces along which lateral spreading is performed	Use of RH-observation increments at observation points	Model fields before nudging period
T3A	A1	30	Yes	sigma	No	EMA
T3A-NONISO	A1	30	No	sigma	No	EMA
T3A-I5	A1	30	Yes	isentropic *	No	EMA
T3A-I5Q	A1	30	Yes	isentropic *	Yes	EMA
T3ADM	A1	30	Yes	sigma	Yes	DMA
T3ADM-I5Q	A1	30	Yes	isentropic *	No	DMA
T3AFC	A1	30	Yes	sigma	Yes	12-h forecast
T3AFC-I5Q	A1	30	Yes	isentropic *	No	12-h forecast
T3AFC-P5Q	A1	30	Yes	isobaric *	Yes	12-h forecast
T2AFC	B	20	Yes	sigma	No	12-h forecast
T2AFC-I5Q	B	20	Yes	isentropic *	Yes	12-h forecast
T2AFC-IQ	B	20	Yes	isentropic **	Yes	12-h forecast

TABLE 3-2. Description of experiments discussed for the lateral spreading of rawinsonde data in cases A1 and B. EMA denotes interpolated Europa Modell Analyses, DMA denotes Deutschland Modell Analyses. In all experiments, screen-level humidity data are also assimilated (see section 3.5) in order to make the enquiry of this section as realistic as possible.
*: applied only to the soundings of Payerne, Lyon, Stuttgart, Munich, Milano. For the other soundings, spreading along σ-surfaces is used.
**: applied to all soundings.

A1 (see Figure 3-2a). In the 24-hour forecast however, the deficit of low cloud over the Swiss Plateau and the Lyon region is larger. A similar trend in quality is also observed with the vertical profiles albeit the differences at the rawinsonde stations are small. In case B, the choice of the weight function has generally little influence.

It appears therefore that for low stratus, the non-isotropic weights cannot adequately account for reduced representiveness of observations along sloping terrain. The positive impact of the non-isotropic weights on the analysis in case A1, both over low and high terrain, suggests that the selected value for Θ_c is reasonable. However, the lack of soundings over high terrain implies that this is a data-poor area which is not influenced by observations in T3A-NONISO unless information from the data-rich low-terrain region is advected.

3.4.2 Lateral spreading along isentropes

This shortcoming of the non-isotropic weights can be overcome by spreading the influence of observations along physically more appropriate surfaces. The potential benefit with idealized conditions has been illustrated in section 2.3.4. Lateral spreading of real data along surfaces different from the model levels has been adopted by Stauffer and Seaman (1994). They spread the data increments given at the model σ-levels without any further vertical interpolation approximately along constant pressure surfaces, but no evaluation of the impact was provided.

Benjamin et al. (1995) spread information along isentropic model surfaces (in an OI scheme), i.e. the influence of observations was extended along quasi-material surfaces. On isentropic surfaces, flow patterns are spatially and temporally more coherent, and

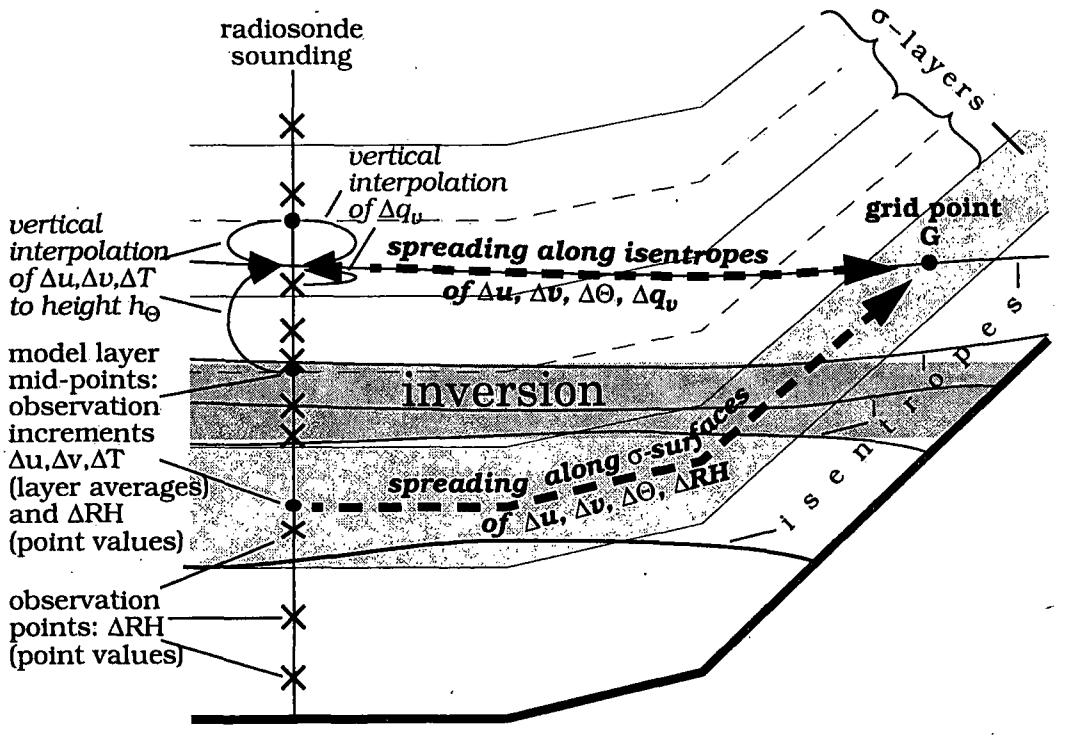

FIGURE 3-14. Illustration of different ways of lateral spreading of the influence of upper-air observations in the environs of steep orography. For further explanation, see text.

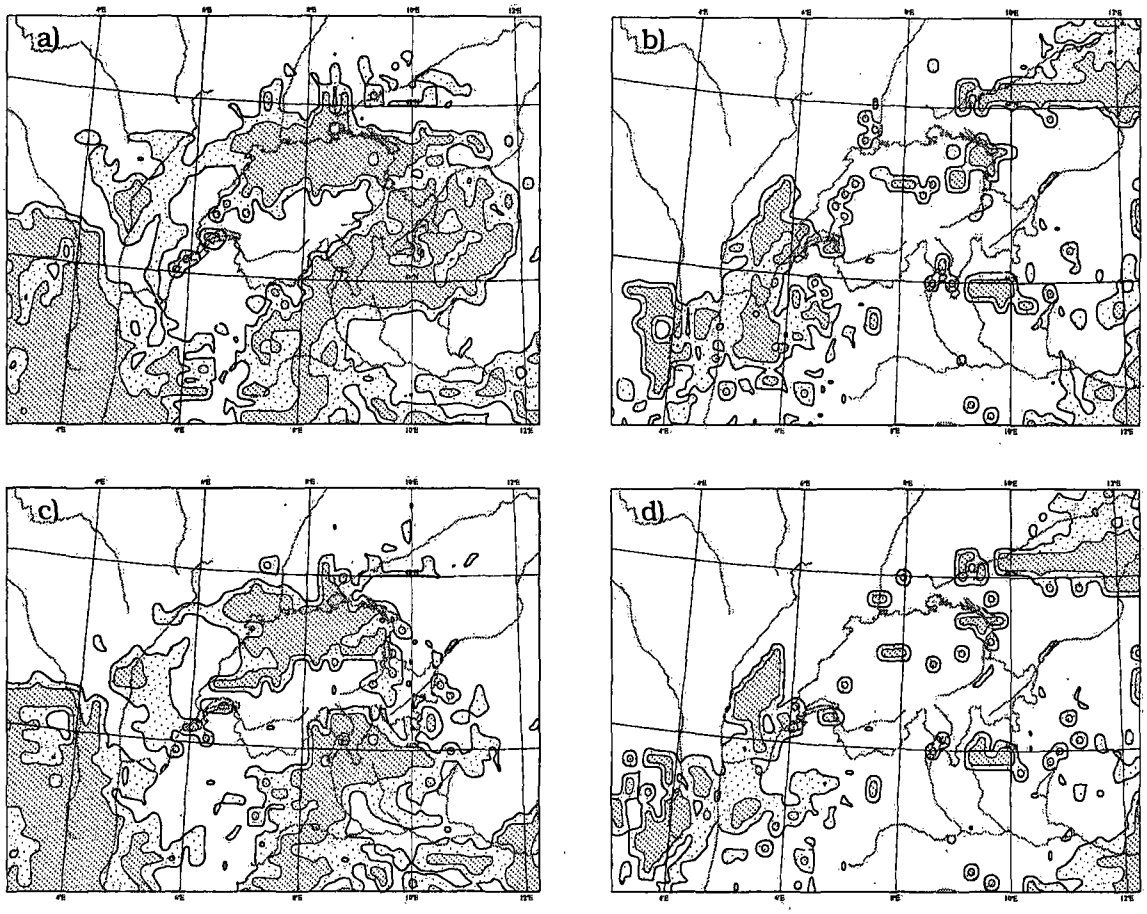

FIGURE 3-15. Low cloud cover as in Figure 3-6. Case A1. Left column: analyses valid for 1200 UTC, 19 November 1993; right column: 24-hour forecasts valid for 1200 UTC, 20 November 1993. a), b): Experiment T3A (conventional scheme); c), d): Experiment T3A-NONISO (non-isotropic weight function).

the isotropic correlation assumption is better founded (Benjamin, 1989). As the vertical resolution increases with the atmospheric stablity in isentropic coordinates, spreading along isentropes can hamper spreading of information across inversions.

Here, these two concepts are combined to spreading along isentropes in a σ-level model (see Figure 3-14). At a grid point G within the horizontal radius of influence of a rawinsonde profile, the observation increment is related to that at the same potential temperature Θ at the rawinsonde location. The vertical interpolation used to convey the increments from the model levels to that height is linear in Θ. This is a good approximation to linear interpolation in log(pressure) which would involve a transcendental equation under the assumption that the temperature varies linearly in log(pressure). The resulting vertically interpolated observation increments of temperature and relative humidity are then transformed into increments of potential temperature and of specific water vapour content q_v (which are conserved quantities with adiabatic flow along isentropes). The transformed increments are finally spread to grid point G, and multiplied with the temporal and (isotropic) horizontal weights.

A disadvantage to isentropic coordinates is that the vertical resolution decreases as the atmospheric stability decreases, e.g. in the PBL (Pielke et al., 1992). Hence in the case of a near-neutral lapse rate at the rawinsonde location, a small error in the simulated

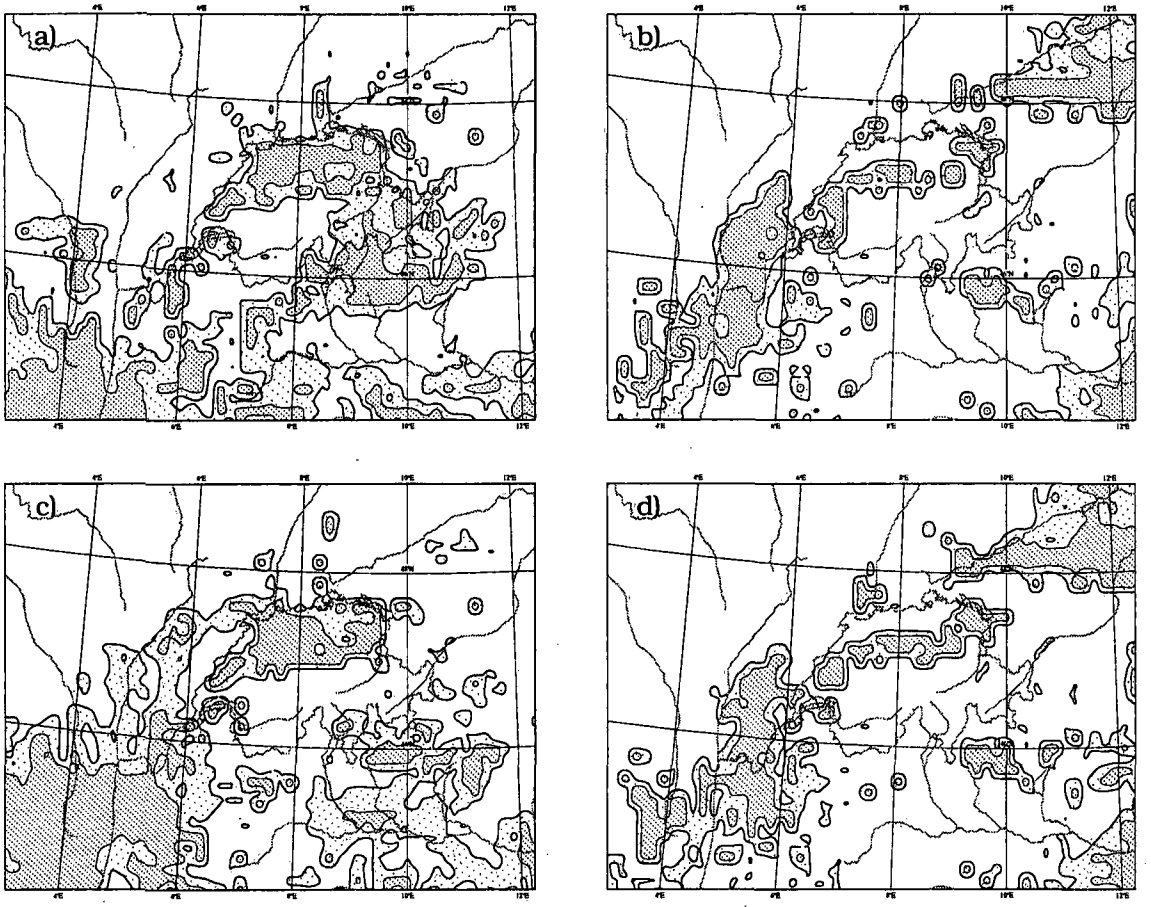

FIGURE 3-16. Low cloud cover as in Figure 3-6. Case A1. Left column: analyses; right column: 24-hour forecasts. a), b): Experiment T3A-I5 (spreading along isentropes); c), d): Experiment T3AFC-I5Q (spreading along isentropes, and nudging period starts from 12-hour forecast instead of interpolated Europa Modell Analysis). See also Table 3-2.

potential temperature would result in a large error in the height h_Θ, from which the increment is spread to a grid point. To circumvent this problem, the following strategy is adopted. If the stability at the height h_Θ is below a threshold γ_T (for which a temperature error of 1 K corresponds to a height error of about 500 m for typical low-tropospheric conditions), the final increment for the grid point G is a weighted linear combination of two increments computed by spreading (i) along isentropes and (ii) along constant pressure surfaces. For a neutral or instable atmosphere, the spreading is performed exclusively along pressure surfaces. At high elevations (above 240 hPa), the observation increments are also spread along the model's isobaric levels.

Also for computational efficiency, the scheme was only applied to the rawinsonde stations close to the Swiss Alps (i.e. Payerne, Lyon, Stuttgart, Munich and Milano) in the first instance (experiment T3A-I5). Relative to T3A and T3A-NONISO, the low cloudiness of the analysis and 24-hour forecast is moderately improved north and west of the Alps in case A1 (Figure 3-16, cf. Figure 3-15, Figure 3-2a), but no improvement is apparent in cases A2 and B.

Several modifications have been devised to improve the scheme's performance:

- The vertical interpolation of observation increments to the height h_Θ of equal potential temperature introduces an additional vertical averaging (cf. Figure 3-14). This

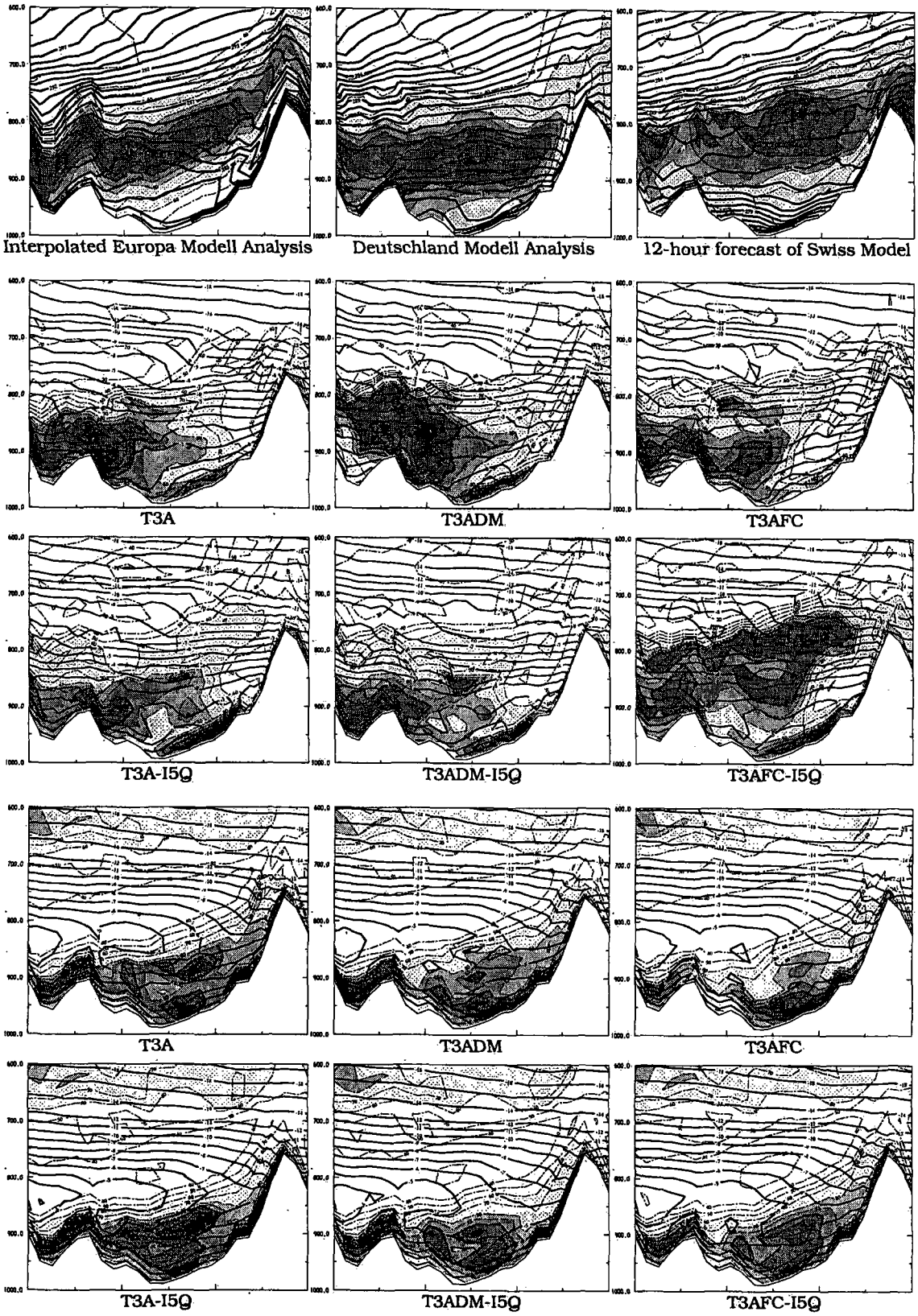

FIGURE 3-17. Vertical cross sections across the French Rhone Valley near Lyon (cf. Figure 3-12). Case A1. Top row: relative humidity (shading and dashed lines, in %) and potential temperature (thick solid lines, in K) at the beginning of the 12-hour nudging period. Rows 2 - 5: relative humidity, and temperature (solid lines, in °C), where rows 2 - 3: analyses (1200 UTC, 19 Nov. 1993); rows 4 - 5: subsequent 24-hour forecasts. For experiment names, see Table 3-2. Above about 90 % humidity (thick dashed lines), the model produces cloudiness except close to the ground.

can reduce the effective vertical gradients and the probability of saturation in the observations. Alternatively, observation increments computed at the observation points of the sounding (which are already used for quality control, see section 2.2) can be used also for the vertical interpolation below 700 hPa. Application of this approach indeed increases the vertical gradients in the analysis, but tends to deteriorate the forecast, possibly due to imbalances caused by assimilating sub-grid vertical scales of wind and temperature which are contained in the point value increments at the observation points. This is avoided if the scheme is applied only to humidity, and a small positive impact limited to the analyses results.

Basic to the scheme is the assumption that the isentropic distribution is realistic in the model. In the previous experiments of this section, the nudging has started from interpolated Europa Modell Analyses (EMA) which exhibit isentropes (Figure 3-17) that are often terrain-following, somewhat noisy, and unrealistic. In contrast, the Deutschland Modell Analyses (DMA) and the 12-hour forecasts of the Swiss Model (SMF) have isentropes (Figure 3-17, top row) which are significantly more horizontal, smooth, and realistic. Comparison is made of 6 experiments (cf. Figure 3-17), where nudging with spreading along (i) σ-surfaces or (ii) isentropes starts from (I) EMA, (II) DMA or (III) SMF. In the analyses, the differences are quite large, but not systematic (cf. Figure 3-17). Spreading along isentropes has a slight tendency to improve the 24-hour forecasts more strongly if the nudging starts from a

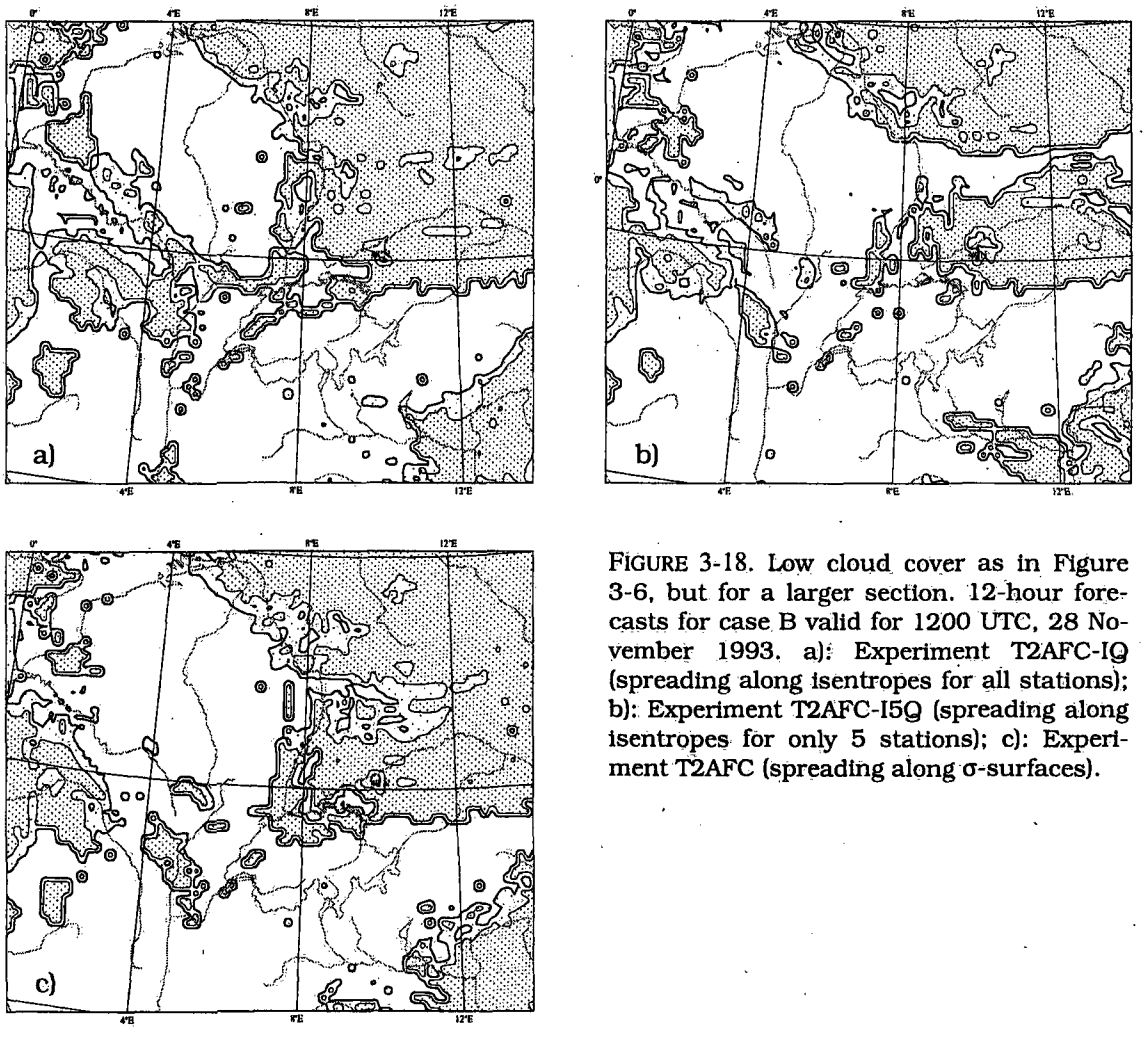

FIGURE 3-18. Low cloud cover as in Figure 3-6, but for a larger section. 12-hour forecasts for case B valid for 1200 UTC, 28 November 1993. a): Experiment T2AFC-IQ (spreading along isentropes for all stations); b): Experiment T2AFC-I5Q (spreading along isentropes for only 5 stations); c): Experiment T2AFC (spreading along σ-surfaces).

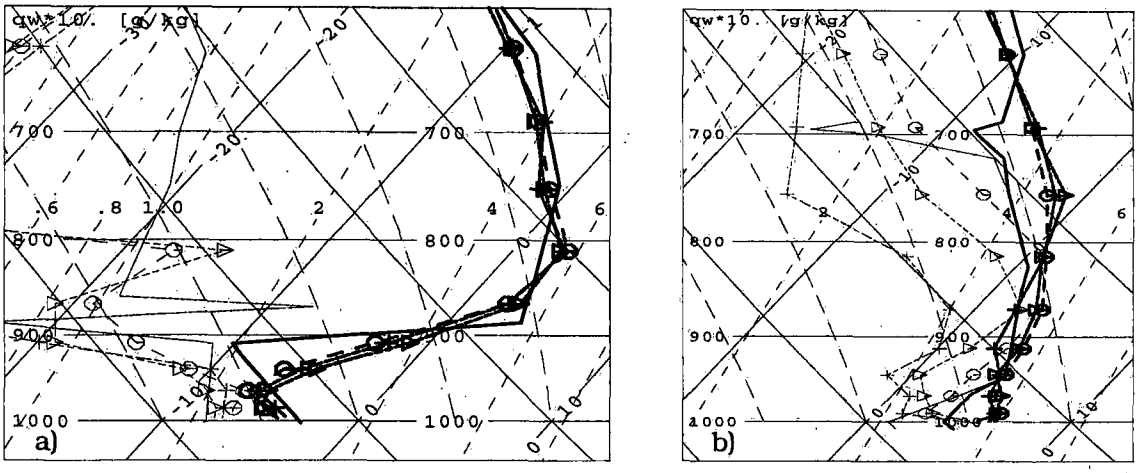

FIGURE 3-19. Vertical profiles as in Figure 3-7. 12-hour forecasts for case B. a): Nancy; b): Udine. The following four profiles are shown: solid lines: observation; circles: experiment T2AFC-IQ (spreading along isentropes for all stations); triangles: experiment T2AFC (spreading along σ-surfaces); crosses: experiment T2AFC-I5Q (spreading along isentropes for Payerne, Lyon, Stuttgart, Munich, Milano only).

realistic isentropic distribution (DMA and SMF). In a further experiment, lateral spreading is performed along isobaric surfaces. It yields results similar to spreading along isentropes, and this indicates that the nudging scheme is relatively insensitive to noise-like features and details of the shape of the surfaces used for lateral spreading.

- Spreading along isentropes for all rawinsonde stations (instead of only 5) has rather little impact in case A1. However in the 12-hour forecast in case B, it significantly improves the low cloud cover (Figure 3-18, cf. Figure 3-3) and the vertical structure at several stations (Udine, cf. Figure 3-19). A clear positive impact is even found in the Swiss Plateau where for the closest rawinsonde stations, spreading along isentropes is used in both experiments. Note further that the lateral spreading scheme does not only have an effect near steep orography, but also over moderate terrain with variations of about 200 to 400 metres. Spreading along σ-surfaces, or a limitation of spreading along isentropes to a subset of stations can result in smoothing of the inversion between the stations (cf. Stensrud and Fritsch, 1994).

In conclusion, increasing the effective vertical resolution of assimilated relative humidity, enhancing the consistency and balance of the model state at the beginning of the nudging period, and applying the new scheme to all soundings each tend to improve the results with spreading along isentropes. With the inclusion of these features, spreading along isentropes renders analyses and forecasts of modest superiority in cases A and B and of similar quality in case C when compared with those produced by spreading along σ-surfaces. However, this benefit from spreading remains small in the vicinity of steep orography. The fact that the dynamics is directly involved in the assimilation process probably makes nudging somewhat more tolerable to (temperate) misspecification of the spreading than 3-D analysis methods. However, previous work (e.g. Wright et al., 1994) indicates that e.g. the assumed vertical location of cloud (i.e. of saturation) relative to the vertical structure of the model fields (e.g. of temperature) is critical also with nudging.

Note finally that the horizontal diffusion along σ-surfaces is likely to be more harmful with spreading along isentropes which directly introduces sharp gradients on the model's σ-surfaces. With a more adequate formulation of the diffusion, one may expect a larger benefit from spreading along isentropes.

3.5 Assimilation of relative humidity surface observations

An accurate specification of the initial humidity is known to be important when the dynamical forcing is weak (cf. Lorenc et al., 1994). It is also well known that humidity has significant small-scale variations in time and space (Lilly and Perkey, 1976; Zou et al., 1995). Because of the lack of temporal and spatial resolution in the conventional rawinsonde network, moisture is not well sampled, and the resulting mesoscale moisture structure is often aliased to larger scales (Kuo et al., 1993). Although the low stratus in the cases treated here is relatively uniform in space and time, it is still not adequately resolved in the horizontal (cf. section 3.1.2). On the other hand, the vertical structure below the cloud top usually is relatively regular down to the ground (see section 3.1.2), and low stratus is often coupled to the ground, particularly near high terrain. For these reasons it is interesting and potentially promising to apply the assimilation of screen-level humidity observations with their high horizontal and temporal resolution to low stratus cases.

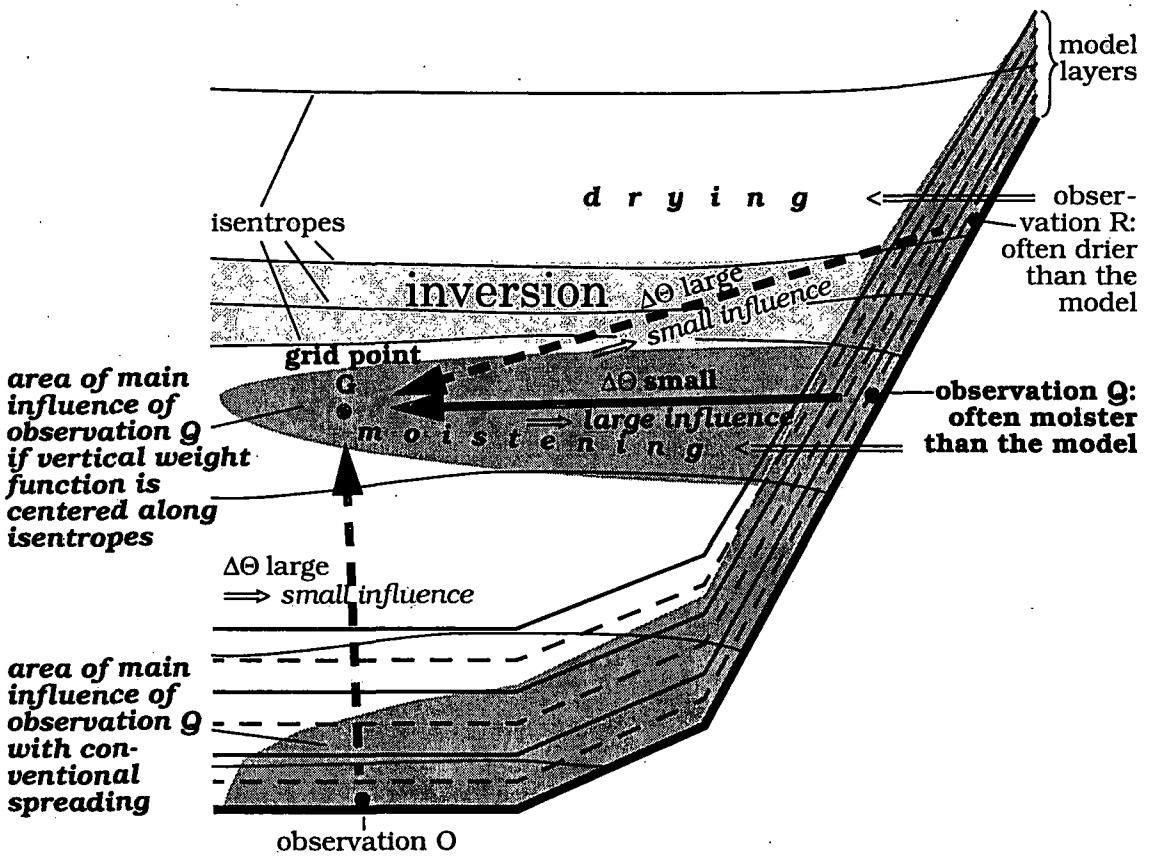

FIGURE 3-20. Illustration of different ways of lateral spreading of the influence of screen-level (humidity) observational information from surface stations located at different altitudes in the environs of steep orography. For further explanation, see text.

The assimilation technique is described in section 2.2 except for the spreading of the influence of the observations. Commonly, the influence of single level data such as screen-level data is at first spread vertically, often as a function of pressure (cf. Maycock and Macpherson, 1994). Alternatively, the boundary layer height was used as a limit for the vertical influence of surface data by Stauffer et al. (1991). In a second step the resulting vertical column of weighted observation increments is spread laterally along the model levels.

This approach is adopted in experiment S3A-I5. A Gaussian vertical weight function (as a function of log(pressure)) is used with an e-folding decay height of about 400 m for relative humidity (cf. Maycock and Macpherson, 1994: a value of 300 m yields the statistical fit used at the UKMO).

As an alternative, a strategy analogous to spreading along isentropes and based on the same considerations (cf. section 3.4) is applied in experiment T3A-I5. Here, the vertical weight function for screen-level data is a Gaussian of the potential temperature difference between the target grid points and the lowest model layer at the observation stations. Figure 3-20 sketches the difference between T3A-I5 and S3A-I5 of the main area of influence for a screen-level observation Q made just below an elevated inversion. Note that the e-folding decay rate of 1 K as selected for the vertical weighting in T3A-I5 is usually less than a rate of 400 m (cf. Figure 3-17). Hence the influence of screen-level data tends to be smaller over flat areas but larger near the Alps compared to S3A-I5.

The impact of the screen-level humidity data is illustrated for case A2. Here, the 30-layer reference experiment N3A-I5 (cf. Table 3-3), which assimilates only rawinsonde data, misses the low stratus over the central and eastern Swiss Plateau in the analysis and 12-hour forecast (cf. Figure 3-21, and cross sections in Figure 3-22). The assimilation of screen-level humidity data in T3A-I5 (with spreading mainly along isentropes) greatly enhances the analyzed low-level humidity and cloud over the Swiss Plateau and adjacent German areas, and causes drying around the Alpine crest. The height of the cloud top coincides with the inversion base at about 1200 m to 1500 m (Figure 3-22) and agrees well with observations (- areas above 1500 m were cloud-free). In the subsequent 12-hour forecast period (right columns of Figure 3-21 and Figure 3-22), the low cloud tends to thin too much, and dissipates partly over the Swiss Plateau. However, the fields of humidity and, due to radiational feedback, particularly of temperature remain significantly more consistent. This includes a higher relative humidity maximum further above the ground, and fractional cloudiness topped by a stronger and horizon-

Experiment name	Use of screen-level humidity data from all surface stations	surfaces along which the influence of screen-level data is largest
N3A-I5	No	-
T3A-I5	Yes	isentropic
S3A-I5	Yes	sigma
T3A750-I5	stations below 750 m only	isentropic

TABLE 3-3. Description of experiments as discussed for the assimilation of screen-level humidity data in case A2. See experiment T3A-I5 in Table 3-2 for the definition of the lateral spreading of rawinsonde data as used here.

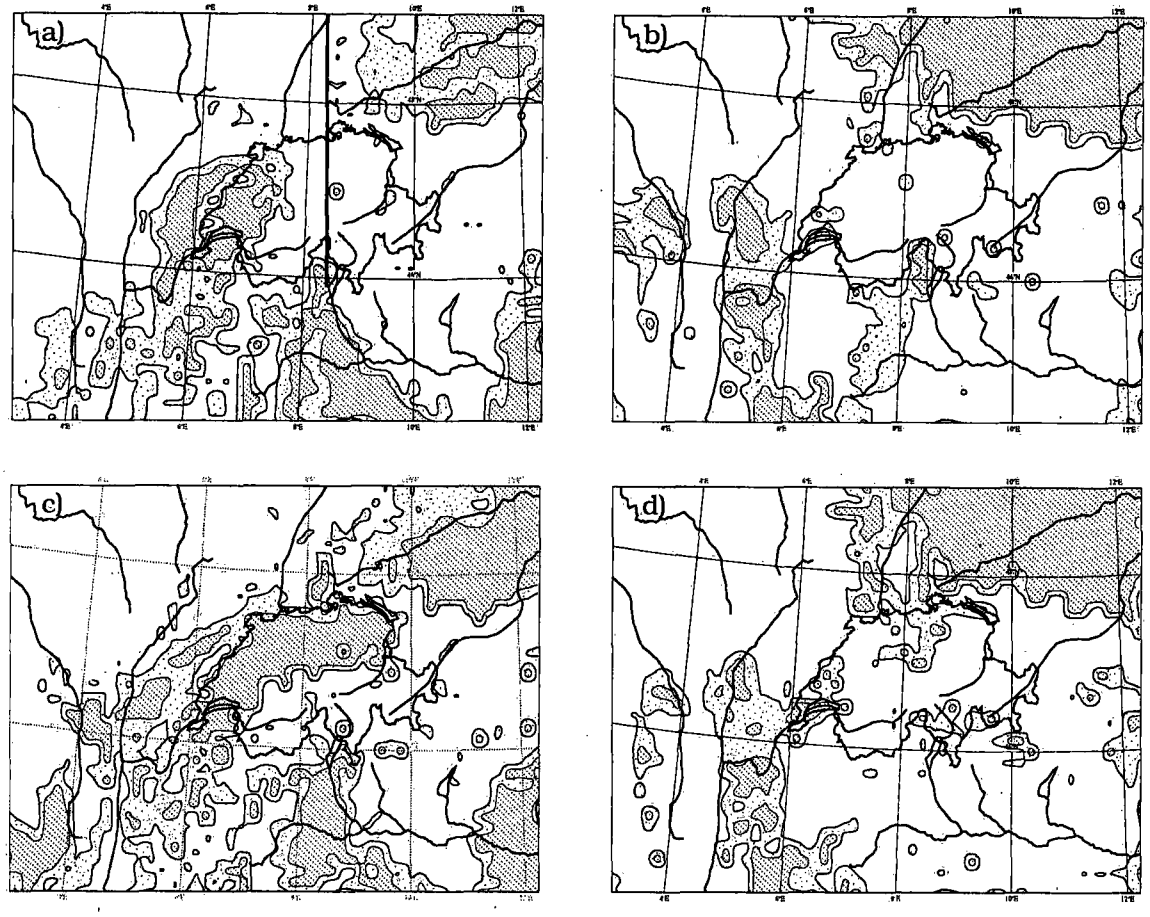

FIGURE 3-21. Low cloud cover as in Figure 3-6. Case A2. Left column: analyses valid for 1200 UTC, 20 November 1993. Right column: 12-hour forecasts valid for 0000 UTC, 21 November. a), b): N3A-I5: assimilation of rawinsonde data only; c), d): T3A-I5: including screen-level humidity, lateral spreading with largest influence along isentropes. See also Table 3-3. The thick black line in a) indicates the position of the cross sections in Figure 3-22.

tally more uniform inversion. Pronounced smoothing of the inversion occurs only very close to the Alpine slope.

In the analysis, the cloud band is absent if screen-level humidity data are assimilated merely from stations below 750 m (experiment T3A750-I5, see Figure 3-22e). This indicates, that the main source of the additional moisture resulting in the cloud band in T3A-I5 are positive humidity observation increments at surface stations between 750 m and 1500 m, which are spread primarily quasi-horizontally along isentropes (cf. Figure 3-20). Since the horizontal half width radius of influence is 115 km these data can influence the whole of the Swiss Plateau. With conventional spreading (experiment S3A-I5), the cloudiness is mainly confined to a near-surface band along the northern Alpine slope (Figure 3-22e) as expected (cf. Figure 3-20). However, dynamical and physical processes spread some of the additional humidity over the whole of the Swiss Plateau (although the wind direction does not indicate significant advection from the northern Alpine slope towards the Plateau). Remarkably, these adjustment processes are strong enough to render the 12-hour forecast of S3A-I5 similar to that of T3A-I5.

In cases A1, B, and C, the use of only rawinsonde data leaves less scope for improvement in the Swiss Plateau. The analyses still benefit slightly from the screen-level hu-

midity data but the effects in the forecasts are mixed. Notably, the low cloud cover is correctly enhanced in the eastern Swiss Plateau in case B, but slightly (erroneously) reduced in the western Swiss Plateau due to dry conditions at the stations on the Jura Mountains. These mixed effects are even enhanced in the 12-hour forecast (Figure 3-23). In case C, the impact is marginal throughout. Some further remarks are appropriate.

- The main benefit from the assimilation of screen-level humidity and from the spreading along isentropes pertains to central and northern Switzerland and its immediate environs where middle and high orography (up to 2500 metres) is well and relatively uniformly represented by the surface observing network. Elsewhere - and close to Payerne - the benefit is generally limited. This indicates that a uniform vertical distribution of representative surface stations is important.
- The area which is primarily affected by the screen-level data (i.e. the eastern Swiss Plateau) is rather flat. Hence, the isentropes tend to approximate the σ–surfaces, and the forcing of the nudging in T3A-I5 is relatively continuous within a σ–layer there. The resulting limitation of the effect of the horizontal diffusion probably contributes to the finding that in the present experiments, the impact of spreading along isenstropes appears to be in better agreement with the theoretical considerations for screen-level data than for rawinsonde data.
- The limited impact of the screen-level humidity data on the forecasts is in line with previous work by Clark (1994) and Maycock and Macpherson (1994) who noted that the benefit on the prediction of fog or low stratocumulus was largely confined to the first 6 to 12 hours of the forecast period. Even a 3-D relative humidity analysis derived from a cloud analysis had impacted positively only during the first 15 forecast hours (Wright et al., 1994).
- The concept of spreading the influence of screen-level humidity data along isentropes is attractive for low stratus cases because of the stable stratification of the atmosphere, and because the representiveness of these data for the free atmosphere is influenced by the relatively uniform horizontal thermal and humidity structure. The problem of representiveness is further alleviated by the restricted selection of surface stations (see section 2.2) which excludes stations from exposed mountain peaks and deep mountain valleys. In other meteorological situations however, it may be potentially dangerous to spread the influence of Alpine screen-level data over an area as large as in T3A-I5. Note that little is known about the surface layer in steep terrain, and boundary-layer parameterization for complex terrain is recognized as a particular weakness in today's NWP models (cf. Binder and Schär, 1995).

FIGURE 3-22. (see right): North-south vertical cross sections of temperature (solid lines) and relative humidity (colour shading) across the Alps and the Swiss Plateau near Zurich (as indicated by the thick black line in Figure 3-21a). Above about 90 % relative humidity (blue colours), the model starts producing cloudiness except close to the ground.
Case A2. Left column: analyses valid for 1200 UTC, 20 November 1993. Right column: 12-hour forecasts valid for 0000 UTC, 21 November 1993. Description of experiments (see also Table 3-3):
a), b): N3A-I5: assimilation of rawinsonde data only;
c), d): T3A-I5: lateral spreading of screen-level humidity with largest influence along isentropes;
e), f)): T3A750-I5: as T3A-I5, but using surface stations below 750 m only;
g), h): S3A-I5: spreading of screen-level humidity: max. influence along σ-surfaces (conventional).

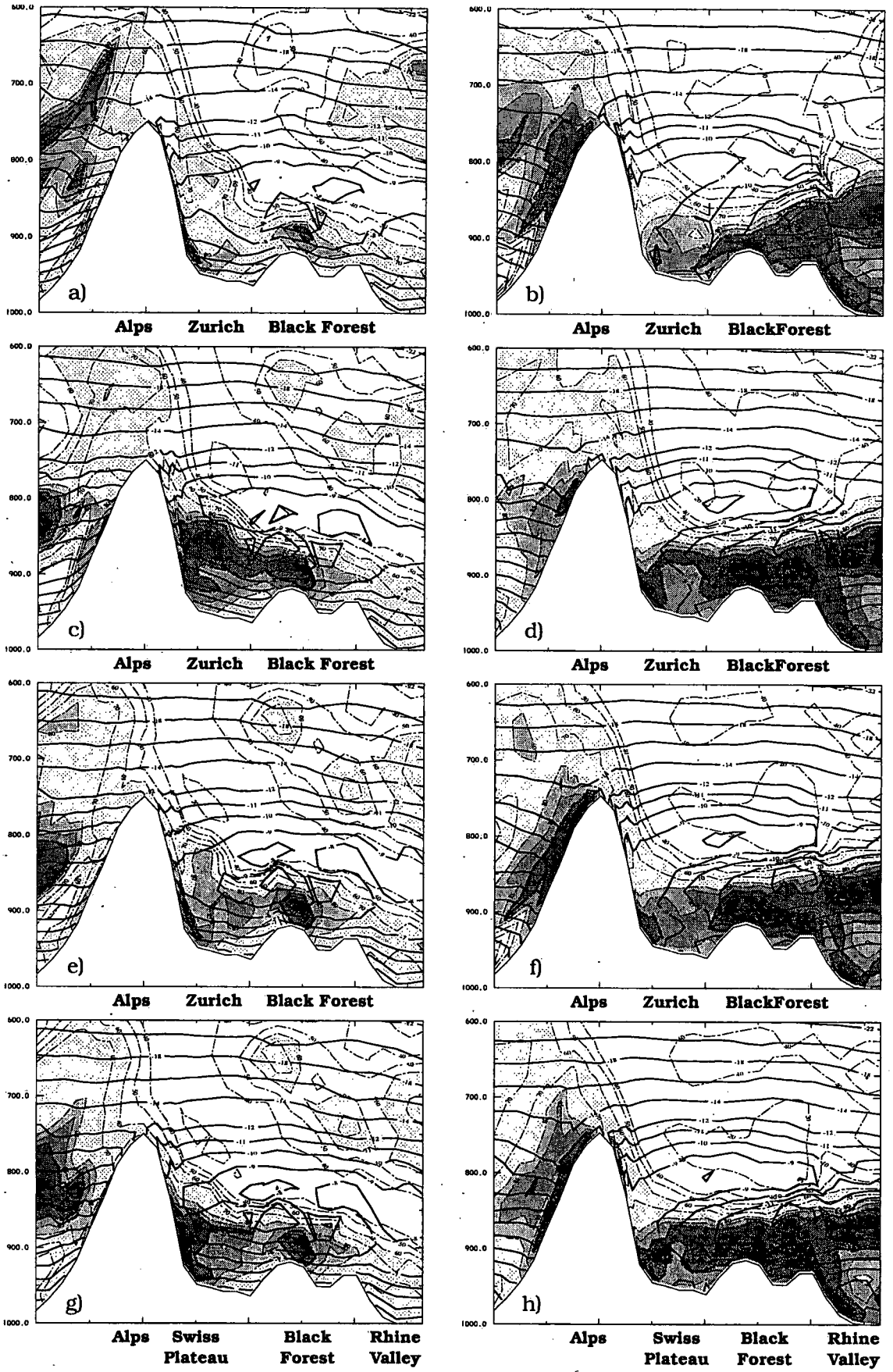
a)
Alps Zurich Black Forest
b)
Alps Zurich BlackForest
c)
Alps Zurich Black Forest
d)
Alps Zurich BlackForest
e)
Alps Zurich Black Forest
f)
Alps Zurich BlackForest
g)
Alps Swiss Plateau Black Forest Rhine Valley
h)
Alps Swiss Plateau Black Forest Rhine Valley

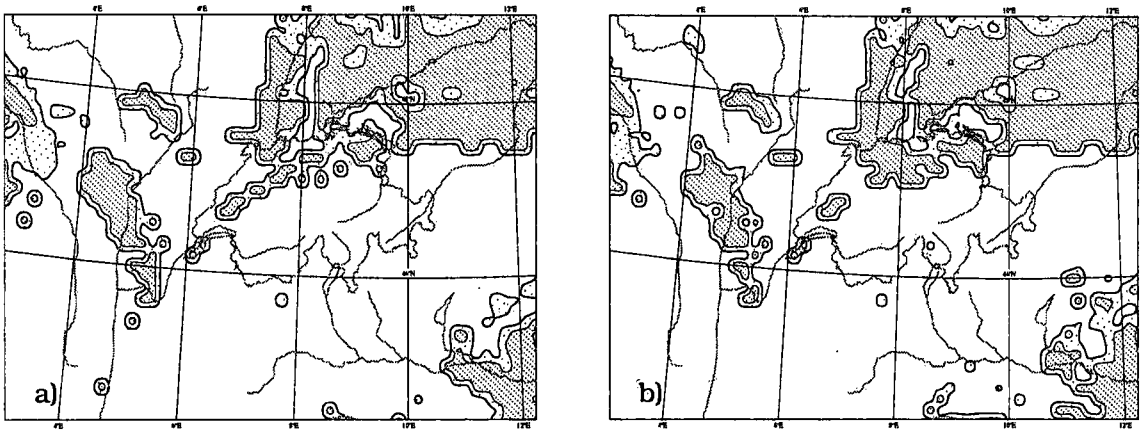

FIGURE 3-23. Low cloud cover as in Figure 3-6. 12-hour forecasts for case B valid for 1200 UTC, 28 November 1993. a): assimilation of rawinsonde data only; b): assimilation of rawinsonde and screen-level data. (Spreading of rawinsonde data along σ-surfaces, influence of screen-level humidity largest along isentropes. Domain equals white square in Figure 3-3, upper right.)

- An increase of the e-folding decay height of the vertical weight function centred along the isentropes somewhat enlarges the influence of the data from those stations where the vertical data density is largest. In case A2, this tends to slightly enhance low cloudiness north and west of the Alps.

Some attention has also been devoted to the assimilation of screen-level wind data. Due to their poor representiveness in rough terrain, only two stations above 700 m are considered (cf. section 2.2). In all cases, the small impact from these data in the analyses disappears during the forecast period, and this agrees with Cardinali et al. (1994).

3.6 Comparison to optimum interpolation

Optimum interpolation (OI) is currently the most commonly used data assimilation method for operational NWP purposes, and is used in the Deutschland Modell (DM). Therefore, consideration of the present nudging scheme in comparison with the state-of-the-art Deutschland Modell analyses is appropriate to provide some indication of the scheme's performance in cases of low stratus near steep orography, and to help estimating the suitability of the nudging technique for operational mesoscale NWP near steep orography.

3.6.1 The analysis of the Deutschland Modell and the experimental set-up

The DM analysis system is a limited-area version of the OI analysis scheme of the ECMWF (Lorenc, 1981; Lönnberg and Shaw, 1987; Shaw et al., 1987). A multivariate analysis is performed for wind components, geopotential and surface pressure, and a univariate analysis is done for relative humidity.

The horizontal forecast error correlations used until February 1994 (pertinent to cases A and B) for the mass and wind fields are based on ECMWF values (Hollingsworth and Lönnberg, 1986; Lönnberg and Hollingsworth, 1986; Lönnberg, 1988), but modified to more narrow correlations. Thereafter (pertinent to case C), new values derived from a statistical verification of EM 6-h forecasts against rawinsonde data have been used.

The new correlations have an even shorter component length scale (Buchhold and Paul, 1995), and have predominantly impacted on the wind fields (Wergen, 1995). The horizontal correlation for the mixing ratio is a simple inverse exponential function with an e-folding decay scale of 600 km, i.e. considerably larger than what is used in the nudging scheme. The vertical correlations are the empirical positive definite functions as derived at the ECMWF (Hollingsworth and Lönnberg, 1986; Lönnberg and Hollingsworth, 1986), but modified to yield more narrow correlations below 700 hPa. They were further modified in September 1994 (concerns case C).

For height correlations and standard deviations of observation errors, use is made of the ECMWF values for North America (ECMWF, 1992). Significant-level data from radiosondes (TEMP, PILOT) are only used below 700 hPa before September 1994 (concerns cases A and B) and below 500 hPa thereafter. All rawinsonde data up to 275 hPa are used for humidity. Further data include aircraft data (AIREP, ASDAR: winds), SATOB, SATEM and screen-level data (pressure, humidity, winds from ships), and total cloud amount and precipitation data are used to impose saturation under certain circumstances.

All forecasts are produced with reduced horizontal diffusion to allow for realistic fine structures near steep orography. However, for the comparison, (i) full diffusion is de-

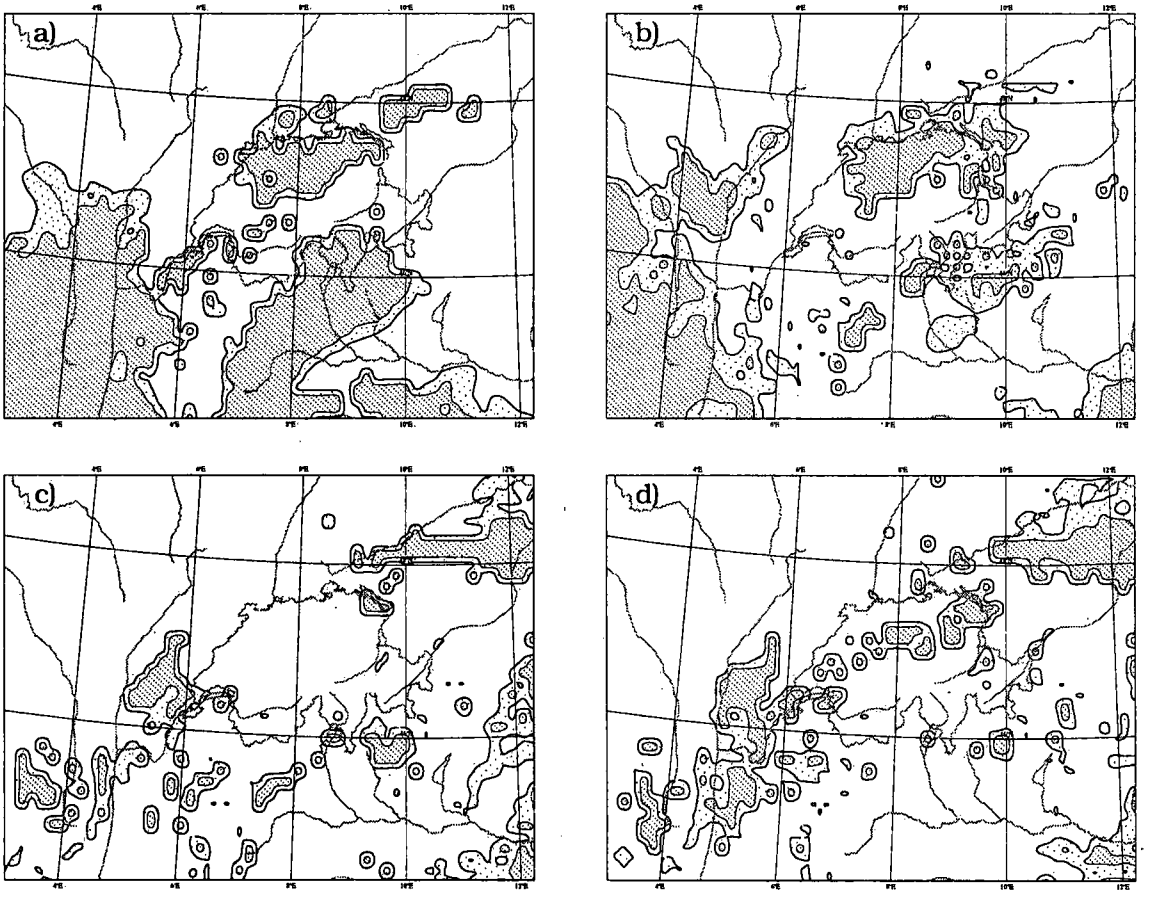

FIGURE 3-24. Low cloud cover as in Figure 3-6. Case A1. Top row: analyses valid for 1200 UTC, 19 November 1993; bottom row: 24-hour forecasts valid for 1200 UTC, 20 November 1993. a), c): Experiment D2A, starting from OI analysis; b), d): Experiment T2AFC starting from nudged analysis.

ployed in the nudging period like in the data assimilation period for the DM analyses, and (ii) the same distribution of 20 model layers is used as for the DM. Note that the data base for the DM analyses includes more data types.

Rawinsonde data are spread along σ-surfaces (since spreading along isentropes is costly for operational NWP purposes at present), and the 12-hour nudging period starts from 12-hour forecasts. The nudging experiments are denoted as T2AFC, and the integrations starting from OI analyses as D2A.

3.6.2 Results

Case A1

D2A correctly analyzes more low cloudiness (Figure 3-24) where the observed cloud top is relatively high (at about 1500 m, i.e. in the Lyon region and in the northeastern Po Valley). However, the vertical temperature and humidity profiles of T2AFC (Figure 3-25)

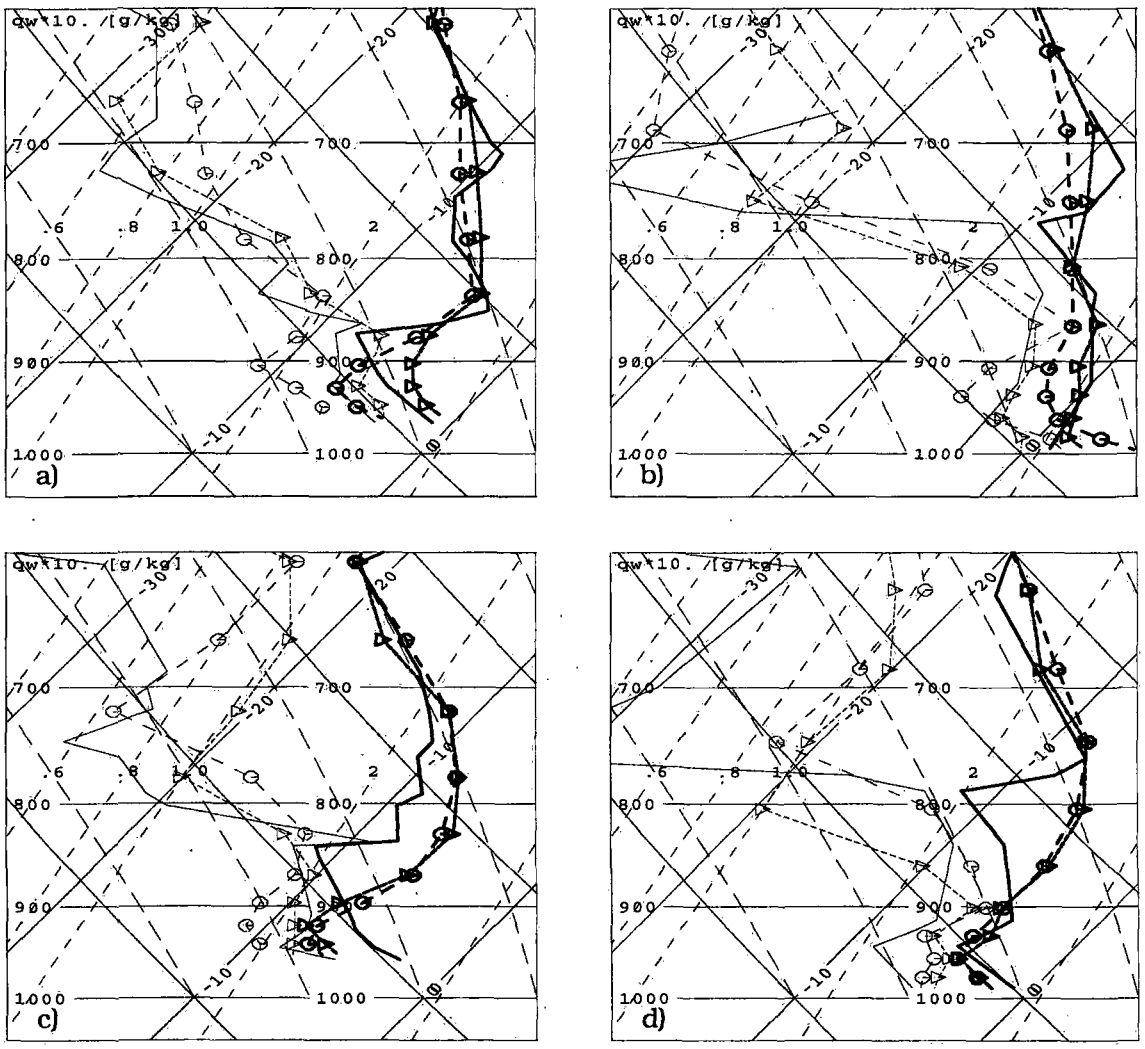

FIGURE 3-25. Vertical profiles as in Figure 3-7. Case A1. Top row: analyses; bottom row: 24-hour forecasts valid for 1200 UTC, 20 November 1993. a), c): Payerne; b), d): Lyon. The following three profiles are shown: solid lines: observation; circles: experiment D2A starting from OI analysis; triangles: experiment T2AFC starting from nudged analysis.

match the rawinsonde soundings clearly better, and this more consistent initial vertical structure imposed by the nudging results in a significantly superior 24-hour forecast, e.g. of the vertical profile at Payerne (Figure 3-25), and of the low cloud cover (Figure 3-26) in the Lyon region and Swiss Plateau.

Case B

Both analyses reproduce the low cloud cover over most of France and Germany very well (Figure 3-26), but T2AFC is clearly superior for the Swiss Plateau. In the 12-hour forecast (compare to Figure 3-3), D2A predicts too much low cloud in the central Po Valley, but too little over north-eastern France and west of the Jura Mountains. In T2AFC, the underestimation of cloud over France is even worse (- note that spreading along isentropes does somewhat better here, cf. Figure 3-18).

The vertical profiles, e.g. at Paris (Figure 3-27), reveal that whilst T2AFC follows the observations exactly, D2A grossly overestimates the humidity above the inversion base, and this is found in a wide area as illustrated in vertical cross sections (Figure 3-29). In contrast to nudging, which analyzes well the typical low stratus structure, the OI

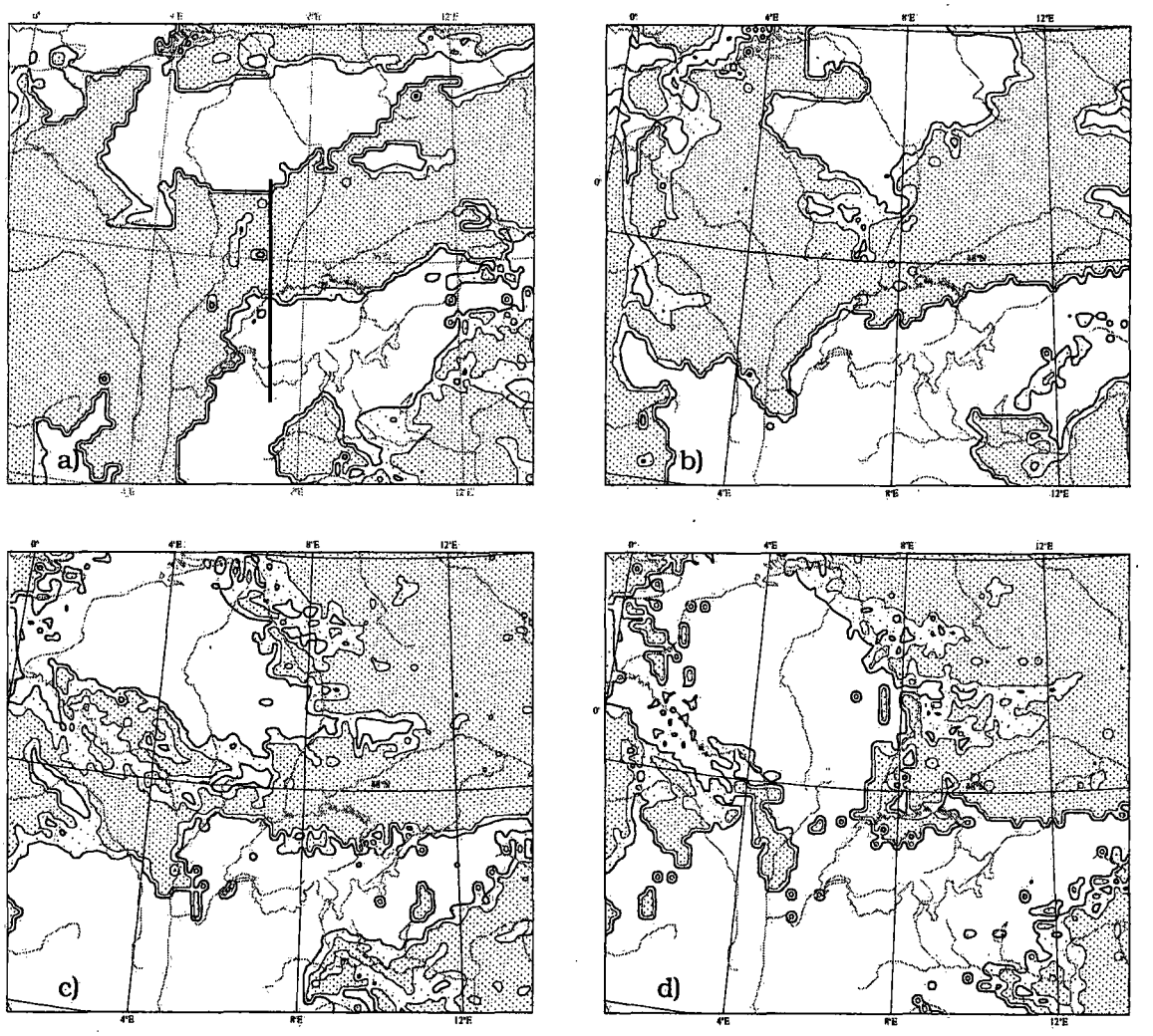

FIGURE 3-26. Low cloud cover as in Figure 3-6, but for a larger section. Case B. Top row: analyses valid for 0000 UTC, 28 November 1993; bottom row: 12-hour forecasts valid for 1200 UTC, 28 November 1993. a), c): Experiment D2A, starting from OI analysis; b), d): Experiment T2AFC starting from nudged analysis. The thick black line in a) denotes the position of the cross sections in Figure 3-29.

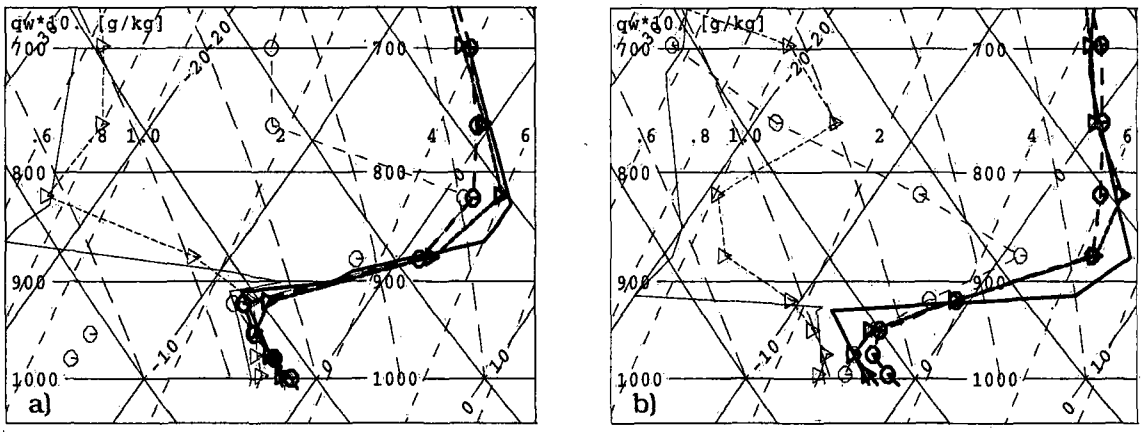

FIGURE 3-27. Vertical profiles for case B as in Figure 3-7. Location: Trappes (Paris). a): Analyses valid for 0000 UTC, 28 November 1993; b): 12-hour forecasts valid for 1200 UTC, 28 November 1993. The following three profiles are shown: solid lines: observation; circles: experiment D2A starting from OI analysis; triangles: experiment T2AFC starting from nudged analysis.

renders horizontally very inhomogeneous the analyzed humidity. Its maximum is too low close to the Alps (cf. also Figure 3-30a), but elsewhere, saturation reaches too high (i.e. above the inversion base), and the vertical relative humidity gradient within and above the inversion is far too weak everywhere.

These characteristic differences pertain in the forecast period, but spurious processes occur (cf. Figures 3-27, 3-29, 3-30), namely vertical smoothing, lowering of the inversion and its base to close to the ground, and moderate drying notably at the cloud top. As a result, saturation and cloudiness is erroneously lost more readily in T2AFC than in D2A which, in this respect, benefits from its humidity surplus. Otherwise however, the observed profiles (e.g. at Paris, Figure 3-27b) are matched still significantly better by T2AFC than by D2A which has also a greater tendency to smoothe inversions and underestimate their top temperatures due to the excessive moisture (Figure 3-29, Figure 3-30d). Near steep orography, e.g. at Payerne (cf. Figure 3-30b), the smoothing and its detrimental effects are significantly enhanced.

Advection of moist cold air at low levels and orographic blocking appears to counter the smoothing effects. In southern Germany, low-level moist cold air is advected from the

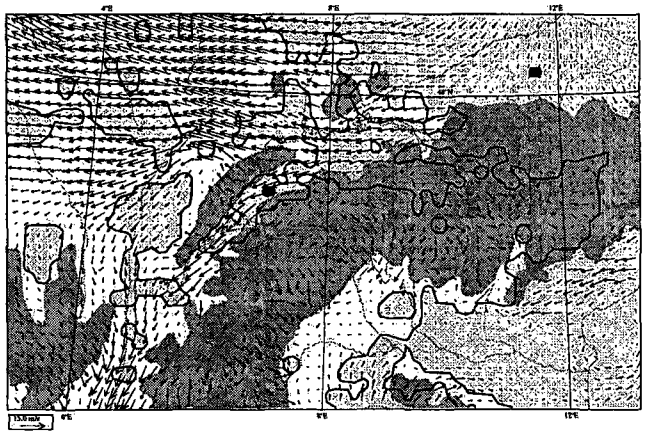

FIGURE 3-28. 24-hour forecast of experiment T2AFC (with a nudged analysis) valid for 0000 UTC, 29 November 1993. (Domain equals white square in Figure 3-3, lower left).
Wind vector field at 925 hPa. Dark shaded areas denote orography above 750 m (which approximates 925 hPa). In these areas, the wind vectors denote the wind field of the lowest model layer. Contoured light shaded areas are covered with more than 20 % low-level cloudiness. The black dots denote the locations of Payerne and Munich.

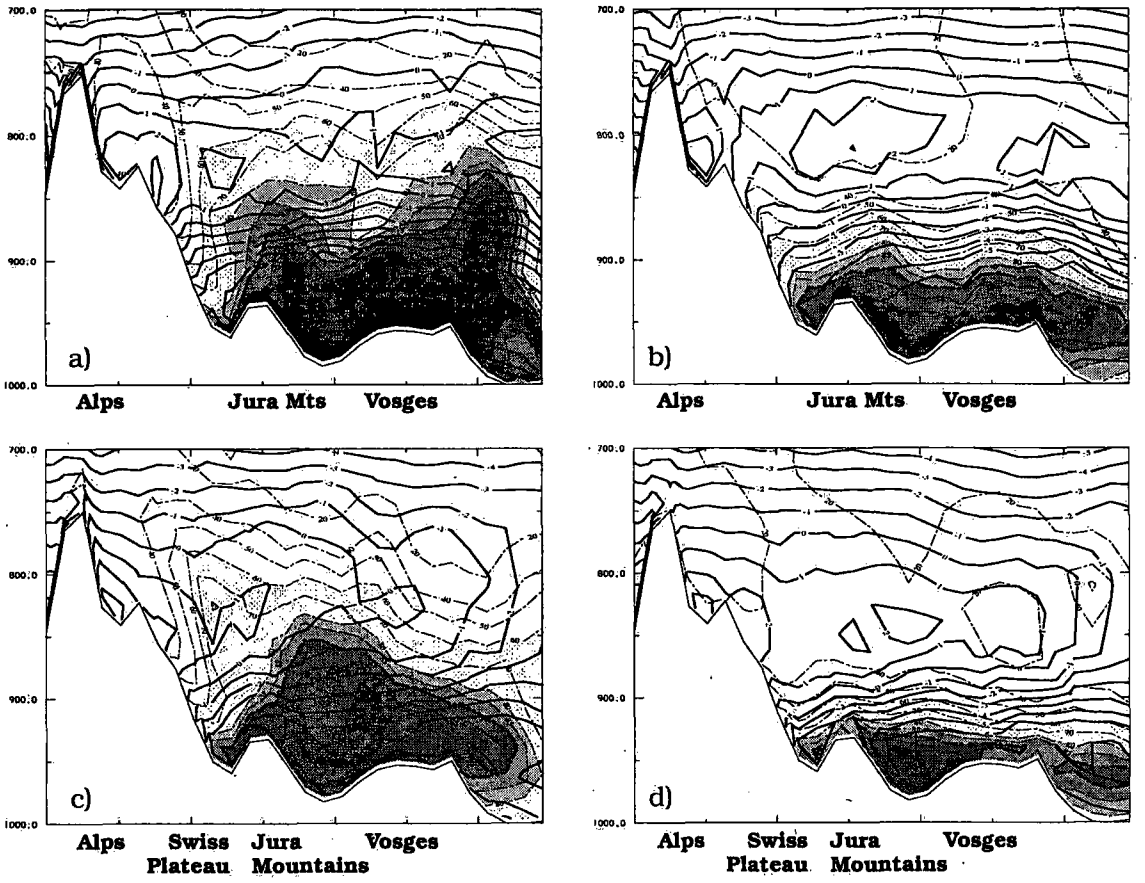

FIGURE 3-29. North-south vertical cross sections of temperature (thick solid lines, in K) and relative humidity (shading and dashed lines, in %) across the Alps and the western Swiss Plateau near Payerne (as indicated by the thick black line in Figure 3-26a). Above about 90 % relative humidity (thick dashed lines), the model starts producing cloudiness except close to the ground. Case B. Top row: analyses valid for 0000 UTC, 28 November 1993; bottom row: 12-hour forecasts valid for 1200 UTC, 28 November 1993. a), c): Experiment D2A, starting from OI analysis; b), d): Experiment T2AFC starting from nudged analysis.

north-east, and flow splitting west of Munich (Figure 3-28) indicates the blocking north of the Alps. Unlike in D2A, the predicted inversion, humidity structure, and cloud top height in T2AFC agree excellently with the observations at Munich (Figure 3-30d) and at Stuttgart. In the Swiss Plateau, the Bise (northeasterly wind) is at its peak at +24 h (Figure 3-28), and the blocking effect between the Jura Mountains and the Alps (cf. section 3.1.2) is indicated (in agreement with observations) by a veering of the wind to the southeast in a thin layer above the crest of the Jura Mountains (cf. Schubiger et al., 1987). In contrast to +12 h (Figure 3-27, Figure 3-30b) and +36 h, low cloud pervades the western Swiss Plateau (Figure 3-28) at +24 h in both experiments, and the inversion at Payerne (Figure 3-30c) is lifted off the ground. This renders more realistic the forecasted vertical structure despite continual vertical smoothing, exceesive humidity in D2A, and a significant low-level cold bias in T2AFC which is probably due to underestimation of relative humidity and enhanced radiational cooling. Note, that the wind profiles with a pronounced shear at the observed inversion height is hardly smoothed in D2A and T2AFC, but the Bise beneath is too strong (Figure 3-30c).

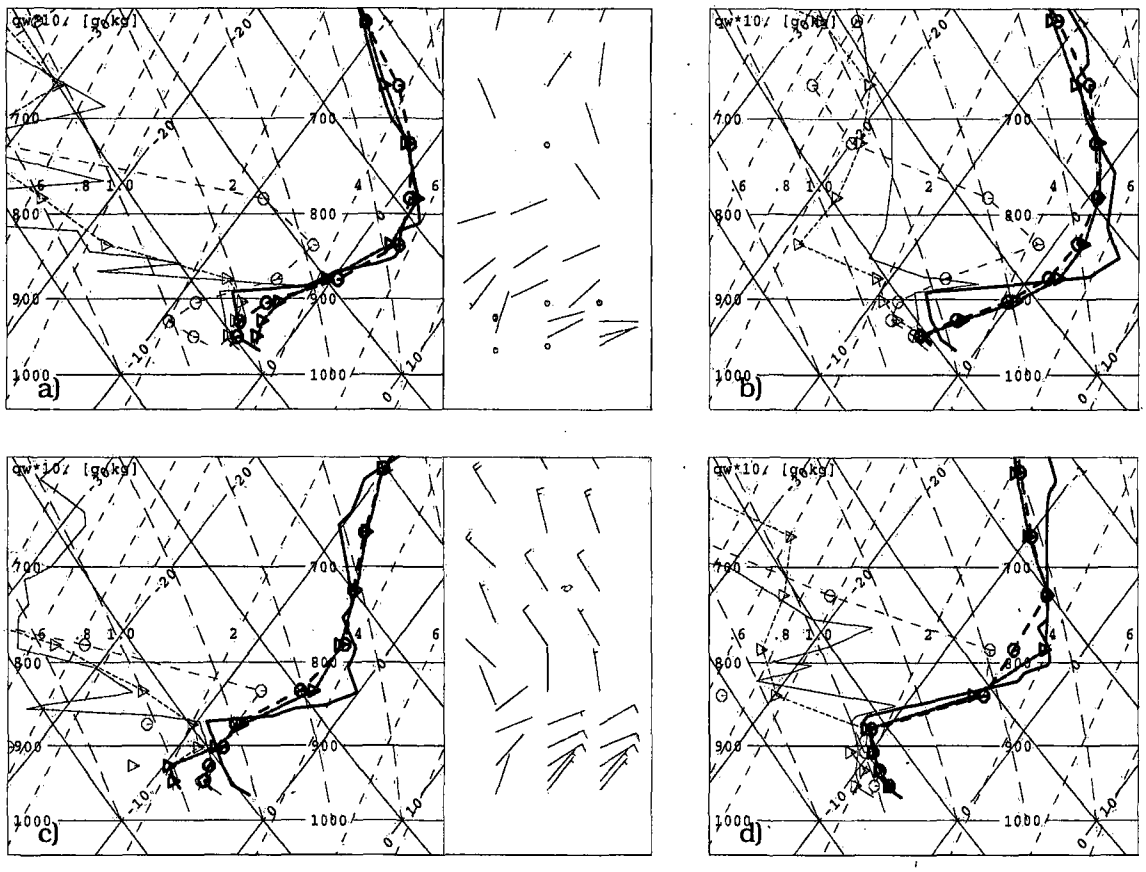

FIGURE 3-30. Vertical profiles for case B as in Figure 3-7.
a): Analyses at Payerne valid for 0000 UTC, 28 November 1993;
b): 12-hour forecasts at Payerne valid for 1200 UTC, 28 November 1993;
c): 24-hour forecasts at Payerne valid for 0000 UTC, 29 November 1993;
d): 12-hour forecasts at Munich valid for 1200 UTC, 28 November 1993.
The following profiles are shown (winds from left to right): solid lines: observation; circles: experiment D2A starting from OI analysis; triangles: experiment T2AFC starting from nudged analysis.

Case C

This case (cf. Figure 3-31) exhibits differences in the vertical structure similar to case B. Whilst the analyzed vertical profiles of T2AFC follow the observations fairly well, D2A produces excess moisture above the observed inversion, however without attaining saturation at any height in some areas. Thus, the OI analysis misses low cloudiness not only in the Swiss Plateau, but also in some regions with less orography (e.g. the Saône basin, areas in southern Germany and eastern Belgium).

In the forecast, the excess moisture induces more low cloud, and again reduces its erroneous dissipation due to vertical smoothing which in T2AFC results in moderate underprediction of low cloud in the Swiss Plateau and north of Switzerland at +12 h. The cloud top height is too low in both experiments. The 24-hour forecasts of D2A and T2AFC are relatively similar (not shown). The conversion of relatively shallow fog in the Po Valley to a thick low stratus with a cloud top height at around 2000 m is well predicted, but the dispersion of the low cloud over northern Germany, eastern Holland and Belgium is not captured.

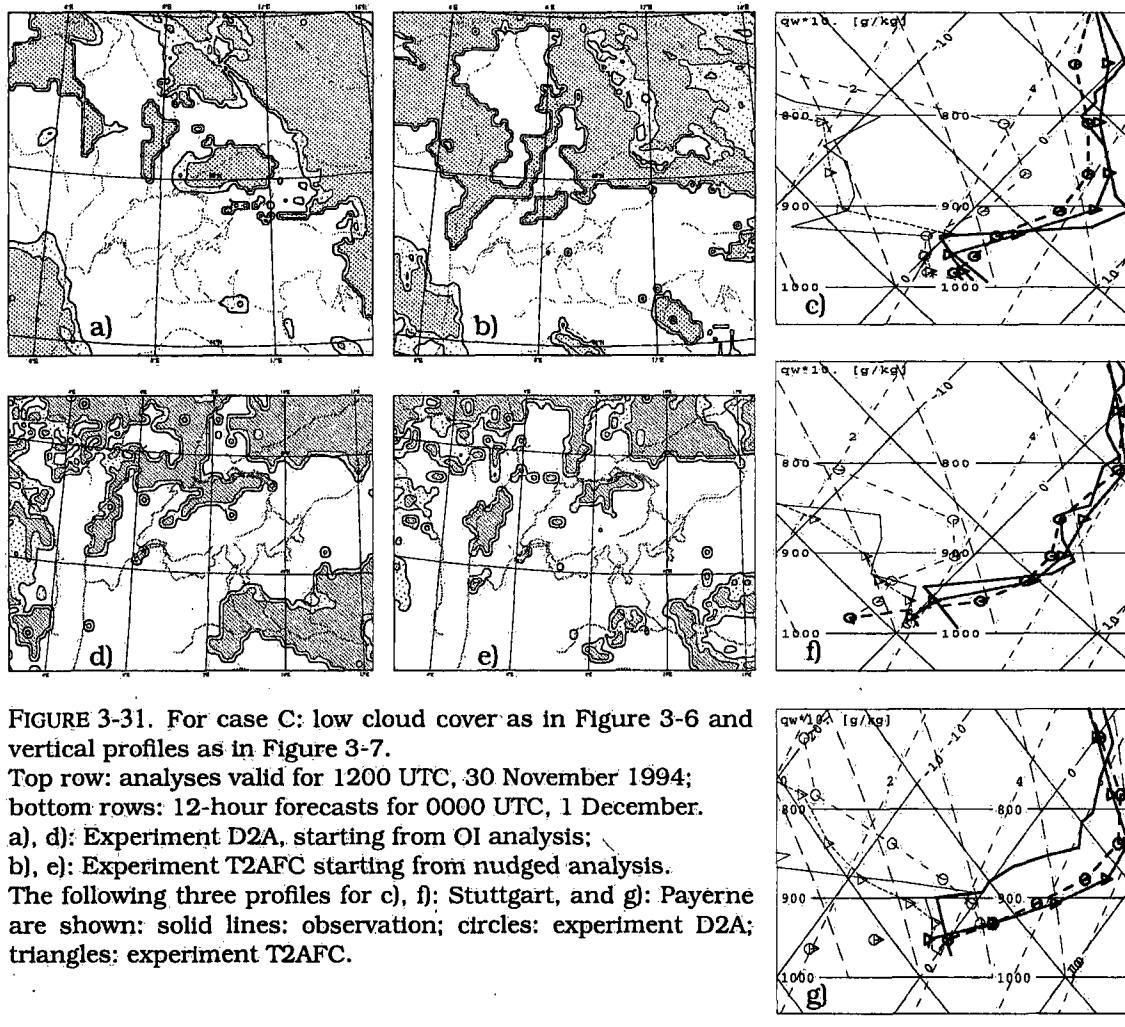

FIGURE 3-31. For case C: low cloud cover as in Figure 3-6 and vertical profiles as in Figure 3-7.
Top row: analyses valid for 1200 UTC, 30 November 1994;
bottom rows: 12-hour forecasts for 0000 UTC, 1 December.
a), d): Experiment D2A, starting from OI analysis;
b), e): Experiment T2AFC starting from nudged analysis.
The following three profiles for c), f): Stuttgart, and g): Payerne are shown: solid lines: observation; circles: experiment D2A; triangles: experiment T2AFC.

3.6.3 Vertical smoothing: cause, and impact on the schemes' performance

In summary, the vertical profiles of the nudging experiments match the observed profiles far better at the analysis time, and often also in the forecast period. Whilst the vertical profiles particularly of humidity are often smoothed in the OI analyses which is probably partly attributable to the vertical forecast correlations, the vertical gradients of the nudged analyses are strong, and their spatial structures are physically consistent with low stratus conditions. However, the SM, alike other models (cf. Bretherton et al., 1994), appears to have a tendency to smoothe strong vertical gradients. Here, this smoothing often causes a warming of the inversion base and thus a lowering of the inversion, unlike e.g. in the ECMWF model, where inversions are often too high (Klinker, 1994). Moreover, it causes a reduction of the specific humidity and thus even a greater reduction of the relative humidity around the inversion base. Finally, saturation and cloudiness can get lost erroneously. This process is hampered in the OI experiments by the overestimated analyzed moisture, and as a result, the finding of case A and of Ballard et al. (1994) that more fog or low cloud over land is correctly retained in the forecasts with nudging as compared to static initialization, does not apply to cases B and C.

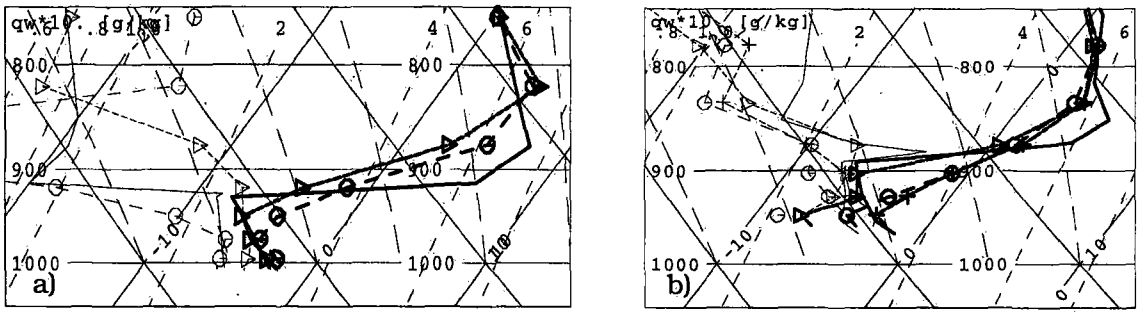

FIGURE 3-32. Vertical profiles as in Figure 3-7. 12-hour forecasts for case B valid for 1200 UTC, 28 November 1993. a) Trappes (Paris): solid lines: observation; circles: complete model; triangles: without humidity advection. b) Payerne: solid lines: observation; circles: complete model; triangles: without advection and diffusion of thermodynamic variables; crooses: without advection of thermodynamic variables.

This prompts the question about the reasons for this vertical smoothing and erroneous break up of low cloudiness, e.g. in case B.

First, erroneous prediction of physical mechanisms enhancing low stratus dissipation (cf. section 3.1.2) is considered. There is no erroneous cloud sheet above the low stratus which would reduce radiative cooling, and no indication of significant (overestimation of) subsidence has been found. Despite a modest overprediction of the wind speed at Paris in case B, no significant error in vertical wind shear occurs which may contribute to enhanced mixing and vertical smoothing of the inversion. Moreover, the advection of low-level moist air from Germany to northern France is simulated correctly since errors in the wind direction are small.

Therefore, the smoothing is caused more likely by spurious effects of the model formulation. As shown earlier in section 3.3, the smoothing effect depends on the vertical model resolution (cf. Figure 3-13) as the 40-layer model version preserves the inversion base height, saturation, and the cloud top height at Paris in case B.

Hence, several experiments have been carried out for case B with 20 layers (and with 40 layers for case 'B0' with analysis time at 0000 UTC, 27 November 1993) to examine the effect of different model components. All experiments start from the same nudged analysis T2AFC-IQ (see Table 3-2), and consist of 12-hour forecasts, in which different model components are switched off in the prognostic equations.

Solar irradiation is found to have a negligible effect on the warming at the cloud top (in accordance with observational experience, cf. section 3.1.2). Elimination of the thermal radiation term results in a faster dispersion of low cloud, i.e. the model's thermal radiation helps to maintain the low stratus by radiational cooling of the cloud top. Completely turning off the horizontal diffusion for the thermodynamic variables has a marginal effect (apart from Payerne). If the same is done for the vertical diffusion, the inversion base becomes cooler, but not higher elevated. This tends to raise the cloud top due to increased relative humidity but otherwise results in less agreement with the observed profiles. Only if the advection for the humidity is turned off then the specific humidity of the analysis is largely preserved in the forecast, saturation is maintained, and the cloud top at Paris (Figure 3-32a) is lowered correctly by merely one model layer. (This agreement with the observations certainly depends on the steadiness of the meteorological situation.)

A sensitivity of fog to the advection scheme used for the thermodynamic variables has already been noted by Ballard et al. (1991). Here, a 12-hour forecast has been made using a timestep of 10 seconds, or alternatively, the nudging and forecast period of case B has been recalculated with the 2-D Semi Lagrangian advection scheme (timestep: 240 seconds). In both experiments, the forecasted vertical structure at Paris and the low cloud cover is similar as in the reference experiment with Eulerian advection and a timestep of 90 seconds. This result, and the dependence on the vertical grid spacing, might indicate that the vertical rather than the horizontal part of the advection contributes mainly to the smoothing. An alleviation of this smoothing effect can be achieved by extra vertical model resolution, or by using a different advection scheme, e.g. shape preserving, particularly for humidity (as suggested by Tiedtke, 1994).

In rough terrain, the issue is more complicated. At Payerne, the lowering of the inversion base to (close to) the ground, e.g. at +12 h in case B, happens even when the advection of both the temperature and the humidity (i.e. total energy and total specific water content) is turned off (Figure 3-32b). It is the combination of advection and (even reduced) diffusion that contribute to this mechanism.

Due to the vertical smoothing, the effective model resolution is less than given by the thickness of the model layers. Hence, the nudging can introduce vertical scales not properly resolved by the present model in practice, and this can result in erroneous low stratus dissipation in the forecast. However, it is desirable to have very strong vertical gradients with low stratus, and a data assimilation scheme providing such gradients is potentially promising. It calls for an improvement of the model dynamics.

4 Control, refinement, and further applications of the nudging scheme

Nudging schemes require the specification of several parameters, e.g. the nudging coefficient, the horizontal correlation scale and the temporal weighting. No general theory exists (apart from the elegant, but computationally expensive adjoint methods) to determine the optimum values for these parameters, and the specification has been guided by some simple considerations and the results of numerical experiments. The main goal of this chapter is to assess the sensitivity of the scheme with respect to various parameters and components, to seek to optimize the parameter values, and to examine the impact of different data. Given the lack of suitable very high-quality gridded data sets for verification, the OSSE (Observing System Simulation Experiment) approach is adopted as the main experimental tool for this task, and applied to a variety of meteorological situations that pertain specifically to the Alpine region. Emphasis is laid upon the elimination of pressure errors related to mesoscale cyclones (section 4.3), and of errors in precipitation patterns associated with mesoscale convective systems and fronts (section 4.4.3). As a supplement, some real data experiments are performed as well. This includes an examination of the scheme's effect on the mixed-layer depth in summertime conditions with weak winds and little cloudiness (section 4.4.2). Finally, the OSSE approach allows consideration of the potential influence of hypothetical observing systems which is deployed to address the impact of simulated hourly profiler observations in an exploratory case study (section 4.5).

4.1 Experimental set-up

4.1.1 The OSSE approach

In this section, an account is given of the basic ideas of and implementation procedures for the OSSE approach, and a brief review of its limitations.

A. Motivation for and basic idea of the OSSE approch

In the context of NWP the performance of a data assimilation scheme is measured in terms of fidelity to observations and the accuracy of the analysis and particularly the subsequent forecast. A limitation of real data experiments is that the analysis and forecast fields cannot be verified against the realized state but only against (inaccurate and/or inadequate) observations or independent (but nevertheless imperfect) analyses. The operational Deutschland Modell (DM) analyses are amongst the best available for the Alpine environs but, as shown earlier, they can contain unrealistic structures notably near steep orography. Thus, there are limitations to verification against independent 3-D analyses. Rawinsonde observations are expected to have realistic structures but these data are sparse compared to the model grid points. This makes it difficult in individual cases to assess the horizontal error structure and renders difficult the tuning of the horizontal correlation scale.

The OSSE approach circumvents these problems, albeit not without introducing different shortcomings. In this approach, a 'reference atmosphere' defined as truth is created by integration of a 'reference model'. Data sets are extracted from the reference atmosphere and defined as (perfect) 'observations'. Systematic and random errors can be

added to these to create simulated 'observations' with observational errors, and this can include mimicking observing systems that do not (yet) exist. The pseudo-observations can then be assimilated into a model that starts from an initial condition different from the one used by the reference model. The difference between the assimilation integration and the reference atmosphere is the 'error' of the assimilation experiment.

Historical reviews and detailed discussions of the OSSE approach can be found in Gilchrist (1984) and Arnold and Dey (1986). In recent years, the approach has mainly been used to assess the potential benefit of future observing systems (e.g. Kuo and Guo, 1989; Baker et al., 1995), and adopted for sensitivity tests on data assimilation techniques and the influence of observation errors (Spero et al., 1994; Chang and Holt, 1994).

B. Guiding principles and limitations

To assess the potential benefit of observing systems or to evaluate a given data assimilation scheme the guiding principle is to set up the experiments as realistically as possible. With respect to the observations, there are two constraints - (i) observation errors should be simulated realistically, and (ii) simulated rawinsonde observations should be given at levels different from those of the assimilation model. With respect to the models, the constraint is that (iii) the reference atmosphere and the assimilation model should relate to each other in the same way as the real atmosphere and the model. Since a model is always a simplification of the real atmosphere the assimilation model should be less sophisticated than the reference atmosphere (Arnold and Dey, 1986). This can be attained using a coarser grid and less physics.

There are two basic approaches to set up an OSSE: the identical twin experiments where the reference model and the assimilation model are identical (this clearly violates constraint (iii)), and the fraternal twin experiments where the two models are different. Direct inferences from identical twin experiments provide an optimistic estimate of an assimilation system's performance (cf. Atlas et al., 1985) for two main reasons.

First, the forecast error can only result from altering the initial conditions, i.e. the only source of forecast error is the model's predictability error growth since the physics and numerics are identical (Williamson, 1973). However, for the purpose of adjusting data assimilation parameters and refining the scheme this may be regarded as an advantage since only the relative performance for different parameter choices is relevant, and it renders easier the interpretation of the results. In the fraternal twin case, the relative performance may be biased since it is possible that for a certain choice of parameters, the assimilation scheme compensates for systematic errors of the assimilation model with respect to the reference model. An analogous argument may be forwarded for using imperfect lateral boundary conditions.

Second, the simulated observations are fully compatible with the assimilation model and with the lateral boundary conditions which is generally not true for real data. As a result, data are less liable to be rejected in the identical twin approach (Morel et al., 1971; Kasahara, 1972), and some of the variables may be implied to an unrealistic extent by the other model variables. This is a general weakness of OSSE's as the fraternal twin approach is able to only reduce but not eliminate it, and it is likely to affect results also for the purpose of adjusting nudging parameters.

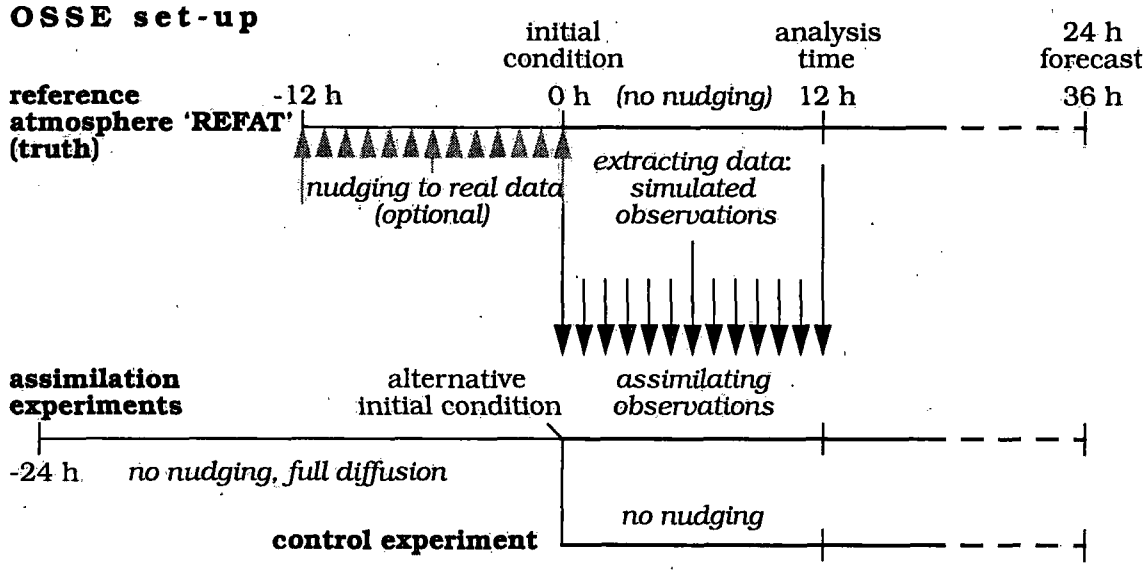

FIGURE 4-1. Sketch of OSSE set-up. The initial condition of the reference atmosphere is defined by DM analyses, or interpolated EM analyses in those cases where the stress lies on the assimilation of surface pressure. In one case the set-up has been modified to enhance a phase error (cf. section 4.3). For more detail, see text.
The term 'error' denotes the difference between the assimilation or control experiments and the reference atmosphere REFAT.

C. *The procedure: set-up of quasi-identical twin experiments*

To permit a clearer interpretation of results for the purpose of adjusting data assimilation parameters, the assimilation model is chosen to be identical to the reference model except for the lower vertical resolution (to satisfy constraint ii). The general set-up is sketched in Figure 4-1. Since the nudging has been shown in the previous chapter to significantly improve the vertical structure with low stratus, a 12-hour nudging period is employed to define the initial condition of the reference atmosphere for those cases for which a detailed vertical structure is expected to be of primary importance (Table 4-1). Also, the number of model layers is larger than for the other cases (Table 4-1). A 24-hour forecast with strong horizontal diffusion produces initial conditions for the assimilation experiments that are expected to differ significantly from the initial conditions of the reference atmosphere. In the first 21 hours, lateral boundary fields from the EM forecast starting at -24 h are used, and during the subsequent 3 hours, a

	cases with significant surface pressure errors	cases with a focus on low stratus or precipitation
initial condition of reference model	DM or EM analysis	12-h nudging period
number of layers of reference model	30 or 26	40
number of layers of assimilation model	20	30
domain size in grid points	97*109 or 121*109	97*91

TABLE 4-1. Specification of some model parameters for the OSSE set-up. Cases with significant surface pressure errors are cases G, H and I as defined in section 4.1.2.

smooth transition is made to the EM analysis at +0 h. Thereafter, only forecast fields from the EM forecast starting at +0 h are used as lateral boundaries both for the reference atmosphere and the assimilation experiments in order to rule out compensatory effects as mentioned above.

D. Simulated observations and specified observation errors

Simulated observations are extracted from the reference atmosphere at exactly those locations where observations of rawinsonde stations and surface stations have been available in reality. This includes the specification of the same station heights so that the interpolation and weights are identical to the real data case.

Observation errors which are to be added to these perfect simulated observations should be realistic. There are two sources of information to estimate appropriate values for rawinsonde errors. The first source are observational studies. The total instrument error consists of a systematic error, a sonde error and a random error (Hooper, 1975). The values given in Table 4-2 are valid for fixed pressure levels (i.e. pressure errors are included in the temperature, wind and humidity errors) and are an approximate average from the WMO International Radiosonde Intercomparisons (Nash and Schmidlin, 1987; Schmidlin, 1988; Ivanov et al., 1991), further observational studies (Richner and Phillips, 1982; Antikainen and Hyvönen, 1983; Elliot and Gaffen, 1991; Nash, 1993; Nash, 1994) and differences of observations to first guess fields of NWP models (Oakley, 1993). The systematic errors or biases of rawinsondes are treated statistically, which allows the computation of rms errors. The second source of information are rms error values used by other meteorological centers in operational data assimilation schemes. Those values are model dependent as they include representativeness errors of the observations which are significant (Kitchen, 1989). The values given in Table 4-2 for the DM analysis correspond to the values used in the ECMWF O.I. scheme for North American observations (ECMWF, 1992).

The rms errors chosen to be added to the prefect simulated observations are somewhat optimistic for winds. This is justified since these errors grow with increasing wind speed (Nash and Schmidlin, 1987) and since the main stress of this study lies on situ-

observation errors	surface pressure	temperature	relative humidity	wind components
systematic errors (bias)	~ 0.5 hPa	~ 0.35 K	~ 5 %	< 0.3 m/s
sonde and random error	~ 0.5 hPa	~ 0.2 K	~ 3.5 %	1 - 2 m/s
rawinsonde measurement rmse	~ 0.7 hPa	~ 0.4 K	~ 6.1 %	1 - 2 m/s
rawinsonde rmse in DM analysis	~ 0.55 hPa	-	-	2 - 3.8 m/s
rawinsonde rmse used for OSSE	0.7 hPa	0.4 K	6 %	1.5 m/s
surface station rmse for OSSE	0.7 hPa	-	6 %	2 m/s
hourly profiler rmse for OSSE		1.0 K	10 %	1.5 m/s

TABLE 4-2. Estimations of observation errors for the Vaisala RS80 rawinsonde valid for beneath about 100 hPa (rows 1 - 3), observational errors for rawinsondes as used in the O.I. analysis for the DM (row 4) and observation errors (independent from pressure level) as used for the OSSE's in this study (rows 5, 6). For further explanation, see text.

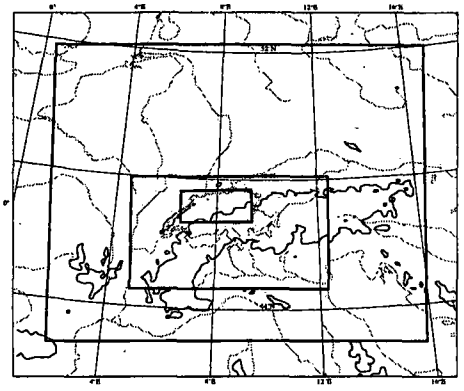

FIGURE 4-2. 3 domains used for objective evaluation within the 97*91 grid point model domain. The two smaller domains are called Alpine domain and Swiss Plateau domain in the text. The 1000 m isoline of the model orography is also shown.

ations with rather weak winds. Relative humidity observations are known to often contain larger errors near saturation or with very dry conditions (Schmidlin, 1993), above 600 to 500 hPa, or due to lag errors in cases of dramatic changes of the environment (Connell and Miller, 1995). The assumed errors for surface station observations are equal to the rawinsonde errors except for winds where a larger rms error accounts for local influences. The 6 % screen-level relative humidity observation error agrees with the UKMO analysis correction scheme (Macpherson, 1995).

E. Evaluation

The experiments are evaluated both objectively and subjectively. Statistics are calculated for temperature, relative humidity, geopotential and winds at 300, 500, 700, 850, and 900 hPa and for surface pressure, screen-level temperature and humidity and 10 m winds. Measures adopted are bias, absolute errors and rms errors (- for wind only the rms of the speed of the wind vector errors are computed). In addition for precipitation, the threat score (number of events forecasted *and* 'observed' above threshold divided by number of events forecasted *or* 'observed' above threshold) and bias score (number of events forecasted above threshold divided by number of events 'observed' above threshold) are determined for different thresholds (0.1, 2, 10, 30 mm per 6 hrs). The threat score is a measure for the spatial (and temporal) accuracy of the forecast which is relatively insensitive to a bias. Threat scores and bias scores with thresholds of 20 % and 80 % are also computed for low cloudiness with low stratus cases.

All statistics are computed on three domains (Figure 4-2): the whole model domain excluding the lateral boundary zone, an 'Alpine domain' in order to evaluate the scheme's performance near in steep orography, and a 'Swiss Plateau domain' covering the environs of the Swiss Plateau where operational verification scores have differed from other relatively flat areas due to the strong influence of the adjacent steep terrain.

4.1.2 Definition of experimental set-up and case descriptions

A large set of OSSE's (Table 4-3) has been carried out for up to 8 meteorological cases. The first benchmarks are the control experiment and the nudging experiment with a standard choice of parameters (see section 2.2). A first set of experiments is designed to facilitate the refinement of the scheme and involves tuning the temporal and horizontal weights and the nudging coefficient. In a second set, further components are examined in relation to the correction of the mass field in the free atmosphere. This includes the temperature correction for surface pressure nudging and the geostrophic wind correc-

Experiment name	temporal weight function	horizontal correlation scale** (km)	nudging coeff. (in 10^{-4} s^{-1})	description / remark
CTRL	-	-	-	(no nudging)
NA	lin. interpol.	130 / 220	6	standard rawinsonde nudging ***
NA**W**	**saw tooth**	130 / 220	6	
NAw**S1**	both	**70 / 100**	6	
NAw**S2**	both	**130 / 130**	6	correlation scale for humidity: 70 km
NAw**CL**	both	130 / 220	**12**	
NAw**CS**	both	130 / 220	**3**	
TAw**S** *	both	**100 / 100**	6	short correlation scale ****
TAwS-**NOPS***	case depend.	100 / 100	6	no surface pressure nudging
TAwS-**PS**	case depend.	100 / 100	6	nudging of surface pressure only
TAws-**TCOR**	case depend.	100 / 100	6	with temperature correction
TAws-**GEO** *	both	100 / 100	6	with geostrophic wind correction
TAwS-**MASS**	both	100 / 100	6	nudging mass field only (incl. humidity)
TAwS-**WIND**	both	100 / 100	6	nudging wind field only
TAVS	**short saw t.**	100 / 100	6	saw tooth time window halfed
TAw	case depend.	130 / 220	6	with surface observations ****
TAW-**ISEN**	saw tooth	130 / 220	6	spreading along isentropes
TAws-**NOQ**	saw tooth	case depend.	6	no humidity nudging
TAS-**4DDA** *	lin. interpol.	100 / 100	6	nudging (4DDA) throughout the period
TAS-**TMIX** *	lin. interpol.	100 / 100	6	no temperature nudging in mixed layer
PAvS-**UV**	both	100 / 100	6	with additional hourly wind profiler data
PAvS-**UVT**	both	100 / 100	6	with wind + temperature profiler data
PAvS-**UVTQ**	both	100 / 100	6	with wind, temp. + humidity profiler data

TABLE 4-3. List of OSSE's discussed in subsequent. Only the first 7 experiments are applied to all of the 8 meteorological cases. For definitions of weight functions, see section 2.2.
About the convention for experiment names:

the meaning of **bold** letters in the names is described by bold declarations in the 3 middle columns and by descriptions in the right column.

small case letters denote that experiments have been carried out with and/or without the property symbolized by that letter.

*: These experiments have also been carried out with real data. For a real data experiment refered to in the text, an '**R**' is prefixed to the name given in the Table.

**: Notation: correlation scales for: upper air observations / surface pressure.

***: Standard rawinsonde nudging: uses only rawinsonde data, deploys linear temporal interpolation, lateral spreading along σ-surfaces, other parameters as indicated in the table.

****: In sections 4.3 to 4.5, these experiments are often denoted 'standard nudging' experiments (irrespective of the correlation scales or temporal weight function) since they are the benchmark for the other experiments in these sections.

tion. In a third set, components that have a more local impact, like screen-level humidity data assimilation, are examined in relation to meteorological phenomena that are sensitive to a variety of dynamical and physical processes and that are often characterized by strong vertical gradients or significant small-scale variability (e.g. precipitation, boundary layer processes). In a final set, the impact of simulated profiler observations is addressed in an exploratory case study. Real data experiments complement the OSSE's where appropriate.

The selection of the meteorological cases has been guided by the aim of the operation of the SM, that is to resolve and forecast meso-α to meso-β-scale phenomena of relevance to forecasting. With regard to the influence of initial conditions, situations with modest advection are more significant. Therefore, two low stratus cases (A1, B0) and three summertime cases (D, E, F) with convection and precipitation have been selected. For the examination of surface pressure assimilation, two cases (G, H) have been added that involve pronounced closed mesoscale cyclones. Finally, the set is complemented by a case dominated by strong northwesterly advection with the intention to test the performance and stability of the scheme with strong large-scale forcing and to examine the impact of the geostrophic wind 'correction' with strong ageostrophic flow over the Alps.

The low stratus cases A1 and B0 have already been presented in chapter 3 (but note that the initial time for case B0 is 24 hrs prior to the analysis time of case B in chapter 3). The remaining cases are briefly decribed here.

Case D: Initial time: 5 July 1993, 0000 UTC: summertime cold front

A cold front traversed toward very hot and humid air in the Alpine area during the evening of 5 July 1993. Lifiting caused violent thunderstorms and wide-spread precipitation over most of the Alps and the regions north of it. Rain amounts in central to northeastern Switzerland were 60 to 90 mm within 24 hours. The front was associated with a sharp turn of the low-level winds from southwest to north(east) and a widespread temperature decrease of 13 K.

Case E: Initial time: 15 July 1993, 1200 UTC: meso-β-scale morning convection

A frontal zone with moderate precipitation extending over Belgium to southern Germany was slowly moving eastward. Warm and humid air over Switzerland became unstable due to slight upper-level cooling in the morning of 16 July. The resulting convection took the form
of a chain of thunderstorms with heavy rain causing damage within a relatively narrow band on the Swiss Plateau. The event was missed totally by all the NWP models and by the local forecasters. Underestimation of moisture in the analyses was deemed to be a contributory. For more details on the meteorological situation, see Field Phase Report (1993) of POLLUMET.

Case F: Initial time: 6 August 1994, 1200 UTC: mesoscale convective systems

Hot and relatively humid air and modest (south-)westerly winds above 800 hPa prevailed in the environs of Switzerland on 6 and 7 August. Widespread convection and thunderstorms developed over the Alps in the evenings, and some moved onto the Swiss Plateau. Mesoscale convective systems produced precipitation over eastern and northern France to southern Germany and the Czech Republic. A convective system approached western Switzerland in the evening of 7 August.

Case G: Initial time: 22 October 1993, 0000 UTC: stationary cyclone southwest of the Gulf of Genoa

An upper-level trough extended southward to the western Mediterranean and induced a relatively intense cyclone that stayed stationary near the Cote d'Azur on October 22 and 23. Moderate precipitation occured in the Alpine region and its environs.

Case H: Initial time: 28 March 1995, 1200 UTC: cut-off low passing over Germany

A secondary mesoscale cyclone moved from England southeastward over Germany. Associated with it were warm cold fronts. Precipitation was strongest on the warm front region, but the northerly winds subsequent to the cold front pressed the cold humid air against the Alps and caused persistent snowfall mainly along the northern slopes and foreland of the Alps.

Case I: Initial time: 27 January 1995, 0000 UTC: northwesterly advection

A strong northwesterly flow and a pronounced post-frontal pressure rise caused ageostrophic flow over and around the Alps during 27 January.

4.2 Benchmark experiments and tuning of nudging parameters

Before presenting the results on the tuning of the scheme's basic parameters it is appropriate to address issues regarding the experimental set-up and the evaluation methods by discussing the control experiments CTRL without nudging and the standard rawinsonde nudging experiments NA. The evaluations in the present section are mainly statistical.

4.2.1 Control experiment without nudging: influence of lateral boundaries

The initial conditions of the assimilation experiments are considerably degraded by the use of out-dated lateral boundary fields prior to the initial time. The effect of the smooth transition to perfect lateral boundary conditions within the last 3 hours prior to the initial time is evident in the initial condition by a narrow stripe of small errors at the lateral boundaries of the domain for instance in case G (Figure 4-3a). In large parts of the inner domain, surface pressure errors exceed 2 - 3 hPa. Subsequently, the pressure errors decrease sharply in CTRL without any data assimilation due to the 'perfect' lateral boundaries (Figure 4-3b, c). The error decrease is strongest in the pressure fields (i.e. surface pressure and geopotential) since there is an integral influence of the lateral boundaries on the pressure field (cf. Vukicevic and Peagle, 1989; cf. section 2.3.3). This decrease is smallest in the environs of mesoscale cyclones or other mesoscale structures that are not primarily a response of the large-scale flow to orographical forcing.

A generally weak sensitivity of geopotential forecasts to the initial condition with limited area models has also been found by other authors (cf. Vukicevic and Errico, 1990). However, recent sensitivity analyses based on the adjoint method and on singular vectors have shown that error growth can also occur in mesoscale models (Errico et al., 1993), but the number of growing small-scale perturbations is relatively small (Ehrendorfer and Errico, 1995).

For wind, temperature and humidity, the error decrease is found to be less pronounced, yet present in all cases (rms error decrease of about 20 - 30 %, mostly con-

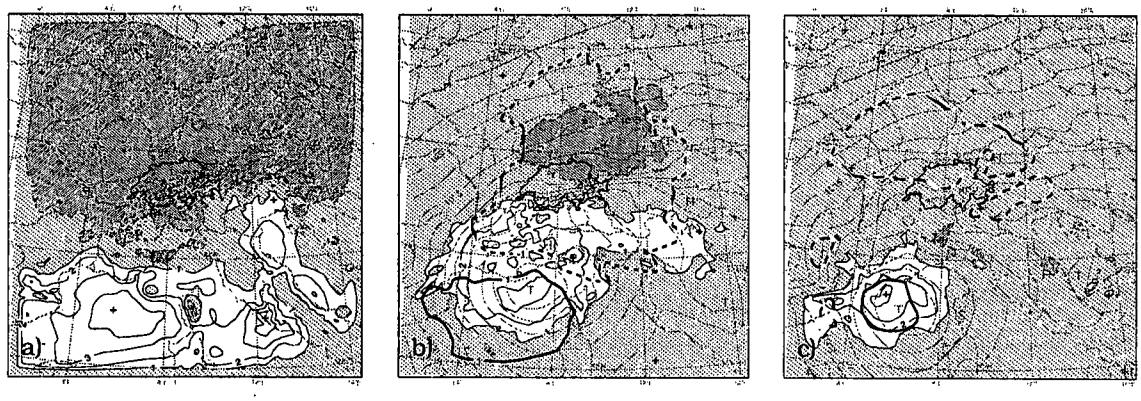

FIGURE 4-3. Error (i.e. difference to reference atmosphere REFAT) of surface pressure (thin black contours and shading) of experiment CTRL for case G. Contour interval is 1 hPa (without 0 hPa contour), positive (negative) errors > 1 hPa are white (dark shaded).
In panels b) and c), the 500 hPa geopotential error of CTRL (thick black contours, solid contour: +10 m, dashed contour: -10 m), and the reduced surface pressure of the reference atmosphere (grey contours, contour interval 2.5 hPa) are also shown.
a): initial condition; b): +12 h (beginning of forecast period); c): +24 h.

fined to the first 12 hours). In case I, the strong advection causes the initial errors to disappear almost entirely within 12 hours, leaving no scope for improvement during the 12-hour nudging period.

4.2.2 Standard rawinsonde nudging experiment: a benchmark

Generally, nudging is found to substantially decrease the bias and the standard deviation in standard rawinsonde nudging experiment NA (cf. Table 4-3) both at the end of the nudging period and in the forecast period. The average rms error reduction is 20 - 50 % at the end of the nudging period and 10 - 30 % at + 36 h. Less or no improvement is achieved where CTRL errors are small. This applies particularly for surface pressure (for instance in case D). Comprehensive examination indicates that there is a slight tendency for the nudging to be more beneficial at low levels. The average relative rms error reduction is similar for wind, temperature or humidity, and it is also similar for the three verification domains (as defined at Figure 4-2).

4.2.3 Horizontal weight function

The horizontal weight functions are designed to model the horizontal forecast error correlations. As opposed to data-poor areas, the errors mainly consist of small-scale structures in data-rich areas like Central Europe (Lönnberg, 1992). The dependence of the appropriate scale for the nudging weight function on the data-density has been experimentally confirmed for instance by Kuo and Guo (1995). They obtained the best results for meso-β-scale nudging if the (Cressman) radius of influence was comparable to the station separation. Unnecessary smoothing is expected with the use of a significantly larger scale (cf. Seaman et al., 1995).

Since the EM covers large data-poor areas, the optimal scales for the SM are expected to be smaller than those specified in standard rawinsonde nudging experiment NA which are based on estimates for forecast errors of the EM. The increased small-scale

horizontal weight function w_r (see (2-7))	example 1	example 2
specified correlation scale of the horizontal weight function	130 km	70 km
half width radius L for 1 observation ($w_r(r=L) = 0.5$)	218 km	118 km
effective half width radius L in the area between 2 observations separated by 250 km (typical for rawinsondes in Central Europe)	135 km	88 km
relative reduction of L when second observation is added	38 %	25 %

TABLE 4-4. Illustration of the adaptation of the horizontal weighting to the data density by the use of (2-5). The effective width of the narrower weight function (example 2) is reduced less than that of the broader weight function (example 1) when the data density is increased.

variability of the model errors near steep orography should strengthen this expectation since rough terrain is significantly more predominant in the SM than in the EM.

However, the present nudging scheme in the SM is expected to be fairly insensitive to the specified scale of the horizontal weight function for three reasons:

- The use of equation (2-5) for multiple observations adjusts the effective scale to the data density to some degree as illustrated in Table 4-4. This will tend to make the scheme relatively insensitive to variations of the specified scale of the horizontal weight function provided that the average observation station separation is of the same order of magnitude as the (formal) half width radius of the horizontal weight function (2-7).
- In a recent study of Kuo and Guo (1995) who also used (2-5) to account for varying data density, only modest sensitivity was observed unless the (Cressman) radius of influence was significantly less than half the average station separation. (Apart from that study, this issue has been little addressed in the literature by means of nudging experiments.)
- The O.I. method is well known to be insensitive to large variations in the horizontal scale of error correlations given relatively dense and accurate data (Seaman, 1992). In comparison, successive correction methods are found to be even less sensitive (Homleid and Breivik, 1995), and since nudging consists of imposing successive corrections during the forward integration of the model, this should also hold for nudging.

This suggests that there is only a (modest) potential for a positive impact if the horizontal correlation scales are reduced by a considerable amount. This is tested in two experiments. In the first experiment (NAS1, cf. Table 4-3) the correlation scales are almost halved for all variables. In the second experiment (NAS2) this reduction is restricted to humidity and surface pressure, based on the considerations that humidity generally has greater small-scale variability (cf. Zou et al., 1995) and that the synoptic scales (accounted for by the standard weight function of surface pressure, cf. Table 2-1) are largely determined by the lateral boundary conditions on the SM domain.

The impact is marginal relative to standard rawinsonde nudging (experiment NA) in both experiments and for all meteorological cases. At most, there is a tendency to a slight degradation of the middle- and upper-level fields in experiment NAS1. Note that although the atmospheric flow has more small-scale structures over rough terrain generally, the statistical evaluation does not indicate that shorter weight functions are advantageous over the Alps. Presumably, the sensitivity is too weak.

4.2.4 Temporal weight function

Here, the two temporal weight functions defined in section 2.2 are compared, i.e. linear temporal interpolation over a maximum interval of 12 hours as used for instance by Stauffer and Seaman (1990) for a horizontal model resolution of 80 km and the saw tooth weight function as used operationally at the UKMO (Lorenc et al., 1991). The characteristic time scale T_c (where $w_t(-T_c/2<t<T_c/2) > 0.5$) for 12-hourly rawinsonde data is 6.5 hours for the linear interpolation, respectively 12 hours with a continuous assimilation cycle, and 3 hours for the saw tooth function. Note that the time scale is automatically adjusted to high-frequency data.

The time scale should be chosen such that the spatial and temporal wavelengths of the features to be analyzed are resolved in a mutually consistent manner (Benjamin and Stamus, 1991). For a horizontal correlation half width radius L of about 220 km for a single observation, the consistent time scale is 6 hours for a 20 m/s advection. However, for a typical mean rawinsonde station separation of around 250 km, the effective correlation half width radius is reduced to about 135 km (Table 4-4). It is even less if the specified correlation scale is reduced. Thus, a time scale of about 3 hours appears to be appropriate. As for the shape of the temporal weight function, Stensrud and Bao (1992) showed in a study with restricted validity that weights that peak at the observation time are preferable to linear temporal interpolation because the variables vary in a quasi-quadratic sense between observation times.

For the SM, experimental results reveal that there is not a clear difference in the overall performance between the two formulations although the differences are significant in some of the cases. Linear temporal interpolation results in better simulations of persistent low stratus, particularly in case A1 and for real data. The saw tooth function is clearly superior in cases F and H where advection significantly changes the location of persistent precipitating mesoscale systems within the nudging period. Specific properties of the two concepts of temporal weighting are discussed further for case H in subsequent sections. In the other cases (D, E, G), the saw tooth function is at most slightly superior with respect to wind and humidity rms errors and precipitation scores.

It should be mentioned that the perfect lateral boundary conditions of the OSSE's tend to bias the results in favour of the saw tooth function which modifies the perfect information from the boundaries less strongly due to its shorter time scale. This is particularly true during the first half of the nudging period as only few soundings are available at 0600 and 1800 UTC. The temporal variation in data density that occurs with the use of the saw tooth function does not appear to have a significant negative impact, possibly because the sensitivity of the forecast to observations valid for the end of the assimilation period is much greater than to earlier observations (cf. Bao and Errico, 1994).

4.2.5 Nudging coefficient

Optimal nudging coefficients can only be determined with use of the computationally expensive adjoint method (Zou et al., 1992; Stauffer and Bao, 1993). Simple physical considerations confine the range of reasonable values. If the nudging coefficients are too small the observational information content won't be well utilized, and too large coefficients cause the artificial nudging effects to overwhelm the dynamics and to disrupt the model adjustment processes which spread the observational information throughout the model domain. An attempt to put the specification on better grounds has been made by Brill et al. (1991) by relating the nudging coefficients to parameters account-

ing for the data accuracy, but it left them with the need to specifiy these secondary parameters based on subjective judgement.

Commonly, a refinement of the nudging coefficients is obtained by comparing the performance of the nudging scheme with various values for the coefficients (cf. Krishnamurti et al., 1988; Wang and Warner, 1988; Ramamurthy and Xu, 1993; Guo and Kuo, 1995). Here, the coefficients are doubled in experiment NAwCL (cf. Table 4-3) and halfed in experiment NAwCS relative to the values (cf. Table 2-1) used in the standard rawinsonde nudging experiment.

Doubling substantially degrades the analyses and particularly the forecasts in all cases. Halving of the coefficients results in a modest deterioration of analyses and forecasts when the saw tooth temporal weight function is applied (experiment NAWCS). With linear temporal interpolation, the reduction of the coefficient has a slight positive impact on analyzed low-level wind and surface pressure. This may be explained by the fact that averaged over the nudging period, linear temporal interpolation produces larger weights. However, the forecasts with the original coefficients are still superior, particularly at low levels and near steep orography. It indicates that the use of the original coefficients controls the large-scale error growth more efficiently in spite of disturbing mesoscale structures developed by the model prior to the forecast period. In the Alpine and Swiss Plateau domains, the use of the original coefficients is even more advantageous relative to the reduced coefficients. This indicates that near steep orography the model sustains and benefits from a stronger forcing by nudging probably because the dynamical and physical forcing itself is increased due to the orography.

4.3 Correcting the mass field in the free atmosphere

4.3.1 Introduction

This section addresses the problem of assimilating mass and wind field data to correct errors in the mass field, particularly in the surface pressure. It has been shown in section 2.3.3 that simple nudging of a single surface pressure observation is not successful, but the geostrophic wind correction has a potential to enhance the assimilation of surface pressure data.

The benefit from nudging surface pressure data in the extra-tropics has not been obvious in the past. The simulations of cyclogenesis by Brill et al. (1991) with a mesh width of 60 km were more accurate when surface pressure analyses were nudged in addition to 3-D analyses. Yet in a companion paper (Manobianco et al., 1991), nudging towards additional, subjective surface pressure analyses in a data-void area failed to produce a realistic simulation of cyclogenesis over the ocean since the model was apparently unable to distribute the corrected total mass correctly in the vertical and to simulate the adjustments between the mass and momentum fields. Ramamurthy and Xu (1993) found that the only impact was a reduction of the spurious pillow effect which is a high-frequency oscillation of the total mass in a limited area model due to inconsistencies at the lateral boundaries. As in Brill et al. (1991), surface pressure nudging affected mainly wavelengths of at least 2000 km. Little is known about surface pressure nudging in meso-β-scale, although it is applied operationally with geostrophic wind corrections to the UKMO meso-β-scale model (Lorenc et al., 1991).

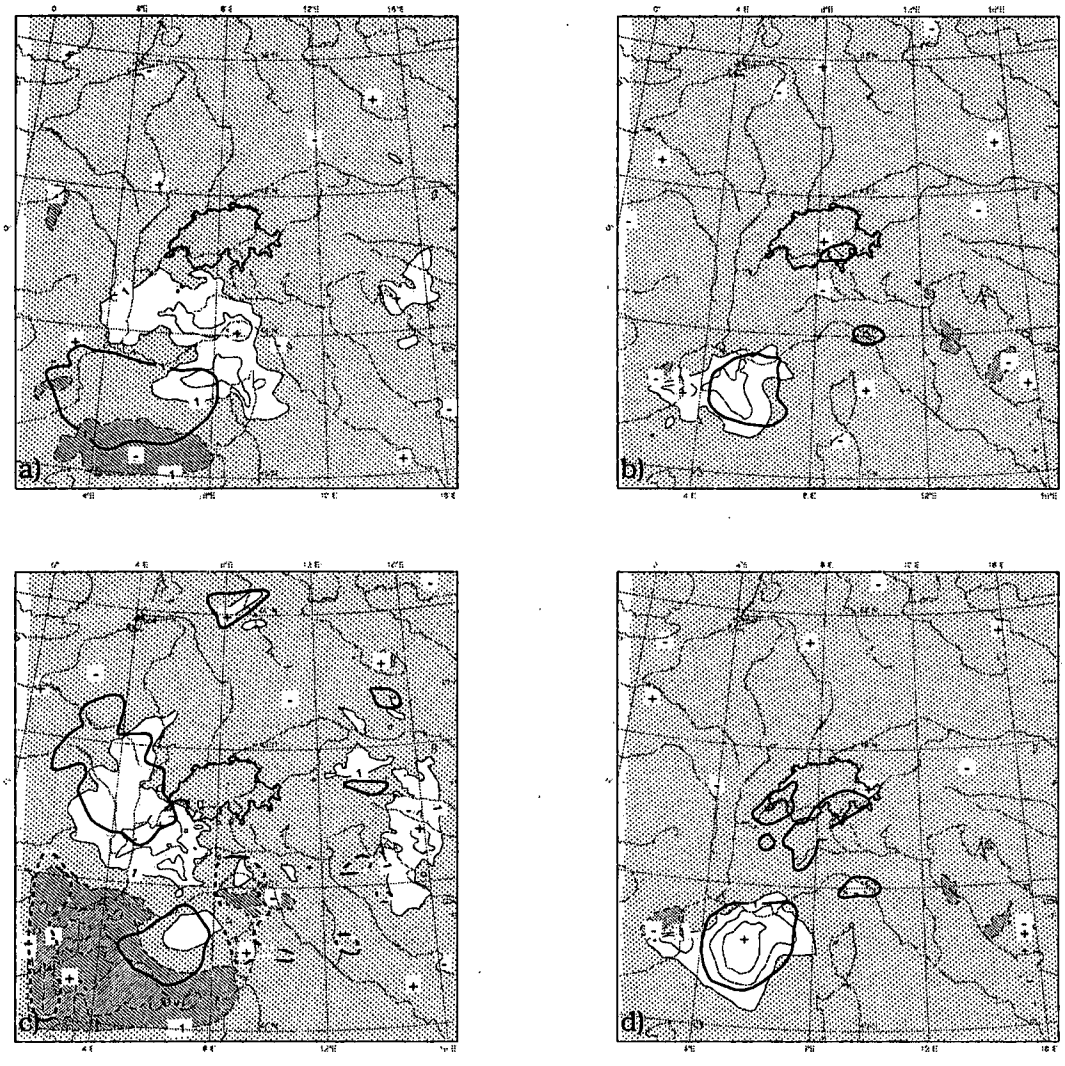

FIGURE 4-4. Error (i.e. difference to REFAT) of surface pressure (contours and shading as in Figure 4-3) and of 500 hPa geopotential (thick black contours, solid contour: +10 m, dashed contour: -10 m) for case G.
a): Experiment TAWS, +12 h (end of nudging period); b): TAWS, +24 h;
c): TAWS-GEO (with geostrophic wind correction), +12 h; d): TAWS-GEO, +24 h.

In the light of this, surface pressure nudging is anticipated to have quite a small effect in the SM for three reasons. First, no pillow effect is observed in the SM. Second, the SM domain is much smaller than that used in the quoted studies, and the synoptic scales are largely determined by the lateral boundary condition. Third, the scales that have been found to be primarily affected by surface pressure nudging are already well resolved by rawinsonde data covering the SM domain relatively uniformly.

The issue is best examined in meteorological cases where areas with significant surface pressure errors in CTRL provide a considerable scope for improvement by nudging. According to section 4.2.1, such errors preferably pertain to the environs of mesoscale cyclones for which the influence of the lateral boundaries is relatively small.

Cases G and H with mesoscale cyclones within an enlarged model domain have been selected for that purpose. They substantially differ from each other in four aspects. In case G, the cyclone is (i) approximately stationary (ii) with its center over the data-void

sea, and (iii) it extends throughout the troposphere. The 500 hPa geopotential field of CTRL (iv) exhibits a pattern with large errors (apart from areas close to the lateral boundary zone) which generally correlates reasonably with the surface pressure error pattern at the end of the assimilation period (Figure 4-1b). In case H, the secondary cut-off low is (i) propagating fairly fast (ii) over a data-rich area, and (iii) the disturbance in the pressure, temperature and wind field is largely confined to the lower troposphere. Thus; the error structure (iv), for instance of temperature, is more shallow than in case G, and 500 hPa geopotential errors are comparatively small. The phase error of the cyclone in the initial condition of the control and assimilation experiments (see Figure 4-1) is enhanced by integrating the model forward from +00 h to +06 h using lateral boundary fields from +00 h to +03 h. The resulting model state is assigned to the time +03 h and forms the initial condition of a 9 h nudging period.

4.3.2 Standard nudging and the influence of surface pressure nudging

Case G

Nudging with standard parameters, except for the narrow horizontal weight function and the use of the saw tooth temporal weight function (experiment TAWS, cf. Table 4-3), sets the benchmark and reduces temperature and geopotential errors by 50 to 80 % relative to CTRL during the nudging period. It adjusts the surface pressure correctly (Figure 4-4a) except in the vicinity of the closed mesoscale cyclone (error reduction: 50 %). The 500 hPa geopotential errors are mainly confined to data-void areas over the northwestern Mediterreanean. Consequently, the lower troposphere is still a bit too cold over northern Italy and southeastern France (despite error reduction of 80 %). 12 hours later, the relation between the magnitude of errors of TAWS (Figure 4-4b) and CTRL (Figure 4-3c) is similar.

Thus, surface pressure is corrected far more successfully in this experiment with realistic data density compared to nudging of a single surface pressure observation in section 2.3.3. However, nudging experiments which do not assimilate surface pressure data (TAWS-NOPS), or use exclusively surface pressure data (TAWS-PS) indicate that the contribution of surface pressure nudging to the reduction of the pressure errors is small (at most 0.5 hPa) and mainly confined to the largest scales.

Case H

The main shortcoming of CTRL (Figure 4-5) consists of the cut-off low being too weak and having propagated too far (south-) east which results in surface pressure errors exceeding ±6 hPa at +12 h (i.e. at the end of the nudging period). Whereas a relatively sharp warm front at 850 hPa is passing the Upper Rhine Valley in the reference atmosphere, it is spread out in CTRL from southern Germany to eastern Austria, and the cold front over northeastern France is displaced to the south. These differences, particularly in the pressure field, qualitatively persist up to about +24 h when the cut-off low is about to cross the eastern boundary of the model domain.

Nudging during 9 hours with standard parameters (experiment TAS; cf. Table 4-3) and linear temporal interpolation largely corrects the position errors of both the cut-off low and the fronts (Figure 4-5c) but tends to smooth horizontal gradients. Thus, the fronts are smeared out, and the surface pressure is too high by about 2 - 3 hPa in the center of the cut-off low and around the fronts. The time series of the 850 hPa temperature over Munich reflects these results. The fronts cross Munich too early in CTRL, and the

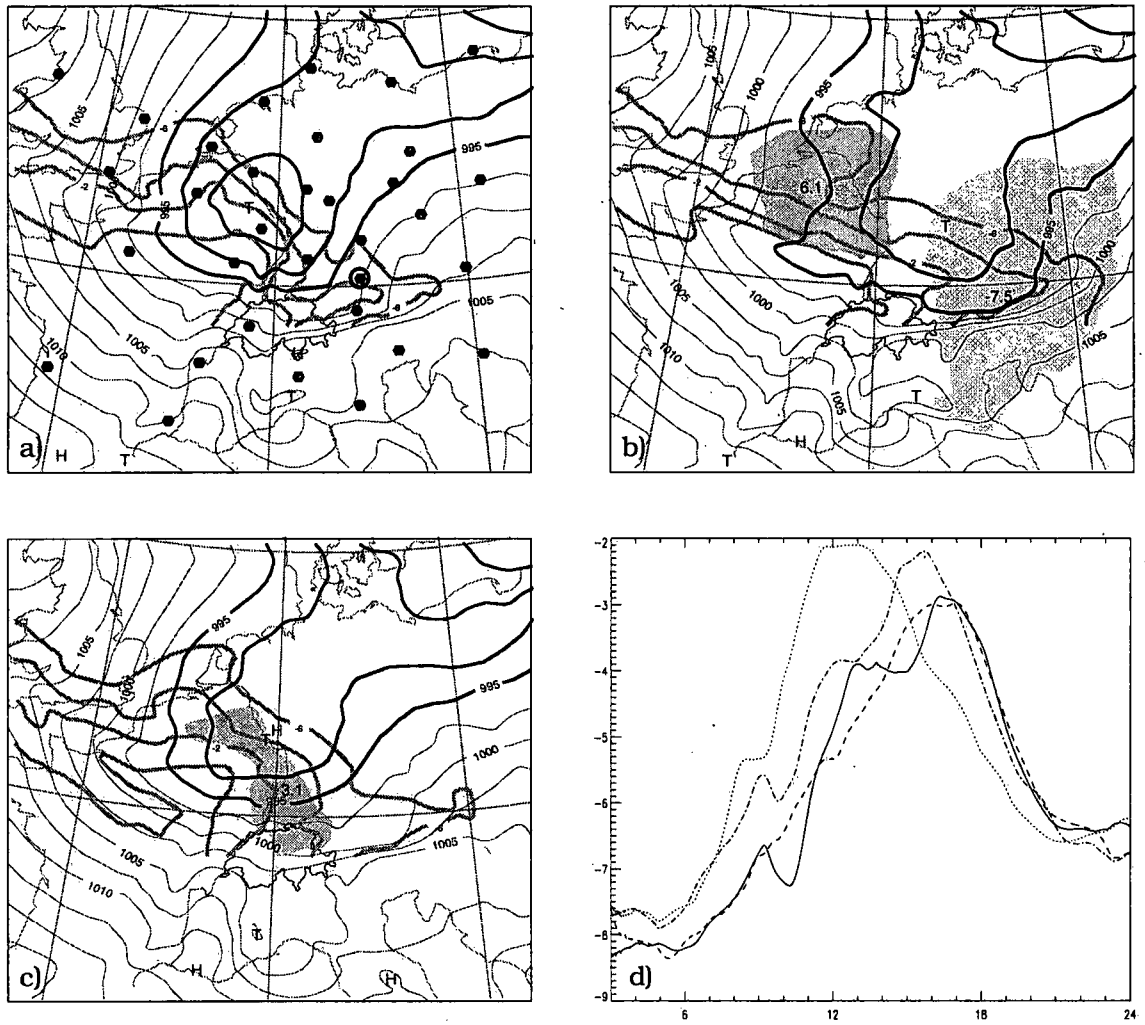

FIGURE 4-5. a) - c): Case H at the end of the nudging period (+12 h).
a): reference atmosphere; b): CTRL; c): standard nudging experiment TAS. Displayed fields:
- reduced surface pressure: black contours in 2.5 hPa intervals, thick contours for ≤ 995 hPa;
- surface pressure error: extreme values and shading where errors exceed 2 hPa; darker shading for positive errors, lighter shading for negative errors;
- 850 hPa temperature: thick grey lines, only contours 0K, -2K, -4K, -6K north of the Alps (this includes the strongest gradients at the warm and cold fronts);
+ locations of rawinsonde stations available at the end of the nudging period: black dots.
d): Time series of 850 hPa temperature at Munich (its location is denoted by the encircled black dot in a)). Solid: reference atmosphere; dotted: CTRL; dashed: TAS; dash-dotted: TAVS (with shortened saw tooth temporal weight function).

temperature maximum after the warm front is 1 K too high. This is corrected in TAS, although some fine scale structures of the frontal temperature rise are completely smoothed.

Excluding surface pressure data from nudging, or nudging of surface pressure data alone has even a smaller impact than in case G. This is not surprising since errors that are largely confined to the lower troposphere as in case H can hardly be expected to be corrected by nudging a vertically integrated quantity such as surface pressure.

The question arises about the cause of the smoothing of the gradients observed in the nudging experiments in this case. It is hypothesized that the linear temporal interpola-

tion of temperature or wind or both may contribute to that smoothing. Using the saw tooth temporal weight function instead corrects indeed the central surface pressure of the cut-off low almost perfectly without substantially smoothing the horizontal temperature gradients but it does not fully correct the phase error. In experiment TAVS (Figure 4-6b), the nudging time scale is reduced further by shortening the saw tooth function so that nudging starts 2 hours instead of 5 hours prior to an observation. The effect of that shortening is not significant at the end of the nudging period except in the northwestern part of the domain, where the surface pressure errors are smaller as the perfect information advected from the lateral boundaries is less modified. It results in the smallest pressure errors of all assimilation experiments at +24 h, but that is at least partly attributable to the specific experimental set-up with perfect lateral boundary fields. The Munich time series (Figure 4-5d) also indicate that the phase error especially of the warm front is not fully corrected earlier in the forecast period. Whether the smoothing is attributable to the temporal interpolation of observed wind or temperature or both will be examined in section 4.3.4.

4.3.3 Attempts to enhance the assimilation of surface pressure data

Since the contribution of surface pressure nudging to the reduction of the pressure errors is small in cases G and H, it is appropriate to test the corrections which are devised to enhance the assimilation of surface pressure data (see chapter 2).

The temperature correction is designed to keep direct upper stratospheric changes small even in case of large direct effects of surface pressure nudging at low levels. Since surface pressure nudging without correction has had a very small effect throughout the atmosphere the main effect of the correction is expected at low levels. This is indeed found in the experimental application (TAWS-TCOR). However, both in cases G and H, the impact on the forecasts is not significant.

Several restrictions (see Table 4-5) are imposed on the geostrophic wind correction in cases G and H (experiment TAwS-GEO, cf. Table 4-3) to diminish unrealistic effects

limitation or weighting	reason
general weight factor : (0.5 or) 0.9	full geostrophy of analysis increments is unrealistic in the mesoscale (cf. Schlatter and Carrière, 1991). 0.5 is used by Lorenc et al. (1991); 0.9 renders larger the correction, allowing a clearer characterization of its effects
general upper limit : (4 or) 10 m/s per hour	wind correction may get too large where nudging substantially increases geopotential gradients. Such an increase preferably occurs at mesoscale cyclones where the curved flow is often substantially ageostrophic
horizontal weight : zero within lateral boundary zone, increasing to 1 within 4 grid pts.	unrealistic geopotential gradients must be expected near the lateral boundaries
vertical weight : parabolic (as a function of model layers), 1 at 650 hPa, 0 at the ground and above 240 hPa	near the surface, the flow field is likely to be strongly ageostrophic in the upper atmosphere, biased temperature observations could lead to strong erroneous geostrophic winds

TABLE 4-5. Description of the restrictions imposed on the full geostrophic wind correction in cases G and H.

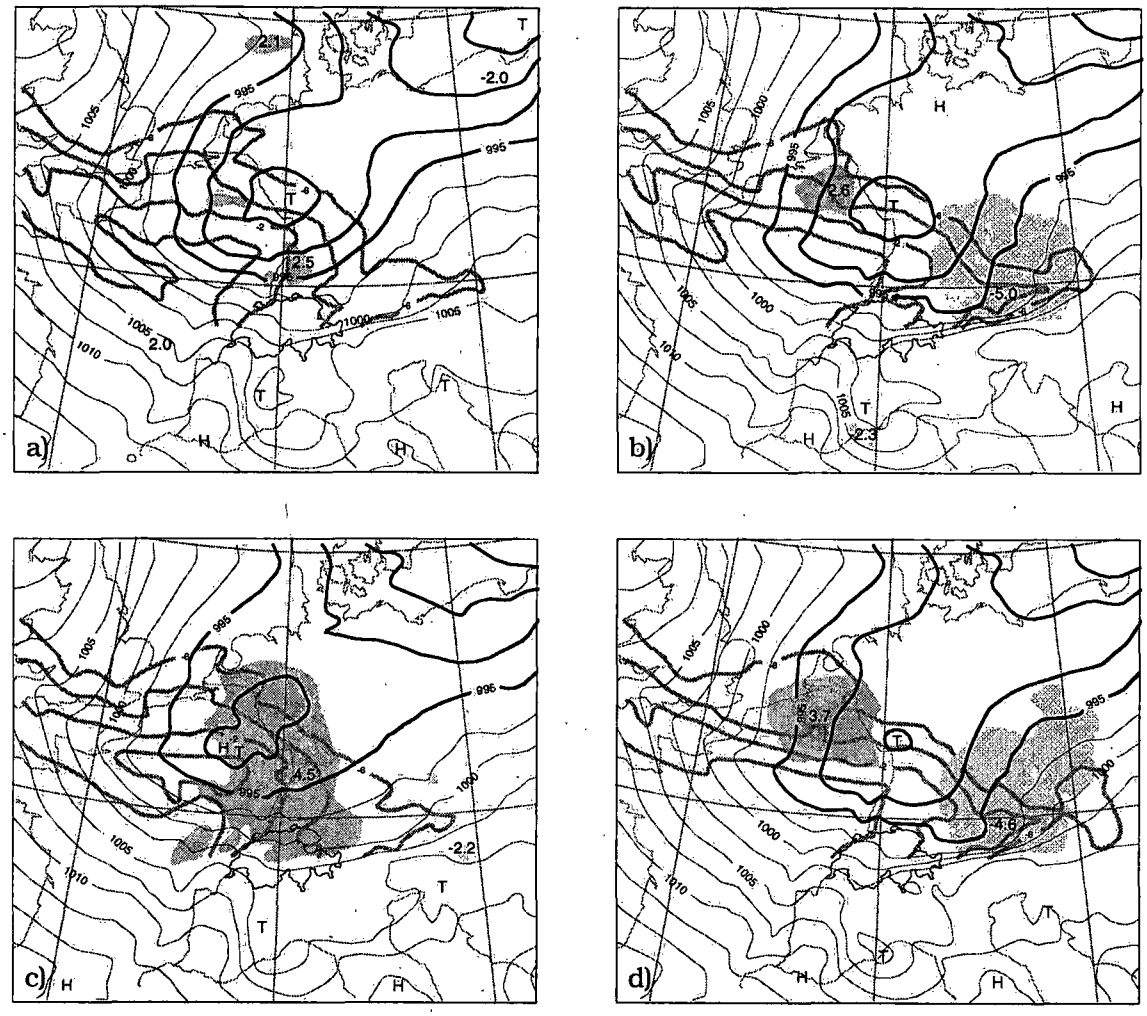

FIGURE 4-6. Reduced surface pressure, surface pressure error and 850 hPa temperature for case H at the end of the nudging period (+12 h) as at Figure 4-5. a): TAS-GEO (with geostrophic wind correction); b): TAVS (with a shortened saw tooth shaped temporal weight function); c): TAS-MASS (nudging mass field only); d): TAS-WIND (nudging wind field only).

which pertain particularly to the mesoscale. If a gridded field of 46 simulated 'buoy' surface pressure observations on the Mediterranean is additionally nudged in case G, the characteristic properties of the impact of the geostrophic wind correction is similar in cases G and H. At the end of the nudging period (Figure 4-6a for case H), the correction improves the surface pressure (by up to 2 hPa) and 500 hPa geopotential near the centers of the cyclones (i.e. in the areas with the largest pressure errors in TAwS). However, it has little influence on the temperature gradients of the fronts or on the pressure errors in their vicinity. Moreover, it introduces 'secondary' surface pressure errors (also up to 2 hPa), e.g. near the lateral boundaries. The net effect of the correction on the wind field does not show much of the expected features, like e.g. a cyclonic circulation around the areas where the surface pressure has been too high in TAwS. With the use of the geostrophic correction, the feedback mechanisms between wind and mass field become complex, and adjustment processes largely cancel the effects of the geostrophic correction in the forecast period.

If the additional 'buoy' surface pressure data are not used in case G, the secondary errors over the sea are more than doubled at the end of the nudging period (Figure 4-4c), and the (12-hour) forecast errors in the center of the cyclone clearly exceed those of experiment TAWS (without geostrophic correction) at +24 h (Figure 4-4d). Thus, the geostrophic wind correction makes the scheme more sensitive to the lack of data over the sea, and possibly to variations in data density in general.

Very little (positive or negative) impact is observed in case I where a geostrophic correction is expected to be clearly inappropriate for the pronounced ageostrophic flow around the Alps. Note however that the strong advection of perfect information from the lateral boundaries sweeps the errors rapidly away.

4.3.4 The influence of wind and temperature data, and the link to geostrophic adjustment theory

Here, the question addressed is whether some results of the idealized experiments with single observations (section 2.3.4) regarding the applicability of the geostrophic adjustment theory can be generalized to realistic conditions with a realistic variety and density of data. For that purpose, experiments are carried out for cases G and H where only the mass field including humidity (experiment TAwS-MASS, cf. Table 4-3) or the wind field (TAwS-WIND) is nudged. The focus is on the correction of the mass and wind fields in areas where major errors occur, i.e. in the (farther) environs of the cyclones rather than specifically near steep orography as in section 2.3. A second purpose of these experiments is to find out whether the smoothing of horizontal gradients in case H can be assigned to the nudging of either wind or temperature.

At the end of the nudging period, nudging effects that are common to cases G and H generally tend to agree qualitatively with those results of the idealized experiments that are not directly related to orography. Mass field nudging yields its main impact on geopotential and wind by nudging temperature. In cases G and H, temperature nudging is effective in reducing the statistical temperature error measures (by 30 % relative to CTRL) and (by 50 to 80 %) mean temperature errors of the lower troposphere (beneath 500 hPa). There, vertical error correlations are relatively narrow, and the adjustments required to eliminate the errors are likely to be rather shallow. In contrast, low-level temperature benefits less from wind field nudging which is found to be more effective in correcting the winds and the 500 hPa geopotential (by 20 to 60 %). Wind field nudging should try to minimize wind errors thoughout the atmosphere. Then, it follows that the smallest wind errors are obtained if the geostrophic wind (and geopotential) errors are minimized in the middle of the atmosphere rather than at its bottom or top. Thus, it appears that also in realistic cases the geostrophic adjustment theory may provide a guideline for roughly estimating some aspects of the impact of nudging surface pressure (see further above), wind, and temperature in the SM.

However, there are limitations to this. Adjustment processes and the influence of the lateral boundaries render the error structures of the 12-hour forecasts after wind field or mass field nudging relatively similar to each other, notably in case G. In this case, the forecast after mass field nudging is slightly superior. In case H, factors not accounted for by the geostrophic theory are important. Nudging of the wind field corrects only about half of the phase error (Figure 4-6d) but preserves the horizontal temperature gradients and corrects the central pressure of the cut-off low. In contrast, mass field nudging (Figure 4-6c) eliminates the phase errors but smoothes horizontal and

temporal gradients at the rapidly propagating fronts and cut-off low. The smoothing occurs as an effect of nudging towards temporally linearly interpolated temperature data over a time interval for which linearity in temperature is a bad approximation around the warm (and cold) front. Without nudging of wind this obviously leads to imbalances (as indicated by large upper-level wind errors), to re-adjustments to the (correctly analyzed) phase, and to a somewhat inferior forecast (which is nevertheless superior to CTRL).

The overall performance of mass field nudging for correcting the mass and wind fields in cases G and H is only slightly inferior to that of wind field nudging. As temperature nudging imposes by far the greatest impact of mass field nudging in this context, this tends to oppose a number of studies that suggest that wind field nudging is significantly more effective than temperature nudging, especially in the mesoscale (cf. Ramamurthy and Carr., 1988; Kuo and Guo, 1989; Ramamurthy and Xu, 1993; Kuo et al., 1993).

4.3.5 Real data experiments

Finally, as simulated observations may have somewhat different properties than real data, for instance regarding their compatibility with the model (cf. section 4.1.1), the influence of surface pressure data and the geostrophic wind correction have been tested with real data replacing the simulated data in cases G and H. (In the largely stationary case G, the nudging period is postponed by 12 hours for a purely practical reason.) Surface pressure and 500 hPa geopotential fields of the assimilation experiments are compared to operational SM analyses. It is assumed that especially surface pressure analyses of the operational SM should be of a sufficiently high quality to serve as reference since (reduced) surface pressure has relatively little small-scale variation and is well resolved by the surface station network, and since the first guesses available for the SM (EM) analyses are likely to be substantially superior to the degraded model states from which the nudging starts in the present experiments (notably in case H).

As in the OSSE's, excluding surface pressure from the full data set to be nudged has marginal impact. Also, adding geostrophic winds corrects a significant part of the surface pressure errors in the vicinity of the cyclones, but introduces secondary errors near the lateral boundaries. The subsequent 12-hour forecasts (+24 h) compare more favourably with the forecasts starting from the operational analyses at +12 h, but not with the operational analyses valid for +24 h. Thus, the benefit from the geostrophic wind correction is at best small, and the results basically confirm the OSSE results.

4.4 Boundary layer, humidity and precipitation

Whilst the previous section was concerned with the relatively large-scale mass (and wind) field of the free atmosphere of which a good simulation forms the basis of a good forecast this section addresses more local aspects of the nudging scheme and of meteorological phenomena which are relevant for modelling and forecasting important weather parameters at or close to the surface. Specific issues are wintertime low stratus, the impact of nudging on the model mixed-layer depth and its diurnal variation in summertime cases with relatively weak winds and little cloudiness, the performance of the nudging scheme in relation to the simulation and prediction of precipitation, and the influence of assimilating temperature, wind, and humidity data on precipitation.

4.4.1 Wintertime low stratus

The motivation here is to provide objective measures to confirm some of the results of chapter 3. Threat scores are computed for low cloudiness using the OSSE approach. It is noted that such measures are of rather limited value (as pointed out in chapter 3) in the context of orographical effects on low stratus, and they should be regarded merely as a supplement and partly as confirmation of the subjective evaluations done chapter 3.

In case A1, low cloudiness threat scores (Figure 4-7) of CTRL for the Alpine and the Swiss Plateau domains are below 0.3 up to +24 h and then rise sharply whilst in case B0, the scores increase far more rapidly (up to 0.85). In both cases, there is a diminishing negative bias of low cloudiness prior to +30 h. Thus, the degraded initial state of CTRL adversely affects the forecast of low stratus by a significant deficit of cloudiness up +24 h.

Standard nudging of rawinsonde data (with the saw tooth temporal weight function, experiment NAW) increases low stratus and improves the scores on each domain in case B0 and (up to +24 h) on the Alpine domain in case A1 (Figure 4-7a). However, it does not improve low stratus on the Swiss Plateau domain in case A1 (Figure 4-7b). A considerable part of the latter domain is substantially influenced by the simulated Stuttgart and Munich soundings which do not indicate saturation. Thus, local information is needed as the horizontal extent of the stratus is limited in this case. Such information is apparently provided by assimilating humidity surface observations in TAW, which enhances the threat scores in the Alpine and particularly the Swiss Plateau domain (Figure 4-7) at the end of the nudging period. However, this improvement is preserved only for strong cloudiness (i.e. for a threat score threshold of 80 %, as opposed to areas, where light cloudiness is included by a threat score threshold of 20 %) and only for 6 hours. As the benefit of the screen-level humidity data lasts no longer than in the real data experiments (cf. section 3.5), this fast decrease of impact in the forecast period is not attributable to inconsistency of the model's boundary layer parameterization with real data of screen-level humidity or to representativeness errors of these data caused by local influences. The decrease is rather likely due to the limitation of the spatial influence of these data or due to a thermal structure in the model that is inconsistent with the humidity structure resulting after the assimilation period. Finally, lateral spreading along isentropes as opposed to σ-surfaces has a very limited impact in the OSSE framework (cf. Figure 4-7).

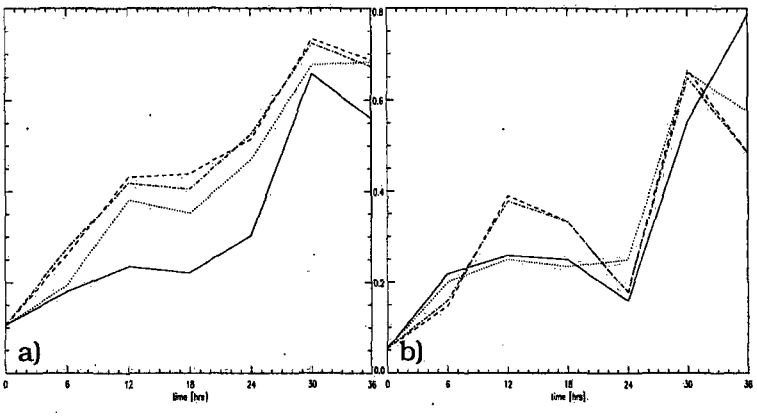

FIGURE 4-7. Evolution of low cloudiness threat scores (cf. section 4.1.1) for OSSE case A1. a): Alpine domain (cf. Figure 4-2), cloud cover threshold: 20 % ; b): Swiss Plateau domain, threshold: 80 %. Solid: CTRL; dotted: NAW (only rawinsonde data); dashed: TAW (with additional screen-level data); dash-dotted: TAW-ISEN (lateral spreading along isentropes). Nudging ends at +12 h.

4.4.2 Mixed layer and its depth in summertime conditions with weak winds and little cloudiness

A realistic modelling of the planetary boundary layer (PBL) and the vertical turbulent exchange of mass and momentum is of primary importance not only for the determination of near-surface parameters, but also for the simulation of relevant meteorological phenomena such as low stratus or convection, and of transport processes of tracers. The mixed-layer depth and its diurnal variation influence the concentration of pollutants such as ozone in typical sunny summertime smog conditions with little large-scale forcing or deep convection - an issue addressed in the Swiss field experiment POLLUMET (POLLUMET, 1996). Here, we merely examine the effect of the nudging on the internal consistency of the SM, i.e. on the mixed-layer depth, and compare its thermal structure to routine rawinsonde measurements. This is in part motivated by the results of Stauffer et al. (1991). Nudging towards 12-hourly temperature analyses also within the PBL led to an almost complete collapse of the mixed-layer depth during the daytime and thus to a breakdown of the diurnal cycle of the PBL. However, Seaman et al. (1995) stressed that this problem was mostly a consequence of the diagnostic technique used to define the mixed-layer depth in their PBL parameterization. By deploying the observation nudging approach for relatively high-frequency (3 to 6 hourly) temperature soundings from a high-resolution rawinsonde network also within the PBL, Seaman et al. (1995) achieved a very realistic mixed-layer depth even in complex terrain with strongly heated summertime conditions.

In the SM, the mixed-layer depth can be diagnosed from in situ turbulent stress which determines the vertical turbulent fluxes. Time series of mixed-layer depth are subjectively evaluated at various grid points in the vicinity of the Alps with a focus on the diurnal variation in the summertime cases D and F. (In case E, which was during a POLLUMET IOP, diurnal variations were small due to significant cloudiness.) Control experiment CTRLA is identical to the complete 30-layer OSSE CTRL integration except that the horizontal diffusion is reduced (by a factor of 5 relative to the operational value) also during the first 24-hour (pre-OSSE) period (cf. Figure 4-1). Although OSSE's have been examined as well, the emphasis is on real-data experiments since the model boundary layer may have properties different from reality, and this could render real data more incompatible with the model (than simulated model data) and provide a potential for disrupting the simulation of the mixed layer and its depth (cf. Stauffer et al., 1991).

To illustrate the influence of the nudging, two examples of mixed-layer depth time series are selected (Figure 4-8a, b) for their pronounced and relatively continuous diurnal signal up to +40 h. (Thereafter, convective systems and precipitation influenced the mixed-layer evolution.) The diurnal cycle of the CTRLA and RTAS-4DDA (standard nudging throughout the period with linear temporal interpolation) mixed-layer depth agree well with general conceptual models of the PBL (cf. Stull, 1988): a rapid increase in the morning due to solar radiative heating of the surface, relatively little change in the afternoon, and a sudden breakdown in the evening due to (longwave) radiative cooling at the surface which induces the generation of a stable nocturnal boundary layer topped by a residual layer.

However, the nudging in experiment RTAS-4DDA reduces the mixed layer depth relative to CTRLA, especially in the afternoon. In a free forecast starting at noon after a nudging period, the influence of the nudging on the growth rate of the mixed-layer depth is quickly lost, but the effect of the corrected 'initial condition' at 1200 UTC per-

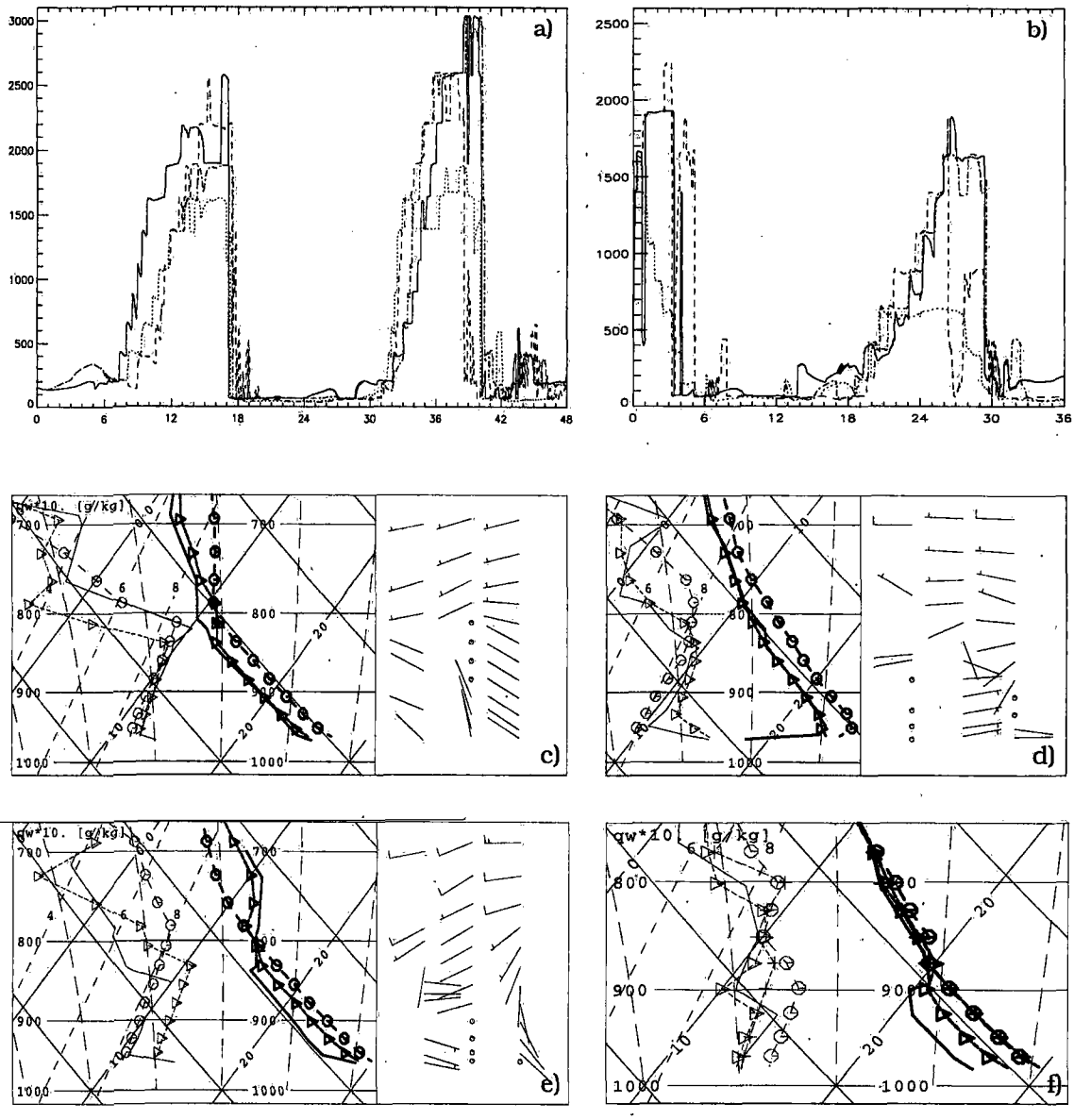

FIGURE 4-8. Top row: time series of mixed-layer depth (in metres). a) for case D at Munich; b) for case F at Stuttgart. Solid: CTRL; dotted: RTAS-4DDA (continuous standard nudging of real data throughout the period with linear temporal interpolation); dash-dotted: as RTAS-4DDA, but free forecast after +12 h; dashed: RTAS-TMIX (as RTAS-4DDA (i.e. also continuous nudging throughout the period), but without temperature nudging within the mixed layer).
Bottom rows: vertical profiles as at Figure 3-7 (emagramme with temperature and dewpoint, horizontal wind). The following profiles are shown (wind columns from left to right): solid lines: observation; circles: CTRL; triangles: RTAS-4DDA: crosses (for f) only): RTAS-TMIX. c): case D, +12 h (valid for 1200 UTC, 4 July 1993); d): case D, +24 h; e): case D, +36 h; f): case F, +24 h (valid for 1200 UTC, 6 August 1994).
The stepwise rise in the mixed-layer depth time series during the forenoon reflects the increasing number of turbulent model layers, and this number of layers can be compared to the number of layers (denoted with symbols, except for the lowest model layer) with constant potential temperature and specific water content in the vertical profiles at noon.

sists up to the breakdown of the mixed-layer depth in the evening (cf. Figure 4-8a). If temperature is not nudged within the mixed-layer (experiment RTAS-TMIX, with nudging throughout the period) as proposed by Stauffer et al. (1991), the mixed-layer depth is often very close to that of CTRLA. Thus, the temperature nudging within the mixed layer is the major factor to the reduction of its depth, and the question arises whether this results in a better agreement with reality.

Gassner (1995) computed the SM mixed-layer depth using a criterion on the vertical profile of potential temperature, compared it to Doppler-SODAR measurements, and found that the diurnal maximum of the SM mixed-layer depth generally tends to be too high and by several hours too late in the afternoon. Note however, that observed (and modelled) mixed-layer depth values for the late afternoon are subject to great uncertainty (Gassner, 1995; Beyrich and Görsdorf, 1995).

Here, the comparison of model and observed mixed-layer depths is based on 1200 UTC vertical profiles of temperature and humidity. For this date, the height of (vertically) constant model values of potential temperature and specific water vapour content (as an alternative definition for the mixed-layer depth) is found to generally agree well with the model's mixed-layer depth from time series.

Figure 4-8 illustrates for the same examples as above that if continuous nudging is applied also in the boundary layer (experiment RTAS-4DDA), the model fits the observed mixed-layer depth as derived from the rawinsonde profiles far better than without nudging (CTRLA). In CTRLA, the mixed layer is 1 to 3 model layers too deep and too warm (probably partly due to incorrect surface heat fluxes), and the excess of low-level heat persists during the night, i.e. throughout the diurnal cycle. In case F, the pronounced observed capping inversion at Stuttgart at noon (+24 h) is likely to hinder the growth of the mixed layer in the afternoon. This is simulated well by RTAS-4DDA whilst the other experiments (CTRLA and RTAS-TMIX) fail to indicate the inversion and exhibit a strong increase of the mixed-layer depth. Similar differences have been obtained at other locations. Note that nudging in RTAS-4DDA also corrects most of the wind, temperature, and humidity errors which are often significant in CTRLA within the daytime mixed layer or nocturnal residual layer (see Figure 4-8).

In conclusion, nudging towards routine rawinsonde (and surface humidity) data, including nudging of temperature profiles within the mixed layer, is fairly effective in correcting the evolution of the mixed layer, namely its depth, wind and temperature, in typical sunny summertime conditions prone to smog. In such cases, the nudging approach has a good potential to significantly improve diagnostic data sets generated with the SM. However in a forecast, the positive impact of the nudging on the mixed-layer depth disappears within 6 to 12 hours.

4.4.3 Precipitation

Verification of precipitation is particularly valuable. Precipitation is the result of, and highly sensitive to, many complex dynamical and physical processes active on all scales of motion, and it is usually characterized by a significant small-scale variability. This makes it very difficult to simulate it accurately. At the same time, it is (one of) the primary goal(s) of most mesoscale models (and in particular of the SM) to deliver accurate and detailed precipitation forecasts. Furthermore, it is not an assimilated variable itself, so that an increase of the precipitation forecast quality often requires an improvement of the fields of several, if not all, the primitive variables.

To this end, OSSE's have been evaluated for cases D, E, F, G and H. In the absence of high quality real-data precipitation analyses, the approach is an efficient tool for the refinement of the nudging scheme since the experimental set-up should have less impact on the relative than absolute forecast quality. This allows to address specific problems related to precipitation, e.g. the benefit from nudging humidity. The performance of the scheme is illustrated for cases F, G and H.

A. Case F: correction of position of mesoscale convective systems

Case F is selected here for the occurence of significant position errors of mesoscale convective systems in CTRL and for the remarkable performance of the nudging scheme. The 850 hPa geopotential field is generally flat, but a considerable low-tropospheric

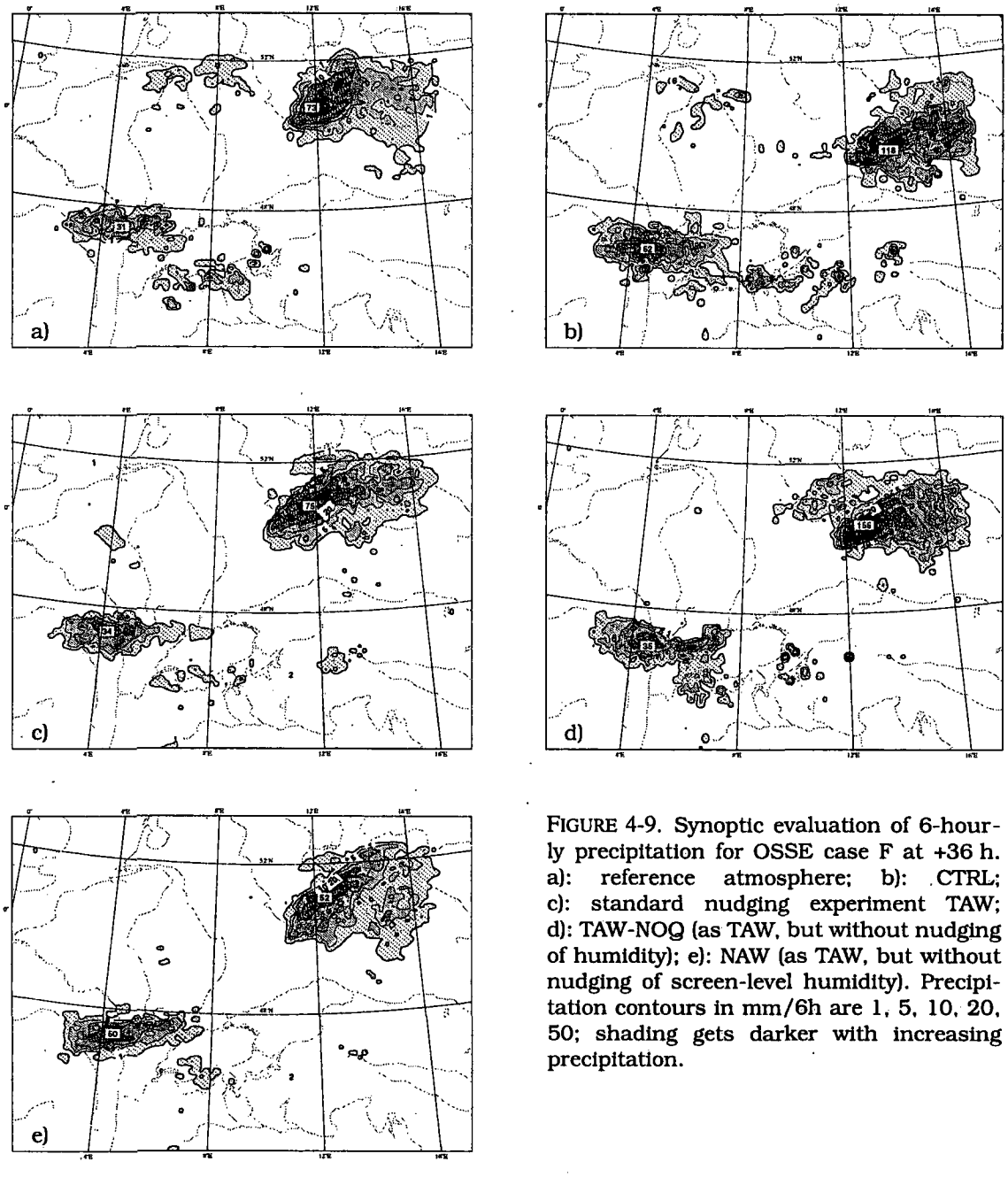

FIGURE 4-9. Synoptic evaluation of 6-hourly precipitation for OSSE case F at +36 h. a): reference atmosphere; b): CTRL; c): standard nudging experiment TAW; d): TAW-NOQ (as TAW, but without nudging of humidity); e): NAW (as TAW, but without nudging of screen-level humidity). Precipitation contours in mm/6h are 1, 5, 10, 20, 50; shading gets darker with increasing precipitation.

north-south temperature gradient causes a substantial westerly geostrophic flow component at 700 hPa and above. This drives the mesoscale convective systems from west to east. However, the systems couple with the low-level wind field, and significant errors in the initial CTRL fields, particularly of humidity and of the weak but rich low-level wind cause significant position errors of the precipitation patterns up to the end of the forecast period (Figure 4-9). The largest system has moved from Central France to northwestern Czechia instead of eastern Germany at +36 h, and a second system with a low-level convergence line northwest of Switzerland is displaced to the south by about 70 km, bringing about erroneous precipitation over western Switzerland. Note that this second system has moved into the model domain only after +24 h. Although perfect information is advected from the west except at low levels the interaction with (wind, temperature and humidity) errors at low levels leads to the position error. Nudging with standard parameters deploying the saw tooth time function (experiment TAW) is not only able to completely eliminate the erroneous precipitation of a convective system early in the forecast (not shown), but to largely correct the position and maxima of precipitation (and reduce primitive variable field errors) up to the end of the forecast period (Figure 4-9).

B. Impact of humidity data

It is widely accepted that the specification of moisture is one of the weakest links in today's data assimilation systems. Several authors (Stauffer and Seaman, 1990; Ramamurthy and Xu, 1993; Kuo et al., 1993; Yap, 1995) found an adverse impact of nudging towards mixing-ratio analyses from rawinsonde data as it led to a serious underforecast of precipitation. Although the most reliable moisture data available still come in the form of rawinsonde dewpoint depression profiles (Ledvina and Pfaendtner, 1995), it is recognized that the errors of these data (cf. section 2.2) and their poor spatial and temporal resolution (cf. section 3.5) may contribute to a degradation of the precipitation fields. Lorenc et al. (1994) found for the UKMO analysis correction scheme that although relative humidity from rawinsonde led to a spin up, its assimilation was nevertheless important for precipitation forecasting, and Cram et al. (1993) noted that humidity analysis nudging decreased mixing ratio rms errors in the subsequent 12-hour forecast period without having a significant feedback effect on the other variables.

To examine the benefit of humidity data on the general forecast quality and specifically on the simulation of precipitation, humidity data are excluded from the data set in experiment TAW-NOQ. The 6-hourly precipitation at +36 h in case F (Figure 4-9) clearly does not agree as well with the reference precipitation as the TAW precipitation does. The position errors of both convective systems are only partly corrected, and the rainfall maximum of the northesterly system is too large. Since the heavy rainfall is associated (and strongly correlated around 700 hPa) with a cyclonic wind vortex and temperature anomaly in that system and with a convergence line in the second system northwest of Switzerland, the positive feedback effect of humidity assimilation on the other variables is significant in this case. A pronounced benefit from rawinsonde humidity data is also observed in case D whilst the impact is small in case E.

Excluding only screen-level humidity data (NAW) has only a slight negative effect on precipitation in case F (Figure 4-9) and tends to have even a slight positive influence in case D. Generally, the benefit from these data for precipitation forecasting hardly appears to be significant.

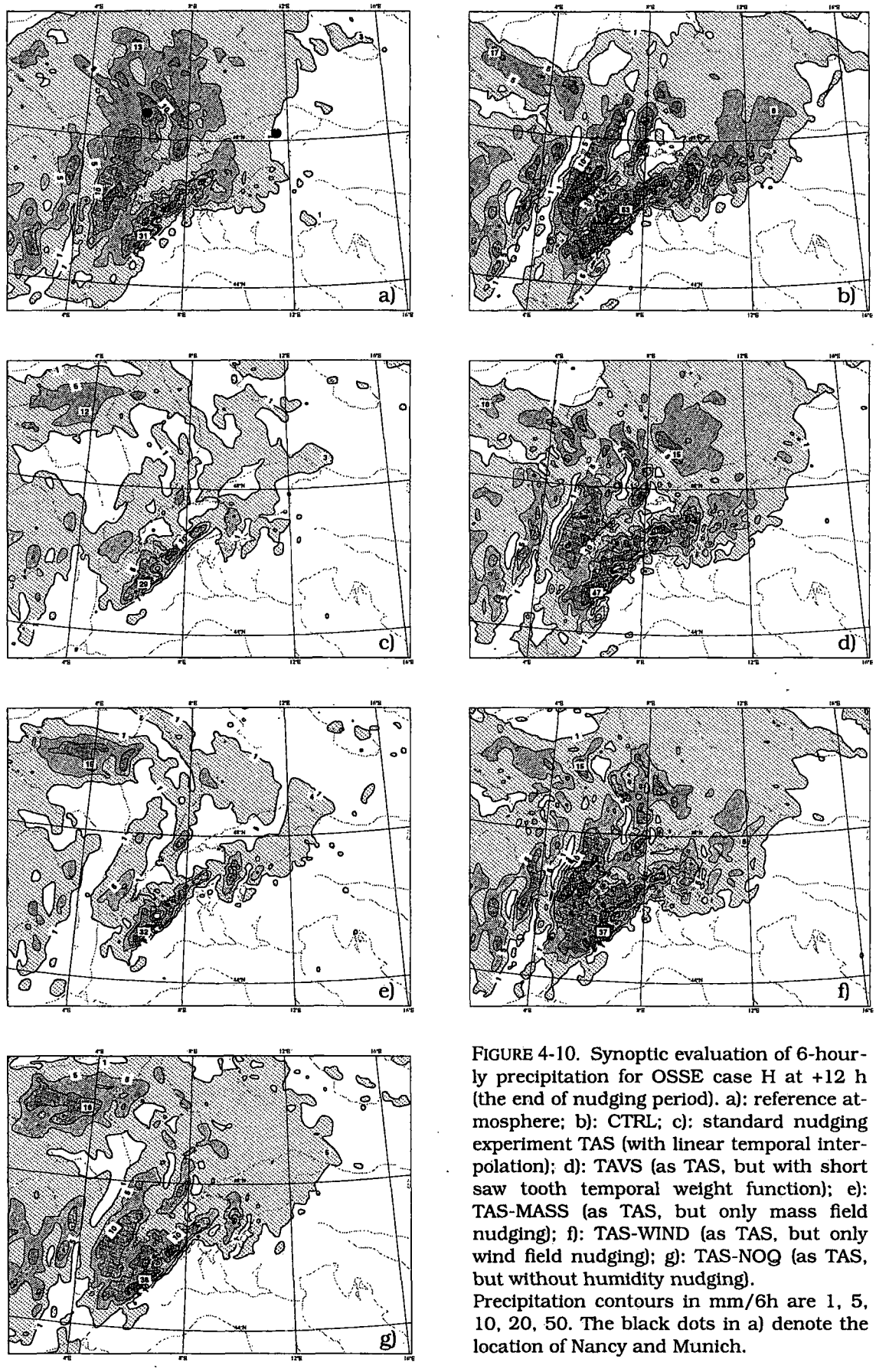

FIGURE 4-10. Synoptic evaluation of 6-hourly precipitation for OSSE case H at +12 h (the end of nudging period). a): reference atmosphere; b): CTRL; c): standard nudging experiment TAS (with linear temporal interpolation); d): TAVS (as TAS, but with short saw tooth temporal weight function); e): TAS-MASS (as TAS, but only mass field nudging); f): TAS-WIND (as TAS, but only wind field nudging); g): TAS-NOQ (as TAS, but without humidity nudging).
Precipitation contours in mm/6h are 1, 5, 10, 20, 50. The black dots in a) denote the location of Nancy and Munich.

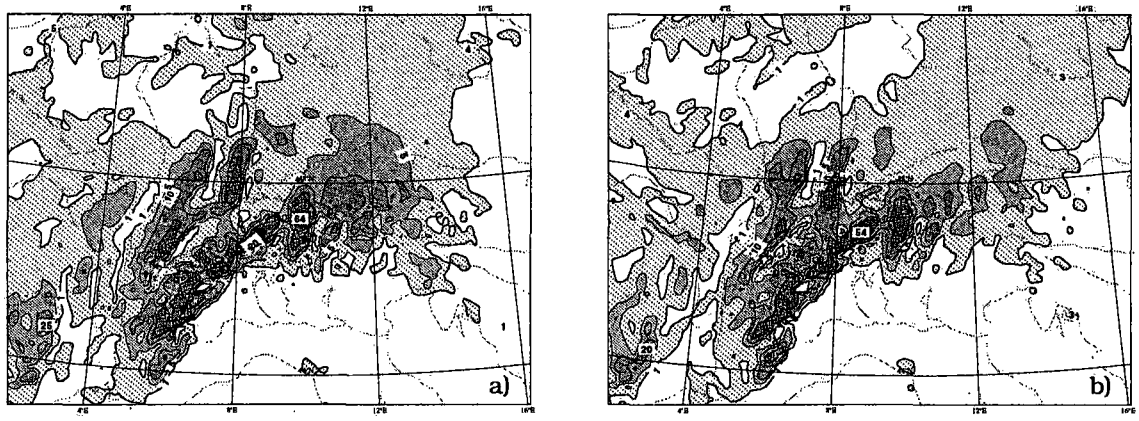

FIGURE 4-11. Synoptic evaluation of precipitation as in Figure 4-10, but for +18 h (6 hour forecast). a): reference atmosphere; b): standard nudging experiment TAS (with linear temporal interpolation).

C. *Case H: influence of the temporal nudging weights on precipitation*

Severe problems with correcting precipitation patterns by nudging within the OSSE framework are encountered in case H. At the end of the nudging period, the main precipitation which is associated with the cut-off low and the warm front is just passing the upper Rhine Valley in the reference atmosphere (Figure 4-10a). Bands of relatively intense precipitation over the northwestern part of the Alps and west of Jura Mountains are at least partly orographically enhanced. Weak precipitation is just reaching Munich. In CTRL (Figure 4-10b), the phase error of the cut-off low (cf. section 4.3) causes the warm frontal precipitation to be displaced southeastward (i.e. centered over Munich) and the orographically enhanced precipitation to be too strong.

Nudging with linear temporal interpolation (experiment TAS, Figure 4-10c) largely corrects the phase error (precipitation is just starting at Munich) but dramatically underestimates precipitation amounts particularly around the center of the cut-off low, the warm front, and all over eastern France. In the early forecast, these errors are significantly reduced, and are mainly to confined to relatively flat areas in Bavaria (Figure 4-11). This is mainly an effect of the perfect lateral boundaries, and of the Alps. Predictability is often enhanced in the presence of significant orography (cf. Vukicevic and Errico, 1990; Weygandt and Seaman, 1994), and for a high mountain ridge such as the Alps, orographically enhanced precipitation tends to be less sensitive to the temperature and humidity structure and to phase errors.

However, underestimation of precipitation in the data assimilation period can have generally a deleterious effect on daily routine forecasts provided that the initial states are deduced from a continuous data assimilation cycle as is common practice. It will then cause a tendency to dry out the model soil and thereby change the model climate. It is often found (cf. Bouttier et al., 1993; Garratt, 1993; Viterbo, 1995) that (convective) precipitation rates are strongly dependent on surface evaporation and thus (namely in the summer season) on the availability of soil moisture. This applies also for the SM (Bayerle, 1995). Therefore, it is appropriate to examine the failure of the nudging to correct the precipitation errors during the assimilation period in the present case.

In view of section 4.3, it appears that the underestimation of the precipitation in TAS is linked to the smearing of the warm front and the cut-off low. Based on this hypothesis,

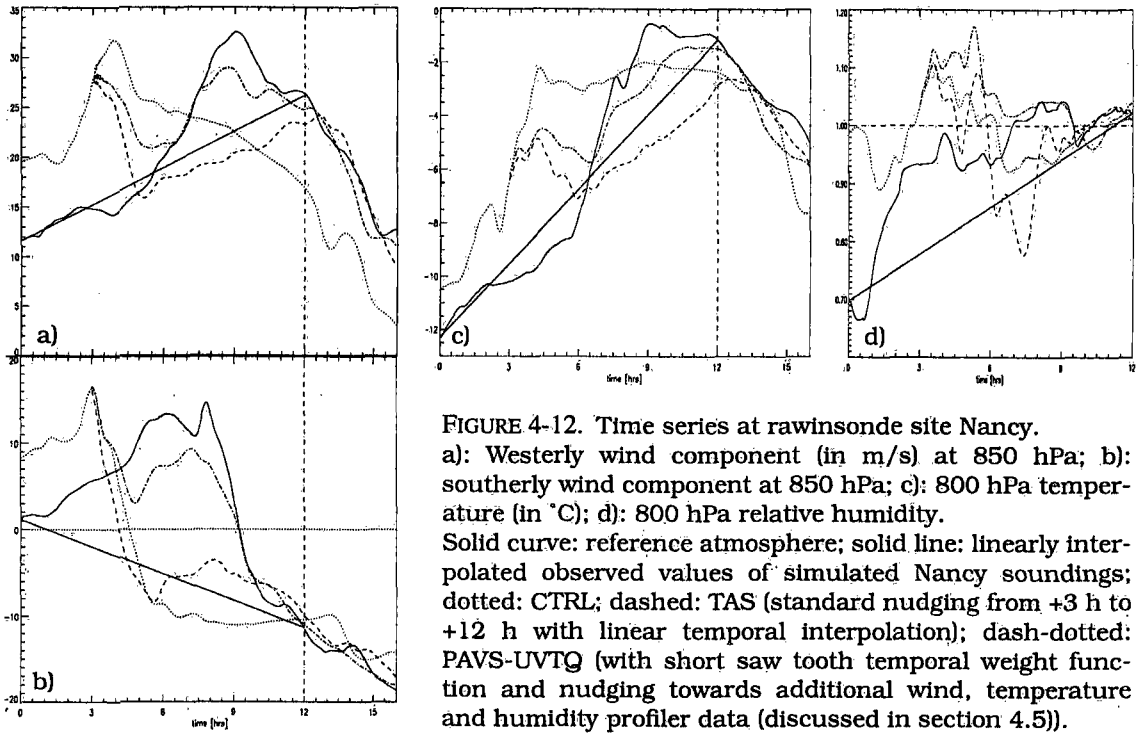

FIGURE 4-12. Time series at rawinsonde site Nancy.
a): Westerly wind component (in m/s) at 850 hPa; b): southerly wind component at 850 hPa; c): 800 hPa temperature (in °C); d): 800 hPa relative humidity.
Solid curve: reference atmosphere; solid line: linearly interpolated observed values of simulated Nancy soundings; dotted: CTRL; dashed: TAS (standard nudging from +3 h to +12 h with linear temporal interpolation); dash-dotted: PAVS-UVTQ (with short saw tooth temporal weight function and nudging towards additional wind, temperature and humidity profiler data (discussed in section 4.5)).

the relatively small effect which the omission of wind field data (experiment TAS-MASS, cf. Table 4-3) has on the warm front (cf. Figure 4-6c) suggests also a small effect on precipitation. This is indeed confirmed in Figure 4-10e. Moreover, experiments TAS-WIND (omission of mass field data) and TAWS (use of the saw tooth temporal weight function) render not only a great improvement of the temperature gradients (cf. Figure 4-6d), but also of the precipitation amounts (Figure 4-10f). At the same time, they fail to eliminate the phase errors of both the warm front and the precipitation, thus indicating a link between the phase correction of the front and the phase correction of the precipitation. (Note that in TAWS, the first hours contributing to the 6-hour sum of precipitation are little influenced by nudging since no sounding is available near strong precipitation at +6 h.)

Why does the nudging fail to eliminate the phase error without diminishing precipitation amounts? Another experiment (TAVS) reveals that from halfing the width of the saw tooth temporal weight function, a small impact results, and this indicates that even this short nudging time window is long enough. However, when the saw tooth function is applied, rawinsonde observations of only one date (+12 h) are utilized in main area of interest in the 9-hour nudging period, and this is not sufficient to properly resolve the exact position of the main gradient of the warm front (cf. Figure 4-5a). The main temperature errors in TAVS occur between the rawinsonde stations, but are small at the stations themselves (except at Stuttgart). Consequently, an observing network that is substantially denser in the horizontal should allow a more complete correction of the phase.

What may be expected from an increase of the temporal data resolution? Linear temporal interpolation also uses the data from +0 h, and this appears sufficient to eliminate the phase errors, albeit at the cost of smoothing gradients due to linearization. Hence, an increase of the data frequency to the extent that the absolute errors of a lineariza-

tion in the interval between observing times become small should allow to correct the phase without significant smoothing of the gradients. In conclusion, insufficient horizontal and/or temporal upper-air data resolution contribute to the precipitation errors in this case.

Two questions remain in relation to the smoothing effects with 12-hourly linear interpolation. First, why does nudging of only the wind field not cause significant smoothing of the fronts or reduction of precipitation amounts? Various time series for wind components and temperature (e.g. for Nancy (Figure 4-12) which is amidst the main precipitation area, cf. Figure 4-10a) reveal that linearity is as bad an approximation for wind as for temperature, and that the wind field tends to be drawn towards the (linearly interpolated) observations even faster and more completely than temperature if all variables are nudged. Thus, linearization and smoothing of the wind occurs but appears to have a limited impact on the magnitude of (small-scale) temperature gradients and on precipitation rates in this case. More disruptive effects may be expected in other cases, e.g. where precipitation is more sensitive to low-level convergence or wind shear.

Second, what is the effect of linear interpolation of humidity? In time series of (low-tropospheric) relative humidity, little evidence for excessive drying is found (cf. Figure 4-12d). However, if humidity is not nudged (experiment TAS-NOQ) then precipitation (Figure 4-10g) is significantly enhanced but still underestimated in most areas. Consequently, the underestimation of precipitation is primarily due to linear interpolation of temperature and humidity data.

D. Real data applications

The real data experiments of section 4.3 that have been carried out for cases G and H with a focus on correcting the mass field in the free atmosphere are also evaluated in analogous way with respect to precipitation. Clearly, the reference precipitation forecasts up to +12 hours starting from the most recent operational analyses are much more likely to contain significant errors compared to the operational surface pressure analyses, but the errors should be assumed still significantly smaller than the errors of the CTRL precipitation forecasts that start from older and degraded initial states.

Although there are some differences if real data instead of simulated data are assimilated in case H, the precipitation patterns are remarkably similar. Notably, the charactistic properties of various experiments regarding the shape of the temporal weight function or the influence of geostrophic wind correction are qualitatively confirmed in the real data application. Thus, the results and conclusions derived above from the OSSE's appear to be valid also for real data applications.

In case G, experiment REF starts from an operational analysis, whilst CTRL starts from 48-hour forecast fields and should be expected to have clearly larger errors. The initial state of RTAWS is obtained after a 12-hour nudging period starting from 36-hour forecasts, and the aim of the nudging towards real data is to 'convey' the CTRL precipitation patterns approximately to those of REF. This is successfully achieved (Figure 4-13): the position of precipitation band north of the Alps as well as its maximum is corrected, the erroneous precipitation over the Alps and Venezia region is eliminated, and the position of the band of heavy rain over the eastern gulf of Lyon is correctly shifted westward. This illustrates the potential for correcting precipitation patterns which the nudging scheme also has for real data.

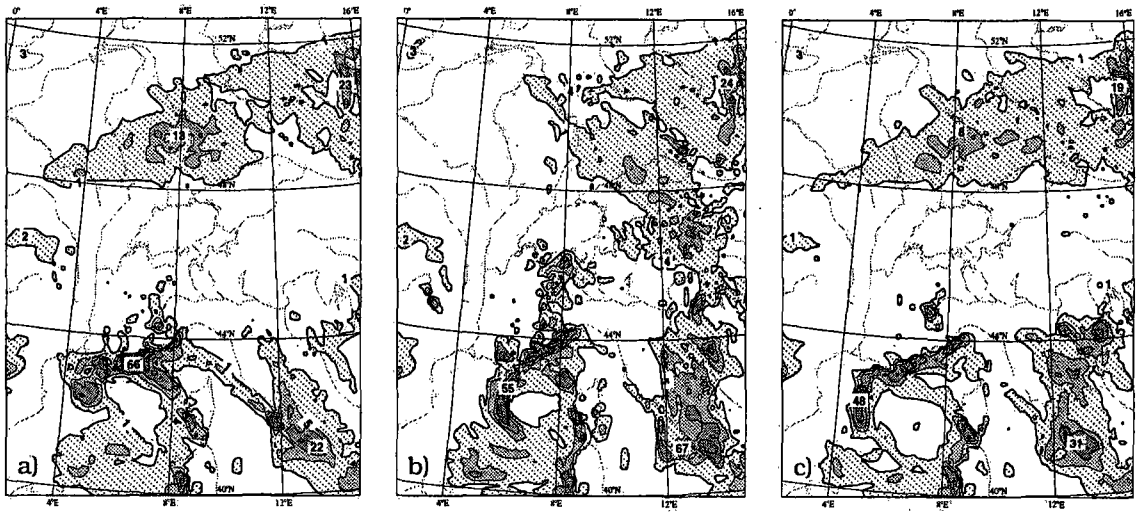

FIGURE 4-13. Synoptic evaluation of 6-hour sums of precipitation for real-data case G. a): reference experiment REF; b): CTRL; c): RTAWS (12-hour forecast after 12 hours of standard nudging towards real data). For further explanation, see text.

For case E, where the operational integrations completely missed the line of thunderstorms with (observed) heavy precipitation within a band along the Swiss Plateau in the morning of 16 July 1993, an experiment with nudging towards real data is performed. It does not capture the event either although the nudging increases the tendency of precipitation in Switzerland (i.e. mainly over the northeastern part of the Swiss Alps). Note that none of the 0000, 0600 (for Payerne) and 1200 UTC rawinsonde profiles in the environs of Switzerland indicated saturation although the humidity was high in most soundings. Thus, these observations did not capture the event itself, and the assimilation of these data could at best have assisted the model to produce the thunderstorms itself. This case illustrates the limits of the performance of the nudging scheme.

4.5 Additional observations: impact of simulated profiler observations

It has been shown in sections 4.3 and 4.4.3 that nudging towards conventional (simulated) rawinsonde data is not able to correct the phase errors of the warm front and the precipitation band of case H without decreasing the gradient of the front and the rate of precipitation. Insufficient temporal and/or horizontal resolution of the upper-air rawinsonde data has been suggested as a major cause for this problem.

The recent advances in the development of remote sensing observing systems will provide considerably more mesoscale, high-frequency data sets in the near future. This applies particularly for wind since wind profilers are commercial. In combination with these profilers, RASS (Radio Acoustic Sounding Systems) can profile virtual temperature. Other systems include spectro-radiometers, lidars, GPS (Global Positioning System, cf. Businger et al., 1996) and combined systems (cf. Stankov, 1995; Han and Westwater, 1995) but these are mostly in the experimental stage and only partly applicable to the mesoscale. The largest operational remote sensing network at present is a demonstration network of 30 wind profilers in the US (NOAA, 1993). Assimilation of

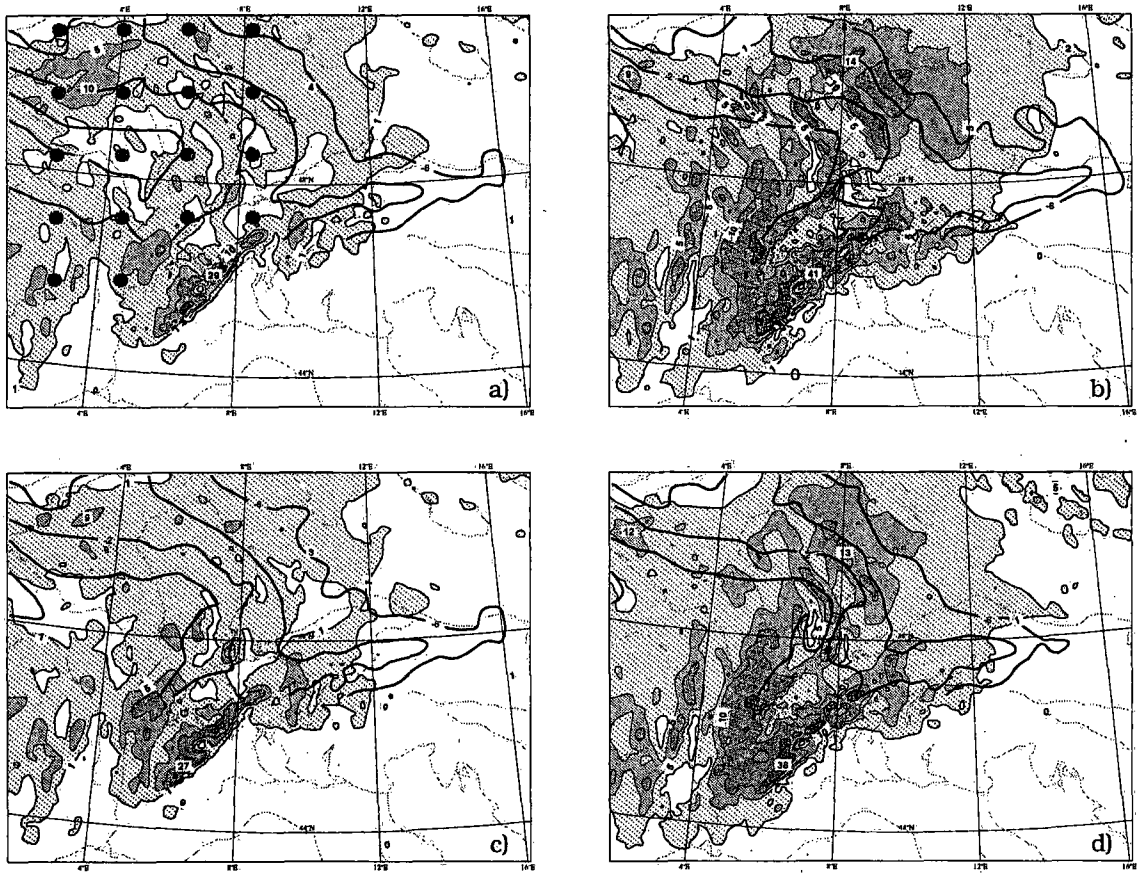

FIGURE 4-14. 6-hourly precipitation (shading, contours for 1, 5, 10, 20, 50 mm/6h as in Figure 4-10) and 850 hPa temperature (black lines, only contours 0K, -2K, -4K, -6K north of the Alps, cf. Figure 4-5) for case H at the end of the nudging period (+12 h).
All experiments include nudging of all rawinsonde and surface data and of a subset of the profiler data. Left row: linear temporal interpolation; right row: short saw tooth temporal weight function.
a), b): PAvS-UV (utilized profiler data: wind); c), d): PAvS-UVT (utilized profiler data: wind and temperature). The black dots in a) denote the locations of the simulated profilers.

real data from that network has proved beneficial in a number of recent studies (Smith and Benjamin, 1993; Smith and Benjamin, 1994; Xu and Ramamurthy, 1994).

It is expected that nudging of high-frequency data sets from remote sensing observing systems, if available, would improve the analysis (e.g. for case H). In the absence of real data, the OSSE technique allows consideration of the potential influence of hypothetical observing systems. This approach was adopted by Kuo and Guo (1989) for nudging high-frequency wind and temperature profiles. Here, the impact of hourly wind, temperature and humidity profiles is addressed for case H in an exploratory manner within the OSSE framework. For this purpose, hourly profiles for the 9-hour nudging period are extracted from the reference atmosphere at 18 grid points (cf. Figure 4-14a) which form a regular grid with a horizontal resolution of about 110 by 150 km in the main precipitation area. For wind components, an rms error (cf. Table 4-2) of 1.5 m/s is added to these perfect 'observations' like for rawinsonde winds, but for temperature, the rms error is increased to 1 K (cf. Browning and Szejwach, 1994) and for relative humidity to 10 %. The additional hourly profiler data of either wind (experiment PAvS-UV, cf. Table 4-3), wind and temperature (PAvS-UVT), or wind, temperature and humidity

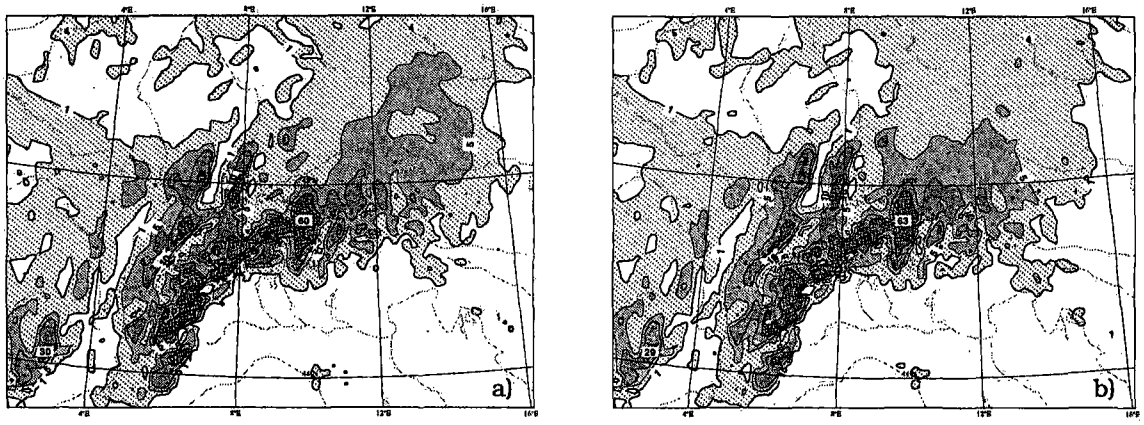

FIGURE 4-15. 6-hourly precipitation as in Figure 4-14 (shading, contours for 1, 5, 10, 20, 50 mm/6h as in Figure 4-10) but for the beginning of the forecast period (+12h to +18 h).
a): PAVS-UV (utilized profiler data: wind); b): PAVS-UVT (utilized profiler data: wind and temperature). In both experiments, the short saw tooth temporal weight function is used.

(PAvS-UVTQ) are then nudged in addition to the rawinsonde and surface data using linear temporal interpolation or the short saw tooth time function.

Clear improvements on the gradients and position of the warm front are brought about only by the profiler data of temperature in addition to wind (Figure 4-14c, d), but not of wind alone (Figure 4-14a, b). Precipitation is at most modestly improved by wind profiler data, and the further improvement induced by the additional nudging of the temperature profiler data is clearly more significant. The impact of assimilating humidity profiler data on top of that is rather weak and mixed (not shown), as precipitation is somewhat increased (and thus improved) with linear temporal interpolation, but somewhat decreased (and deteriorated) if the saw tooth function is used.

Temperature profiler data appearing to have a larger impact than the wind profiler data contrasts with the results of Kuo and Guo (1989) who neglected rawinsonde data but assumed a uniform profiler network covering the entire model domain (with an rms error of 1 m/s for simulated wind data and 1 K for temperature data). Specifically, they noted a significant improvement of the temperature field by use of only wind profiler data through the model's large-scale adjustment. Such an effect of the wind profiler data on temperature is not apparent in the present experiments. This may be partly attributable to the assimilation of rawinsonde temperature data which already largely corrects the temperature field except for meso-β-scale errors at the fronts.

Comparing the two concepts of temporal weighting for rawinsonde data when additional wind and temperature profiler data are also nudged, it is obvious that linear temporal interpolation of the 12-hourly rawinsonde data within (and outside) the profiler network still causes smoothing of the warm front and underestimation of precipitation. Thus, the benefit from the profiler data is limited. In contrast, when the (short) saw tooth function is deployed, nudging of the additional hourly profiler data renders an almost complete correction of the phase of the warm front and the main precipitation, and smoothing remains weak at the end of the nudging period. The overall performance is clearly the best in this latter experiment (PAVS-UVT), and the 6-hour precipitation forecast (Figure 4-14b) is very similar to the reference forecast (Figure 4-11a).

With the use of additional profiler data of wind only, precipitation (Figure 4-14a) is erroneously enhanced over the western part of the Czech Republic in the 6-hour forecast. This may be due to inconsistencies at the (northeastern) edge of the profiler network, where there is a strong inhomogeneity in horizontal data density during the first 7 hours of the nudging period (from +3 h to +10 h). It is remarkable that this effect is absent if the temperature profiler data are also utilized.

The benefit from the increase of the temporal (and horizontal) resolution of independent data relative to linear interpolation of 12-hourly rawinsonde data is also illustrated in the Nancy time series (Figure 4-12). If all profiler data are additionally nudged and the short saw tooth function is deployed the tendency for the wind and temperature evolution to be smoothed is strongly reduced, and drying is avoided. Rather, the warming brought about by the warm front at Nancy is split into two distinct parts, with an intermediate period of relatively little temperature change from +4 h to +8 h.

The nudging of the hourly data basically interrupts the eastward propagation of the cut-off low and the warm front, so that most of the phase error is eliminated by +8 h. Examination of horizontal temperature fields reveals that during that phase adjustment, considerable transient horizontal smoothing occurs even by nudging of the hourly data. Subsequently, however, these data help to re-intensify the horizontal gradients so that smoothing weakens by the end of the nudging period. The transient horizontal smoothing hardly affects mean precipitation amounts.

In order to estimate the sensitivity to the observation frequency, profiler data are assumed to be available only every 6 hours (at +6 h and +12 h). The resulting deterioration of the warm front and 6-hourly precipitation is modest at the end of the nudging period. Yet, the phase error of the warm frontal precipitation of the subsequent 6-hour forecast is centred between the phase errors that result when hourly respectively no profiler data are utilized. If only profiler data at +12 h are considered (which corresponds to an increase of the horizontal resolution only) the benefit from these additional data almost disappears. Nevertheless, it cannot be concluded generally that an increase of only the horizontal data density is not beneficial since the major errors associated with the warm front and the associated precipitation band have already left the area of the profiler network by +12 h.

It is clear from these experiments is that there are flow situations where significant improvements result from the assimilation of additional 6-hourly vertical profiles of wind and notably temperature from a profiler network. The benefit from this network is further increased when the data are available at an hourly rate.

5 Conclusion

A nudging scheme has been developed for assimilation of rawinsonde and screen-level data into a mesoscale model for the Alpine region, and applied to routine observations to examine its potential capabilities and limitations for NWP purposes. Aspects of primary interest are the impact of different data, the influence of steep orography particularly with low stratus, and the benefit from the nudging for mixed-layer simulation in typical summertime smog conditions. Here, the main results are summarized, and possibilities for further improvement of numerical forecasts are outlined.

5.1 Summary of the main results

a. Impact of different data

1. Linear **geostrophic adjustment theory** provides a guideline for estimating the degree of (i) assimilation of the observational information, and (ii) mutual adjustment of the mass and wind fields with a mesoscale model. However, the adjustment is only partly geostrophic, and the residual flow is often substantially modified by orography, significant advection, and non-linearity in time of the flow fields within the time scale of the temporal nudging weights (e.g. with fronts).
2. Nudging of **surface pressure** has only a small effect, limited mainly to the larger scales. However, most of the pressure error is eliminated by nudging the wind and temperature profiles from the rawinsonde network. The remaining error is typically concentrated at mesoscale flow structures such as mesoscale cyclones.
3. Nudging of vertical **temperature** profiles is found to be as important as nudging of **wind** profiles, particularly in the boundary layer. This applies to 12-hourly rawinsonde data and to (simulated) hourly profiler data.
4. Errors in **precipitation** patterns are reduced fairly efficiently by the nudging scheme. In particular, this has been shown in OSSE's for position errors of precipitation associated with mesoscale convective systems or fronts. Nudging of **humidity** profiles is beneficial in most cases, but screen-level humidity data have little impact on precipitation.
5. In an exploratory case study, significant benefit for the simulation of warm frontal precipitation and temperature gradients results from the assimilation of additional hourly vertical profiles of wind and particularly of temperature from a relatively dense, **simulated profiler** network.
6. The **lateral boundaries** have an integral influence on the pressure field, and in the presence of strong advection, their influence on short-range forecasts dominates over influence of the initial conditions.

b. Tuning and refinement of the scheme

7. A **nudging coefficient** of $6 \cdot 10^{-4}$ s^{-1} for all variables is appropriate for the SM. The degradation caused by halving the coefficients is small over flat terrain but more pronounced near steep orography.
8. Little sensitivity to the scale of the **horizontal weight function** is found, provided that the scale is comparable to the station separation, and that the (upper-air) data are as accurate, dense, and uniformly distributed as in the further envi-

rons of the Alps.

9. 12-hourly linear interpolation and a saw tooth shaped **temporal weight function** with a time window of 6 hours render similar the overall performance of the nudging. However in individual cases, differences are often significant: linear interpolation is superior with persistent low stratus near steep orography and corrects the position of steadily propagating features (e.g. fronts) more efficiently, but tends to be inferior otherwise, e.g. in relation to mesoscale (frontal or convective) precipitation. Halfing of the time scale of the saw tooth function has a far smaller impact.

10. 12-hourly linear interpolation of rawinsonde data tends to render **almost linear** the **evolution** of the temperature and humidity fields. This smoothes horizontal temperature gradients of propagating fronts, and leads to underestimation of frontal precipitation particularly during the assimilation. A similar tendency to an almost linear evolution of the wind field appears to have less effect.

11. The use of a **geostrophic wind correction** devised to enhance the assimilation of surface pressure data does not result in improved forecasts. It increases the scheme's sensitivity to the scale of the horizontal weight function, and to variations in the data density, e.g. in the presence of data-poor areas over the sea.

12. No significant deleterious, spurious increase of **inertia-gravity wave activity** results from the nudging of rawinsonde and screen-level data except with the use of the geostrophic wind correction. Hence, the scope for benefit from noise control procedures is limited.

Specific problems arise near steep orography, when rawinsonde observation increments over low terrain are spread laterally upslope along the terrain-following σ-surfaces to high terrain, i.e. areas for which the observation is not often representative, particularly with low stratus. Two approaches are tested to tackle this problem.

13. Use of a **non-isotropic horizontal weight function** to restrict an observation's direct influence to representative areas tends to degrade forecasts of low stratus, probably because the data-poor area over high terrain (e.g. the Alps) does not directly benefit from observational information with this approach.
Spreading of rawinsonde data increments **along isentropes** (which is a new concept for σ-layer models) or isobaric surfaces leads to modest improvement of the low cloud cover and the vertical thermal and humidity structure in the analyses and forecasts. Consistent application of this new concept to all rawinsonde stations (instead of a subset located near steep orography) can be important, and the effect over moderate terrain with variations of few hundred metres can be as large as over steep orography.

c. Application to low stratus with a focus on orographic effects

14. Nudging is able to improve the vertical structure of the initial state relative to the operational SM analyses during episodes of low stratus. Near steep orography, the improvement on the representation of inversions, humidity gradients and cloud cover pertains in the forecast period only if the **horizontal diffusion** along the model's σ-layers is strongly reduced. With the operational coefficient, the horizontal diffusion contributes to an enhanced vertical coupling and a significant reduction of stability and humidity gradients near steep orography.

15. With **extra vertical model resolution**, nudging of rawinsonde data is able to in-

troduce finer vertical structures and increase the effective resolution of the initial state. This is often a requirement for a benefit of the forecast from extra resolution. A second requirement is the reduction of the horizontal diffusion. Since the onset and dissolution of (low) cloud has strongly non-linear radiational feedback, extra resolution need not have a merely gradual impact but may change fundamental properties of the forecast.

16. Nudging towards **screen-level humidity data** from a high-resolution network of surface stations **at various altitudes** can substantially improve the analyses near steep orography, but a significant benefit on the humidity and temperature structure does not often pertain to 12-hour forecasts. In the analyses, the benefit is enhanced if the main influence of these data is spread along isentropes instead of σ-surfaces.

17. **Nudging** often yields more consistent analyses and forecasts of inversions, of associated vertical humidity gradients and, namely near steep orography, of wintertime low stratus cloud cover and cloud top heights; **compared to optimum interpolation**. However on occasions, forecasts starting from nudged analyses with their strong vertical gradients tend to erroneously dissipate low cloud due to spurious vertical smoothing. The advection scheme and, near steep orography, even the reduced horizontal diffusion are shown to contribute to this process. Forecasts starting from optimum interpolation analyses are less subject to these proceedings since their vertical relative humidity gradients are weak as a result of the use of (broad) vertical forecast error correlations.

d. Mixed layer and its depth with typical summertime smog conditions

Related to Pollumet, time series of mixed-layer depth are computed for summertime cases with weak winds and little cloudiness. The diurnal maximum of the mixed-layer depth predicted by the SM generally tends to be too high and by several hours too late in the afternoon.

18. Continuous nudging towards routine rawinsonde and screen-level humidity data, and in particular nudging of (linearly interpolated) 12-hourly temperature profiles within the mixed layer, corrects well the evolution of the **mixed layer**, namely its **depth**, temperature and wind, in typical sunny summertime conditions prone to smog. In such cases, the nudging approach has a good potential to significantly improve diagnostic data sets generated with the SM. However in a forecast, the positive impact of the nudging on the mixed-layer depth disappears within 6 to 12 hours.

5.2 Perspective

It is concluded from the above that nudging towards direct observations is an appropriate method for assimilation of rawinsonde and screen-level data into a mesoscale model for the Alpine region. The technique also appears to offer promising perspectives for operational NWP. However, a conclusive answer to this requires a comparison of nudging with the presently operational analyses schemes in a much larger number and variety of meteorological events, and this includes objective verification against real observations. Also, the effects of the nudging scheme ought to be studied in continuous 4DDA cycles of several days or weeks.

The present study has supported projects at the SMA and the DWD aimed at providing a more comprehensive comparison, improving the present code (e.g. in relation to computational efficiency), and implementing and examining the nudging technique in a next-generation, non-hydrostatic, very high-resolution (pre-)operational model. The present results and encountered problems suggest a variety of issues which are important for further improvement of nudged analyses and subsequent forecasts, particularly for low stratus events. These can be subdivided in three groups: model refinements, refinements of the assimilation scheme, and its extention by use of additional data.

In relation to the SM, the rather pronounced decrease of the sensitivity to the initial condition with increasing forecast time indicates that the primary requirement for improvement of 24- to 48-hour forecasts may be to refine the model formulation. However, the present work (e.g. on the influence of the horizontal diffusion) also indicates that the more refined the model, the more scope there is for further enhancement of the forecast quality by improved initial conditions. Reversely, the more accurate and detailed the initial conditions, the more important a refined model formulation becomes.

a. Model refinements

Thus, requirements on the model depend on the analysis scheme. In particular, the strong vertical temperature and humidity gradients present in the nudged analyses requires that spurious vertical smoothing in the model is as small as possible. For the SM, this calls for a more appropriate horizontal (see Ballard et al., 1991) and vertical advection scheme, especially for the humidity variable(s). Since a general operational reduction of the horizontal diffusion along the sloping σ-surfaces is problematic, a selective reduction or preferably a more appropriate formulation of the diffusion of the thermodynamic variables is also required in the presence of steep orography. The effective vertical resolution may be further enhanced by parameterizing vertically sub-grid scale cloud, e.g. explicitly by distinguishing between volumetric cloud fraction and cloud cover (Dastoor, 1994), or implicitly by diagnosing fractional cloudiness not only as a function of relative humidity and height but also of other properties, e.g. inversions (Slingo, 1987).

Note that, given the forecast aims - e.g. low stratus prediction in the (western) Swiss Plateau - much of the benefit obtained from these measures may also be expected from an appropriate increase of the vertical and horizontal resolution. (In other words, the SM with the present resolution (and formulation) is in fact not quite adequate for (low stratus) forecasting in the western Swiss Plateau.)

For improved forecasting of the mixed-layer depth, a more appropriate surface flux parameterization appears to be indispensable.

b. Refinements of the nudging scheme

The stringent time constraints of operational short-range NWP are likely to inhibit the application of the present formulation of spreading along isentropic or isobaric surfaces. However, a different implementation of these concepts can significantly enhance the computational efficiency at the cost of much increased needs on computer memory by keeping fixed the surfaces used for the spreading during e.g. one hour (i.e. temporal variations of the horizontal gradients of potential temperature (or surface pressure) are neglected for the spreading in this period).

Alternative ways to account for reduced representiveness due to orography is to limit the lateral spreading specifically in consideration of barrier effects of mountain ridges (cf. Lanzinger, 1990), or to vary the horizontal correlation scale as a function of height (cf. Fast, 1995). However, the experiments with non-isotropic horizontal weights indicate that the potential of such measures may be rather limited.

In contrast, further efforts to examine and optimize the temporal nudging weights are justified by the large differences in impact between linear temporal interpolation and the saw tooth function. A difficult but crucial task for operational purposes is the development of more comprehensive quality control procedures.

c. *Use of additional data*

In consideration of the positive impact of the assimilation of screen-level humidity data and temperature profiles within the mixed layer an examination of nudging towards surface temperature data appears worthwhile. A potential exists notably near steep orography if the data increments are spread mainly along isentropes.

The rawinsonde network does not provide sufficient resolution to capture the fine-scale horizontal upper-air moisture structures which are required for realistic mesoscale cloud and precipitation fields in the assimilation and (early) forecast period. Routinely available additional data sources, e.g. satellite cloud imagery, total precipitable water, radar and rain gauge precipitation, and cloud observations from SYNOPs may be used to adjust the model's moisture field, latent heating rates, and surface fluxes (see section 1.1). Present preliminary results (section 4.5) suggest that further significant benefit is expected from the exploitation of future observing system such as profilers of wind and temperature (RASS). In particular, the promotion of future routine temperature profilers should not be neglected due to a concentration of efforts on wind profilers.

References

Andersson, E., J. Pailleux, J.-N. Thépaut, J. R. Eyre, A. P. McNally, G. A. Kelly, and P. Courtier, 1994: Use of cloud-cleared radiances in three/four dimensional variational data assimilation. Quart. J. Roy. Met. Soc., **120**, 627 - 653.

Anthes, R. A., 1974: Data assimilation and initialization of hurricane prediction models. J. Atmos. Sci., **31**, 702 - 719.

Antikainen, V. and V. Hyvönen, 1983: The accuracy of Vaisala RS 80 radiosonde. Proc. of Fifth Symp. on Meteorol. Observations and Instrumentation, 11-15 April 1983, Toronto, Canada, 134 - 140.

Arnold, C. P., and C. H. Dey, 1986: Observing-systems simulation experiments: Past, present, and future. Bull. Amer. Meteor. Soc., **67**, 687 - 695.

Atlas, R., E. Kalnay, W. E. Baker, J. Susskind, D. Reuter, and M. Halem, 1985: Observing system simulation experiments at GSFC. Proc. NASA Symposium on Global Wind Measurements, Columbia, 65 - 71.

Atkins, M. J., 1974: The objective analysis of relative humidity. Tellus, **26**, 663 - 671.

Bachmann, M., and J. Bendix, 1993: Nebel im Alpenraum. Eine Untersuchung mit Hilfe digitaler Wettersatellitendaten. Bonner Geogr. Abhandl., Heft 86, ISSN 0373-0468.

Baierle, U., 1995: *Die sommerliche Wasserbilanz in einem regionalen Klimamodell. Diplomarbeit am Lab. f. Atmosphärenphysik der ETH Zürich*, 93 pp.

Baker, W. E., G. D. Emmitt, F. Robertson, R. M. Atlas, J. E. Molinari, D. A. Bowdie, J. Paegle, R. M. Hardesty, R. T. Menzies, T. N. Krishnamurthy, R. A. Brown, M. J. Post, J. R. Anderson, A. C. Lorenc, and J. McElroy, 1995: Lidar-measured winds from space: A key component for weather and climate prediction. Bull. Amer. Meteor. Soc., **76**, 869 - 888.

Ballard, S. P., B. W. Golding, and R. N. B. Smith, 1991: Mesoscale model experimental forecasts of the Haar of Northeast Scotland. Mon. Wea. Rev., **119**, 2107 - 2123.

Ballard, S. P., S. D. Jackson, and B. Macpherson, 1994: Short-range forecasting of stratocumulus: Initialization v. prediction. ECMWF Workshop Proc. on 'Parameterization of the Cloud Topped Boundary Layer', 8 - 11 June 1993, 403 - 429.

Bao, J.-W., and R. M. Errico, 1994: Sensitivity of forecasts and analyses to the observations in FDDA using the dynamical relaxation (nudging) method. Proc. of 10th AMS Conf. on NWP, Portland, 584 - 585.

Barwell, B. R., and A. C. Lorenc, 1985: A study of the impact of aircraft wind observations on a large scale analysis and numerical weather prediction system. Quart. J. Roy. Meteor. Soc., **111**, 103 - 129.

Barwell, B. R., and R. A. Bromley, 1988: The adjustment of numerical weather prediction model to local perturbations. Quart. J. Roy. Meteor. Soc., **114**, 665 - 689.

Bell, R. S., 1989: Developments in regional data assimilation at the Meteorological Office. Report on HIRLAM workshop, Oslo 1989.

Bell, R. S., 1994: The beneficial impact of changes to observations usage in the UK Met. Office operational data assimilation system. Proc. of 10th AMS Conf. on NWP, Portland, 485 - 487.

Bell, R. S., and O. Hammon, 1989: The sensitivity of fine-mesh rainfall and cloud forecasts to the initial specification of humidity. Meteorol. Mag., **118**, 152 - 158.

Bengtsson, L., M, Ghil, and E. Källén, 1981: Dynamic meteorology: Data assimilation methods. Springer-Verlag, 330 pp.

Benjamin, S. G., 1989: An isentropic meso-α-scale analysis system and its sensitivity to aircraft and surface observations. Mon. Wea. Rev., **117**, 1586 - 1603.

Benjamin, S. G., and N. L. Seaman, 1985: A simple scheme for objective analysis in curved flow. Mon. Wea. Rev., **113**, 1184 - 1198.

Benjamin, S. G., K. A. Brewster, R. Brümmer, B. F. Jewitt, T. W. Schlatter, T. L. Smith, and P. A. Stamus, 1991: An isentropic three-hourly data assimilation system using ACARS aircraft observations. Mon. Wea. Rev., **119**, 888 - 906.

Benjamin, S. G., and P. A. Stamus, 1991: Experiments with 1-h and 3-h assimilation sysles using mesoscale aircraft and surface data. Proc. on 9th AMS Conf. on NWP, Denver, 186 - 189.

Benjamin, S. G., D. Kim, and T. W. Schlatter, 1995: The Rapid Update Cycle: A new mesoscale assimilation system in hybrid (t-s) coordinates at the National Meteorological Center. WMO/TD-No. 651. Proc. of 'Second WMO International Symposium on Assimilation of Observations in Meteorology and Oceanography'. Tokyo, 13 - 14 March 1995, Vol. I, 337 - 342.

Bergthorsson, P., and B. R. Döös, 1955: Numerical weather map analysis. Tellus, **7**, 329 - 340.

Bergot, T., and D. Guedalia, 1994: Numerical forecasting of radiation fog. Part I: Numerical model and sensitivity tests. Mon. Wea. Rev., **122**, 1218 - 1230.

Beyrich, F., and U. Görsdorf, 1995: Composing the diurnal cycle of mixing height from simultaneous sodar and wind profiler measurements. Bound.-Layer Meteor., **76**, 387 - 394.

Binder, P., and C. Schär, Editors, 1995: Mesoscale Alpine Programme Design Proposal. Available from the Swiss Meteorological Institute.

Blumen, W., 1972: Geostrophic adjustment. Rev. Geophys. Space Phys., **10**, 485 - 528.

Bougeault, P., 1992: Current trends and achievements of limited area modelling. WMO/TD No. 479, WMO Programme on Weather Prediction Research, PWPR report series No. 1, appendix 6, 21 pp.

Bouttier, F., J.-F. Mahfouf, and J. Noilhan, 1993: Sequential assimilation of soil moisture from atmospheric low-level parameters. Part I: Sensitivity and calibration studies. J. Appl. Meteorol., **32**, 1335 - 1351.

Branscome, L. E., D. A. Douglas, and R. Carpenter, 1994: Influence of drainage flows and surface processes on fog formation in a river valley. Proc. of 6th AMS Conf. on Mesoscale Processes, Portland, 560 - 561.

Bretherton, C. S., E. Klinker, and J. Coakley, 1994: Comparison of ceilometer, satellite and synoptic measurements of boundary layer cloudiness and the ECMWF diagnostic cloud parameterization scheme during ASTEX. Proc. of 8th AMS Conf. on Atmospheric Radiation, 253 - 255.

Brill, K. F., L. W. Uccellini, J. Manobianco, P. J. Kocin, and J. H. Homan, 1991: The use of successive dynamic initialization by nudging to simulate cyclogenesis during GALE IOP 1. Meteorol. Atmos. Phys., **45**, 15 - 40.

Brown, R., and W. T. Roach, 1976: The physics of radiation fog: II - A numerical study. Quart. J. Roy. Meteor. Soc., **102**, 335 - 354.

Browning, K. A., and G. Szejwach, 1994: Developments in observational systems for weather forecasting. Meteorol. Appl., **1**, 3 - 22.

Buchhold, M., and G. Paul, 1995: The regional and high-resolution data assimilation systems at the DWD. WMO/TD-No. 665, Research Activities in Atmospheric and Oceanic Modelling. CAS/JSC Working Group on Numerical Experimentation, Report No. 21, Ed. A. Staniforth, 1.10 - 1.11 .

Businger, S., S. R. Chiswell, M. Bevis, J. Duan, R. A. Anthes, C. Rocken, R. H. Ware, M. Exner, T. VanHove, and F. S. Solheim, 1996: The promis of GPS in atmospheric monitoring. Bull. Amer. Meteor. Soc., **77**, 5 - 18.

Cardinali, C., E. Andersson, P. Viterbo, J.-N. Thépaut, and D. Vasiljevic, 1994: Use of conventional surface observations in three-dimensional variational data assimilation. ECMWF Tech. Memo. No. 207. 31 pp.

Carr, F. H., M. H. Ramamurthy, D. J. Rusk, and G.-P. Lou, 1993: Observing system experiments: Relative model response to various FGGE datasets in the tropics. Mon. Wea. Rev., **121**, 3106 - 3122.

Carr, F. H., and Q. Zhao, 1994: The initialization of cloud water/ice in NMC's Eta Model. Proc. of 10th AMS Conf. on NWP, Portland, 303 - 305.

Chang, S. W., and T. R. Holt, 1994: Impact of assimilating SSM/I rainfall rates on numerical prediction of winter cyclones. Mon. Wea. Rev., **122**, 151 - 164.

Charney, J., M. Halem, and R. Jastrow, 1969: Use of incomplete historical data to infer the present state of the atmosphere. J. Atmos. Sci., **26**, 1160 - 1163.

Clark, P., 1994: Case studies of fog in the UK Met Office mesoscale model. Proc. of 10th AMS Conf. on NWP, Portland, 15 - 17.

Clifford, S. F., J. C. Kaimal, R. J. Lataitis, and R. G. Strauch, 1994: Ground-based remote profiling in atmospheric studies: an overview. Proc. of the IEEE, **82**, (3), 313 - 354.

Coiffier, J., P. Chapelet, and N. Marie, 1987: Study of various quasi-Lagrangian techniques for numerical models. Proc. of ECMWF Workshop on 'Techniques for Horizontal Discretization in Numerical Weather Prediction Models', 19 - 46.

Connell, B. H., and D. R. Miller, 1995: An interpretation of radiosonde errors in the atmospheric boundary layer. J. Appl. Meteorol., **34**, 1070 -1081.

Côté, J., S. Gravel, and A. Staniforth, 1995: A generalized family of schemes that eliminate the spurious resonant response of semi-Lagrangian schemes to orographic forcing. Mon. Wea. Rev., **123**, 3605 - 3613.

Courtier, P., 1994: Introduction to numerical weather prediction data assimilation methods. ECMWF Seminar Proc. on 'Development in the Use of Satellite Data in Numerical Weather Prediction', 6 - 10 Sept. 1993, 189 - 207.

Courtier, P., 1995: Variational methods. Geophys. Mag., Series 2. Special issue on the 'Second WMO International Symposium on Assimilation of Observations in Meteorology and Oceanography'. Tokyo, 13 - 14 March 1995, IV-i-1 - V-i-19.

Courtier, P., J. Derber, R. Errico, J.-F. Louis, and T. Vukicevic, 1993: Important literature on the use of adjoint, variational methods and the Kalman filter in meteorology. Tellus, **45A**, 342 - 357.

Courtier, P., J.-N. Thépaut, and A. Hollingsworth, 1994: A strategy for operational implementation of 4D-Var using an incremental approach. Quart. J. Roy. Meteor. Soc., **120**, 1367 - 1387.

Cram, J. M., J. S. Snook, S. C. Albers, and J. A. McGinley, 1993: A brief description of, and preliminary results from, the LAPS modeling/4DDA system. Proc. of 5th AMS Conf. on Aviation Weather Systems, Vienna, J10 - J14.

Cram, J. M., S. C. Albers, D. L. Birkenheuer, J. R. Smart, and P. A. Stamus, 1995: Meso-β-scale data assimilation in LAPS. WMO/TD-No. 651. Proc. of 'Second WMO International Symposium on Assimilation of Observations in Meteorology and Oceanography'. Tokyo, 13 - 14 March 1995, Vol. I, 343 - 348.

Cressman, G., 1959: An operational objective analysis system. Mon. Wea. Rev., **87**, 367 - 374.

Daley, R., 1991: Atmospheric data analysis. Cambridge University Press, 457 pp.

Dastoor, A. P., 1994: Cloudiness parameterization and verification in a large-scale atmospheric model. Tellus, **46A**, 615 - 634.

Davidson, N. E., and K. Puri, 1992: Tropical predition using dynamical nudging, satellite-defined convective heat sources, and a cyclone bogus. Mon. Wea. Rev., **120**, 2501 - 2522.

Davies, H. C., 1976: A lateral boundary formulatin for multi-level prediction models. Quart. J. Roy. Meteor. Soc., **102**, 405 - 418.

Davies, H. C., and R. E. Turner, 1977: Updating prediction models by dynamical relaxation: An examination of the technique. Quart. J. Roy. Meteor. Soc., **103**, 225 - 245.

Derber, J. C., 1989: A variational continuous assimilation technique. Mon. Wea. Rev., **117**, 2437 - 2446.

Duynkerke, P. G., 1991: Radiation fog: a comparison of model simulation with detailed observations. Mon. Wea. Rev., **119**, 324 - 341.

ECMWF, 1992: Research Manual 1, 3/92 3rd edition, ECMWF data assimilation. Scientific doc., ECMWF Research Department.

ECMWF, 1995: NWP progress report for 1994. WMO/TD-No. 708. NWPP report series No. 21, 39 - 57.

Ehrendorfer, M., and R. M. Errico, 1995: Mesoscale predictability and the spectrum of optimal perturbations. J. Atmos. Sci., **52**, 3475 - 3500.

Eigenwillig, N., and G. Ungewitter, 1993: Contributions to an improved forecasting of fog in Southern Germany. Proc. on 1st European Conf. on Applications of Meteorology, Oxford, 27. 9. - 1. 10. 1993.

Elliot, W. P., and D. J. Gaffen, 1991: On the utility of radiosonde humidity archives for climate studies, Bull Amer. Meteor. Soc., **72**, 1507 - 1520.

EWGLAM, 1995: LAM Newsletter No. 24. 16th EWGLAM Meeting and 1st SRNWP Network Meeting. Norrköping, Sweden, 17 - 21 October 1994, 236 pp.

Errico, R. M., T. Vukicevic, and K. Raeder, 1993: Comparison of initial and lateral boundary condition sensitivity for a limited-area model. Tellus, **45A**, 462 - 477.

Fast, J. D., 1995: Mesoscale modeling and four-dimensional data assimilation in areas of highly complex terrain. J. Appl. Meteorol., **34**, 2762 - 2782.

Filiberti, M. A., L. Eymard, and B. Urban. 1994: Assimilation of satellite precipitable water in a meteorological forecst model. Mon. Wea. Rev., **122**, 486 - 506.

Fitzjarrald, D. R., and G. G. Lala, 1989: Hudson Valley fog environments. J. Appl. Meteorol., **28**, 1303 - 1328.

Gandin, L. S., 1963: Objective analysis of meteorological fields. Hydrometeoizdat (in Russian). English translation by Israel Program for Scientific Translations, Jerusalem, 1965, 242 pp.

Gandin, L. S., 1988: Complex quality control of meteorological observations. Mon. Wea. Rev., **116**, 1137 - 1156.

Garand, L., C. Grassotti, J. Halle, and G. L. Klein, 1992: On differences in radiosonde humidity-reporting practices and their implications for numerical weather prediction and remote sensing. Bull. Amer. Meteor. Soc., **73**, 1417 - 1423.

Garratt, J. R., 1993: Sensitivity of climate simulations to land-surface and atmospheric boundary layer treatments - A review. J. Climate, **6**, 419 - 449.

Gasser, M., 1995: *Untersuchung der planetaren Grenzschicht mit einem auf digitalen Betrieb umgebauten Doppler Sodar.* Ph. D. thesis, Dissertation No. 11168 ETH Zürich, 98 pp.

Gayno, G. A., N. L. Seaman, A. M. Lario, and D. R. Stauffer, 1994: Forecasting visibility using a 1.5-order closure boundary layer scheme in a 12-km non-hydrostatic model. Proc. of 10th AMS Conf. on NWP, Portland, 18 - 20.

Ghil, M., S. Cohn, J. Tavantzis, K. Bube, and E. Isaacson, 1981: Application of estimation theory to numerical weather prediction. Dynamic meteorology: Data assimilation methods. Bengtsson, L., Ghil., M., and E. Källén, eds, Springer-Verlag, 139 - 224.

Gilchrist, A., 1984: Observing system experiments - review and outlook. ECMWF Seminar/Workshop Proc. on 'Data Assimilation Systems and Observing System Experiments with Particular Emphasis on FGGE', 3 - 11 Sept., Vol. 1, 145 - 164.

Golding, B. W., 1990: The Meteorological Office mesoscale model. Meteor. Mag., **119**, 81 - 96.

Golding, B. W., 1993: A study of the influence of terrain on fog development. Mon. Wea. Rev., **121**, 2529 - 2541.

Guedalia, D., and T. Bergot, 1994: Numerical forecasting of radiation fog. Part II: A comparison of model simulation with several observed fog events. Mon. Wea. Rev., **122**, 1231 - 1246.

Guo, Y.-R., and Y.-H. Kuo, 1995: Testing of Newtonian nudging technique in data assimilation on the meso-beta-scale. Proc. of 4th AMS Conf. on Atmospheric Radiation Measurement (ARM), Science Team Meeting, Charleston, 28. 2. - 3. 3. 1994, 167 - 171.

Gustafsson, N., P. Lönnberg, and J. Pailleux, 1995: Data assimilation for high resolution limited area models. Geophys. Mag., Series 2. Special issue on the 'Second WMO International Symposium on Assimilation of Observations in Meteorology and Oceanography'. Tokyo, 13 - 14 March 1995, V-i-1 - V-i-20.

Haltiner, G. J., and R. T. Williams, 1980: Numerical prediction and dynamic meteorology. 2nd ed., J. Wiley and Sons, 477 pp.

Han, Y., and E. R. Westwater, 1995: Remote sensing of tropospheric water vapor and cloud liquid water by integrated ground-based sensors. J. Atmos. Ocean. Tech., **12**, 1050 - 1059.

Harms, D. E., S. Raman, and R. V. Madala, 1992: An examination of four-dimensional data-assimilation techniques for numerical weather prediction. Bull. Amer. Meteor. Soc., **73**, 425 - 440.

Hayden, C. M., 1973: Experiments in the four-dimensional assimilation of Nimbus 4 SIRS data. J. Appl. Meteorol., **12**, 425 - 436.

Henmi, T., 1990: Assimilation of wind field over complex terrain. Proc. of 5th AMS Conf. on Mountain Meteorology, Boulder, 118 - 124.

Hoke, J. E., and R. A. Anthes, 1976: The initialization of numerical models by a dynamical initialization technique. Mon. Wea. Rev., **104**, 1551 - 1556.

Hollingsworth, A., 1986: Objective analysis for numerical weather prediction. Short and Medium-Range Weather Prediction, Proc. WMO/IUGG NWP Symposium, Tokyo, 11 - 59.

Hollingsworth, A., and P. Lönnberg, 1986: The statistical structure of short-range forecast errors as determined from radiosonde data. Part I: The wind field. Tellus, **38A**, 111 -136.

Homleid, M, and L.-A. Breivik, 1995: Preparations for the assimilation of ERS-1 surface wind observations into numerical weather prediction models. Tellus, **47A**, 62 - 79.

Hooper, A. N., 1975: Studies of radiosonde performance. WMO Technical Note No. 140, WMO No. 394.

Huang, X.-Y., 1996: Initialization of cloud water content in a data assimilation system. Mon. Wea. Rev., **124**, 478 - 486.

Huang, X.-Y., and H. Sundquist, 1993: Initialization of cloud water content and cloud cover for numerical prediction models. Mon. Wea. Rev., **121**, 2719 - 2726.

Huang, X.-Y., A. Cederskov, and E. Källén, 1994: A comparison between digital filtering initialization and nonlinear normal-mode initialization in a data assimilation system. Mon. Wea. Rev., **122**, 1001 - 1015.

Ingleby, B., 1995: Vertical averaging of radiosonde data. WMO/TD-No. 665, Research Activities in Atmospheric and Oceanic Modelling. CAS/JSC Working Group on Numerical Experimentation, Report No. 21, Ed. A. Staniforth, 1.2 - 1.3 .

Ingleby, N. B., and A. C. Lorenc, 1993: Bayesian quality control using multivariate normal distribution. Quart. J. Roy. Meteor. Soc., **119**, 1195 - 1225.

Ivanov, A. A., S. Kats, S. Kurnosenko, J. Nash, and N. Zaitseva, 1991: WMO International Radiosonde Intercomparison. Phase III (Dzhambul, USSR, 1989). Final report. WMO/TD-No. 451. Instruments and Observing Methods Report No. 40, 135 pp.

Jacobsen, I., and E. Heise, 1982: A new economic method for the computation of the surface temperature in numerical models. Beitr. Phys. Atm., **55**, 128 - 141.

Järvinen, H., J.-N. Thépaut, and P. Courtier, 1996: Quasi-continuous variational data assimilation. Quart. J. Roy. Meteor. Soc., **122**, 515 - 534.

Kalman, R. E., and R. S. Bucy, 1961: New results in linear filtering and prediction theory. Trans. ASME, J. Basic Eng., **83D**, 95 - 108.

Karlsson, E., and J. E. Falk, 1984: An operational numerical model for prediction of fog and stratus. Proc. Nowcasting II Symposium, Norrkoping, 1984, ESA SP-208, 335 - 340.

Kasahara, A., 1972: Simulation experiments for meteorological observing systems for GARP. Bull. Amer. Meteor. Soc., **53**, 252 - 264.

Kim, D., T. W. Schlatter, and D. Dévényi, 1994: A new mesoscale objective analysis with Bessel basis functions. Proc. of 10th AMS Conf. on NWP, Portland, 151 - 153.

Kistler, R. E., and R. D. McPherson, 1975: On the use of a local wind correction technique in four-dimensional data assimilation. Mon. Wea. Rev., **103**, 445 - 449.

Kitchen, M., 1989: Representativeness errors for radiosonde observations, Quart. J. Roy. Meteor. Soc., **115**, 673 - 700.

Klinker, E., 1994: Analysis and diagnosis of the ECMWF model during ASTEX. ECMWF Workshop Proc. on 'Parameterization of the Cloud Topped Boundary Layer', 8 - 11 June 1993, 15 - 20.

Krishnamurti, T. N., K. Ingles, S. Cocke, R. Pasch, and T. Kitade, 1984: Details of low latitude medium range numerical weather prediction using a global spectral model (II). Effect of orography and physical initialization. J. Meteor. Soc. Japan, **62**, 613 - 649.

Krishnamurti, T. N., H. S. Bedi, W. Heckley, and K. Ingles, 1988: Reduction of the spinup time for evaporation and precipitation in a spectral model. Mon. Wea. Rev., **116**, 907 - 920.

Krishnamurti, T. N., G. D. Rohaly, and H. S. Bedi, 1994: On the improvement of precipitation forecast skill from physical initialization. Tellus, **46A**, 598 - 614.

Krishnamurti, T. N., S. K. R. Bhowmik, D. Oosterhof, and G. Rohaly, 1995: Mesoscale signatures within the tropics generated by physical initialization. Mon. Wea. Rev., **123**, 2771 - 2789.

Kuo, Y.-H., and Y.-R. Guo, 1989: Dynamic initialization using observations from a hypothetical network of profilers. Mon. Wea. Rev., **117**, 1975 - 1998.

Kuo, Y.-H., Y.-R. Guo, and E. R. Westwater, 1993: Assimilation of precipitable water measurements into a mesoscale numerical model. Mon. Wea. Rev., **121**, 1215 - 1238.

Kuo, Y.-H., X. Zou, and Y.-R. Guo, 1996: Variational assimilation of precipitable water using a nonhydrostatic mesoscale adjoint model. Part I: Moisture retrieval and sensitivity experiments. Mon. Wea. Rev., **124**, 122 - 147.

Kvamstø, N. G., 1994: Cloudiness validation in the ECMWF model. ECMWF Workshop Proc. on 'Parameterization of the Cloud Topped Boundary Layer', 8 - 11 June 1993, 345 - 365.

Lafaysee, C., Editor, 1994: Utilization of UHF/VHF radar wind profiler networks for improving weather forecasting in Europe. COST 74 final report, European Commission, Luxembourg, 333 pp.

Lanzinger, A., and R. Steinacker, 1990: A fine mesh analysis scheme designed for mountainous terrain. Meteorol. Atmos. Phys., **43**, 213-219.

Le Dimet, F. X., and O. Talagrand, 1986: Variational algorithms for analysis and assimilation of meteorological observations: theoretical aspects. Tellus, **38A**, 97 - 110.

Ledvina, D. V., and J. Pfaendtner, 1995: Inclusion of Special Sensor Microwave/Imager (SSM/I) total precipitable water estimates into the GEOS-1 data assimilation system. Mon. Wea. Rev., **123**, 3003 - 3015.

Lee, H.-S., and T. N. Krishnamurthy, 1995: Impact of physical initialization on cloud forecasts. Meteorol. Atmos. Phys., **56**, 261 - 273.

Leidner, S. M., D. R. Stauffer, and N. L. Seaman, 1994: High-resolution forecasting in the California coastal zone using four-dimensional data assimilation. Proc. of 10th AMS Conf. on NWP, Portland, 528 - 530.

Lenschow, D. H., 1990: Factors affecting the structure and stability of boundary-layer clouds. Proc. on AMS Conf. on Cloud Physics, San Francisco, 23 - 27 July 1990, 37 - 42.

Lewis, J. M., and J. C. Derber, 1985: The use of adjoint equations to solve a variational adjustment problem with advective constraints. Tellus, **37A**, 309 - 322.

Lilly, D. K., and D. J. Perkey, 1976: Sensitivity of mesoscale predictins to mesoscale initial data. Proc. on 6th AMS Conf. on Weather Forecasting and Analysis, Albany, 174 - 179.

Lönnberg, P., 1988: Developments in the ECMWF analysis system. ECMWF Seminar Proc. on 'Data Assimilation and the Use of Satellite Data'. Reading, 5. - 9. Sept. 1988, 75 - 119.

Lönnberg, P., 1992: Optimization of statistical interpolation. Finnish Meteorol. Institute, Contributions, No. 6, 42 pp.

Lönnberg, P., and A. Hollingsworth, 1986: The statistical structure of short-range forecast errors as determined from radiosonde data. Part II: The covariance of height and wind errors. Tellus, **38A**, 137 - 161.

Lönnberg, P., and D. Shaw, 1987: ECMWF Data Assimilation. Scientific Doc., ECMWF Research Manual 1, 10/87, 2nd Revised Ed.

Lorenc, A. C., 1981: A global three-dimensional multivariate statistical interpolation scheme. Mon. Wea. Rev., **109**, 701 - 721.

Lorenc, A. C., 1984: Data assimilation by repeated insertion into a forecast model - principles, practice, problems, and plans. Proc. of ECMWF Seminar/Workshop on 'Data Assimilation Systems and Observing System Experiments with Particular Emphasis on FGGE', 3 - 11 Sept., Vol. 2, 191 - 214.

Lorenc, A. C., 1986: Analysis methods for numerical weather prediction. Quart. J. Roy. Meteor. Soc., **112**, 1177 - 1194.

Lorenc, A. C., R. S. Bell, and B. Macpherson, 1991: The Meteorological Office analysis correction data assimilation scheme. Quart. J. Roy. Meteor. Soc., **117**, 59 - 89.

Lorenc, A. C., D. Barker, R. S. Bell, B. Macpherson, and A. J. Maycock, 1994: On the use of radiosonde humidity observations in mid-latitude NWP. UK Met. Office, Forecasting Research Scientific Paper No. 28, 16 pp. plus figs.

Louis, J.-F., 1979: A parametric model of vertical eddy fluxes in the atmosphere. Boundary-Layer Meteor., **17**., 187 - 202.

Lynch, P., and X.-Y. Huang, 1992: Initialzation of the HIRLAM model using a digital filter. Mon. Wea. Rev., **120**, 1019 -1034.

Lyons, W. A., C. J. Tremback, and R. A. Pielke, 1995: Applications if the Regional Atmospheric Modeling System (RAMS) to provide input to photochemical grid models for the Lake Michigan Ozone Study (LMOS).

Macpherson, B., 1995: Assimilation of moisture data in the UK Met Office mesoscale model. LAM Newsletter No. 24. 16th EWGLAM Meeting and 1st SRNWP Network Meeting. Norrköping, Sweden, 17 - 21 October 1994, 207 - 212.

Macpherson, B., 1996: Radiosonde balloon drift - does it matter for data assimilation? Meteorol. Appl., **2**, 301 - 305.

Majewski, D., 1985: Balanced initial and boundary values for a limited area model. Contrib. Atm. Phys., **58**, 147 - 159.

Majewski, D., 1991: The Europa-Model of the Deutscher Wetterdienst. ECMWF Seminar Proc. on 'Numerical methods in atmospheric models', Vol II, 9 - 13 Sept., 147 - 191.

Majewski, D., 1995: Regional operational prediction. WMO/TD No. 699, WMO Programme on Weather Prediction Research, PWPR report series No. 7. International Workshop on Limited-area and Variable Resolution Models. Bejing, 23. - 27. Oct., 29 -35.

Manobianco, J., L. W. Uccellini, K. F. Brill, and Y.-H. Kuo, 1992: The impact of dynamic data assimilation on the numerical simulations of the QE II cyclone and an analysis of the jet streak influencing the precyclogenetic environment. Mon. Wea. Rev., **120**, 1973 - 1996.

Manobianco, J., S. Koch, V. M. Karyampudi, and A. J. Negri, 1994: The impact of assimilation satellite-derived precipitation rates on numerical simulations of the ERICA IOP 4 cyclone. Mon. Wea. Rev., **122**, 341 - 365.

Martner, B. E., Wuertz, D. B., Stankov, B. B., Strauch, R. G., Westwater, E. R., Gage, K. S., Ecklund, W. L., Martin, C. L., and W. F. Dabberdt, 1993: An evaluation of wind profiler, RASS, and microwave radiometer performance. Bull. Amer. Meteor. Soc., **74**, 599 - 613.

Mathur, M. B., 1995: Amelioration of convective and nonconvective condensation with the assimilation of rainfall for improving inital conditions. Mon. Wea. Rev., **123**, 1851 - 1861.

Maycock, A. J., and B. Macpherson, 1994: Developments in mesoscale data assimilation at the UK Met. Office. Proc. of 10th AMS Conf. on NWP, Portland, 561 - 563.

McDonald, A., and J. E. Haugen, 1992: A two-time level, three-dimensional semi-Lagrangian, semi-implicit, limited-area grid-point model of the primitive equations. Mon. Wea. Rev., **120**, 2603 - 2621.

McNider, R. T., A. J. Song, D. M. Casey, P. J. Wetzel, W. L. Crosson, and R. M. Rabin, 1994: Towards a dznamic-thermodynamic assimilation of satellite surface temperature in numerical atmospheric models. Mon. Wea. Rev., **122**, 2784 - 2803.

Mellor, G. L., and T. Yamada, 1974: A hierarchy of turbulence closure models for planetary boundary layers. J. Atmos. Sci., **13**, 1791 - 1806.

Meteorological Office, 1994: Handbook of Aviation Meteorology, 3rd ed., London, HMSO. ISBN 0-11-400365-3 .

Miller, P. A., and S. G. Benjamin, 1992: A system for the hourly assimilation of surface observations in mountainous and flat terrain. Mon. Wea. Rev., **120**, 2342 - 2359.

Mills, G. A., and L. W. Logan, 1994: Upgrades to the Australian limited area data assimilation system. Austral. Meteor. Mag., **43**, 167 - 180.

Miyakoda, K., and A. Rosati, 1977: One-way nested grid model: The interface condition and the numerical accuracy. Mon. Wea. Rev., **105**, 1092 - 1107.

Morel, P., C. Leteure, and G. Rabreaa, 1971: On initialization and non-synoptic data assimilation. Tellus, **23**, 197 - 206.

Müller, E., 1981: Turbulent flux parameterization in a regional-scale model. ECMWF Workshop Proc. on 'Planetary Boundary Layer Parameterization', 25 - 27. Nov. 1981, 193 - 220.

Musson-Genon, L., 1987: Numerical simulation of a fog event with a one-dimensional boundary layer model. Mon. Wea. Rev., **115**, 592 - 607.

Nash, J., 1993: Characteristic errors in radiosonde temperature observations identified in the WMO radiosonde comparisons. Proc. of Eighth Symp. on Meteorol. Observation and Instrumentation, 17-22 January 1993, Anaheim, California, 98 - 103.

Nash, J., 1994: Upper wind observing systems used for meteorological operations. Ann. Geophysicae **12**, 691 - 710.

Nash, J., and F. J. Schmidlin, 1987: WMO International Radiosonde comparison (UK 1984, USA 1985). Final report. WMO Instruments and Observing Methods Report No. 30. WMO Geneva.

Nielsen, N. W., B. H. Sass, and J. Jørgensen, 1996: Mesoscale forecasts with an atmospheric limited area model. Meteorol. Appl., **2**, 351 - 361.

NOAA, 1993: The NOAA wind profiler demonstration network: background and overview. 201-01 - 09, NOAA/ERL/FSL Report, 14 pp.

Oakley, T., 1993: Compatibility of radiosonde geopotential measurements 1990, 1991 and 1992. WMO/TD-No. 587. Instrument and Observing Methods Report No. 56, 90 pp.

Økland, H., 1970: On the adjustment toward balance in primitive equation weather prediction models. Mon. Wea. Rev., **98**, 271 - 279.

Orlanski, I., 1975: A rational subdivision of scales for atmospheric processes. Bull. Amer. Meteor. Soc, **56**, 527 - 530.

Pielke, R. A., W. R. Cotton, R. L. Walko, C. J. Tremback, W. A. Lyons, L. D. Grasso, M. E. Nicholls, M. D. Moran, D. A. Wesley, T. J. Lee, and J. H. Copeland, 1992: Meteorol. Atmos. Phys., **49**, 69 - 91.

POLLUMET, 1996: *Luftverschmutzung und Meteorologie in der Schweiz.* To appear in the *Schriftenreihe Umwelt*, published by the *Bundesamt für Umwelt, Wald und Landschaft (BUWAL)*, Bern, Switzerland.

Puri, K., and M. J. Miller, 1990: The use of satellite data in the specification convective heating for diabatic initialization and moisture adjustment in numerical prediction models. Mon. Wea. Rev., **118**, 67 - 93.

Rabier, F., E. Klinker, P. Courtier, and A. Hollingsworth, 1996: Sensitivity of forecast errors to initial conditions. Quart. J. Roy. Meteor. Soc., **122**, 121 - 150.

Ramamurthy, M. K., and F. H. Carr, 1987: Four-dimensional data assimilation in the monsoon region. Part I: Role of temperature and moisture data. Mon. Wea. Rev., **115**, 1678 - 1706.

Ramamurthy, M. K., and F. H. Carr, 1988: Four-dimensional data assimilation in the monsoon region. Part I: Experiments with wind data. Mon. Wea. Rev., **116**, 1896 - 1913.

Ramamurthy, M. K., and T.-X. Yu, 1993: Continuous data assimilation experiments with the NMC Eta Model: A GALE IOP I case study. Mon. Wea. Rev., **121**, 3082 - 3105.

Richner, H., and P. D. Phillips, 1982: The radiosonde intercomparison SONDEX, Spring 1981, Payerne, Pure Appl. Geophys., **120**, 851-1198.

Ritter, B., and J.-F. Geleyn, 1992: A comprehensive radiation scheme for numerical weather prediction models with potential applications in climate simulations. Mon. Wea. Rev., **120**, 303 - 325.

Rivest, C., A. Staniforth, and A. Rober, 1994: Spurious resonant response of semi-Lagrangian discretizations to orogrphic forcing: Diagnosis and solution. Mon. Wea. Rev., **122**, 366 - 376.

Roach, W. T., 1994: Back to basics: Fog: Part 1 - Definitions and basic physics. Weather, **49**, 411 - 415.

Roach, W. T., 1995: Back to basics: Fog: Part 2 - The formation and dissipation of land fog. Weather, **50**, 7 - 11.

Roach, W. T., R. Brown, S. J. Caughey, B. A. Crease, and A. Slingo, 1982: A field study of nocturnal stratocumulus: I. Mean structure and budgets. Quart. J. Roy. Meteor. Soc., **108**, 103 - 123.

Rossby, C. G., 1938: On the mutual adjustment of pressure and velocity distribution in certain simple current systems, II. J. Marine Research, Vol. 1, 1938, 239 - 263.

Ruffieux, D., 1995: Remote sensing tools for the observation of the atmosphere. Part I: Inventory, research, and operational aspects. SMI internal report, 33 pp. Available from the Swiss Meteorological Institute.

Ruggiero, F. H., K. D. Sashegi, R. V. Madala, and S. Raman, 1994: Four-dimensional data assimilation of surface observations in a limited-area model. Proc. of 10th AMS Conf. on NWP, Portland, 572 - 574.

Schlatter, T. W., and J.-M. Carrière, 1991: A correlation model allowing for divergent wind analyses and supporting three-hour assimilation of mesoscale data. Proc. of 9th AMS Conf. on NWP, Denver, 58 - 61.

Schmidlin, F. J., 1988: WMO International Radiosonde Intercomparison. Phase II (USA 1985). WMO/TD-No. 312. WMO Instruments and Observing Methods Report No. 29, 113 pp.

Schmidlin, F. J., 1993: Radiosonde measurements: How accurate are they? How accurate must they be? Proc. of Eighth Symp. on Meteorol. Observation and Instrumentation, 17-22 January 1993, Anaheim, California, 93 - 97.

Schrodin, R., Editor, 1995a: *Dokumentation des EM/DM-Systems*. Available from the Deutscher Wetterdienst, Research Dept.

Schrodin, R., Editor, 1995b: Quarterly Report of the Operational NWP-Models of the Deutscher Wetterdienst. Research Dept., January 1995. Available from the Deutscher Wetterdienst.

Schubiger, F., G. de Morsier and H.C. Davies, 1987: Numerical studies of mesoscale motion in a mixed layer over the northern Alpine foreland. Bound. Layer Met., **41**, 109 - 121.

Schubiger, F., and G. de Morsier, 1992: *Erstellung von Anfangs- und Randdaten für das hochauflösende Regionalmodell (HRM) und zugehörige Experimente*. Internal report (*Arbeitsbericht Nr. 169*) of the Swiss Meteorological Institute (SMI), 34 pp. Available from SMI.

Schwartz, B. E., and C. A. Doswell, 1991: North American rawinsonde observatins: Problems, concerns, and a call to action. Bull. Amer. Meteor. Soc., **72**, 1885 - 1896.

Seaman, N. L., 1990: Continuous dynamic assimilation by Newtonian nudging: a four-dimensional approach to data assimilation. HIRLAM report, Copenhagen, 3. - 5. Sept., 111 - 116.

Seaman, R. S., 1992: The influence of background field characteristics on statistical interpolation an quality control. Austral. Meteor. Mag., **40**, 1 - 10.

Seaman, N. L., D. R. Stauffer, and A. M. Lario-Gibbs, 1995: A multiscale four-dimensional data assimilation system applied in the San Joaquin Valley during SARMAP. Part I: Modeling design and basic performance characterisics. J. Appl. Meteorol., **34**, 1739 - 1761.

Shaw, D. B., P. Lönnberg, A. Hollingsworth, and P. Undén, 1987: The 1984/1985 revisions of the ECMWF mass and wind field analysis. Quart. J. Roy. Meteor. Soc., **113**, 553 - 566.

Simmons, A. J., 1995: High-performance computing requirements for medium-range weather forecasting. ECMWF Newsletter No. 69, 8 - 13.

Simmons, A. J., R. Mureau, and T. Petroliagis, 1995: Error growth and estimates of predictability from the ECMWF forecasting system. Quart. J. Roy. Meteor. Soc., **121**, 1739 -1771.

Sisdselrud, L., 1995: Recent limited area modeling in Norway. LAM Newsletter No. 24. 16th EWGLAM Meeting and 1st SRNWP Network Meeting. Norrköping, Sweden, 17 - 21 October 1994, 99 - 104.

Slingo, J. M., 1987: The development and verification of a cloud prediction scheme for the ECMWF model. Quart. J. Roy. Meteor. Soc., **113**, 899 - 927.

Slingo, A., R. Brown, and C. L. Wrench, 1982: A field study of nocturnal stratocumulus; III: High resolution radiative and microphysical observations. Quart. J. Roy. Meteor. Soc., **108**, 145 - 165.

Smith, R. B., 1979: The influence of mountains on the atmosphere. Advances in Geophysics, B. Saltzmann, Ed., Vol. **21**, Academic Press, 87 - 230.

Smith, R. N. B., 1994: Experience and developments with the layer cloud and boundary layer mixing schemes in the UK Meteorological Office united model. ECMWF Workshop Proc. on 'Parameterization of the Cloud Topped Boundary Layer', 8 - 11 June 1993, 319 - 339.

Smith, T. L., and S. G. Benjamin, 1993: Impact of network wind profiler data on a 3-h data assimilation system. Bull. Amer. Meteor. Soc., **74**, 801 - 807.

Smith, T. L., and S. G. Benjamin, 1994: Relative impact of data sources on a data assimilation system. Proc. of 10th AMS Conf. on NWP, Portland, 491 - 493.

Snook, J. S., J. M. Cram, and J. M. Schmidt, 1995: LAPS/RAMS. A nonhydrostatic mesoscale numerical modeling system configured for operational use. Tellus, **47A**, 864 - 875.

Spero, T. L., N. L. Seaman, and D. R. Stauffer, 1994: Structure-weighted observation nudging for dynamic initialization in the Penn State/NCAR mesoscale model. Proc. of 10th AMS Conf. on NWP, Portland, 575 - 577.

Stankov, B. B., 1995: Ground- and space-based humidity profiling in a cloudy atmosphere with strong elevated temperature inversions. Proc. of 4th AMS Conf. on Atmospheric Radiation Measurement (ARM), Science Team Meeting, Charleston, 28. 2. - 3. 3. 1994, 305 - 311.

Stauffer, D. R., and N. L. Seaman, 1990: Use of four-dimensional data assimilation in a limited-area mesoscale model. Part I: Experiments with synoptic-scale data. Mon. Wea. Rev., **118**, 1250 - 1277.

Stauffer, D. R., N. L. Seaman, and F. S. Binkowski, 1991: Use of four-dimensional data assimilation in a limited-area mesoscale model. Part I: Effects of data assimilation within the planetary boundary layer. Mon. Wea. Rev., **119**, 734 - 754.

Stauffer, D. R., and J.-W. Bao, 1993: Optimal determination of nudging coefficients using the adjoint equations. Tellus, **45A**, 358 - 369.

Stauffer, D. R., and N. L. Seaman, 1994: Multiscale four-dimensional data assimilation. J. Appl. Meteorol., **33**, 416 - 434.

Stauffer, D. R., N. L. Seaman, J. M. Fritsch, C. W. Porter, and J.-W. Bao, 1994: Non-hydrostatic real-case forecasting of wintertime aviation-sensitive events using 4-km resolution and four-dimensional data assimilation. Proc. of 6th AMS Conf. on Mesoscale Processes, Portland, 435 - 438.

Stensrud, D. J., and J.-W. Bao, 1992: Behaviors of variational and nudging assimilation techniques with a chaotic low-order model. Mon. Wea. Rev., **120**, 3016 - 3028.

Stensrud, D. J., and J. M. Fritsch, 1994: Mesoscale convective systems in weakly forced large-scale environments. Part II: Generation of a mesoscale initial condition. Mon. Wea. Rev., **122**, 2068 - 2083.

Stull, R. B., 1988: An introduction to boundary layer meteorology. Kluwer Academic Publishers. ISBN 90-277-2769-4. 576 pp.

Tanguay, M., E. Yakimiw, H. Ritchie, and A. Robert, 1992: Advantages of spatial averaging in semi-implicit semi-Lagrangian schemes. Mon. Wea. Rev., **120**, 113 - 123.

Temperton, C., 1988: Implicit normal mode initialization. Mon. Wea. Rev., **116**, 1013 - 1031.

Temperton, C., and D. L. Williamson, 1981: Normal mode initialization for a multi-level grid point model. Part I: Linear aspects. Mon. Wea. Rev., **109**, 729 - 743.

Thépaut, J.-N., and P. Courtier, 1991: Four dimensional variational data assimilatino using the adjoint of a multilevel primitive equation model. Quart. J. Roy. Meteor. Soc., **117**, 1225 - 1254.

Thépaut, J.-N., R. Hoffman, and P. Courtier, 1993: Interactions of dynamics and observations in a four-dimensional variational assimilation. Mon. Wea. Rev., **121**, 3393 -3414.

Thépaut, J.-N., P. Courtier, G. Belaud, and G. Lemaître, 1996: Dynamical structure functions in a four-dimensional variational assimilation: A case study. Quart. J. Roy. Meteor. Soc., **122**, 535 - 561.

Thiébaux, H. J., H. L. Mitchell, and D. W. Shantz, 1986: Horizontal structure of hemispheric forecast error correlations for geopotential and temperature. Mon. Wea. Rev., **114**, 1048 - 1066.

Thiébaux, H. J., and M. A. Pedder, 1987: Spatial objective analysis. Academic Press, 299 pp.

Tiedtke, M., 1989: A comprehensive mass flux scheme for cumulus parameterization in large-scale models. Mon. Wea. Rev., **117**, 1779 - 1800.

Tiedtke, M., 1993: Representation of clouds in large-scale models. Mon. Wea. Rev., **121**, 3040 - 3061.

Tiedtke, M., 1994: The ECMWF prognostic cloud scheme. ECMWF Workshop Proc. on 'Parameterization of the Cloud Topped Boundary Layer', 8 - 11 June 1993, 341 - 343.

Turton, J. D., and R. Brown, 1987: A comparison of a numerical model of radiation fog with detailed observations. Quart. J. Roy. Meteor. Soc., **113**, 37 - 54.

Ungewitter, G., 1984: *Zur Vorhersage von Nebeleinbrüchen im Alpenvorland. Theoretische Ueberlegungen und praktische Anwendungen zur thermischen Zirkulation zwischen einem Nelbelgebiet und seiner Umgebung.* Met. Rdsch. **37**, H. 5; 138-145.

Viterbo, P., 1995: Initial values of soil water and the quality of summer forecasts. ECMWF Newsletter No. 69, 2 - 8.

Vrhovec, T., 1990: Analysis of mesometeorological temperature fields. Meteorol. Atmos. Phys., **43**, 235-240.

Vukicevic, T., and J. Paegle, 1989: The influence of one-way interacting lateral boundary conditions upon predictability of flow in bounded numerical models. Mon. Wea. Rev., **117**, 340 - 350.

Vukicevic, T., and R. M. Errico, 1990: The influence of artificial and physical factors upon predictability estimates using a complex limited-area model. Mon. Wea. Rev., **118**, 1460 - 1482.

Wade, C. G., and B. Schwartz, 1993: Radiosonde humidity observations near saturation. Proc. of 8th Symposium on Meteorological Observations and Instrumentation, Anaheim, 44 - 48.

Wang, J., and W. B. Rossow, 1995: Determination of cloud vertical structuree from Upper-air observations. J. Appl. Meteorol., **34**, 2243 - 2258.

Wang, W., and T. T. Warner, 1988: Use of four-dimensional data assimilation by Newtonian relaxation and latent-heat forcing to improve a mesoscale-model precipitation forecast: A case study. Mon. Wea. Rev., **116**, 2593 - 2613.

Wanner, H., 1979: *Zur Bildung, Verteilung und Vorhersage winterlicher Nebel im Querschnitt Jura-Alpen.* Geographica Bernensia 7.

Wanner, H., and M. Furger, 1990: The Bise - climatology of a regional wind north of the Alps. Meteorol. Atmos. Phys. **43**, 105-115.

Warner, T. T., Y.-H. Kuo, J. D. Doyle, J. Dudhia, D. R. Stauffer, and N. L. Seaman, 1992: Nonhydrostatic, mesobeta-scale, real-data simulation with the Penn State University/National Center for Atmospheric Research mesoscale model. Meteorol. Atmos. Phys., **49**, 209 - 227.

Wergen, W., 1992: The effect of model errors in variational assimilation. Tellus, **44A**, 297 -313.

Wergen, W., 1995: Recent LAM activities at DWD. LAM Newsletter No. 24. 16th EWGLAM Meeting and 1st SRNWP Network Meeting. Norrköping, Sweden, 17 - 21 October 1994, 77 - 79.

Weygandt, S. S., and N. L. Seaman, 1994: Quantification of predictive skill for mesoscale and synoptic-scale meteorological features as a function of horizontal grid resolution. Mon. Wea. Rev., **122**, 57 - 71.

Whiteman, C. D., 1982: Breakup of temperature inversions in deep mountain valleys. Part I: Observations. J. Appl. Meteorol., **21**, 270 - 289.

Williamson, D. L., 1973: The effects of forecast error accumulation on four-dimensional data assimilation. J. Atmos. Sci., **30**, 537 - 543.

Woodage, M. J., 1985: The preparation of data for the Meteorological Office 15-level forecst model. Meteorol. Mag., **114**, 1 -13.

Working Group Report, 1994: Parameterization in forecast and climate models. ECMWF Workshop Proc. on 'Parameterization of the Cloud Topped Boundary Layer', 8 - 11 June 1993, Working Group 3, 15 - 20.

World Meteorological Organization, 1974: Manual on codes. Vol. II. Regional codes and national coding practices. Geneva, WMO No. 306.

Wright, B. J., and B. Golding, 1990: The Interactive Mesoscale Initialization. Meteorol. Mag., **119**, 234 - 244.

Wright, B. J., W. H. Hand, and B. Macpherson, 1994: Assimilation of satellite data for mesoscale analysis. ECMWF Seminar Proc. on 'Developments in the Use of Satellite Data in Numerical Weather Prediction'. Reading, 6. - 10. Sept. 1993, 111 - 128.

Xinmei, H., T. J. Lyons, and R. O. Pitts, 1990: Fog formation at Perth airport. Austral. Meteor. Mag., **38**, 99 - 106.

Xu, T., and M. K. Ramamurthy, 1994: Four-dimensional assimilation of wind profiler data with NMC Eta Model. Proc. of 10th AMS Conf. on NWP, Portland, 569 - 571.

Yap, K.-S., 1995: Impact of a Newtonian assimilation and physical initialization on the initialization and prediction by a tropical mesoscale model. Mon. Wea. Rev., **123**, 833 - 861.

Young, S. H., and J. W. Zack, 1994: The use of non-standard data to improve the initialization of relative humidity in mesoscale models. Proc. of 10th AMS Conf. on NWP, Portland, 326 - 327.

Zou, X., I. M. Navon, and F. X. LeDimet, 1992: An optimal nudging data assimilation scheme using parameter estimation. Quart. J. Roy. Meteor. Soc., **118**, 1163 - 1186.

Zou, X., Y.-H. Kuo, and Y.-R. Guo, 1995: Assimilation of atmospheric radio refractivity using a nonhydrostatic adjoint model. Mon. Wea. Rev., **123**, 2229 - 2249.

Zupanski, D., and F. Mesinger, 1995: Four-dimensional variational assimlation of precipitation data. Mon. Wea. Rev., **123**, 1112 - 1127.

Zupanski, M., 1993: Regional four-dimensional variational data assimilation in a quasi-operational forecasting environment. Mon. Wea. Rev., **121**, 2396 - 2408.

Zupanski, M., 1994: Regional four-dimensional variational data assimilation at NMC: Results with full-physics Eta-Model using direct observations. Proc. of 10th AMS Conf. on NWP, Portland, 587 - 588.

Acknowledgements

The present work would not have been possible without the friendly agreement between and the generous support of four institutions involved: The Swiss Meteorological Institute (SMA), the Laboratory for Atmospheric Physics of the ETH Zürich (LAPETH), the Swiss National Funds for Scientific Research (NFR), and the Deutscher Wetterdienst (DWD). I'm indebted to the NFR for the financial support (as project, No. 2122-33655.92), and to the SMA for providing me with the required infrastructure.

I'm most grateful to Prof. H. C. Davies, LAPETH, for his scientific guidance. I will remember him not only for his excellent scientific quality and his brilliant writing skills, but most gladly for his great sensitivity and wisdom in leading me all the way to the end of my study. What I have learnt on this way from his advice will accompany me on my future way. Thanks!

It is also a pleasure to express my gratitude to Jean Quiby for fruitful early discussions, and most importantly for providing me with the optimum conditions for my working. I much appreciated the friendship and the uncomplicated and constructive collaboration in his group. Namely, thanks go to Peter Binder and Francis Schubiger for early discussions, their general support, and the help with the data collection and graphics, to Jean-Marie Bettems and Guy de Morsier for their assistance related to the world of computers, and to Andrea Rossa for his aid with the production of the cross sections and for the discussions on important non-meteorological subjects.

My appreciation also goes to Christoph Schär for helpful remarks on the manuscript, and to the numerical meteorology group at the DWD for supporting advice related to the refinement of the assimilation scheme and for the friendly collaboration.

Not only did the present work give me the opportunity to learn a lot about data assimilation, low stratus, and the way of science, but also about myself, which made it a most valuable experience from a personal point of view. For their great support in various ways, I want to express my deepest gratitude namely to Jürg Schwarz, Jivka Joos, Ghandali Hasler, Gilles Heysteck, and my mother Martha. I thank them and all my friends for their love and for making my life so lively. They are very precious to me.

Liste der Veröffentlichungen der SMA

Nr.	Verfasser	Titel	Seiten	Jahr
1a	Uttinger H., Ambrosetti F.	Die Niederschlagsstunden in Zürich	22	1962
1b	Ambrosetti F.	Die Niederschlagsstunden in Locarno-Monti	12	1965
2	Thams J.C. et al	Die Ergebnisse des Grossversuches III zur Bekämpfung des Hagels im Tessin in den Jahren 1957-1963 (vergriffen)	32	1966
3	Grütter M.	Die bemerkenswertesten Niederschläge der Jahre 1948-1964 in der Schweiz	20	1966
4	Schram K., Thams J.C.	9. Internationale Tagung für Alpine Meteorologie in Brig und Zermatt, 14. - 17. Sept. 1966	366	1967
5	Ambrosetti F., Thams J.C.	Die direkte Sonnenstrahlung auf die Flächen eines nach Süden orientierten Würfels ohne Grundfläche in Locarno-Monti	16	1967
6	Schram K., Thams J.C.	Der Tagesgang der Abkühlungs- und Aufwärmegrösse in Locarno-Monti (vergriffen)	20	1968
7	Ambrosetti F., Schram K., Thams J.C.	Die Intensität der direkten Sonnenstrahlung in verschiedenen Spektralbereichen in Locarno-Monti (vergriffen)	13	1968
8	Uttinger H.	Die Zahl der Tage mit Windspitzen von mindestens 20 Metern pro Sekunde in Zürich (1934-1967)	22	1968
9	Mäder F.	Untersuchung über die Windverhältnisse in Bodennähe bei verschiedenen Wetterlagen	42	1968
10	Schram K.	Die Windverhältnisse in der bodennahen Luftschicht an einem Hang von etwa 25 Grad Neigung (vergriffen)	13	1968
11	Schüepp M.	Kalender der Wetter- und Witterungslagen von 1955 bis 1967	44	1968
12	Ackermann P.	Die neue Radiosondenstation Payerne der MZA (vergriffen)	36	1968
13	Junod A.	Contribution à la méthodologie granulométrique des aérosols amicroscopiques	70	1969
14	Joss J., Schram K. et al.	Untersuchungen zur quantitativen Bestimmung von Niederschlagsmengen mittels Radar (vergriffen)	37	1969
15	Courvoisier H.W.	Die quantiative Niederschlagsprognose winterlicher zykloner Witterungslagen auf der Alpenordseite der Schweiz (vergriffen)	15	1970
16	Schram K., Thams J.C.	Die kurzwellige Globalstrahlung und die diffuse Himmelsstrahlung auf dem Flugplatz Zürich-Kloten	18	1970

Nr.	Verfasser	Titel	Seiten	Jahr
17	Kasser P., Schram K., Thams J.C.	Die Strahlungsverhältnisse im Gebiet der Baye de Montreux	46	1970
18	Gutermann Th.	Vergleichende Untersuchungen zur Föhnhäufigkeit im Rheintal zwischen Chur und Bodensee	68	1970
19	Ginsburg Theo	Die statistische Auswertung von langjährigen Temperaturreihen	42	1970
20	Primault B.	Du risque de gel et de sa prévision	20	1971
21	Piaget A.	Utilisation de l'ozone atmosphérique comme traceur des échanges entre la troposphère et la stratosphère	72	1971
22	Zenone E.	Die Gewitterverhältnisse in den südlichen Zentralalpen und Voralpen	24	1971
23	Kirchhofer W.	Abgrenzung von Wetterlagen im zentralen Alpenraum	72	1971
24	Primault B.	Le climat, élement du plan d'aménagement Das Klima, eine der Grundlagen der Landesplanung The climate as an element of the land management	28 1 Karte	1971
25	Fröhlich C., Wierzejewski H.	Die verschiedenen Messverfahren zur Bestimmung der Strahlungsintensität mit dem Kompensationspyrheliometer und die Entwicklung eines verbesserten Modells	36	1972
26	Bouët M.	Le foehn du Valais	12	1972
27	Zenone E.	Die Gewitterverhältnisse in den südlichen Zentralalpen und Voralpen	32	1972
28	Catzeflis J., Primault B., Strehler H.	Analyse de la pluviosité dans le Valais central	15	1972
29	Courvoisier H.W.	Die Niederschlagswirksamkeit markanter, hochreichender Kaltlufteinbrüche im Sommer in der Schweiz	11	1973
30	Sevruk B.	Erfahrungen mit Totalisatoren mit schiefen, geneigten und bodenebenen Auffangflächen im Einzugsgebiet der Baye de Montreux. Einfluss der Temperatur auf die Messung des Niederschlages mit Totalisator	44	1973
31	Strehler H.	Beziehungen zwischen Witterung und Zuckerrübenmerkmalen im Spätsommer	20	1975
32	Courvoisier H.W.	Katalog objektiv-statistischer Wetterprognosen für die Alpensüdseite und das Oberengadin	24	1975
33	Primault B.	Essais d'évaluation climatologique du risque de gel	28	1975
34	Kirchhofer W.	Stationsbezogene Wetterlagenklassifikation	50	1976
35	Piaget A.	L'évolution orageuse au nord des Alpes et la tornade du Jura vaudois du 26 aout 1971	114	1976

Nr.	Verfasser	Titel	Seiten	Jahr
36	Bouët M.	Contribution à l'étude de la variation diurne de pression en Suisse romande	23	1976
37	Zenone E.	Die Gewitterverhältnisse in den südlichen Zentralalpen und Voralpen	60	1976
38	Primault B., Quiby J.	Diagrammes psychrométriques différenciés en altitude	36	1977
39	Courvoisier H.W.	Katalog objektiv-statistischer Wetterprognosen für die Alpennordseite, das Wallis sowie Nord- und Mittelbünden	58	1978
40	Gutermann Th., Mäder F. (Redaktion)	15. Internationale Tagung für alpine Meteorologie, Grindelwald 19. - 23. September 1978, Tagungsbericht 1. Teil	332	1978
41	Gutermann Th., Mäder F. (Redaktion)	15. Internationale Tagung für alpine Meteorologie, Grindelwald 19. - 23. September 1978 Tagungsbericht 2. Teil	63	1979
42	Courvoisier H.W.	Starkniederschläge in der Schweiz in Abhängigkeit vom Druck-, Temperatur- und Feuchtefeld	59	1981
43	Urfer Ch.	Mittlere Temperatur- und Windverteilung im Dischmatal bei Davos bei typischen sommerlichen Witterungslagen	32	1981
44	Altherr, J.-D., Dupanloup M., Ganter Y., Junet E.	Prévision objective des hauteurs de précipitations et de l'ensoleillement relatif au moyen de l'analyse discriminante	43	1982
45	Courvoisier H.W.	Abgeschlossene Höhentiefs und ihre Wetterauswirkungen in der Schweiz	44	1984
46	Perret R.	Une classification des situations météorologiques à l'usage de la prévision	127	1987
47	Courvoisier H.W.	Regionale Wetterauswirkung und Prognose von Staulagen in der Schweiz	22	1988
48	Gutermann Th., Mäder F. (Redaktion)	21. Internationale Tagung für alpine Meteorologie, Engelberg, 17. - 21. September 1990 Tagungsbericht 1. Teil	437	1990
49	Gutermann Th., Mäder F. (Redaktion)	21. Internationale Tagung für alpine Meteorologie, Engelberg 17. - 21. September 1990 Tagungsbericht 2. Teil	135	1991
50	Defila C.	Pflanzenphänologie der Schweiz	238	1991
51	Binder P.	Aspects of precipitation simulation in numerical weather prediction Towards an operational mesoscale NWP model	148	1992
52	Brändli J.	Niederschlag, Verdunstung und Wasserbilanz der Station Zürich SMA von 1901-1990	109	1993

Nr.	Verfasser	Titel	Seiten	Jahr
53	de Montmollin A.	Comparaisons de différentes méthodes de calcul de la température journalière dans leurs influences sur les longues séries d'observations	144	1993
54	Fankhauser Gregori A.	Einfluss der Witterung auf den Ertrag und die Qualität von Zuckerrübenkulturen	116	1993
55	Wolfensberger Hermann	Chronik der Totalisatoren, Handbuch zu den Niederschlags-Totalisatoren	390	1994
56	Schraff Christoph H.	Data Assimilation and Mesoscale Weather Prediction: A Study with a Forecast Model for the Alpine Region	138	1996